

**PROCEEDINGS OF 2020 IEEE SIXTH INTERNATIONAL CONFERENCE ON
N**

BIO SIGNALS, IMAGES AND INSTRUMENTATION

FEBRUARY 27 - 28, 2020



DEPARTMENT OF BIOMEDICAL ENGINEERING

2020 Sixth International Conference on Bio Signals, Images, and Instrumentation (ICBSII)

Copyright ©2020 by IEEE.

Copyright and Reprint Permission: Abstracting is permitted with credit to the source. Libraries are permitted to photocopy beyond the limit of U.S. copyright law for private use of patrons those articles in this volume that carry a code at the bottom of the first page, provided the per-copy fee indicated in the code is paid through Copyright Clearance Center, 222 Rosewood Drive, Danvers, MA 01923.

For reprint or republication permission, email to IEEE Copyrights Manager at pubs-permissions@ieee.org. All rights reserved. Copyright ©2020 by IEEE.

- For papers in which all authors are employed by the US government, the copyright notice is: U.S. Government work not protected by U.S.copyright
- For papers in which all authors are employed by a Crown government (UK, Canada, and Australia), the copyright notice is: 978-1-7281-1047-9/20/\$31.00 ©2020Crown
- For papers in which all authors are employed by the European Union, the copyright notice is: 978-1-7281-1047-9/20/\$31.00 ©2020 European Union
- For all other papers the copyright notice is: 978-1-7281-1047-9/20/\$31.00 ©2020IEEE

ISBN : 978-1-7281-1047-9/20

IEEE Meetings, Conferences & Events (MCE)

445 Hoes Lane Piscataway,

NJ 08854 USA

Fax: +1 732 981 1769

Email: ieee-

mce@ieee.orgAvailability:

Monday-Friday

08:00 - 16:30 Eastern Standard Time

IEEE: Advancing Technology forHumanity

Proceedings of the

2020 IEEE Sixth International Conference on Biosignals, Images and Instrumentation

Department of Biomedical Engineering
SSN College of Engineering



In association with

Centre for Healthcare Technologies



ICBSII - 2020
(27th – 28th February
2020) Editorial Board

Chief Editor:

Dr. A. Kavitha, Prof & HoD/BME

Co- Editor:

Ms. B. Divya, AP/BME

Contents

Message from theChiefPatron	ix
Mrs. Kala Vijayakumar, President, SSN Institutions	
Message fromthePatron	x
Dr. S. Salivahanan, Principal, SSN College of Engineering	
Convener’sMessage.....	xi
Dr. A. Kavitha, Professor & Head, BME	
Message fromtheCoordinators.....	xii
Dr. J. Vijay, Associate. Prof/BME, Dr. S. Arun Karthick, Associate. Prof/BME	
Message from theOrganizing Secretary	xiv
Dr. S. Bagyaraj, Associate. Prof/BME	
ConferenceOrganizingCommittee... ..	xv
Technical AdvisoryCommittee	xvi
ReviewCommittee.....	xvii
StudentOrganizingTeam	xxi

Keynote Speakers

Dr.JustinDauwels	xxiii
Dr.PerungoThirumaraiChelvan	xxiv
Dr.DeepakJoshi	xxv
Dr.G.S.Bhuvaneshwar,	xxvi
Dr. BasheerAhamedGulam	xxvii
Dr.Ing.EkoSupriyanto	xxviii

Research Papers

Session-I

1. Design of a Standardised Semi-Automated Sensory Device for Two Point Discrimination testing in the footsole M. S. Gansehmurthy, Dr. R. Periyasamy	2
.....	
2. Development of a non-invasive non-contact optical device for estimating TcB in Neonates K. Vignesh Kumar , Dr. R. Periyasamy	7
.....	
3. Intelligent wearable device for early detection of myocardial infarction using IoT V. Kavya , G. R. Suresh	12
.....	
4. Region Specific Weight Measuring System for Bedridden patients G. Annie Nancy , B. Rashmi , R. Kalpana	16
.....	
5. Microfluidic device for Multitarget separation using DEP techniques and its applications in clinical research Mohamed Zackria Ansar B.I , Mohamed Yousuff Caffiyar , Mohammed Kashif .A	20
.....	
6. Smart Health Monitoring System using IOT and Machine Learning Techniques Honey Pandey , S. Prabha	26
.....	

Research Papers

Session-II

1. A Deep Learning Approach on Segmentation of Bone for BMD Measurement from DEXA ScanImages	
S. M. Nazia Fathima , R. Tamilselvi , M. Parisa Beham , A. Nagaraj	
.....	32
2. MAMMSIT: A Database For The diagnosis and detection of Breast Cancer in Mammographyimages	
M. Parisa Beham , N. Kayalvizhi , R. Tamilselvi , A. Nagaraj	
.....	37
3. Shape Description of FDG uptakes in Pre and Postoperative fused PET/CTImages	
J. AngelinJeba , S. Nirmala Devi	
.....	42
4. BRAMSIT: A Database for Brain Tumor Diagnosis andDetection	
R. Tamilselvi , A. Nagaraj , M. Parisa Beham , M. BharkaviSandhiya	
.....	48
5. Molecular Docking Analysis of CFTRInhibitors	
M. Brindha , R. Shelishiyah , S. Vasanthavalli	
.....	53
6. Analysis of Histogram Distance Measures for Change Detection In BrainSymmetry	
K. Suresh , U. Sakthi , N. Sri Madhava Raja , R. Prabhu	
.....	57

Research Papers **Session-III**

1. Delay and Power Efficient FIR Architecture for Noise Suppression of EOGSignal Gundugonti Kishore Kumar , Balaji Narayanam , D Hema Malini	64
2. Analysis of Obstructive Sleep Apnea using ECGSignals A. K. Jayanthi , SubhikshaSomanathan , Shivani Yeshwant	69
3. Fractal Characterization of Auditory EvokedPotentials Suman Paria , Uttaran Bhattacharjee , Nilotpal Das , Dr Monisha Chakraborty	74
4. Optimal filtering of Single channel EEG Data using LinearFilters AshmitaBera , Nilotpal Das , Dr. Monisha Chakraborty	78
5. Fractal Characterization of ECG signals: Indian Classical Music asstimulus Nilotpal Das , Dr Monisha Chakraborty	83
6. FGPA Implementation Of Epileptic Seizure Detection Using ELMClassifier J Prabin Jose , M. Sundaram , G. Jaffino	89

Research Papers

Session-IV

1. Machine Learning Techniques for Prediction from various Breast Cancer Datasets Shalini M , Dr. S. Radhika.	95
2. A Review on Image Processing Approaches for Glioma Grading Seema P.D. , Christy Bobby T.	100
3. Establishing Authenticity on DICOM images using ECC algorithm Veena Suresh , S Rajashree	106
4. Efficient medical image compression based in integer wavelet transform R.Krishnaswamy , Dr. S. Nirmala Devi	109
5. Blood Vessel Segmentation on Retinal Fundus Image-A Review P.Hosanna Princy , M.Lavanya , S.Sivasubramanian , Archana MK	114
6. Analysis of Alzheimer Disease using Optimization Techniques D. Chitradevi , S. Prabha	120
7. Vowel Identification from Neural Signals during Articulated Speech Ashley Bishop, Anandha Sree Retnapandian, Sandhya Chengaiyan, Kavitha Anandan	125
8. Effect of Virtual Reality on the EEG Sub-Band Frequency Powers of Autistic and Control groups Chrisilla S, Anna Masciantonio, Divya B, Vidhusa S, Kavitha A	130
9. Analysis of Physiological Signals During Therapeutic Yoga Practice R.Anandha Prabha, E.S.SelvaPriya, L.Suganthi, T.Nandini, D.Sindu , M.Muthu Vijay	134
10. A Novel VLSI Architecture of CORDIC Based Image Registration Anirban Chakraborty, Ayan Banarjee	140

*Dedicated to
All the Staff and Students
of the Department of Biomedical Engineering*

From the Chief Patron Mrs. Kala Vijayakumar

President, SSN Institutions



SSN Institutions (SSN) nurture the all-round development of the students, focusing not only on academic excellence but also on honing life skills such as leadership, discipline, team spirit and time management. Students are encouraged to think critically and creatively. SSN prides itself on providing holistic education to its students.

Biomedical Engineering is a multi-disciplinary branch of study which brings together healthcare and technology, the front runners in the modern world. I congratulate the Department of Biomedical Engineering for organizing the 6th International Conference on Bio signals, Images and Instrumentation, in association with the Centre for Healthcare Technologies of SSN. This conference will provide the participants and the students a unique opportunity to develop enriching perspectives by interacting with some of the renowned experts in these fields, from all over the world. I am certain that the talks by eminent scientists, researchers, industry-experts and the papers presented will stimulate lively discussions and will lay a strong foundation for further advanced research in these fields. I appreciate the untiring, excellent teamwork carried out by the faculty of Biomedical Engineering department towards organizing this conference.

I extend my felicitations to the BME department and wish the conference all success.

Mrs. Kala Vijayakumar,
Chief Patron,
ICBSII – 2020

From the Patron

Dr. S. Salivahanan

Principal, SSN College of Engineering



I am pleased that the department of Biomedical Engineering is organizing the 6th International conference on Bio signals, Images and Instrumentation in a manner befitting the stream.

Biomedical engineering is a multidisciplinary field integrating Engineering and healthcare. It focuses on the advances that improve human health and health care at all levels. The department's engagement in wide spectrum of activities with involvement of students and faculty along with strategic planning process has strengthened it.

This International Conference was conceived with the thought of bringing scientists, engineers and researchers together from various domains all over the world. It has been a platform where some of the greatest minds of the country and abroad could interact, exchange ideas and work together towards a common goal.

I congratulate the entire team of Biomedical Engineering Department for structuring it to perfection and wish them all success.

Dr. S. Salivahanan,
Patron,
ICBSII – 2020.

From the Convener

Dr. A. Kavitha

Professor & Head,
Department of Biomedical Engineering
SSN College of Engineering



Education is a holistic endeavor, creating new paths with endless boundaries and priming the mind to orient one to the world. That being said, it gives me immense pleasure to present the Sixth International Conference on Bio-signals, Images and Instrumentation.

Biomedical engineering discipline is one which catalyzes interactions between biologists, physical scientists, and engineers to benefit medicine and human health. This serves society by conducting research that develops quantitative linkages across scales in the human body and uses that development to build new tools to improve human health. The outcomes of research assume a whole new level of importance and significance.

The department is frequently organizing workshops, seminars, project exhibitions and guest lectures on diverse concepts related to the core and interdisciplinary subjects in biomedical engineering to equip the students in gaining a comprehensive knowledge of the industrial requirements to the fullest.

The Centre for Healthcare Technologies, a multidisciplinary research initiative, concentrating on research through innovation in healthcare, in association with the Department of Biomedical Engineering, is organizing the 6th International Conference on Biosignals, Images and Instrumentation, hoping to instill research aptitude in students and provide a great platform for the researchers to showcase their work in various domains of Biomedical Engineering.

Alone we can do little; together we can do so much. With confidence, we aim higher and higher, raising our bars towards the next success!!!

Dr. A. Kavitha
Convener,
ICBSII – 2020

From the Coordinators

Dr. J. Vijay

Associate Professor,
Department of Biomedical Engineering
SSN College of Engineering



I extend a hearty welcome to all to the IEEE sponsored Sixth International Conference on Bio signals, Images and Instrumentation (ICBSII2020) February 27-28, 2020 in SSN College of Engineering. It gives me an immense pleasure to once again put our hands together in organizing the Department's annual extravaganza!

This Conference provides an excellent opportunity for Researchers, Scientists, Academicians and Students from all over the world to share their ideas, experiences and the work done by them. It is a platform which helps students to explore new ideas and build upon the existing ones. It also provides an opportunity to exchange ideas with experts and scholars from various fields.

The Conference will involve various talks from Experts, Presentation Of Papers and a Forum for discussion to unveil different facets of Science and Engineering.

I would like to thank the management of SSN College of Engineering, Mrs. Kala Vijayakumar, President, SSN Institutions and Dr. S. Salivahanan, Principal, SSN College of Engineering for granting the department a delightful opportunity to organize such a magnificent event that enables the department as a whole to grow on a global level. I would also like to thank all the members who have contributed towards organizing the occasion to make it a grand success!

Dr. J. Vijay
Coordinator,
ICBSII-2020

From the Coordinators

Dr. S. Arun Karthick

Associate Professor,
Department of Biomedical Engineering,
SSN College of Engineering



On behalf of the Biomedical Engineering Department, it is with great pleasure that I welcome you to the 6th International Conference on Bio signals, Images and Instrumentation (ICBSII 2020) on February 27th and 28th, 2020 in SSN College of Engineering, Kalavakkam. This two-day conference features Keynote talk from distinguished scientist of International standing. Keynote presentations often lead to thought-provoking insights that can be applied to one's research problems, so I am convinced that, like me, you are very much looking forward to such stimulating talks. This conference will provide a platform for researchers, scientists and industry practitioners from all over the country to present, discuss and share their knowledge on novel approaches and solutions in the field of Biomedical Engineering for the betterment of society.

My sincere gratitude to the management of SSN College of Engineering, Mrs. Kala Vijayakumar - President, SSN Institutions and Dr. S. Salivahanan - Principal, SSN College of Engineering, without whom a prolific occasion of this magnitude would not be possible. I would like to thank ICBSII 2020 committee members for their support, constructive feedback, and timely help. Finally, I would like to take this opportunity to thank all Keynote Speakers, External Reviewers, Student Volunteers and Contributing Authors presenting at ICBSII 2020.

I sincerely hope that you will enjoy the Technical Program about to unfold in the next two days and that will leave you with fond memories of ICBSII 2020.

Dr. S. Arun Karthick
Coordinator,
ICBSII –2020

From the Organizing Secretary

Dr. S. Bagyaraj

Associate Professor,

Department of Biomedical Engineering

SSN College of Engineering



Welcome to IEEE sponsored Sixth International Conference on Bio signals, Images and Instrumentation (ICBSII 2020) on February 27th to 28th, 2020 in SSN College of Engineering. The purpose of this Conference is to bring Researchers and Industry Practitioners together to present and discuss novel approaches and solutions. The outcomes in the field of Biological, Medical, Health Care, Pharmaceutical, Biotechnology, Bioinformatics, Computer Science, Information Technology and Communication to create synergy, support Interdisciplinary Research, and to exchange ideas and explore new avenues of collaborations.

For this conference, research papers on the mentioned issues were collected from India and Abroad. Papers collected in this international conference were rigorously reviewed by the scientific program committee members. According to the review results, the program committee members have selected twenty-four high quality papers to be presented in this conference. Many researchers from all over the world have kindly helped us to prepare and organize ICBSII-2020. The conference turned out to be a forum for scientists and researchers all over the world to share their ideas, experiences, findings, and conclusions of their work in due course of their scientific research.

I would like to thank the ICBSII-2020 organization and technical program committee for their support, constructive feedback, and timely proposal review. I extend my sincere gratitude to the management of SSN College of Engineering, Mrs. Kala Vijayakumar-President, SSN Institutions and Dr. S. Salivahanan-Principal, SSN College of Engineering for granting the department a wondrous opportunity to organize and conduct this productive occasion helping us to take it forward to the global level. Finally, I would also like to take opportunity to thank all external reviewers and contributing authors for producing high quality papers to be presented at ICBSII2020.

Dr. S. Bagyaraj
Secretary,
ICBSII – 2020

Conference Organizing Committee

Chief Patron

Ms. Kala Vijayakumar, President, SSN Institutions

Patron

Dr. S.Salivahanan, Principal, SSN College of Engineering

Convener

Dr. A. Kavitha, Professor and HOD/BME

Coordinators

Dr. J. Vijay

Dr. S. Arun Karthick

Organizing Secretary

Dr.S. Bagyaraj

Treasurer

Dr. K. Nirmala

Ms. B.Divya

Committee Members

Dr. V. Mahesh

Dr. S. Pravin Kumar

Dr. L. Suganthi

Dr. B. GeethanjaliDr.

R. Subhashini Ms.

M.Dhanalakshmi

Dr. SachinGaurishankarSarate

Ms. R. Nithya

Technical Advisory Committee

International Advisory Committee Members

- **Dr. Sriram Balasubramanian**, Asso. Prof., Drexel University, USA
- **Dr. Kong Pui Wah**, Asso. Prof., NTU, Singapore
- **Dr. Teo Ee Chon**, Asso. Prof., NTU, Singapore
- **Dr. M. Murugappan**, Asso. Prof., KCST, Kuwait
- **Dr. EkoSupriyanto**, Asso. Prof., Universiti Teknologi Malaysia, Malaysia
- **Dr. S. Arunachalam**, Asso. Prof., JIC, Kingdom of Saudi Arabia
- **Dr. Tinashe Mutswangwa**, Senior Lecturer., UCT, South Africa
- **Dr. Sekar Raju**, Asso. Prof., Xi'an jiaotong-Liverpool University, China
- **Dr. J. Jesu Christopher**, Senior Scientist, ASTRAZENCA, Cambridge, UK
- **Dr. S. Ramji**, Queen's University Belfast, UK
- **S. Ramesh**, University of Malaya, Malaysia
- **P. Sasikumar**, Higher Colleges of Technology, UAE

National Advisory Committee Members

- **Dr. S. Ramakrishnan**, Prof., IIT Madras
- **Dr. S. Muttan**, Prof., Anna University
- **Dr. Renu John**, Associate Professor & Head of the Department BME., IIT Hyderabad
- **Dr. R. Periyasamy**, Assistant. Prof., NIT Raipur
- **Mr. K. Mohanavelu**, Scientist E, DEBEL., DRDO, Bangalore
- **Mr. S. Sivagnanam**, Additional Industrial Advisor., Govt. of India, MSME
- **Dr. Niranjan D. Khambete**, Biomedical Head., Pune Govt. Hospital, Pune
- **Dr. G. Sudhir**, Orthopaedic Spine Surgeon., SRMC, Chennai
- **Dr. G. Kumaramanickavel**, Director of Research., Narayana Nethralaya
- **Dr. B. Minimol**, Asso. Prof., Gov. Model Engineering College, Kochi
- **Dr. C.M. Sujatha**, Asso. Prof., Anna University, Chennai

Review Committee

International List of Reviewers:

- **Dr. Vivek PadmanaabhanIndramohan,Senior Lecturer Brimingham City University,UK**
- **Dr. Kong PuiWah,Associate Professor Nanyang Technological University, Singapore**
- **Dr. Teo EeChon,Professor Nanyang Technological University,Singapore**
- **Dr. R. Sivaramakrishnan, Research Scientist National Institutes Of Health,USA**
- **Dr. S. Pravin Kumar,Research Specialist Palacký University Olomouc CzechRepublic**
- **Dr. Rahuman,Sheriff Project Leader Biomodels European Bioinformatics Institute ,UK**
- **Dr. R. Yuvaraj, Research Scientist Nanyang Technological University,Singapore**
- **Dr. Aleksandra Kawalajanik,Research Scientist Opole University OfTechnology**
- **Dr. EkoSupriyanto,ProfessorIjn-Utm Cardiovascular Engineering Centre,UTM**
- **Dr. Sriram Balasubramanian,Associate Professor Drexel University,USA**
- **Dr.M.Murugappan,AssociateProfessorKuwaitCollegeOfScienceAndTechnology,Kuwait**
- **Dr. S. Arunachalam,Associate Professor Jic, Kingdom Of SaudiArabia**

IEEE Members:

- **Dr.AKavitha, Professor and Head Department of Biomedical Engineering,SSNCE**
- **Dr. N.Venkateswaran, Professor Department of ECE,SSNCE**
- **Dr.MaheshVeezhinathan, Associate Professor Department of Biomedical Engineering,SSNCE**
- **Dr.O. Uma Maheswari, Assistant Professor (Senior Grade) Department of ECE, CEG Campus, AnnaUniversity,**
- **Dr. Suganthi Lakshmanan, Associate Professor Department of Biomedical Engineering,SSNCE**
- **Dr.S.Prabakar, Professor & Head Department of Biomedical Engineering, Dr.NGP Institute of Technology,Coimbatore**
- **Dr.R.Periyasamy, Assistant Professor Department of Biomedical Engineering, NIT,Raipur**
- **Dr.T.S.Karthik, Associate Professor Department of ECE, B.V.Raju Institute of Technology, Telengana.**
- **Dr.R.M.Akila, Professor Department of ECE, KPR Institute of Engineering and Technology, Coimbatore**
- **Dr.Balaji.V, Associate Professor Department of ECE, KPR Institute of Engineering and Technology,Coimbatore**
- **Dr. B. Jaishankar, Associate Professor Department of ECE, KPR Institute of Engineering and Technology,Coimbatore**
- **Dr.M.Kayalvizhi, Associate Professor and Head Department of Biomedical Engineering Agni College of Technology, Thalambur,Chennai**
- **Dr.S.Karthika, Associate Professor Department of IT,SSNCE**

Indian Reviewers:

- **Dr.C. M. Sujatha, Assistant Professor Department of ECE, Anna University**
- **Dr. G. Kavitha, Assistant Professor (Senior Grade) MIT campus, Anna University**
- **Dr. A. Mythili, Associate Professor Sensor and Biomedical Technology Division, School of Electronics Engineering (SENSE), VIT Vellore campus.**
- **Dr. K. Kamalanand, Assistant Professor MIT campus, Anna University**
- **Dr. B. Minimol, Associate Professor Department of Electronics & Biomedical Engineering, Model Engineering College, Kerala**
- **Dr. R. Tamilselvi, Professor Department of ECE, Sethu Institute of Technology, Madurai.**
- **Dr. D. Vaithyanathan, HOD Department of ECE, NIT, Delhi**
- **Dr. A. K. Jayanthi, Professor Department of Biomedical Engineering, SRM University, Chennai.**
- **Dr.S.Poonguzhali, Associate Professor Department of ECE, CEG Campus, Anna University**
- **Dr. P. Rajasekar, Senior Assistant Professor Department of Biotechnology, Rajalakshmi Engineering College, Chennai**
- **Dr. S.Sasikala, Associate Professor Department of ECE, CEG Campus, Anna University**
- **Dr. Jaganathan M, Associate Professor School of Electronics Engineering, VIT, Chennai.**
- **Dr. K. Adalarsasu, Associate Professor School of EEE, Sastra University, Tanjavur**
- **Dr. Ganesh Vaidyanathan, Principal SVCE, Chennai.**
- **Dr. M. G. Sumithra, Professor Bannari Amman Institute of Technology, Sathyamangalam.**
- **Dr. T. R. Ganesh babu, Professor Muthyammal Engineering College, Rasipuram**

- **Dr. M. C. Jobin Christ, Associate Professor Department of Biomedical Engineering, Rajalakshmi Engineering College, Chennai.**
- **Dr. E. Priya, Beatrice Associate Professor Department of ECE, Sri Sairam Engineering College, Chennai.**
- **Dr. K. Vidhya, Professor School of ECE, Saveetha University, Chennai.**
- **Dr. B. Padmapriya Associate Professor Department of Biomedical Engineering PSG College of Technology**
- **Dr. Judith Justin, Professor Department of Biomedical Instrumentation Engineering, Avinashilingam University**
- **Dr. D. Balasubramanian, Professor Department of ECE, GKM college of Engineering and Technology**
- **Dr. S. Bagyaraj, Associate Professor Department of Biomedical Engineering, SSN College of Engineering**
- **Dr. J. Vijay, Associate Professor Department of Biomedical Engineering, SSN College of Engineering**
- **Dr. S. Arun Karthick, Associate Professor Department of Biomedical Engineering, SSN College of Engineering**

Student Organizing Team

Registration:

- Varshini V– Third Year,UG
- Sharmilee S– ThirdYear,UG
- Rishika V– Third Year,UG
- Shwetha Sridhar– ThirdYear,UG
- Srividya S– Third Year,UG

Conference Proceedings:

- Arthika J – ThirdYear,UG
- Srinidhi V – ThirdYear,UG
- Haridhra Suresh–Third Year,UG

Food Committee:

- Pranav KrishnaR–ThirdYear,UG
- ThejasviNrupeshPuvvada–ThirdYear,UG
- Abhijith K S–ThirdYear,UG
- Arshad Ahmed S – Third Year,UG
- Saranya V– ThirdYear,UG
- Rajkumar A J– ThirdYear,UG

Hall Arrangements:

- Sri Yukesh S –ThirdYear,UG
- Kavin M–ThirdYear,UG
- Annamalai R V –ThirdYear,UG

Design:

- Parvathi AR–ThirdYear,UG
- Radhika B–ThirdYear,UG
- Reshma C.A – ThirdYear,UG

Transport:

- BharathRaaj N– Third Year, UG
- Ansar Ahamed S – Third Year,UG
- Gurucharan M K– Third Year,UG

**2020 IEEE Sixth International
Conference on Bio signals, Images and
Instrumentation
ICBSII 2020**

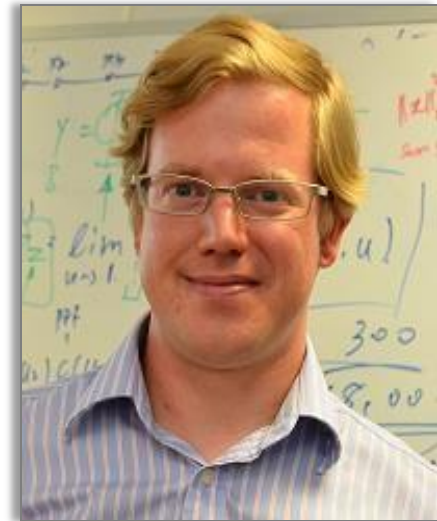
KEYNOTE SPEAKERS' PROFILE

Artificial Intelligence for Applications in Psychiatry

Dr. Justin Dauwels

Abstract:

Many tasks in medicine still involve substantial manual work. In many cases there is strong potential for intelligent automation by A.I., leading possibly to a reduction in costs and man-hours, while increasing the quality of clinical service. In this talk, we will consider applications of A.I. in the domain of psychiatry. Specifically, we will give an overview of our research towards automated behavioral analysis for assessing the negative symptoms of mentally ill patients. Many tasks in medicine still involve substantial manual work. In many cases there is strong potential for intelligent automation by A.I., leading possibly to a reduction in costs and man-hours, while increasing the quality of clinical service. In this talk, we will consider applications of A.I. in the domain of psychiatry. Specifically, we will give an overview of our research towards automated behavioral analysis for assessing the negative symptoms of mentally ill patients.



Dr. Justin

Dauwels Associate Professor NTU,
Singapore Deputy Director, ST
Engineering – NTU
corporate lab

Justin Dauwels is an Associate Professor in School of Electrical & Electronic Engineering at Nanyang Technological University (NTU). He also serves as Deputy Director of the ST Engineering – NTU corporate lab. He obtained his PhD degree in Electrical Engineering at the Swiss Polytechnical Institute of Technology (ETH) in Zurich in December 2005. His research on intelligent transportation systems has been featured by the BBC, Straits Times, Lianhe Zaobao, Channel 5, and numerous technology websites. Besides his academic efforts, the team of Dr. Justin Dauwels also collaborates intensely with local start-ups, SMEs, and agencies, in addition to MNCs, in the field of data-driven transportation, logistics, and medical data analytics.

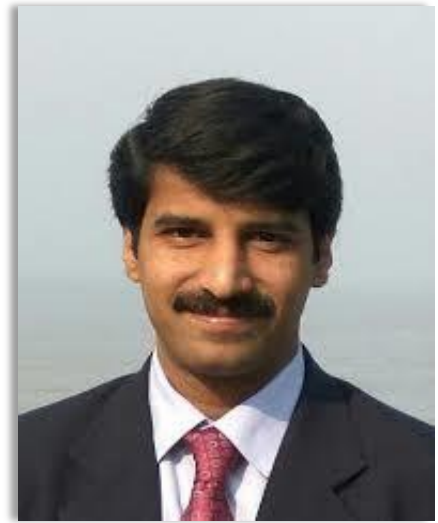
A paradigm shift in the medical field- Biomedical Engineering Dr.PerungoThirumaraiChelvan

Abstract:

Science is evolving and so is the medical field. Evidence-based medicine(EBM)is the current trend, having moved away significantly from the traditional empirical therapies. We are in the era of analyzing genes and cellular functions. Treatment advances had been made to diagnose and treat disease at the molecular level. All these were made possible by the advances in the field of Biomedical engineering which along with the technical expertise has produced a paradigm shift in the medical field.

Biosignals like ECG, EEG, and EMG etc. have become inevitable intheevaluationofpatients.BiomedicalimageslikeCTscan,MRI, PETscanhavehelpedtodiagnoseaccuratelyevenaminutepathology which otherwise may not be possible. Biomedical instrumentations including Endoscopy, laparoscopy, robotics(AI) have significantly advanced in the recent years making therapeutic procedures and surgeries to be performed easier, faster, highly precise, pain-free, scar-lesswithveryfastrecovery.Laparoscopygivesusamagnified view of the operative field which helps the surgeon to perform better. Laparoscopy is a minimally-invasive surgery using a few smallincisionsonthepatient'sbodytoinsertthetoolsandtelescope and conduct the surgical operation. Laparoscopic video processing can be used to extract valuable knowledge and help to develop the skills of the surgeons. Next level of laparoscopy is the introduction of artificial intelligence in the medicalfield.

We briefly introduce the Bio Signals, Images and instruments and thedevelopmentvertimehighlightingtheirinevitablenatureinthe current medicalfield.



Dr.PerungoThirumaraiChelvan
Unit Head, Chennai Division
Asian BariatricsHospital

Dr.PerungoThirumaraiChelvanis a Bariatric, Metabolic and Gastrointestinal surgeon, from Chennai, India. Heobtained his MBBS degree in 2004 from Stanley Medical college hospital in Chennai. He pursued his Master's in the General Surgery from Chengalpet Medical college hospital between 2006 and 2008. After graduation, he underwent his basic laparoscopic training at the Lifeline multi-specialty hospital - a high volume gastrointestinal surgery center in Chennai. Dr.Perungo mastered the technique of bariatric surgery at the Asian Bariatrics hospital under the guidance of the doyens in the field namely Dr.MahendraNarwaria and Dr.SanjayPatolia.

Dr.Perungo has a surgical experience of more than 10 years. His bariatric surgical experience spans over 1000 successful procedures including sleeve gastrectomy, Gastric bypass, Revision bariatric surgeries and Metabolic surgery. He has pioneered and excelled in the novel Laprosc bariatric surgery.

Dr.PerungoThirumaraiChelvanis also a Fellow of the Royal College of Surgeons, Edinburghsince theyear2011.Inaddition, he is a Registered Member of the General Medical Council, UK.

Forcemyography: A paradigm shifts from Electromyogram for Rehabilitation Engineering Deepak Joshi

Abstract:

Despite of its various shortcomings, electromyography (EMG) is still the benchmark biosignal in rehabilitation engineering including prosthetic control. The intuitive control is prime feature of EMG that makes it globally acceptable. However, EMG is associated with various disadvantages like sweating, complex signal processing, and sensitive placements to anatomical location. Recently, our group at IIT-Delhi proposed an alternate method named Forcemyography (FMG), which is a mechanical manifestation of muscles contraction, for rehabilitation engineering and prosthetics control. We show that FMG outperforms EMG in locomotion classification for prosthetic control with a potential to be useful in rehabilitation engineering. The talk will present some of the FMG-related work in the Neuromechanics laboratory at IIT Delhi. In addition, the recent work in FMG-related Parkinson's diagnosis and signal modelling for FMG will be discussed.



Deepak Joshi,
Assistant Professor, IIT Delhi

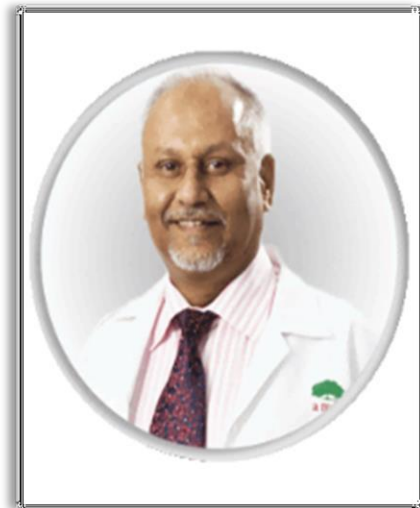
Dr. Deepak Joshi received his PhD in Biomedical Engineering from Indian Institute of Technology (IIT) Delhi. During his tenure at Department of Electrical and Computer Engineering in National University of Singapore (NUS), he worked on the development of Artificial Hand with integrated sensors to create an illusion of touch from human hand. This work received the most popular article in IEEE Transaction on neural system and rehabilitation engineering. He continued his research works at Institute of Neuroscience (ION), Newcastle University in United Kingdom (UK). He further obtained his postdoctoral at University of Oregon in United States of America (USA). Before joining IIT Delhi, he was working as an Assistant professor with Indian Institute of Information Technology (IIIT), Allahabad. Dr. Joshi is currently exploring Visual motor control for seamless transition in powered prosthesis and the role of artificial proprioception in lower limb prosthesis and gait rehabilitation. Besides that, he is actively engaged in projects related to development of Biomedical Instrumentation for applications specific to assistive devices for elderly and disabled.

Clinical Engineering: Evolution of a Discipline

Dr. Basheer Ahamed Gulam

Abstract:

Clinical Engineering is an up going Biomedical & Biomechanical science. Most of the western world hospitals have a Clinical Engineering department. The department of Clinical Engineering plays an important role beginning from procurement process and facilitates effective management of medical devices which are especially used in healthcare facilities. Additionally, clinical engineering department increases lifecycle of medical devices, optimizes spare parts and technical services' costs of medical devices in order to improve the quality of healthcare. They also support the institution with advance patient care with technological support and with Management Skills. Clinical Engineers Support a Healthcare industry with their technology, hospital economics, social, management, & safety features. Clinical Engineering techniques and methodologies are mainly focused on safe, appropriate and economical management of technologies, as well as on governance and management (limited to specific responsibilities) of healthcare facility. The main aim of Clinical Engineering is to support the use of biomedical technology by health professionals and hospital organizations with appropriate skills in order to reach the best compromise between clinical efficacy/efficiency.



Dr. Basheer Ahamed Gulam
Senior Orthopaedic Surgeon

Dr. Basheer Ahamed Gulam completed his M.B.B.S from Coimbatore Medical College, Coimbatore, India. He earned his post-graduation in Orthopaedic Surgery from Kilpauk Medical College, Chennai. He has shined his academic career with Postgraduate Diploma in Sports Medicine from the Board of the Royal College of Surgeons and Physicians in Ireland (Dip. Sports Med RCS & P). He is a member of Sports & Exercise Medicine from UK (Edinburgh) (MFSEM) and Fellow in Sports & Exercise Medicine from the Royal College of Physicians and Surgeons Dublin, Ireland (FFSEM.RCS&P). He has rich experience in consultation as Orthopaedic Surgeon and Sports Medicine from many Hospitals. He currently works in the American Mission Hospital in the Kingdom of Bahrain as Orthopaedic Surgeon.

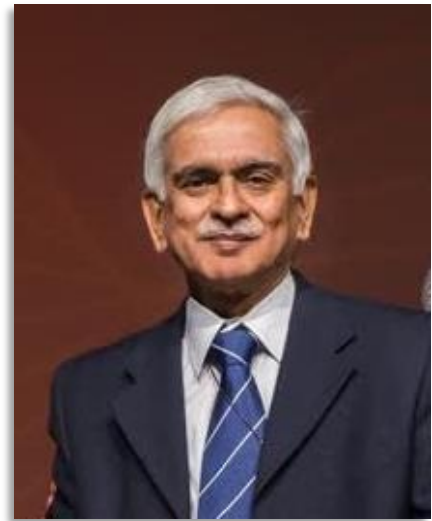
Development Of Medical Devices - A Roadmap

Dr. G.S. Bhuvaneshwar

Abstract:

Development of a medical device involves multiple aspects and stages. One needs to understand the user needs and the technical challenges of the product development to start with. The development then moves on to choice of design, testing of the materials involved. The next stages involves 3 to 4 cycles of prototyping and testing. The prototypes need to be tested to demonstrate that they meet the design requirements and the user needs.

For medical devices, it is also necessary to demonstrate its safety and performance. This involves multiple stages of testing leading finally to Clinical trials. The "Development of the Chitra Heart Valve prosthesis" is used as a case study to highlight the various steps and stages of a high risk product development, including the final stages of pilot production and clinical trials.



**Dr. G.S.
Bhuvaneshwar** Independent
Consultant, Adjunct
Professor, IIT Madras
Visiting Professor, IIT Hyderabad

Dr. G. S Bhuvaneshwar graduated with a B.Tech (Electronics) in 1972 and M.S. (Bioengineering), 1975 from IIT Madras. He obtained a PhD in Biomedical Technology from SCTIMST in 1994. Notable awards include the Distinguished Alumnus Award of IIT Madras in 1999, Materials Society of India Medal lecture and NRDC awards for meritorious inventions. In May 2016 he was elected "Fellow, Biomaterials Science & Engineering (FBSE)" by the International Union of Societies of BSE at the World Biomaterials Congress, Montreal, Canada. From Sep 2012 to Dec 2015, he was Director of Innovation at Triviron Healthcare Pvt, LTd., Chennai – a leading company of Indian origin with a major focus in *In vitro* Diagnostics.

Previously, he retired as Head of the Biomedical Technology Wing of Sree Chitra Tirunal Institute for Medical Sciences & Technology (SCTIMST), Trivandrum in 2012 after a long & distinguished career spanning 36 years.

Cardiovascular Management In 4th Industrial Revolution Era

Dr. Ing. EkoSupriyanto

Abstract:

Cardiovascular Diseases (CVDs) are the leading causes of death worldwide. Proper management of cardiovascular system is a method to prolong life expectancy due to CVDs. In this talk, cardiovascular management in 4th Industrial Revolution Era will be discussed. This includes the online CVD risk prediction and prevention, smart sensor-based CVD detection, artificial intelligence supported CVD diagnosis, robot supported CVD treatment, blockchain based dynamic clinical pathway of CVD management in Hospital, as well as CVD home telemonitoring. Objective of technology 4.0 integration in CVD management is to improve accuracy, access and patient safety as well reduce cost and time for CVD management. We have developed web and mobile apps for CVD risk prediction and lifestyle recommendation. Two methods which are decision trees and artificial neural network have been used to predict CVD risk. We will also introduce transesophageal echocardiography tele robotic system for CVD intervention and surgery monitoring. These systems have partly tested in few cardiac hospitals. Test results show that the prediction system has better accuracy than other risk predictors, whereas smart clinical pathway is able to reduce the cost and time for CVD treatment, and tele robotic system can improve patient and operator safety.



Dr. Ing. EkoSupriyanto

Director of IJN-UTM Cardiovascular Engineering Centre, Universiti Teknologi Malaysia

Dr. Ing. EkoSupriyanto obtained his PhD in Electronics Engineering from University of Federal Armed Forces Germany, Hamburg. He worked as an academic staff at this university and a product development manager in a private company in Duesseldorf, Germany, before he moved to Malaysia. He is a visiting professor at Ilmenau University of Technology, Germany and guest professor at Department of Radiology, Padjajaran University, Indonesia. His involvement in computer application for medicine started from 1996 for the dialysis machine safety monitoring system. He has 15 patents in the area of biomedical and computer based products. He also obtained more than 24 awards for his achievement from international institutions. He has more than 120 publications in international journals and proceeding and author of few international books. He is an active speaker in WSEAS conferences since 2009. He spoke about more than 36 papers and is the session chairman.

**2020 IEEE Sixth International
Conference on Bio signals, Images and
Instrumentation
ICBSII 2020**

**SESSION I
RESEARCH PAPERS**

**2020 IEEE Sixth International
Conference on Bio signals, Images and
Instrumentation
ICBSII 2020**

**SESSION I
RESEARCH PAPERS**

Design of a Standardised Semi-Automated Sensory Device for Two Point Discrimination testing in the foot sole

M.S. Ganeshmurthy
Junior Research Fellow, Department of ICE
National Institute of Technology
Tiruchirappalli, India
ganzmurthy@gmail.com

Dr.R. Periyasamy
Assistant Professor: Department of ICE
National Institute of Technology
Tiruchirappalli, India
periyasamy@nitt.edu

Abstract— Evaluation of sensibility in diabetic patients is a crucial factor to spot the group with different neuropathies, which play a crucial role within the development of foot ulcers. Various modalities of touch like pressure, vibration perception threshold (VPT) and two-point discrimination (TPD) are routinely used to evaluate nerve injuries within the hand and, more recently; it is developed to check sensory loss or sensibility within the lower extremity. The two-point discrimination (TPD) test is one of the common tests for neurosensory tests to enact mechanoperception in clinical settings. Despite numerous studies within the functional sensibility of the upper extremity using the TPD test, there are relatively only a couple of reports on TPD within the lower extremity region. The aim of the proposed design may be a digitized handheld isobaric aesthesiometer to supply an equal force on the two prongs and to live TPD within the foot sole, which determines the degree of sensational loss and help the clinicians to understand the severity of peripheral nerve damage in diabetes.

Keywords— Two-point discrimination, Handheld Device, Monofilament, Foot sole, sensory loss

I. INTRODUCTION

A sensory examination is one of the most common parts of the scientific neurological assessment. It is generally accepted that there are five sensory evaluation methods they are vision, hearing, taste, smell, and touch. The main aspect in the sensory examination consist of sectoral and peripheral nerve testing of the cutaneous sensibility, including a sense of mild touch, pain, temperature, vibration, and proprioception [2]. The Human plantar sensation may play an important role in many movement, including postural control, walking, and the scientific testing of diabetic peripheral neuropathy. The International Neuropathy Code define diabetic peripheral neuropathy (DPN) as the presence of symptoms of peripheral nerve dysfunction in patients with diabetes after elimination of other causes.[3] This condition affects 30%-50% of the patient community with diabetes and this ubiquity tends to increase proportionally with the period of diabetes[4]. Neuropathy often presents with a loss of protective sensation, defined as a level of sensory loss, where the patient can sustain an injury without recognizing any of the inciting injury [3]. The progression from small injury into ulceration and, ultimately, evolution into a permanent wound with elemental infection has been cited and the most common series of case leads lower amputation

The study is funded by Department of Science and Technology, Government of India; Sanction Reference Number: SP/Y0/393/2018©, Dt: 28/09/2018.

A. The Semmes-Weinstein Monofilament Test

In 1899, Max Von Frey introduced different sizes of width of monofilament to investigate the cutaneous sensation. [9] The testing mechanism was designed from horsehair seated inside a cylinder. The filament was imposed horizontal to the skin until there was a noticeable bend of the fiber. The patient then provided a verbal evaluation whether the sensation was perceived. Psychologists Florence Semmes and Sidney Weinstein further processed this device in 1960. [10] They developed a set of 20 nylon monofilaments to evaluate gross sensory loss in the hands of patients with brain injury. After gaining increased perception from its use in leprosy research at the Gillis W. Long Hansen's Disease Center in Carville, LA, the Semmes-Weinstein Monofilament (SWM) test was identified as the standard evaluation tool for the patients with Diabetic Peripheral Neuropathy (DPN). [11] The Semmes-Weinstein Monofilament (SWM) is a noninvasive screening equipment that is not only easy to learn also relatively economical and immediately accessible. These factors depict it the single most often used test to evaluate sensory neuropathy; however, the Semmes-Weinstein Monofilament (SWM) test turn out to be more of an theoretical-based technique with limited practical use. For the test to be execute properly, the subjects may need repeated evaluations at the same site to detect the stimulant. In extension, a series of irregular applications of monofilament may be required to put down any assumption by thepatient.

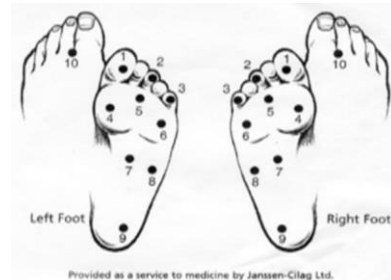


Fig. 1. Foot Test sites for sensory examination

The 10 most periodically used test regions on the foot are pictured in Figure 1. The particular regions of the foot examined during the assessment may affect both accuracy and preciseness. Smeja et al [12] determine that evaluation of the forefoot had reasonable reproducibility, but anatomical sites placed adjacent had only average reproducibility. How many regions of sensory loss are required to decide a loss of protective sensation? The benchmark for this have varied depending on the protocol decided by the investigator. Armstrong et al [13] noted that failure to observe pressure in 4 out of 10 locations is 97% sensitive and 83% precise to determine loss of protective sensation.

B. Two Point Discrimination (TPD) Test

Pinprick examination involves the light application of an antiseptic safety pin at the forefoot with ample manual pressure to slightly deform the skin. Uncommon discovery is concluded if a patient cannot determine the applied stimulus. One of the essential intimation for this testing method is to identify the focal area of sensory damage. However, this method is highly tendentious, thus the results are low replicable. [12] Also, the concern for antiseptic and careless skin damage may restrict its clinical application.



Fig. 2. Two Point Discriminator

[11] Description of two or more insensate regions is considered a decisive result. In a prospective examination of patients with diabetes who had Vibration perception threshold (VPT) greater than 25 volts, the IpTT had an similar sensitivity, specificity, and operating attribute when correlated with the Semmes-Weinstein Monofilament (SWM) test. [15] If this approach resemblance the result of the monofilament exam, the authors query why a clinician would adopt to scrutinize with a device that is more time consuming and requires apparatus.



Fig. 3. Baseline Aesthesiometer

[13] Device used to assess two-point discrimination is Aesthesiometer. It consists of a small ruler scale in millimetre with two mobile tips cover with vinyl. The vinyl finish helps to minimize the influence of temperature on knowing the point of contact. It is a miniature compact instrument developed to identify the smallest distance that two points of touch on the skin that could be identified. [13] In 1989, Dellon [7] created a innovative method to assess the two-point discrimination with the introduction of the Pressure Specified Sensitive Device (PSSD), which uses a computer-support program to compute pressure threshold on the skin for both one-point and two-point stationery contact. This exclusive device contains 1-2 metallic points located at exact intervals. The distance (in millimetres) separating the prongs is inversely associated to the perception density for that anatomical site; therefore, an increment in two-point discrimination value outside of the standard deviation compared with the amount of axonal impairment. [7]



Fig. 4. Pressure Specified Sensitive Device (PSSD)

Like other scrutinizing methods, the Pressure Specified Sensitive Device (PSSD) is tendentious because results are based solely upon the patient's sensory feedback; however, according to Dellon, the PSSD is the most authentic digitized

system to date suited to record sensation in the lower extremity. [7] From the existing TPD measuring devices the following problems are noted first to apply equal force on both of the prongs to accurately measure TPD values if the force is not equal the result may subject to biasing based on the pressure applied by the operator secondly to avoid manual errors while calculating the distance between the filaments. To address these issues we propose a handheld device, which consist of 10g monofilament to apply equal force of 10g and distance sensor to calculate the distance accurately to avoid human errors, and automated the movement between the filament and TPD values are stored in SD card for further processing.

II. MATERIAL AND METHODS

A. Automated IAEM Hardware Design

The handheld Isobaric Aesthesiometer (IAeM) consists of two monofilaments one is Monofilament(S) that is fixed on one end of the handheld device and the other is Monofilament(M) which is movable and it is driven by Stepper motor for precise movement and both the filaments are 10g force Monofilament. A laser based distance sensor is placed on the fixed Monofilament(S) to measure the distance between the two monofilaments then the distance data is transmitted to the microcontroller.

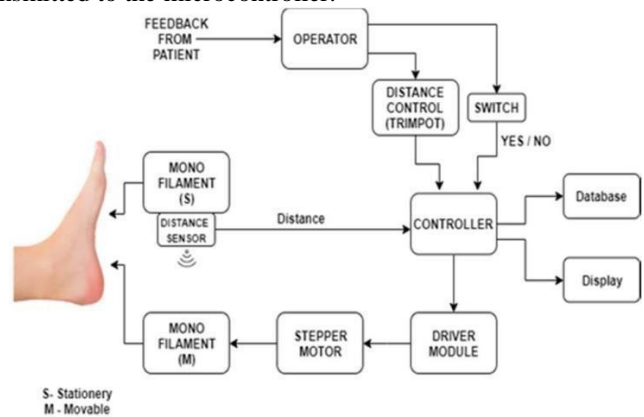


Fig. 5. Block Diagram of Automated IAeM device

The two filaments provide a 10g force that is applied on the foot of diabetic subject to detect the sensation and to diagnose the peripheral neuropathy. The operator can change the distance between the monofilament to repeat the test for different region of the diabetic foot and the patient's feedback is recorded by using a yes / no switch by the operator. The controller collects the distance data as well as the patient feedback from the operator and store the data in the database for further processing. The Atmega 328p microcontroller is used as the main controller for distance acquisition and display module. The VL6180X Time of Flight Distance Ranging Sensor is used to acquire the distance between the two monofilaments and the distance is displayed in the 0.96" inch OLED Display. The range of the TOF sensor varies from 5mm to 200mm. Both the TOF sensor and OLED display are connected in I2C configuration, which is connected to the Analog pin 4 and 5 respectively. The Distance data as well as the patient's feedback data collected and stored in the SD card using the SD card module for further processing and the

module is a four-wire module connected to atmega328 controller through SPI port. The Movable Monofilament is attached to the stepper motor, the A4988 Motor driver drives it, and the Atmega 328p microcontroller controls the driver. There are two signals STEP and DIRECTION is necessary to control the speed and rotational direction of the stepper motor. MS1, MS2, MS3 are the Micro stepping signal are pulled too low to operate the motor in desired configuration. The A4988 driver is powered by separate 9V battery for proper biasing for the stepper motor. It is controlled by the 10K ohm trim pot by the user to move the monofilament to get to the desired distance at resolution of 1mm. The Monofilament used in diabetic foot screening is used for this device. Its length is 90mm and around 35mm is fixed on one end and remaining 55mm where the bending occurs to test the foot. The Holder of size 6mm x 70mm is used for the enclosure of the monofilament and a rubber stopper is used on the end to arrest the oscillation of the monofilament during bucking. The Electronic Design are enclosed in the 3D printed casing is designed using Tinker CAD an online 3D designing platform. The dimension of the casing is 275 x 120mm portable for the handheld device the material used for 3D printing is ABS and layer height is 0.2mm. The Monofilament(S) is fixed on one end of the Device itself and sensor and display placement makes it easily by the user. The casing includes spacing for two-9V battery backup for the handheld and portable function minimize size. The Arduino Integrated Development Environment (IDE) is used to program Atmega controller via USB serial com port. At start initialize all the modules and then update the distance from the TOF-sensor using I2C protocol. The acquired distance is displayed in the OLED display using two-wire protocol. If the acquired distance is the desired distance, then stop the trim pot else rotate the pot until the desired distance is attained. The Operator get the feedback form the patients, the corresponding buttons are pressed, and the final distance and TPD data stored in SD Card for further processing. Since the OLED and Distance sensor are connected using the same I2C bus each device is distinguished by the controller by a unique 7bit I2C address.

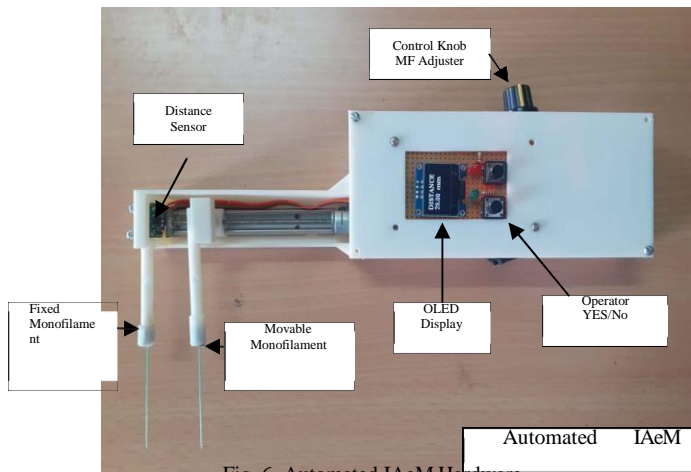


Fig. 6. Automated IAeM Hardware

The IAeM hardware is a dual 9V battery operated handheld device to measure Dynamic TPD in foot and hand areas. The minimum TPD value can be measured using this device is 10mm and the maximum value is 100mm with an accuracy in change of distance as minimum as 1mm. The TPD data measured automatically stored in SD card and the values are

displayed in OLED display. The device can be operated in the foot sole area by applying a constant force of 10gms using a two monofilaments (fixed and movable) and TPD data is measured and the process is repeated by varying the distance between the monofilament and TPD data is recorded for each iteration in different parts of the foot sole area.

B. Experimental Setup – Evaluation of the Automated IAeM Hardware

In order to test the force applied by the Automated IAeM device from reference [11] the Strain Gauge Cantilever Beam experiment is taken. We replicated the same to identify the force applied on both the filament are 10g and equal. The Experiment is as follows. The Steel Beam of length is 15cm is taken and the 120-ohm Strain gauge with Gauge Factor 2.1 is pasted on the top and bottom of beam as shown in the fig below



Fig. 7. Placement of strain gauge on the steel beam

The 120-ohm Strain gauge is pasted at 8cm from the fixed edge of the beam. The beam is mounted on the stand and the force is exerted on the other edge of the beam. The SG-1 and SG-2 are connected to the Wheat Stone Bridge in Halfbridge configuration. If No External force is applied, the bridge is balanced and the output of the bridge is zero.

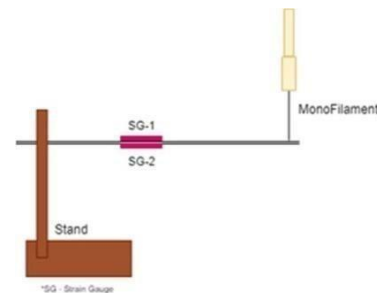


Fig. 8. Cantilever Beam with zero force

If an External force applied, i.e. Monofilament is pinched on one end of the beam the due to the stress applied on SG-1 & SG-2 the bridge is unbalance and the output of Wheatstone bridge is in the order of millivolts.

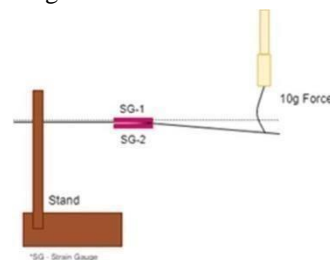


Fig. 9. Cantilever Beam with 10g force applied

The Output of Wheatstone Bridge is amplified using a Differential Amplifier using Opamp UA741. The voltage produced by the beam for standard loads also taken into account to calculate the force exerted by monofilament The NI My DAQ is used to analyze the output signal of the high gain amplifier and to log the data for post processing of the signal

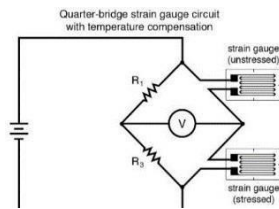


Fig. 10. Wheatstone bridge in Half bridge configuration

C. Amplifier Design

The output of Wheatstone bridge is in the order of millivolts it should be amplified using a two stage amplifier in that first is the Signal Conditioning stage to acquire the voltage from the Wheatstone bridge and the second stage is the Amplifier stage operating in non-inverting mode of gain 2200. There is an offset voltage in both the amplifier that needs to be eliminated using an offset null pin in the IC741.

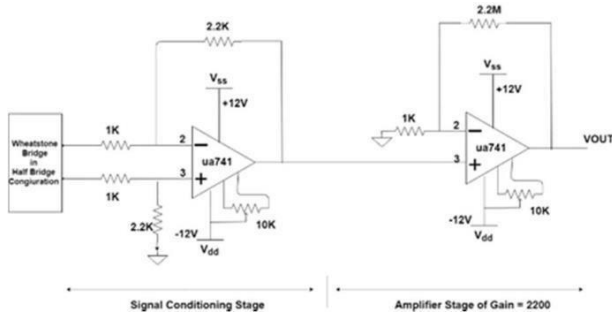


Fig 11. Amplifier Stage circuit diagram

The 10K trim pot is connected across pin 1 and 5 to reduce the offset produced by each stage. The output Vout on the final stage is in the order of volts for the 10gm minimum force applied the output voltage is 1.6Volts, which is recorded using My DAQ data acquisition for further processing.

D. Hardware Setup and Evaluation Outcomes

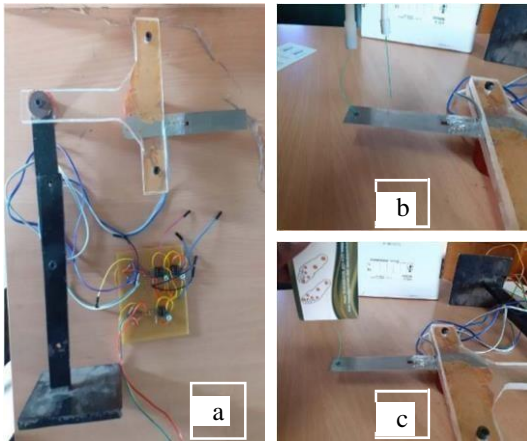


Fig 12. a) Complete Hardware setup, b) Handheld device Monofilament force acted on the beam, c) Standard SWM 10g monofilament acting on beam

The experiment is done as follows the first the standard weight of 100gms is placed on the beam to measure the voltage level so force will be 100gms x 9.8m/s gravity is nearly 10N then SWMF standard 10gm monofilament is applied on the beam and the voltage level is measured and finally IAeM hardware is applied on the beam where each monofilament is applied on the beam separately and the

corresponding voltages have been noted. From these voltage levels, the corresponding force is calculated and it is compared with standard 10gm SWMF for validation and the force acted upon using IAeM device is observed as 10gm force. The force exerted by both the filament are plotted using LabVIEW using My DAQ data acquisition module and they are both exerting 10gm force of equal values makes it eligible for clinical usage from these results we conclude that the force exerted by both the hands of the IAeM device are equal to that of the 10g monofilament thus validating the device for clinical use to measure TPD values. Using this device, we can perform two-point discrimination test on the diabetic foot subject to identify the sensation loss that leads to foot ulcer. Compared to the standard sensation-prescreening test like SWMF, Aesthesiometer and Biothesiometer this Device produces results accurately since elimination of manual errors

TABLE 1: VOLTAGE VALUES FOR CORRESPONDING FORCE APPLIED

S.No	Force Applied	Wheat stone Bridge Output in mv	Output after Amplification in Volts
1.	No Force	0	0
3.	10gm SWMF	0.35mv	1.6 volts
4.	IAeM device 10gm Movable Filament	0.35mv	1.6volt
5.	IAeM device 10gm Fixed Filament	0.35mv	1.6 volts

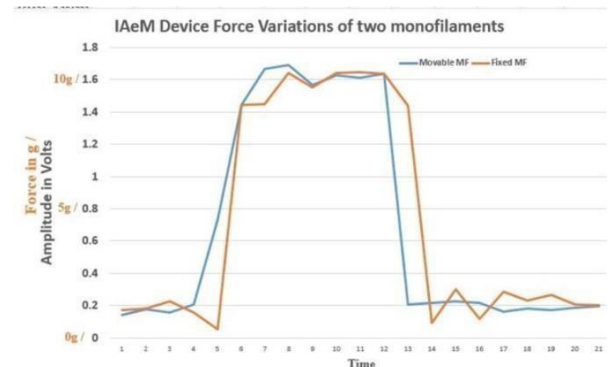


Fig 13. Comparison of Force variation of the Two Filaments in IAeM device

III. RESULTS

Eight healthy subjects of both gender from different age group were recruited and each subject undergone TPD (Two Point Discrimination) test in foot sole carried out in the heel & fore foot area. For testing out the device these two test area is taken from the 10 locations also the TPD values recorded from the first five normal subjects Heel area undergone repeatability test to validate the device for using n number of times. The sample are collected in the following manner. The diagnosis should be done in a calm and relaxed environment and the subject should not be able to see where the examiner places the filament. First, to make the subject knows what to expect apply the monofilament on the inner wrist. This also used to 'warm' the monofilament up. Apply enough force to cause the filament to buckle. The total duration of the

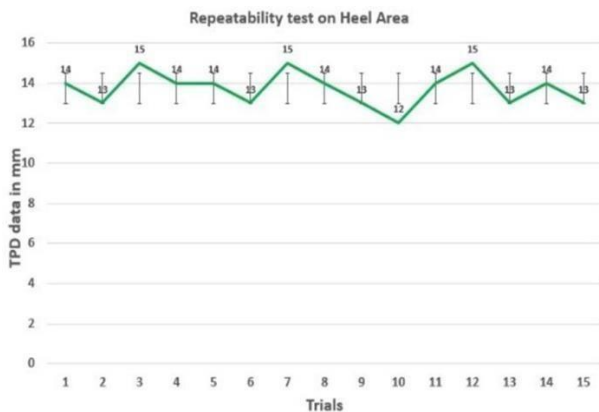
application, skin contact, and removal of the filament should be not more than 2 seconds and the patient have to give a feedback whether they feel single point or two point the test is repeated at different distances until the patient felt the single filament and the corresponding TPD data is noted. Randomize the progression of using the filament during the entire examination. The region can be recorded multipletime to ensure accurate results. The TPD data recorded with IAeM device in each subjects in the right heel consists of distance between the two monofilament and patient sensation feedback data stored in the SD card. To obtain stable results for repeatability, you must be able to execute the same method numerous times. Ideally, the same examiner conducts the same procedure using the same materials and measuring device under the same environmental conditions and does all the trials in a brief period. In order to test the repeatability of the device the TPD test recorded in heel area of one normal subject around 15 trials continuously within an interval of 5 secs. This time is taken since the monofilament need 2 to 3 secs to regain its posture after bucking.

Fig 14. Repeatability test on heel area

From fig (14) it show that the error bar is very less so variation of the device for n number of times is also less. To calculate repeatability, the Standard deviation mean of the data is calculated using the formula

$$\sigma = \sqrt{\frac{1}{N} \sum_{i=1}^N (x_i - \bar{x})^2}$$

(1)



Where μ is the mean of the TPD values and N is the number of trial which is 15 and σ is the Standard Deviation Mean (SDM) which is 0.78 and the value is less than 1 which indicates the variation is of the device for repeating n number is not more than 1mm thus validating the device for repeated usage. By performing the repeatability test, we can assure that the device is performing same for n number of trials increases the reliability of the device more and to analyze the TPD values of the same area for n number of times makes the TPD values more accurate as possible. The TPD data of the normal subject is analyzed by plotting the data collected in heel and forefoot area if it follows the law of mobility that “TPD improves with the mobility of the body part” thus the TPD value of forefoot should be lesser compared to Foot area.

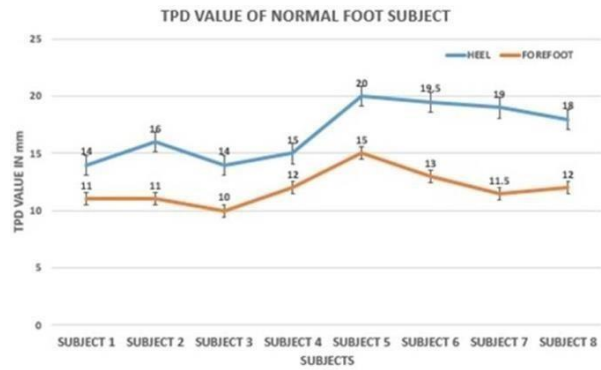


Fig. 15. TPD values of Normal Subject

TABLE 2: TPD DATA OF THE NORMAL SUBJECTS

S.NO	SUBJECT	HEEL (mm)	FORE FOOT (mm)
1	NORMAL	14	11
2		16	11
3		14	10
4		15	12
5		20	15
6		19.5	13
7		19	11.5
8		18	12

From table 2, it is observed that the TPD data in the heel area is greater than the forefoot thus; forefoot is more sensitivity than the heel area and follows the law of mobility. To test the device normal 8 subjects is recorded with aesthesiometer and handheld device in the heel area

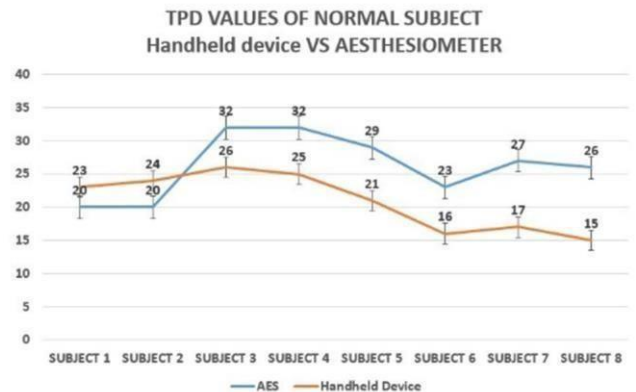


Fig 16. Proposed handheld device vs Aesthesiometer

From the fig (16) it is observed that the TPD data is higher and the variation is more in the aesthesiometer thus standard device has the disadvantage of variation in TPD value based on the operator hand while recording the data thus make the device invalid for clinical usage compared to that the handheld device deliver a constant force of 10g regardless of the operator hand motion make the device more valid for clinical usage.

IV. DISCUSSION

Cutaneous sensitivity methods are used to determine reduced sensory loss and to identify neuropathies and abnormalities of sensory function. The TPD test is frequently used to examine the upper extremities and airways cutaneous sense in considerable populations. Nylon monofilaments tests and the diapason test pitch have been used most often in the sensitivity evaluation of the lower extremities. Few studies have used the two-point discriminator for lower extremities,

particularly for the sole of the feet. Although majority studies on the reproducibility of the TPD test in upper extremities have yielded good results, there is some proof that the test may not be as stable in asymptomatic persons. Studies that used this method on the sole of the foot, despite recorded convincing results, did not state reproducibility data. The mechanical characteristics of the monofilaments depend on humidity, temperature and age. Different forces produced by single monofilaments leads to errors in fidelity and accuracy. The nylon polymer monofilaments have a contradictory chemical structure, is water absorbent, and are not suitable for use in humid environment if stability of the material is needed. Numerous application lowers the buckling forces of the monofilaments as plasticity of filaments is increased. Commercially available monofilaments have distinct variability within and between devices from different suppliers. Their physical bending force varies extensively from their designated buckling threshold value. How much variation in the forces is acceptable for the TPD is unknown? This will lead to the standardization of the TPD assessment procedure. This paper proposed a design of an automated Handheld Device to measure the Two-point discrimination data on the foot sole area. To deliver the constant force we used a 10g monofilament on both the prongs and evaluated the force exerted by the both prongs are equal thus make it suitable for measuring TPD test and the results of force compared with that of the standard monofilament thereby improving the TPD measurement accuracies. After evaluation, the device is validated using a repeatability test that is the TPD data is recorded in the heel area for n number of times to ensure accuracy and the repeatability test value is 0.88 which is less than 1mm make it valid for clinical usage compared to aesthesiometer where the variation is much higher. The TPD test is a distinct tool for clinical assessments, although previous research studies have not considered the test as reliable as nylon monofilaments. Another advantage of the handheld device is that all the TPD data are measured using TOF (Time of Flight) Distance sensor and it is stored in SD card thus eliminating the human error while reading the TPD data from the device. The Patients feedback is also recorded using a yes or no button and it linked with corresponding TPD data make it easier for post processing. Although the proposed handheld instrument could be used to avoid variations, unless a standard protocol is developed for measuring the Two Point Discrimination (TPD), the variation cannot be contained even with this instrument. The only short come is that the minimum distance it can measure is only 10mm so for measuring toes and fingers it need to be redesigned to measure distance with accuracy of 1mm which is necessary for recording TPD data in hand and other sensitive areas Still, the Two Point Discrimination (TPD) test on the sole of the feet was expected to have good intra-observer reproducibility for the examination of functioning normal subjects and diabetic subjects. Studies that assess the

stability of the Two Point Discrimination (TPD) test to analyze the peripheral neuropathy thus numerous subjects with peripheral neuropathy are still required. Furthermore, inter-observer reproducibility testing of the TPD test are also required.

ACKNOWLEDGMENT

The study is funded by Department of Science and Technology, Government of India; Sanction Reference Number: SP/Y0/393/2018©, Dt: 28/09/2018. Department of Instrumentation and Control Engineering, NIT-Trichy have provided the laboratory facilities.

REFERENCES

- [1] Abbott CA, Carrington AL, Ashe H, et al. The North-West Diabetes Foot Care Study: Incidence of and risk factors for, new diabetic foot ulceration in a community-based patient cohort. *Diabet Med.* 2002;19(5):377-384.
- [2] American Diabetes Association. Foot care in patients with diabetes mellitus. *Diabetes Care.* 1998;21(suppl 1):S54-S55.
- [3] Birke JA, Sims DS. Plantar sensory threshold in the ulcerated foot. *Lepr Rev.* 1986;57(3):261-267.
- [4] Boulton AJ. Guidelines for diagnosis and outpatient management of diabetic peripheral neuropathy. *Diabetes Metab.* 1998;24:S55-65.
- [5] Coppini DV, Young PJ, Weng C, Macleod AF, Sönksen PH. Outcome on diabetic foot complications in relation to clinical examination and quantitative sensory testing: a case-control study. *Diabet Med.* 1998;15(9):765-771.
- [6] Dellon AL. Treatment of symptomatic diabetic neuropathy by surgical decompression of multiple peripheral nerves. *Plast Reconstr Surg.* 1992;89(4):689-697.
- [7] Guyton GP, Saltzman CL. The diabetic foot: Basic mechanisms of disease. *Instr Course Lect.* 2002;51:169-181.
- [8] Kamei N, Yamane K, Nakanishi S, et al. Effectiveness of Semmes-Weinstein monofilament examination for diabetic peripheral neuropathy screening. *J Diabetes Complications.* 2005;19(1):47-53.
- [9] Lipsky BA, Berendt AR, Embil J, De Lalla F. Diagnosing and treating diabetic foot infections. *Diabetes Metab Res Rev.* 2004;20:S56-64.
- [10] Mueller MJ. Identifying patients with diabetes mellitus who are at risk for lower-extremity complications: use of Semmes-Weinstein monofilaments. *Phys Ther.* 1996;76(1):68-71.
- [11] Manivannan M, Periyasamy R, Suresh Devashayam., Handheld Isobaric Aesthesiometer for measuring Two-point Discrimination. International Conference on Research into Design IISc, Bangalore., Jan 2015
- [12] Pham J, Armstrong DG, Harvey C, Harkless LB, Giurini JM, Veves A. Screening techniques to identify people at high risk for diabetic foot ulceration: a prospective multicenter trial. *Diabetes Care.* 2000;23(5):606-611
- [13] Smith KD, Emerzian GJ, Petrov O. A comparison of calibrated and non-calibrated 5.07 nylon monofilaments. *Foot Ankle Int.* 2000;21(10):852-855.
- [14] Weisberg LA, Garcia C, Strub R. Sensory disorders. In: Weisberg LA, ed. *Essentials of Clinical Neurology.* 3rd ed. Amsterdam: Elsevier Health Sciences, 1996.
- [15] Yong R, Karas TJ, Smith KD, Petrov O. The durability of the Semmes-Weinstein 5.07 monofilament. *J Foot Ankle Surg.* 2000;39(1):34-38.

Development of a non-invasive non-contact optical device for estimating TcB in Neonates

K.Vignesh Kumar

Senior Research Fellow, Department of ICE
National Institute of Technology
Trichy, India
vigneshkumar13579@gmail.com

Dr.R.Periyasamy

Assistant Professor, Department of ICE
National Institute of Technology
Trichy, India
periyasamy@nitt.edu

Abstract— Neonates tend to get affected with jaundice due to accumulation of unsaturated bilirubin in their body within few days of birth and needs special care to save them from kernicterus and death. The current method of diagnosis uses Total Serum Bilirubin (TSB) value as a gold standard to estimate concentration of bilirubin. TSB is obtained through an invasive and painful blood sampling technique. As an alternative Transcutaneous Bilirubin (TcB) is used clinically to estimate the concentration of bilirubin, where a probe is placed on the forehead of neonate and illuminated with a light source. The study reported in this paper explores the possibility of using 460nm Lights rays in a non-invasive and non-contact mode to estimate the concentration of bilirubin in neonates. A portable device with 460nm light source and photodiode has been developed to measure the skin reflectance in neonates and a correlation study has been conducted between the skin absorbance and TcB measured using NeoBil on 8 neonates (Day of Life < 4 days). The study results reported an acceptable correlation between TcB and Skin Absorbance of 460nm light with a correlation coefficient of 0.93. The result provides a valuable ground work for development of a non-invasive non-contact optical device for measuring the transcutaneous bilirubin in neonates.

Keywords— *Bilirubin, Jaundice, Hyperbilirubinemia, Neonates, Non-Invasive Technology.*

I. INTRODUCTION

Neonatal jaundice occurs in about 60% of term and 80% of pre-term neonates within few hours of birth due to increased level of bilirubin concentration evident from the yellowish discoloration of the skin [1]. This physiological disorder leads to serious brain damage and even result in death if untreated and hence there is a vital need to have an early diagnosis. Physicians practice the visual inspection of the skin or sclera to diagnose the presence of neonatal jaundice and prescribe for blood sampling to estimate the TSB, as it remains to be the gold standard of measuring the bilirubin concentration. Though this test is practiced world-wide as the standard for measuring the bilirubin value, it has limitations of inducing pain and discomfort to neonates. Further this test is a time consuming process and needs to be conducted by a trained clinical professional. In neonates with higher level of bilirubin concentration, the blood sampling needs to be done frequently to keep track of the level of jaundice. Transcutaneous bilirubin (TcB) has been found to address these issues from the study

conducted by Moattar Raza Rizvi et al , 2019 [1] where TSB values estimated through blood sampling and TcB Values estimated using Bilicheck on 100 neonates with mean gestational age 39 had a high correlation ($r^2=0.88$). Earlier the research work by Afsaneh Sadeghian et al, 2017 on 280 neonates with in the age group of 11-15 days reported a high accuracy of BiliCheck (TcB) in estimating the level of bilirubin concentration non-invasively[2]. Similarly the study conducted by Andra Kurnianto et al, 2017 comparing the bilirubin concentration estimated through blood sampling (TSB) and TcB (Using BiliCheck) reported a high correlation ($r =0.897$) for TSB and TcB measurements on the forehead [3]. The results obtained were identical to the comparative study conducted between TcB estimated using JM-105 (TcB) and TSB estimated from blood sampling on 150 Asian origin infants with age below 28 days [4]. The results obtained from the previous research works provide a concrete support for the use of non-invasive techniques in estimation of bilirubin concentration as viable method to predict the severity of jaundice. However, neonatal care needs more sophistication with diagnostic techniques having minimal surface interaction as they are very sensitive to touch and prone to skin infections. Hence this study explores the possibility of developing a non-invasive and non-contact device to measure the level of bilirubin in neonates using skin reflectance technique. Yunus Karamavus et al 2019, had developed a prototype using the Visible light spectrum between 400nm-700nm and conducted a study on 314 babies to estimate bilirubin concentration. The results were compared with the bilirubin concentration estimated using Drager JM-103 and TSB and they reported that the three devices were able to predict the jaundice level with a correlation value between 0.93-0.94 [5]. They had also reported a high absorption of bilirubin in the range of 420nm-480nm. Animesh Halder et al 2019, developed a spectroscopy based model to calculate the bilirubin concentration in neonates using wavelength range from 452 nm to 500 nm. The device was tested on 1028 neonates (500 for calibrating and 528 for validating the developed prototype) and results were compared with the TSB values obtained from the standard biochemical tests reporting a high correlation coefficient ($r = 0.95$) [6]. A literature review on various methods of identifying jaundice in neonates published by Fahmi Akmal et al 2018, reports light absorbance and reflectance as one of the techniques with supporting research works conducted using light source between 425nm to 575nm and obtaining TcB results with high correlation ($r=0.89$) to TSB [7]. The research work by Akash

The study is funded by Department of Science and Technology, Government of India; Sanction Reference Number: IDP/MED/29/2016, Dt: 17/10/2017.

Chandra et al 2017, had developed a device using 460nm light source to estimate the bilirubin concentration, which when tested using mock bilirubin samples and reported a correlation of 0.99 with relative error less than 0.9% [8].

The literatures discussed so far provides a valuable support for developing a non-invasive and non-contact device using 460nm light source for estimating the bilirubin concentration in neonates. This study reports the design, development and validation of a portable device for measuring the concentration of bilirubin using skin reflectance technique and assessing the severity of jaundice in neonates.

II. HARDWARE DESIGN

A battery operated device for measuring bilirubin concentration using skin reflectance technique has been designed and developed at NIT-Trichy Bio photonics Laboratory. The device design contains a light source that will be used to illuminate the neonatal skin, a detector with high responsivity at the peak absorption wavelength, a control and processing unit to drive the Light source, log the reflected light intensity and calculate the concentration of bilirubin based on skin reflectance using Beer lambert law (Fig2.1).

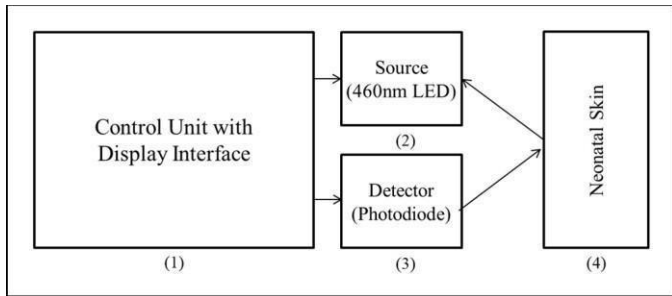


FIGURE 2.1 BLOCK DIAGRAM OF PROPOSED NON INVASIVE & NON CONTACT SYSTEM FOR ASSESSING THE SEVERITY OF JAUNDICE IN NEONATES.

A probe head has been fabricated with 460nm LED light source which has peak absorption in bilirubin [9] and BPW21R Photodiode as the detector that has high responsivity at 460nm light (Fig 2.2). The developed device measures the intensity of light in terms of voltage.

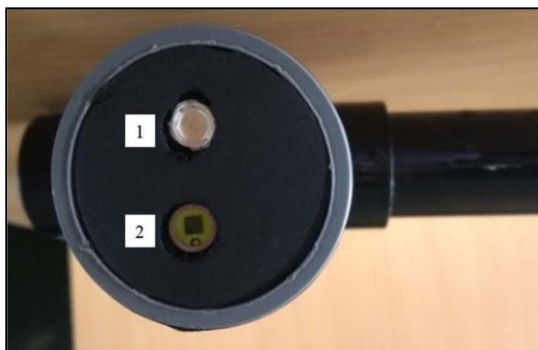


FIGURE 2.2 PROBE HEAD; (1) 460NM LED LIGHT SOURCE (2) BPW21R PHOTODIODE DETECTOR

The probe head was fixed in a portable supporting structure with height adjustable beam (Fig 2.3). The supporting structure can be placed in the neonatal warmer or neonatal bed without disturbing the position of the neonate. The height adjustable beam and the locking knob help placing the detector firmly at a specific distance (5 mm) above the study location on the body of the neonate without touching the skin[10].

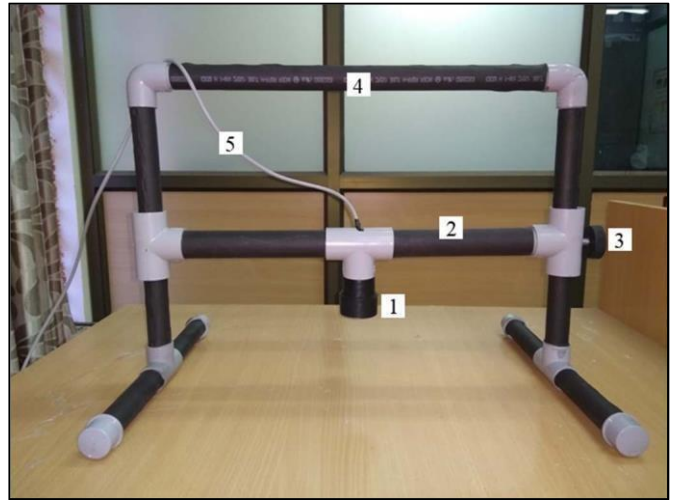


FIGURE 2.3 PORBE SETUP – (1) PROBE HEAD; (2) HEIGHT ADJUSTABLE BEAM; (3) LOCKING KNOB; (4) SUPPORTING FRAME; (5) CONNECTION TO CONTROL UNIT

The probe is connected to the control that has been developed using Arduino UNO embedded development board (Fig 2.4). The control unit has been programmed to drive the light and simultaneously capture the reflected light intensity in order to calculate the bilirubin concentration. A trigger button has been provided to illuminate the light source. The illumination time has been fixed for a period of 2 seconds to avoid prolonged exposure of neonates to monochromatic light source.



FIGURE 2.4 – (1) CONTROL UNIT; (2) LCD DISPLAY; (3) TRIGGER SWITCH; (4) POWER SWITCH

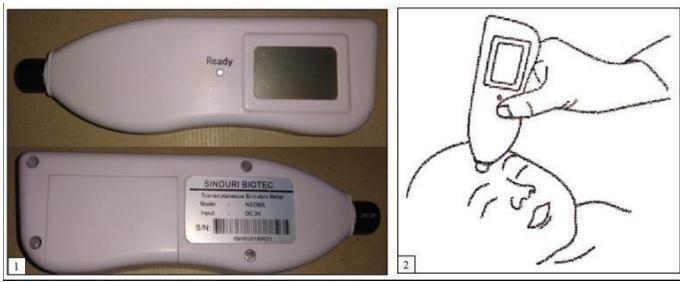


FIGURE 3.1 (1) NEOBIL- TcB MONITOR (2) POSITIONING OF PROBE ON FOREHEAD OF NEONATE

The intensity of transmitted (I_{in}) and received light (I_{out}) was applied in Beer Lambertz law (Equation 1) to quantify the absorbance or optical density(OD) of the neonatal skin and calculate the concentration of bilirubin.

$$OD = -\log\left(\frac{I_{out}}{I_{in}}\right) \dots\dots\dots (1)$$

The device was designed to operate with low power LED light source using DC voltage and the structures were fabricated with light-weight materials thereby eliminating the risk of electrical or physical injury to the neonates during examination.

III. METHODOLOGY

The developed non-invasive and non-contact device was experimented on neonates who were suspected to be affected with jaundice. The study was conducted to measure the skin reflectance of 460nm light source when illuminated on skin surface of neonates suffering from jaundice and formulate an equation for calculating bilirubin concentration. In order to validate the device TcB values from Neobil (existing technology used clinically for TcB measurement) was used as a reference (Fig 3.1 (1)). Three trials were conducted using Neobil on the forehead of the neonate (Fig 3.1 (2)) and the mean bilirubin concentration was considered for the comparison.

Similarly three trials were conducted on the upper trunk of the neonate using the developed device to log the intensity of the light reflected from the neonatal skin (Fig 3.2). The absorbance of 460nm light rays will be high on the skin of the neonates suffering from jaundice and hence the optical density will be high during this physiological change in their body. This phenomenon is discussed in Section IV. A study on relation

TABLE I: TcB VALUES FROM NEOBIL

Subject	TcB- NeoBil (mg/dL)
1	10.4
2	10.6
3	13.1
4	13.4
5	13.5
6	13.6
7	15.4
8	15.6



FIGURE 3.2 POSITIONING OF DEVELOPED PROBE OVER THE STUDY LOCATION OF THE SUBJECT NEONATE

between the optical density of the neonatal skin and bilirubin concentration measured using the Neobil was conducted to formulate a transfer function using linear regression modelling. This transfer function was applied to the optical density calculated by the developed device to calculate the bilirubin concentration. The aim of the study was to achieve a correlation coefficient greater 0.9, which has been reported as the acceptable range in research works discussed in Section I.

IV. RESULT AND DISCUSSION

The study was conducted on 8 neonates who were suspected to have jaundice based on visual diagnosis as per the protocol explained in Section III. The neonates considered for the study were less than 4 days of age and did not have any other physiological abnormalities. The study was conducted in an isolated room with dim lighting to avoid interference. Table I represents the bilirubin concentration measured using Neobil TcB and Table II represents the bilirubin concentration estimated by the developed device.

Figure 4.1 represents the drop in voltage due to absorption of transmitted light with respect to the concentration of bilirubin and Figure 4.2 represents the rise of Optical density with respect to increase in the concentration of bilirubin. The results achieved are synchronous to the results reported by Akash Chandra et al 2017 in their study conducted using mock bilirubin samples. A correlation coefficient of 0.93 was achieved between the TcB measured using Neobil and optical density estimated by the developed device represented, thereby

TABLE II : TcB VALUES FROM THE DEVELOPED DEVICE

Subject	Input Light Intensity (Volts)	Output Light Intensity (Volts)	Optical Density of Neonatal Skin	TcB Developed Device (mg/dL)
1	4.850	1.860	0.42	10.8
2	4.850	1.815	0.43	11.0
3	4.850	1.580	0.49	12.4
4	4.850	1.520	0.50	12.8
5	4.850	1.465	0.52	13.2
6	4.850	1.425	0.53	13.4
7	4.850	1.118	0.64	15.9
8	4.850	1.098	0.65	16.1

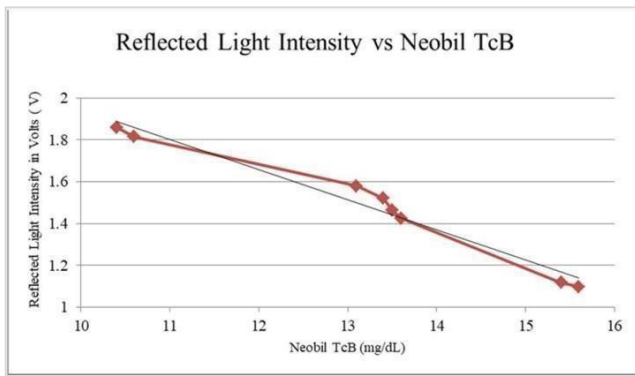


FIGURE 4.1 COMPARISON OF SKIN REFLECTANCE VS TCB ESTIMATED BY NEOBIL

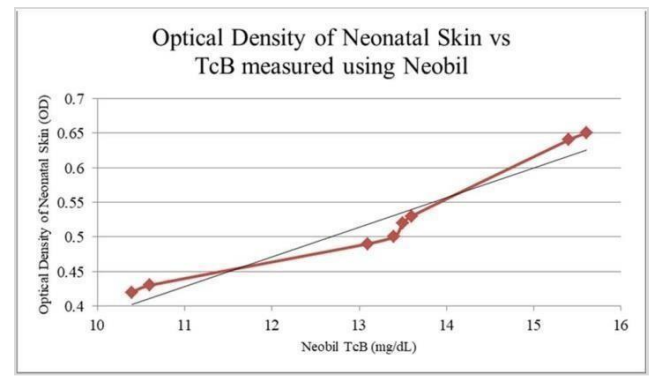


FIGURE 4.2 COMPARISON OF OPTICAL DENSITY VS TCB ESTIMATED BY NEOBIL

resulting a linear regression equation $Y = 0.043X - 0.0433$ where Y is the optical density and X is the concentration of the bilirubin.

By using this regression equation, the results obtained from the developed prototype had a good correlation with the TcB values estimated by Neobil. An absolute error of -0.7 to + 0.5 mg/dL was observed when comparing the results obtained by both the devices; however an error of 1 mg/dL is clinically accepted. The developed device was able to estimate the bilirubin concentration with an accuracy of ± 0.7 mg/dL and a sensitivity of 0.1 mg/dL (Table III).

The results achieved from the current study proves a proportional absorption of transmitted light intensity with respect to bilirubin concentration and supports the concept of identifying neonatal jaundice using light interaction with skin discussed in the literature survey published by Fahmi Akmal et al 2018. Similar results of correlation were obtained in the research work conducted by Yunus Karamavus et al 2019, but they have used multi spectral wavelengths to quantify the concentration of bilirubin whereas we have used a signal wavelength method of estimating bilirubin concentration. The spectroscopy model developed by Animesh Halder et al 2019 has comparatively reported a higher correlation to the device

TABLE III : COMPARISON OF TCB VALUES ESTIMATED BY NEOBIL AND DEVELOPED DEVICE

Subject	Measurements from NeoBil		Measurements from Developed Device		
	TcB- NeoBil (mg/dL)	Neobil (mg/dL)	Values Obtained in Developed Device (mg/dL)	Absolute Error (mg/dL)	Relative error
1	10.4	10.4	10.8	0.4	0.03
2	10.6	10.6	11.0	0.4	0.04
3	13.1	13.1	12.4	-0.7	-0.05
4	13.4	13.4	12.8	-0.6	-0.05
5	13.5	13.5	13.2	-0.3	-0.02
6	13.6	13.6	13.4	-0.2	-0.01
7	15.4	15.4	15.9	0.5	0.03
8	15.6	15.6	16.1	0.5	0.03

used in this study but conducting examination in the region of study (nail plate) suggested has many practical difficulties and may cause inconvenience to the patient as well the clinical professionals whereas the region of study chosen for our study (upper trunk) proves to be very convenient location for examination. However their study has been conducted in 1028 neonates and our study has to be conducted on more number of subjects to prove the dominance of the developed device.

V. LIMITATIONS

Though this system was experimented on 8 neonates suspected to have been affected with jaundice, more number of neonates have been examined in the same method to achieve better accuracy in estimating the concentration of bilirubin.

VI. CONCLUSION AND FUTURE WORK

The clinical testing of the developed prototype proves the viability of the device to be used in hospitals for examination of neonates. The device will be further developed using fiber optic model to reduce the size of the probe head so that the examination can be conducted in all the five jaundice identification zones prescribed in Kramer's rule.

ACKNOWLEDGMENT

We would like to express our sincere appreciation for the guidance of Dr. R. Mahalakshmi M.B.B.S., D.G.O., Jeyam Nursing Home, Trichy and the clinical professionals for their valuable assistance in sample collection from neonates in their hospital. The study is funded by Department of Science and Technology, Government of India; Sanction Reference Number: IDP/MED/29/2016, Dt: 17/10/2017. The laboratory facilities have been provided by Department of Instrumentation and Control Engineering, NIT-Trichy.

REFERENCES

- [1] Moattar Raza Rizvi, Farah Mansoor Alaskar, Raid Saleem Albaradie, Noor Fatima Rizvi and Khaled Al-Abdulwahab, "A Novel Non-invasive Technique of Measuring Bilirubin Levels Using BiliCapture," Oman Medical Journal, vol 34 No. 1, pp 26-33, January 2019.
- [2] Afsaneh Sadeghian, Ghazale Neymati, Pouneh Zolfaghari, Elahe Yahyaei, Mehrisadat Mirghasemi and Mohammad Bagher Sohrabi, "Validation of Transcutaneous Bilirubin in Comparison with Serum Bilirubin for the Detection of Hyperbilirubinemia in Neonates," International Journal of Health Studies, vol 3(3), pp 29- 32, March 2017.

- [3] Andra Kurnianto, Herman Bermawi, Afifa Ramadanti and Erial Bahar, "Transcutaneous bilirubinometry to estimate total serum bilirubin in neonatal jaundice," *Paediatrica Indonesiana*, vol 57 No.1, pp 8 -11, January 2017.
- [4] Andra Kurnianto, Herman Bermawi, Erial Bahar, Afifa Ramadanti and Indrayadi, "The correlation study of transcutaneous bilirubin measurements in neonates," *European Journal of Biotechnology and Bioscience*, vol 4, issue 11, pp34-37, November 2016.
- [5] Yunus Karamavus and Mehmed Özkan, "Newborn jaundice determination by reflectance spectroscopy using multiple polynomial regression, neural network, and support vector regression," *Biomedical Signal Processing and Control*, vol 51, pp 253-263, March 2019.
- [6] Animesh Halder, Mukut Banerjee, Soumendra Singh, Aniruddha Adhikari, Probir Kumar Sarkar, Arnab Madhab Bhattacharya, Prantar Mallick, and Samir Kumar Pal, "A Novel Whole Spectrum-based Non-invasive Screening Device for Neonatal Hyperbilirubinemia," *IEEE Journal of Biomedical and Health Informatics*, vol 23 issue 6, pp 2347 – 2353, November 2019.
- [7] Fahmi Akmal Dzulkifli, Mohd Yusoff Mashor and Karniza Khalid, "Methods for Determining Bilirubin Level in Neonatal Jaundice Screening and Monitoring: A Literature Review," *Journal of Engineering Research and Education*, vol 10, pp 1-10, December 2018.
- [8] Akash Chandra, N.P. Guhan Seshadri and R. Periyasamy, "Skin reflectometry technique for measurement of bilirubin concentration to detect jaundice", *Proc. 2017 International Conference on Biomedical Engineering and Bioinformatics*, September 2017, pp. 22–26, doi. 10.1145/3143344.3143352
- [9] Vignesh Kumar Kanamail and Dr. R.Periyasamy, "A Study on Development of a Non Invasive Optical based Instrument to estimate the Bilirubin Concentration in the Blood Serum", *2019 TEQIP III Sponsored International Conference on Microwave Integrated Circuits, Photonics and Wireless Networks*, May 2019, pp.72-76, doi. 10.1109/IMICPW.2019.8933183
- [10] N. Ali, S. Z. M. Muji, A. Joret, R. Amirulah, N. Podari and N. F. Dol Risep, "Optical technique for jaundice detection", *ARNP Journal of Engineering and Applied Sciences*, vol 10, pp 9929- 9933, November, 2015

Intelligent Wearable Device For Early Detection Of Myocardial Infarction Using IOT

V.Kaviya

Dept. Biomedical Engineering
St.Peter's Institute of Higher Education and Research
Chennai , India
vk111961@gmail.com

G.R.Suresh

Dept. Biomedical Engineering
St.Peter's Institute of Higher Education and Research
Chennai , India
sureshgr@rediffmail.com

Abstract:-Heart attacks take the maximum toll of human life all over the world. Heart disease is reportedly killing approximately 17 million people in the world, and a similar scene is seen in india , where 3 million people die because of CVDs (cardio-vascular diseases), which include heart attack and stroke. Patients suffering from heart diseases need a earlier detection system to have a urgent treatment before it's too late. More over some existing methodology helps in detecting heart attack only if the patient is under doctor or expert observation and hence it is not possible for all the cases. To overcome the above disadvantage we have developed a system which will help to provide earlier detection of myocardial infarction, which avoid overdue of medical treatment . The proposed system is combined with a data collection and computational algorithm which can collect the multiple data continuously, according to the health risk conscious in each patient. In case of heart attack the system sends alert to person device and doctor or medical assistance through GSM. So, that medical assistant can reach the patient with the help of GPS location and provide early medical treatment.

Keywords - Heart Attack , myocardial infarction ,Data Collection, IoT , Algorithm Sensors, Monitoring, Diagnosis.

I. INTRODUCTION

The heart attack is one of the most common and serious disease, which can lead to death if not treated early. There are many devices available in hospitals which helps in detecting heart attack, but this can be only possible when the patient is under physician observation. Hence, all the time it is not possible.

But now a days technology as been covered a long way to make human life easier. Specially in medical field technology as reached high level through which collection and transferring of data from patient to hospital can be possible from any place. In the sense it is not necessary to a person to be always under medical assistant observation.

Previously some of the works has been performed based on different communication network technology in monitoring cardiac condition by collecting certain parameter[2][5].

The objective is to develop a reliable and convenient system that can monitor an essential parameter and send through wireless automation [1] . Now a days everyone is using mobile phones. Recent mobiles are available with good processor and enough memory space. This benefit of advance technology can be used for transmitting sensed parameter through IoT (Internet of Things) [3][4].

This paper proposes a continuously monitor vital parameter and detect the occurrence of heart attack and reduce the response time and allow the person to know that he or she is about to get a heart attack and send the data to medical assistant so, that they can take preventive measures and give medical care within a censorious stage , thus extremely upgrade the possibility of survival .

II. PROPOSED SYSTEM

The stable monitoring system involve three phase of working , which includes

- Sensor or Data collecting module,
- computational module,
- communication module.

In this three phase, data collecting module includes sensors which senses and collects data and sends to computational module, this module undergo some computational process to detect occurrence of heart attack .The communication transfer the data to medical assistant .

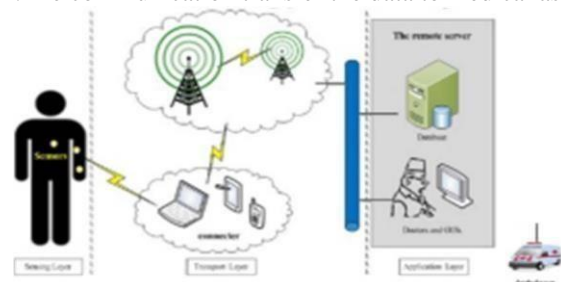


Fig. 1: System Architecture of the Proposed System

A. Sensor or data collecting Module

The data collecting module involve connections of multiple sensors. The sensors being

- Temperature sensor
- Heart rate sensor
- Pressure sensor
- Cardiac pcode sensor

This sensors will be in attached with the person to processor. These sensor act as an tool to detect specific biological or physiological process and transmit data.

1) Temperature Sensor

LM35 sensor is an temperature integrated analog sensor which does not require external calibration to provide typical accuracies .

2) Heart rate sensor

The Heart rate Sensor measures heart rate in beats per minute using LED light source, this LED light passes through the skin and measures the reflected light . It works on the principle of light modulation by blood

flow through finger at each pulses .

3) Pressure sensor

The pressure sensor comprise piezo-resistive sensor it compute the fluctuation in blood pressure waveform from the body which is corresponding to arterial pressure waveform.

4) Cardiac poded

Cardiac biomarker are substance released into blood when the heart is damaged or stressed , it is measured to evaluate the heart function .The release of cardiac biomarker can indicate the occurrence myocardial infarction.. There are several tests available to detect cardiac enzyme, one of the test is ECG.

Thus , cardiac poded is an solitary ECG electrode helps in measuring the modulation in ECG wave.

B. Computational Module

The Computation module involves Pi3 processor in which buzzer, GSM (RS232) interface module and GPS are connected . This module play a vital role in providing accurate information about occurrence of myocardial infarction .So ,that in case of emergency the data and location of person can be send for medical assistance.

1) Raspberry pi3: The Raspberry Pi works like an computer. It enable the software program to run. Her the software will be installed which consist of different algorithm that helps in detecting the occurrence of heart attack accurately.

C. Communication Module

The communication module consists of following sub-modules. They are: doctor system and patient mobile. The main concern of the communication is patient data and sensor data.

- Patient sensor data
- Date and time
- Location etc.

This system allow authoritative user to communicate i.e., user information should match the particular in database. This module sends the alert to person mobile in case of heart attack and sends a alert and location of the person to doctor.so, that the medical assistant can give early treatment to save life. This transmitting of information is performed with the help of GSM and GPS.

- 1) **GSM** (Global System for Mobile):-A GSM is an modem which comprise sim and manipulates in data transmitting service. Here it helps in transfers measured parameter and person condition to person mobile and doctor.
- 2) **GPS** (The Global Positioning System):- They are found in most smartphones ,and they are used to track commerce all over the globe. Here it helps to detect the location of person in emergency.

III. WORKING ALGORITHM

The algorithm plays an imperative role in accomplishing accurate output for collected input. Algorithm assist in computing occurrence of heart attack in advance by undergoing arithmetical computation with respect to given input.

The principle algorithm used in this system is machine learning algorithm under this multiple process are involve where sub-algorithm were used.

Machine learning is an implementation of artificial intelligence (AI) that furnish system the ability to learn automatically and enhance from experience.

Machine learning involves following process

- Preprocessing of dataset
- Feature selection
- Machine learning classifiers
- Cross-validation method
- Classifiers performance evaluation method.

A. Preprocessing of dataset

The preprocessing of data base essential part in machine learning where the data of heart attack are collected from kaggle database and preprocessed. Through which training and test of machine is done.

Machine learning –heart attack dataset which is preprocessed involves following :-

- Number of records :300
- Number features used :14 (list of feature used is mention in Table I.)

TABLE I. LIST OF FEATURE USED

Feature used		
S.no	Feature used	Description
1.	Age	(age in years)
2.	Gender	(1=male ; 0= female)
3.	cp	chest pain type
4.	restbps	resting blood pressure (in mm Hg on admission to the hospital)
5.	chol	serum cholesterol in mg/dl)
6.	fbs	fasting blood sugar > 120mg/dl)(1= true ; 0= false)
7.	restecg	resting electrocardiographic results
8.	thalach	maximum heart rate achieved
9.	exang	exercise induced angina (1=yes ; 0= no)
10.	oldpeak	ST depression induced exercise relative rest
11.	slope	the slope of the peak exercise ST segment
12.	ca	number of major vessel(0-3) coloured by fluoroscopy
13.	thal	3= normal; 6=fixd defect; 7= reversible defect
14.	target	1=0

B. Feature selection

Feature selection is an second important part in machine learning. It is used in order to avoid irrelevant or redundant data that helps in acquire error less output.

Under feature selection three sub- algorithm is used

- 1) Relief Feature Selection Algorithm
- 2) Minimal-Redundancy-Maximal Relevance Feature Selection Algorithm
- 3) Least Absolute Shrinkage and Selection Operator
 - Relief feature selection is used to extract feature from given input from the dataset .
 - Minimal-Redundancy-Maximal Relevance Feature Selection Algorithm eliminates the redundancy and gives relevant data.
 - Least absolute shrinkage and selection operator select features are based on updating new the absolute value of features coefficient.

C. Machine learning classifiers

In order to classify the condition of person (normal or abnormal), machine learning classification algorithms are used.

Here, three algorithm are used

- 1) Support Vector Machine
- 2) Naive Bayes
- 3) Decision Tree Classifier

K-Nearest Neighbor (it is used only when different data are collected)

SVM is a supervised machine learning algorithm which can be used for classification or regression problems. It uses a technique called the kernel trick to transform your data and then based on these transformations it finds an optimal boundary between the feasible outputs.

Naive Bayes comes under the class of generative models for classification. It models the posterior probability from the class conditional densities. So the output is a probability of belonging to a class.

In general, decision trees are constructed via an algorithmic approach that recognize ways to split a data set based on different conditions. The goal is to create a model that predicts the value of a target variable based on several input variables.

The K-nn algorithm uses 'feature similarity' to forecast the values of any new data points. In the sense that the new point is assigned a value based on how closely it resembles the points in the trainingset.

D. Cross-validation method

The k-fold cross-validation (CV) method is used to evaluate how accurate the system is predicting during performance .This technique involves randomly dividing the dataset into K-groups or folds of approximately equal size. The first fold is kept for testing and the model is trained on K-1.

E. Classifiers performance evaluation method

In classifier performance evaluation method , confusion matrix is used ,which checks whether the predicted value by the system is correct or not ,which is given in Table II.

Overall Classification accuracy can be given by:-

$$\text{Classification accuracy} = \frac{TP+TN}{TP+TN+FP+FN} \times 100 \quad (1)$$

Overall Classification error can be given by:-

$$\text{Classification error} = \frac{FP+FN}{TP+TN+FP+FN} \times 100 \quad (2)$$

TABLE II . EVALUATION IN CONFUSION MATRIX

Confusion matrix			
Predicted value	Actual value	Result	Description
Positive (1) ^a	Positive (1)	True positive (TP)	The system has predicted the person do have heart attack ,which is correct and the person have heartattack.
Negative (0) ^b	Negative (0)	True negative (TN)	The system has predicted the person is healthy , which is correct and the person is healthy.
Negative (0)	Positive (1)	False positive (FP) (type error 1)	The system has predicted that theperson is healthy which is incorrect but the person do have heartattack
Positive (1)	Negative (0)	False negative (FN) (type error 2)	The system has predicted that theperson do have heart attack which is incorrect but the person is healthy.

^a For all Positive (1) indicate Heart attack

^b For all Negative (0) indicate Healthy

I. RESULTS AND ANALYSIS

After setting up the system, check all the connections. Once the system is ready, start the programme. Person as to place the index finger on the sensor. The sensor starts sensing the parameter, this can be monitored in screen .the condition of the person whether healthy or having chance of having heart attack can be seen in web page. This web page will be in contact with hospital assistance.

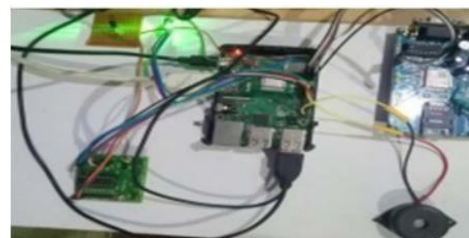


Fig.2: connection of sensor and modules

The system is checked by giving heart attack data, Once the system detects the symptoms of heart attack it gives alert message to persons mobile. The system has configured maximum range of data. Once the system starts measuring the data, it automatically stores the data in database, which helps doctor in knowing previous data so that further treatment can be take.. The readings will be refreshed consistently giving the extension for constant seeing of the patient.

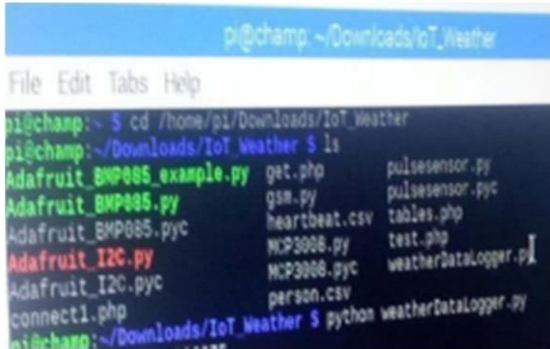


Fig 3: Collecting data from sensor

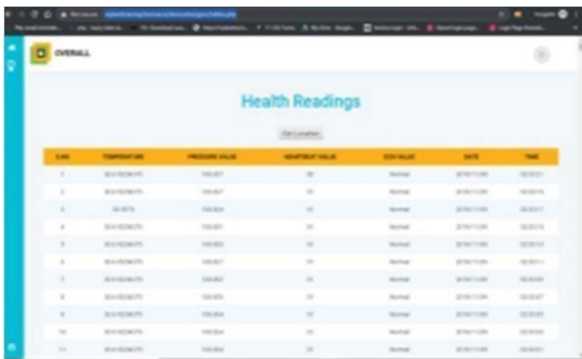


Fig 4:- Web page

II. CONCLUSION

The key objective of this project is to instantly heed Medical attention to the patient’s in emergency and send the patient health condition to the doctor.

A prototype application is developed which consider in measuring parameter continuously and help indetecting heart attack earlier.

The measuring parameter involve heart rate, body temperature , blood pressure, and ECG. It helps the person in emergency by sending the alert to doctor with location and persons health condition. In addition it is easy to carry and reliable to use by a person hence the is no need to stay continuously under medical assistance.

Along with that, a Web Application is developed which allows the doctors to know the condition of the patient and interact with them.

It stores the data received from patient trough cloud . which helps to access the before condition of the patient .

REFERENCES

- [1] Matthew D'Souza, Montserrat Ros, Adam Postula, “Wireless Medical Information System Network for Patient ECG Monitoring” Digital System Design: Architectures, Methods and Tools, DSD 2006, 9th EUROMICRO Conference 2006.
- [2] Roy, Soumya, and Rajarshi Gupta, “Short range centralized cardiac health monitoring system based on Zigbee communication”, In Global Humanitarian Technology Conference-South Asia Satellite (GHTCSAS), IEEE 2014.
- [3] Mohammed, Junaid, Chung-Horng Lung, Adrian Oceanu, Abhinav Thakral, Colin Jones and Andy Adler, “Internet of Things: Remote patient monitoring using web services and cloud computing”, In Internet of Things (iThings), 2014 IEEE International Conference on, and Green Computing and Communications (GreenCom), 2014.
- [4] Dohr, Angelika, Robert Modre-Opsrian, Mario Drobics, Dieter Hayn, and Günter Schreier, “The internet of things for ambient assisted living. In Information Technology”, New Generations (ITNG), 2010 Seventh International Conference on 2010.
- [5] Malhi, Karandeep, Subhas Chandra Mukhopadhyay, Julia Schnepfer, Mathias Haefke and Hartmut Ewald, “A Zigbee-based wearable physiological parameters monitoring system”, IEEE sensors journal, 2012.

Region Specific Weight Measuring System for Bedridden patients

G. Annie Nancy
Department of Electrical and
Electronics Engineering
Loyola- ICAM College of Engineering
and Technology,
Chennai, India
g.annienancy@gmail.com

B. Rashmi
Department of Biomedical Engineering
Rajalakshmi Engineering College
Chennai, India
rashmilatha7024@gmail.com

R. Kalpana
Department of Biomedical Engineering
Rajalakshmi Engineering College
Chennai, India
kalpana.r@rajalakshmi.edu.in

Abstract—Weight measurement is one important aspect, especially for monitoring long term bedridden patients or for post-operative subjects. Presently, though overall weight is measured regularly, periodicity is in the order days owing to practical difficulties like portability of equipment and shifting of patients. Even in this case, region-wise weight measurement is not done. This problem is addressed in the proposed method, where localization of region that contributes to weight change can be identified along with amount of weight change. Since no movement of subject is required, observation interval can be reduced to hours from days. This is achieved by dividing the mild steel sheet holding the subject and placing load sensors beneath the sheets. This is done after understanding and critically reviewing load and height distribution in human body. Load sensors, along with artificial neural network is able to sense the change up to 1 gram with information about location. Entire experiment was done using human phantom model. Result of the proposed method exhibits accuracy of 96% and above with linearity in measurement. Our present efforts are towards making this prototype into a real time weight measuring system.

Keywords—Weight measurement, human phantom, load cells, artificial neural network.

I. INTRODUCTION

Long term bedridden subjects are often vulnerable to health complications and hence regular observation and care are required to prevent organ dysfunction or deterioration [1, 9]. When a human is subjected to bed his/ her physical movement is restricted/ arrested leading to two major complications: one being accumulation of fluid because of physical inactiveness and two is bed sores due to lack of oxygen circulation. The condition of accumulation of fluid is known as edema and is associated with changes in body weight. [2]. In case of certain emergency body weight becomes one important component in deciding the drug and dosing [3,6]. This necessitates periodic weight measurement, however this becomes a challenge when the subject is lying in bed.

Though visual examination and close observation for any physical change are primary sources of information, this becomes unreliable among immobile or unconscious or elderly subjects [4]. Lin et al [7] suggested a mathematical way of estimating weight by measuring mid arm circumference and knee height. Though the authors claim to have more than 90% correlation between estimated value and measured value, edema condition

Darnis et al [17] compared various models used to estimate body weight from anthropometric measures. In their observation this method is associated with error. Since weight is one of the important data in assessing subjects including in post operative conditions, the author suggest for the provision specialized equipment in emergency unit.

Kaweesak Chittawatanarat et.al [5] examined ICU subjects. They collected body weights, height, age and gender at the time of admission into ICU. They observed for any change in weight on daily basis. They concluded that if the change in weight becomes more than 5%, it becomes indicative of fluid accumulation.

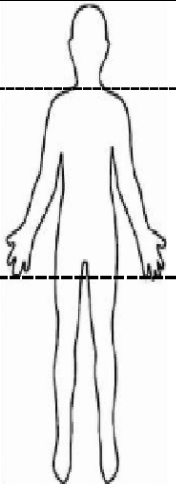
Computed tomography and Magnetic resonance imaging, are other modalities to qualitatively localize fluid accumulations [8, 10, 11, 12, 13]. However these methods become difficult to implement due to immobile condition of subjects, expense and radiation involved. Bio impedance and hydration sensors are other non invasive techniques [14, 15 and 16] to estimate the body fluid shifts. This involves complex instrumentation and still clinically not in use

In summary if measuring techniques are made simple, localization of fluid accumulation and accuracy becomes difficult. However these problems are overcome in high end modalities where regular monitoring becomes impossible. Hence a simple technique is proposed to periodically monitor the weight change and to localize the occurrence; this method involves placing of multiple load sensors by partitioning the cot based on physical structure of the human body. Measurement along with decision making algorithm is able to localize for the change in weight. Entire experiment was conducted on prototype setup.

II. DESCRIPTION OF THE SYSTEM

Attempted in this work is weight estimation of bedridden subjects lying in supine position. Here, single point shear beam type load cells (CZL 635-5 Kg capacity) are used. The analog outputs from the load sensors are fed to Arduino Mega 2560 R3 board after amplification by HX711 amplifier. The entire experiment is conducted using a human phantom model. This phantom is developed in three parts: first part is the head, second being trunk and the third is leg. . These three parts are joined together to form the whole single human phantom model.

TABLE I. HEIGHT AND WEIGHT DISTRIBUTION OF PHANTOM

Human Body	Height distribution		Weight Distribution
		Head	16%
	Trunk	27%	56%
	Leg	57%	37%

Height and weight are the two parameters required to develop the phantom. The weight distribution for these three parts is taken from the literatures [22, 23 and 24]. To know the height distribution, 100 volunteers were recruited in the age group between 25 years and 35 years [Mean – 30.07 and Standard Deviation – 3.38]. Using a graduated scale fixed on a smooth wall total height and region wise heights of the participants are measured. Mean of height and weight distribution is presented in Table 1. Following are the two approaches used to develop the prototype.

A. Method 1: To determine region wise weight by making segments based on physical structure and weight distribution.

In this method region wise weight and total weight are measured using three load cells. One end of these load cells are positioned in cantilever arrangement and are fixed to a common rigid support. The other free end of these load cells are connected to the mild steel sheets. These sheets are separated by a distance of 5mm in between as shown in Figure 1.

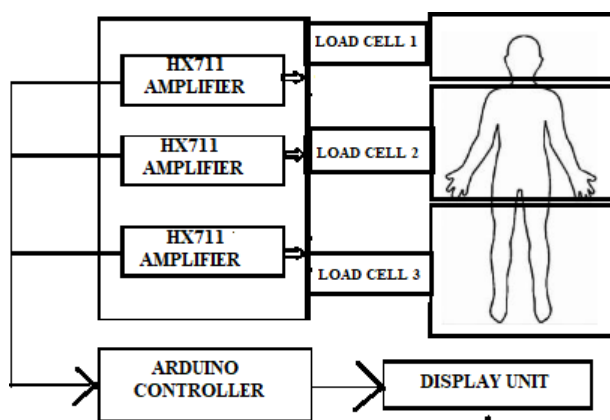


Fig. 1. Schematic diagram for method 1

Known weights are placed in each region and verified for the accuracy upto a resolution of 1 gram. After ensuring

the correctness in the measurement setup, the phantom model is placed on the mild steel sheets such that the head portion lies on the first sheet, trunk on the second and leg position on the third sheet. Weight displayed by each load cell is in agreement to the original manufactured weight of the phantom as illustrated in Table 2. Care should be taken such that head trunk and leg portion lies on the corresponding sheets. However any movement in the sideward direction does not affect the result. By this way this method gives region wise weight and the total weight. (Sum of the three weights)

TABLE II. REGION-WISE WEIGHT MEASUREMENT

Phantom Part	Actual Weight (in grams)	Measured Weight (in grams)
Head	210	209.99
Trunk	1680	1679.12
Leg	1110	1109.18
Total	3000	2998.29

B. Method 2: To localise the region that causes the weight change.

We have seen in the earlier method that the weight of human phantom was measured in three segments. But these segments are broader and do not give information on localised weight change. To address this, in this method multiple load cells are placed under each segment, where first segment holding only the head has one load sensor in the centre of that segment. Second and third segments are divided into six cells, each holding load cells in cantilever arrangement. These load cells are placed in (2x3 and 3x2) format. One end of the sensors is directly attached to the centre of each cell, whereas the other end is free to receive the load. Weights measured by all these 13 load cells are digitally displayed after suitable amplification. All the amplifiers are powered by 5V, 2A switched mode power supply. The entire arrangement is illustrated in Figure 2.

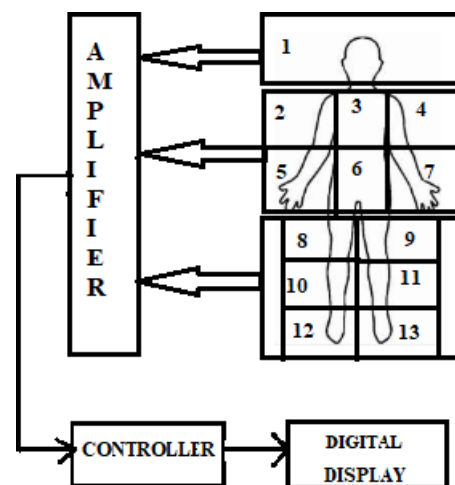


Fig. 2. Schematic diagram for method 2

After making this measurement system ready it is calibrated by placing known concentrated weights directly on each cell. When known additional weights are added changes are observed in the load cell directly below the weight and among four neighbouring load cells. Therefore changes happening in the load cell readings indicate addition of weight in neighbouring cells. However when weight displayed by all load cells are added, it does not correspond to the total weight. After understanding the functionality of the system human phantom is placed such that head, trunk and leg lies on the three segments of the mild steel sheets correctly. When any part of the phantom is extra loaded, then nearby load cells shows variations.

At first we added 10 grams weight in region1 (head) and measured the readings of all the 13 load cells. Then this extra weight was removed and added in region2 (right upper arm) and readings of load cells were noted. Similar procedure is repeated by placing the same extra 10 gms weight in other regions. This gives 13 records, each having

13 load cells measures and target indicating the cell in which load is being added, thus making fourteen columns in each record. In the same way, another 10 sets of records was created by adding in steps of 5 grams upto 60 grams. This resulted in dataset of $13 \times 11 = 143$ records (rows) each having 14 columns (13 readings and one target). Based on these observations, to determine the cell number in which weight change has happened, usage of artificial neural network (ANN) is one feasible approach.

III. LOCALISATION OF WEIGHT CHANGE

Artificial neural network is a mathematical tool, widely used for making decision by taking input from the system being analysed [18, 19]. It operates by the interconnection of neurons with data transmission based on set of instruction [20, 21]. ANN constructed here involves 13 neurons (N) in the input, 9 neurons (M) in the hidden layer and one neuron as output as shown in Fig.3. The readings of 13 load cells are fed to the input layer, which transfer it to the hidden layer with suitable weights (w_{ij}).

Output of hidden layer $y_k = f_1(W_{ij}x_i)_{N,M}$ where W_{ij} is the weight matrix (9×13 in size) between input and hidden layer, $i = 1,2,3, \dots, 13$ $j = 1,2,3, \dots, 9$ $k = 1,2,3, \dots, 9$ and f_1 is the sigmoidal training function.

Finally output of ANN is $y = f_2(W_k y_k)_M$ where W_k is the weight matrix (9×1 in size) between hidden layer and output. y_k is the column vector of size 9×1 resulting in single valued output and f_2 is the linear squashing function

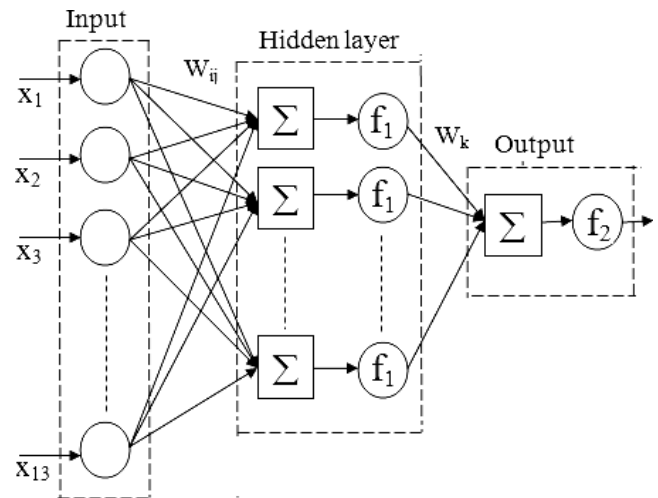


Fig . 3. Architecture of back propagated neural network

The database that is created (as discussed in previous section) is used for training the network. Initially data from column1 to 13 are given as input. With random values for weight between 0 and 1, output of the network is compared with the target (column 14). Using least means square algorithm and back propagation technique, weights are updated till the error reaches tolerance value. Now the network is fixed by the weights, completing training phase. For testing the network, phantom is loaded with known weight at any position between 1 and 13 and the readings of 13 load cells are fed to the network as input. Output of the network now will indicate the region number in which extra load is placed. This when compared with actual position, gives error less than 4%. This level of accuracy is maintained in all our trials, involving different known loads at different position in the phantom. The result of the network is presented in the Table III.

TABLE III. PERFORMANCE ANALYSIS OF ARTIFICIAL NEURAL NETWORK

Load (grams)	10	15	20	25	30	35	40	45	50	55	60
% Accuracy	96.32 ± 1.12	97.14 ± 0.94	97.2 ± 0.86	98.2 ± 0.98	98.4 ± 0.79	99.25 ± 0.08	99.61 ± 0.05	98.02 ± 0.09	97.44 ± 0.86	97.01 ± 1.08	96.69 ± 1.24

CONCLUSION

Attempted in this work is to find weight of human body in supine position. Two methods are proposed here; in one, region-wise as well as total weight is measured. To narrow down the region-wise measurement, second method with multiple loadcells is proposed. This method is able to find small change in weight (upto 1 gram) and display the location. This gives accuracy of more than 96% as given in Table 3 and gives good linearity as given in Figure 4.

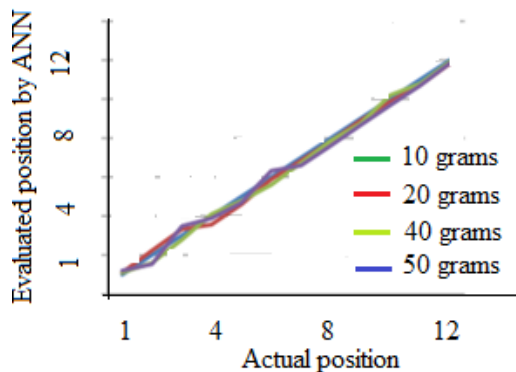


Fig. 4. Position evaluation by the network

In real time application, if the readings are recorded and stored, periodic comparison could be done. This could be useful in understanding the physical changes happened in the body. If the changes are observed over period of observation, then the subject may be referred to further imaging tests. This could help in early diagnosis of any body fluid accumulation and prevent organ failure. Though the present work is with phantom model, this idea could be extended for real time implementation which could be useful for bedridden subjects as well as in hospitals for monitoring post-operative subjects.

REFERENCES

- [1] X. Wu, Z. Li, J. Cao, J. Jiao, Y. Wang, G. Liu, et al., "The association between major complications of immobility during hospitalization and quality of life among bedridden patients: A 3 month prospective multi-center study," *PLoS ONE*, vol. 13(10), pp. 1- 14, 2018.
- [2] A. S. Desai, L. W. Stevenson, "Rehospitalization for Heart Failure Predict or Prevent?," *Circulation*, vol. 126(4), pp. 501-6, 2012.
- [3] W. L. Hall, G. L. Larkin et al., "Errors in weight measurement in emergency department: Comparing Performance by providers and patients," *Journal of Emergency Medicine*, vol. 27, pp. 219-224, 2004.
- [4] T. R. Coe et al., "The accuracy of visual estimation of weight and height in pre-operative supine positions," *Anaesthesia*, vol. 54(12), pp. 1228-9, 1999.
- [5] Kaweesak Chittawatanarat, Todsaporn Pichaiya, Kamtoma Chandacham, "Fluid accumulation threshold measured by acute body weight change after admission in general surgical intensive care units: how much should be concerning?" *Journal of Therapeutic clinical risk management*, vol. 11, pp. 1097-1106, 2015.
- [6] C. M. Fernandes, S. Clark, A. Price, G. Innes, "How accurately do we estimate patients' weight in emergency departments?" *Can Fam Physician*, vol. 45, pp. 2373-2376, 1999

- [7] B. W. Lin, D. Yoshida, et al., "A better way to estimate adult patients' weights," *The American Journal of Emergency Medicine*, vol. 27(9), pp. 1060-1064, 2009.
- [8] Y. Goh, Y. Y. Dan, W. Chua, P. Jagmohan et al., "Diagnostic utility of whole body CT scanning in patients with unexplained weight loss," in *PLoS ONE*, vol. 13(7): e0200686, 2018
- [9] J. McMin, C. Steel, A. Bowman, "Investigation and management of unintentional weight loss in older adults" in *BMJ clinical review* 2011.
- [10] Dominic Gascho, Lucia Ganzoni, Philippe Kolly, Niklaus Zoelch, et al., "A new method for estimating patient body weight using CT dose modulation data," *European Radiology Experimental*, vol. 1, pp. 23, 2017.
- [11] Sam Hassibi, Nabeel Farhatziz, Michael Zaretsky et al., "Optimization of Fetal Weight Estimates Using MRI: Comparison of Acquisitions," in *American Journal of Roentgenology*, vol. 183, pp. 487-492, 2004
- [12] M. Borgia, J. West, J. D. Bell et al., "Advanced body composition assessment: from body mass index to body composition profiling," *Journal of Investigative Medicine*, vol. 66(5), pp. 1-9, 2018.
- [13] M. Djukic, P. Jelic, M. Bulajic and D. Narancic, "One solution for the weight measurement process update using embedded computer," 13th International Conference on Advanced Technologies, Systems and Services in Telecommunications (TELSIKS), pp. 419-422, 2017.
- [14] L. A. L. Fernandes, M. Azadmehr, E. A. Johannessen and P. Häfliger, "An Osmotic Pressure Sensor for Monitoring the Level of Hydration in Biological Fluids," *IEEE Sensors Journal*, vol. 16(11), pp. 4331- 4337, June-2016.
- [15] O. I. Al-Surkhi, P. J. Riu and M. Y. Jaffrin, "Monitoring body fluid shifts during haemodialysis (HD) using electrical bioimpedance measurements," proceedings of 1st Middle East Conference on Biomedical Engineering, Sharjah, pp. 108-113, 2011.
- [16] A. Resendiz, D. Odicho, V. Gabrielian and A. Nahapetian, "Edemeter: Wearable and continuous fluid retention monitoring," pp. 153-158, 13th International Conference on Wearable and Implantable Body Sensor Networks (BSN), San Francisco, CA, 2016.
- [17] S. Darnis, N. Fareau, C. E. Corallo, S. Poole et al., "Estimation of body weight in hospitalized patients," *QJM-Int Transaction of medicine*, vol. 105(8), pp. 769-74, 2012
- [18] B. Karlik, E. Oztoprak, "Web-based telemedical consultation and diagnosis model by multiple artificial neural networks," *Ukrainian Journal of Telemedicine and Medical Telematics*, vol. 5, pp. 156-160, 2007.
- [19] A. Filippo, L. Alberto, M. P. Eladia et al., "Artificial neural networks in medical diagnosis," *Journal of applied Biomed*, vol. 11, pp. 47-58, 2013.
- [20] R. Kalpana, S. Muttan, "Assessment of geriatric - specific changes in brain texture complexity using a back propagation neural network classifier," *Complex Syst*, vol. 20, pp. 305-324, 2012.
- [21] U. Madhanlal, R. Kalpana, P. Soundararajan, "Assessment of chronic kidney disease using skin texture as a key parameter: for South Indian population," *Healthcare Technology Letters*, vol. 4(6), pp. 223-227, 2017.
- [22] Stanley Plagenhoef, F. Gaynor Evans, Thomas Abdelnour, "Anatomical Data for Analyzing Human Motion," in *Research Quarterly for Exercise and Sport*, vol. 54:2, pp. 169-178, 2013.
- [23] Paolode Leva "Adjustments to Zatsiorsky-Seluyanov's segment inertia parameters," in *Journal of Biomechanics*, vol. 29(9), pp. 1223-1230, 1996.
- [24] R. Drillis, R. Contini, M. Bluestein, "Body segment parameters: a survey of measurement techniques," *Artif Limbs* 1964;8:44-68.

Microfluidic device for Multitarget separation using DEP techniques and its applications in clinical research

Mohamed Zackria Ansar B.I
Department of Electronics and
Communication Engineering
C.Abdul Hakeem College of
Engineering & Technology
Melvishram,India
zackriaansarbi@gmail.com

Mohamed Yousuff Caffiyar
Department of Electronics and
Communication Engineering
C.Abdul Hakeem College of
Engineering & Technology
Melvishram,India
cmd.yousuf@gmail.com

Mohammed Kashif .A
Department of Electronics and
Communication Engineering
C.Abdul Hakeem College of
Engineering & Technology
Melvishram,India
kashifmd134@gmail.com

Abstract—This paper presents a time-dependent simulation of two dimensional multiparticle separation using dielectrophoresis method in COMSOL Multiphysics software. The Simulation was made for various microparticles of size ranging (2 μ m to 10 μ m) by applying various electrode potential that creates resultant dielectrophoretic force corresponding to the various channel width. The values of channel width, inflow velocity and applied electrode potential are compared. In this work, we simulated a new model with triangular arrangements of electrode which is capable of separating multiple particles at low voltage of 9-10vpp. Our model shows that particle size of 2 μ m, 6 μ m and 12 μ m can be successfully separated from the mixture by applying suitable DEP force and subsequently controlling the predetermined flow rate at the inlets.

Keywords-COMSOL, DEP force; Triangular Electrodes, Microfluidics, Multiple particles

I. INTRODUCTION

All the living organisms in the world is made of cells that range in micron sized dimensions. The primary process involved for diagnosis of diseases is blood test involving cell separation from the patient blood sample. Manual blood test sometimes leads to wrong test results which in turn serves as the source for wrong medication causing severe harm to the patients or often leading to the allergies. Sometimes can cause death. Several methods have been employed for the isolation, primarily between platelets (PLTs) and red blood cells (RBCs), such as centrifugation, mechanical filtration, and the detection of antibodies [1]. Advancement in the technologies of microfluidic and analytical devices integrated on a mini chip-scale platform have become a promising alternative for more accurate and safe diagnostic testing ,or point-of-care(POC) for the patients aiming least errors[2].

Although, these techniques are macro-scale techniques they have the following disadvantages: (1) the non continuous separation process, which takes more time for analysis; (2) the requirements of a large size and the adaptation of samples; and (3) the requirement for highly trained staff to work on an enormous and expensive tool. Microfluidics offers a practical toolkit for microparticles separation with many benefits, (i) less quantity of samples; (ii) Reduced examining time; (iii) compact size.

Recently, various separation techniques have been successfully applied to separate target particles depending upon their properties of the particles considered. Nada et.al. develop a simulation model to separate platelets from the blood using DEP. They used COMSOL simulation

environment to demonstrate the model. However their model is not demonstrate for simultaneous separation of multiple particles and also, the model does not characterize the impact of electrode geometries arrangements and its electrode potentials[3]. Iliescu et.al demonstrated separation of Viable and nonviable yeast cells using negative DEP. The separation method consists of trapping one population to the bottom of the microfluidic channel using positive DEP, while the other population that exhibits negative DEP is levitated and flowed out[4]. Dongkyu Lee et.al. presented a review on DEP based cell sorting as next generation technologies. They demonstrated various DEP activated cell sorting techniques which includes DEP trapping, traveling wave DEP systems, DEP field-flow fractionation and DEP barriers subsequently they shown the strong and weak points of each DACS [5]. Later On, Tatsumi et.al. developed a ladder type electrode arrangement in a microfluidics channel to analyse and measure the performance of particle manipulation such as motions of the particle, sorting reliability, the direction of the particle, timing and response etc., [6]. Yao et.al. reviewed various electrode arrangement for sorting of microparticles and cells using DEP techniques. Their analysis shows that, the electrode arrangement in the microfluidic device is a key factor to realize an effective dielectrophoretic force [7].

Finite element modelling (FEM) is becoming a vital tool in modern testing. Jing Jin et.al. developed a new model of DEP manipulation on microparticles using Liquid Marbles (LM). In their work, they report that, concept of accurately positioning a floating LM using a pair of electrodes. They formulated an analytical model to describe the DEP force and obtained a governing equation that determines the LM position for various electrode configurations. [8]. Dielectrophoretic is used primarily to characterize particle acceleration while subjected to gradients of electric fields. Zhao et.al. developed two electrode-pads arrangements that are embed in a set of asymmetric orifices on the opposite sidewalls for lateral migration of yeast cells. They investigated the DEP behaviours of yeast cells in suspending media with different ionic concentrations and over a large range of the AC electric field frequency [9]. Our model aims to test the separation of micron-sized particles ranging from 2 μ m to 12 μ m by the use of application of dielectrophoresis. In order to separate the micron sized particles from human body these technique is highly suitable for it. In the dielectrophoretic process, the particles are drawn to the area with large intensities of electrical fields, while the particles are repelled to the region with small intensities of electrical fields. Dielectrophoretic differs greatly from electrophoresis, because dielectrophoretic force does not require the particle

to be charged. All particles exhibit dielectrophoretic activity in the presence of electric fields. While electrophoresis using a uniform electric field requires particle to be charged.

In DEP, there are two forces which expose positive dielectrophoresis (pDEP) and negative dielectrophoresis (nDEP) particles on suspended particles. pDEP are the particles that moves towards the region where there is strong electric field in case if they are polarizable than medium. nDEP represents the particle that moves away from the strong electric field if these particles are less polarizable than surrounding medium. Several review papers have demonstrated various mechanism for multiple target separation particle separation. [10]. Yousuff et.al demonstrated a three-particle separation using inertial microfluidics but the system is difficult when separating a particle which have close size differences [11]. Simulation model for separation of WBC and RBC is reported earlier however the model does not report any guidelines for separation of multiple particles [12]. Punjiya, M., Nejad, H.R., Mathews, J. et al provided the numerical scaling analysis for individual cell trapping and electroporation using low voltage AC fields that was restricted to only embryonic cells [13].

In this paper, we proposed a microfluidics device that is capable to separate multiple particles ranging from 2µm to 15µm with a novel electrode arrangement (triangular arrangement of electrodes). The device's efficiency was analyzed for separation of three particles precisely in three collection outlets with minimal electrode potentials (9vpp). Our device further provides a guideline for separation of multiple particles with varied size distributions (closest to wide range of distributions).

The paper is organized as follows: Section II presents the methods followed; design and modeling of the device. Section III presents the results of the design. The discussion is presented in section IV. Finally; the conclusion is shown in Section V.

II. MATERIALS AND METHODS

A. Dielectrophoresis

Dielectrophoresis (DEP) is the phenomenon in which the force is exerted by the dielectric particles when subjected to non-uniform electric field. The separation force in electrical field E which is inhomogeneous and time- varying is proportional to the volume of the cell, as illustrated by equation (1). Thus, cells having different dielectric characteristics will experience differential DEP forces when subjected to an inhomogeneous dc electric field.

$$\mathbf{F}_{\text{ext}} = 2\pi r_p^3 \epsilon_0 \text{real}(\epsilon_f^*) \text{real}\left(\frac{\epsilon_p^* - \epsilon_f^*}{\epsilon_p^* + 2\epsilon_f^*}\right) \nabla |\mathbf{E}_{\text{rms}}|^2 \quad (1)$$

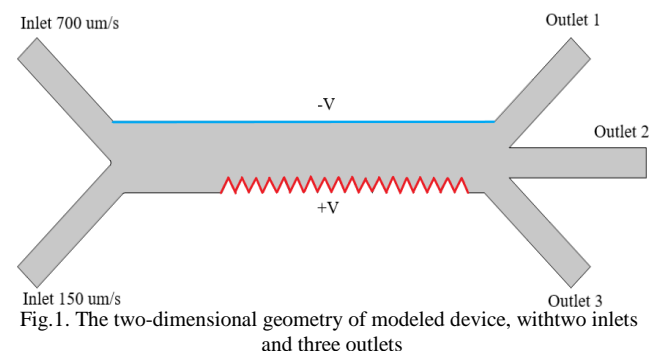
where ϵ_m refers to the permittivity of the medium, r is the radius of the particle, $\text{Re}(\mathbf{K}_{\text{CM}})$ is the real part of the Clausius-Mossotti factor, which is defined as:

$$\mathbf{K}_{\text{CM}} = \frac{\epsilon_p - \epsilon_m}{\epsilon_p - 2\epsilon_m} \quad (2)$$

Where ϵ_p and ϵ_m are the complex permittivities of the particle and suspending medium considered, respectively. Consequently, the \mathbf{K}_{CM} is dependent on the complex permittivities of the suspending medium and particles. Positive DEP (pDEP) attracts the particle to the high electric field region when the suspending medium is less polarizable than particles (i.e., $\text{Re}(\mathbf{K}_{\text{CM}}) > 0$). When the suspending medium is more polarizable than particle (i.e., $\text{Re}(\mathbf{K}_{\text{CM}}) < 0$), negative DEP (nDEP) is created in order to repel the particle away from the highly electric field.

B. Geometry of the separation device

The model consists of two inlets, three outlets and a separation region where a non-uniform electric field is generated by electrode arranged in triangular manner changes the paths of the particle when sufficient electrode potential is provided. Blood containing mixed cells (healthy cells and infected cells) are injected at the entrance and particles of various size comes from three outlets. Blood mixture cells are injected at the inlet 2 and buffer comes from three outlets. The channel width is 100 µm and the flow is laminar in the separation region (Reynolds number < 0.5). Fig.1 shows the schematic of the two-dimensional modeled geometry. The inflow velocity at the inlet 1 is (700 µm/s) and inflow velocity at the inlet 2 is (150 µm/s) to focus the particles at the respective outlets. The electrode potential is chosen in such a way that micron-sized particles are sufficiently experiences the dielectrophoretic force. As shown in fig.1. the electrode is shown in triangular manner that provides the positive potential and the upper wall is supported with electrode that provides the negative potential and the overall phenomenon generates the suitable non-uniform electric field results in DEP force.



C. Numerical Analysis

In order to evaluate each convection, computational calculation were validated, and dielectrophoretic forces (DEF) were found to be sensible on the cells. COMSOL Multiphysics software package has been used to analyze the two-dimensional finite element model, where it returns the electrical field distribution and the flow within the geometry of the device.

The following physical phenomena is used in our model:

- (1) Creeping flow to demonstrate the fluid flow.
- (2) Trace particle-fluid flow for calculating the path of Platelets, WBCs and RBCs under the effect of dielectrophoretic force and drag.
- (3) Electric currents to show the electric field in the device's microchannel.

The geometry of the devices including its channel and electrodes were defined under the graphics section of the COMSOL Multiphysics software. Samples and buffer inlets with channel widths of 42 μm and height of (210 μm to -210 μm), merge into the separation channel of 100 μm width and 560 μm length. The outlets are of same dimensions as that of the inlets followed by selecting appropriate materials for each domain and the required potential is provided at the respective electrode boundaries.

Below table1 shows the parameter values of RBCs, WBCs, and Platelets

TABLE 1. PARAMETERS USED TO CALCULATE KCM OF RBCs, WBCs AND PLATELETS

Cells	Diameter (μm)	Conductivity σ (S/m)	Relative Permittivity ϵ_r
RBCs	2	0.25	50
WBCs	6	0.25	59
PLTs	12	0.31	59

The meshing stage was then done using a variety of types of components, as shown in Table 2. The meshing model, as shown in Fig 2, was made using settings of the default simulation software.

TABLE 2. MESH ELEMENT STATISTICS

Property	Value
Average element quality	0.806
Number of Elements in Mesh	5029
Number of Degree Of freedom	366
Edge elements	668
Vertex elements	54

I. RESULTS

Many steps were taken to determine the quality of blood differentiation and the amount of abstraction of red blood cells when the dielectrophoretic voltage between neighboring liquid electrodes was applied. Fig. 3 demonstrate a perfect isolation of the red blood cells and White blood cells away from the electrodes because of the existence of negative DEP (nDEP), making those cells of larger size leave the separation

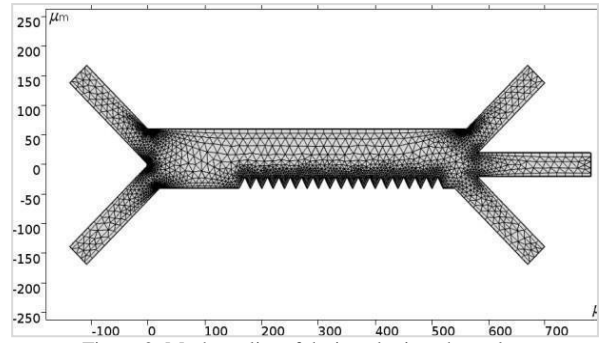


Figure 2: Mesh quality of designed microchannel

region in the correct path. The effect on the left side clearly displays the path of the white blood cells and platelets, which are too small to be clearly prevented and remain with the laminar flow on the left path and leave the separation region on the left path. The concentration level of red blood cells applied for this paper is lower than the concentration level of platelets to improve visualize the platelet and White blood cell path. The flow speed used at the upper inlet is 700 $\mu\text{m/s}$ and the lower inlet is 150 $\mu\text{m/s}$ to focus cells in the direction of the middle at the entrance because of the parabolic flow profile. Follow the path of the cell through the recursive update of the place after the flow field and the DEP speed, given the starting position somewhere in the cell entry. Fig.3 Provides the logical paths of the cells within the geometry of the device. This can be evidenced; it is conceivable to choose a combination of focusing envelope and nDEP where the PLT diverges enough to move towards the left direction channel while the RBC stays on the right due to the bifurcation shifting as a laminar splitter. The numerical "Stability" verification in sorting evaluating by impact on the logical path of cell starting place. As shown in the results of the simulation, the device will retain sort efficiency with varying output position by a small portion of the cell diameter, where the blood flow is highly focused on the left part of the tube.

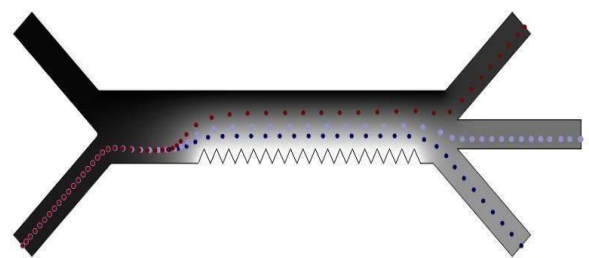


Fig. 3. Particle paths with dielectrophoresis force applied. The RBCs are displayed in red, WBCs in light blue and the platelets in blue.

The cells are separated at specific frequencies after flowing between the sorting electrodes based on their different dielectric property. The frequency used for this initial model is 110 kHz where each of platelets, White blood cells, red blood cells is experiencing negative DEP (nDEP). Nevertheless, because of the difference in size, the

dielectrophoretic intensity becomes stronger for the red blood cells than for the platelets.

A first variation to the configuration of the original system was conducted using a voltage of 9Vpp but in incremental steps of 200kHz at different frequencies varying from 60kHz to 2MHz as shown in Table 3. The proposed device was able to separate platelets, WBCs and RBCs effectively from the samples. Separation efficiency was found to be 100% at 110 kHz (the highest value that was reported in the literature [1]), and 97% at 300kHz. However, when the frequency was lowered than 110 kHz or frequency is increased from 1MHz to 1GHz the particles were not separated and followed as following a similar path, as shown in Fig.4.

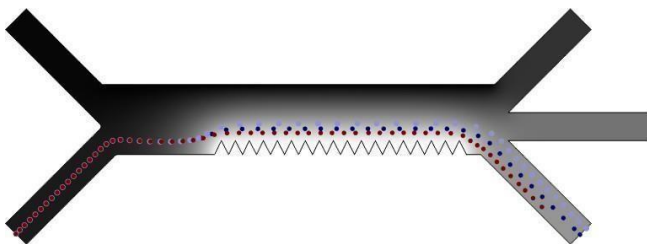


Fig. 4. The particles are released at the same time and follow a similar path (separation failure), for frequencies higher than 600kHz. RBCs are displayed in red, WBCs in light blue and PLTs in blue.

TABLE 4. FREQUENCY CHANGE EFFECT ON SEPARATION OF BLOOD CELLS

Applied Electrode Potential	Inlets Flow Speed (Upper/Lower)	Frequency	Separation (Efficiency)
9 V _{PP}	700µm/s-150µm/s	60kHz	Not- Separated
9 V _{PP}	700µm/s-150µm/s	110kHz	Separated At 3 outlets (effec: 100%)
9 V _{PP}	700µm/s-150µm/s	>100 kHz to 600kHz	Separated At 3 outlets (effec: 98.8% to 97%)
9 V _{PP}	700µm/s-150µm/s	1MHz to 1GHz	Not- Separated

A second variation was performed on the device, using different electrode potential at 110 kHz frequency; Table 5. The simulations showed that when applying voltages below 9 VPP and higher than 15 VPP the device was not able to separate RBCs, WBCs and platelets simultaneously from samples and followed a similar path, but it was capable of PLTs separation using 10 VPP and 25VPP only. It is worth mentioning that the separation efficiency at 30 VPP was not optimal and inappropriate, so this was considered as an unsuccessful value, as inconsistent results could be produced.

TABLE 5. EFFECT OF ELECTRODE POTENTIAL ON SEPARATION OF BLOOD CELLS

Applied Electrode potential	Inlets Flow Speed (Upper/Lower)	Frequency	Separation result (outlets)
5 VPP	700µm/s-150µm/s	110kHz	RBCs gets separated
9 VPP	700µm/s-150µm/s	110kHz	Perfect isolation of three particles
20 VPP	700µm/s-150µm/s	110kHz	WBCs and PLTs gets separated
25VPP	700µm/s-150µm/s	110kHz	PLTs gets separated

A third variation to the original device's design was performed to validate the operation of the device, using different flow speed velocities; Table V. Model simulations revealed that when applying inlet flow velocities from 150 to 500 µm/s flow speed at lower inlet and 700 to 1200 µm/s at upper inlet the device was still able to separate platelets, WBCs and RBCs from other samples, but for lower inlet flow speed of 1600 µm/s and above, the particles were released at the simultaneously and follow a similar path (separation failure).

TABLE 6. EFFECT OF FLOW SPEED VELOCITY ON SEPARATION OF BLOOD CELLS

Amplitude	Inlets Flow Speed (Upper/Lower)	Frequency	Separation (Efficiency)
10V _{PP}	700 µm/s- 100 µm/s	100kHz	Separated (98.9%)
10V _{PP}	900µm/s-130 µm/s	100kHz	Separated (97.3%)
10 V _{PP}	1000µm/s-180 µm/s	100kHz	Separated (96.3%)
10V _{PP}	1400µm/s-220 µm/s	100kHz	Non-Separated
10V _{PP}	600µm/s-500µm/s	100kHz	Non-Separated
15 V _{PP}	700µm/s-150µm/s	100kHz	Separated (99.8%)

IV. DISCUSSION

A modified solution was applied in this paper to separate red blood cells, White Blood Cells and Platelets simultaneously from blood using fractionation of the field flow through dielectrophoresis. The micro-fluid device used combining prefocusing and fractionation functions to specifically trap cells on their size-based location. From the simulation findings shown in this paper the logical cell path was obtained. Through generating a non-uniform electric field and positioning the opposing polarity electrodes, the particle tracks were changed. Simulations were observed in COMSOL Multiphysics software.

The findings of the research simulation were first tested by contrasting it with the original design tests applied by ayad nada[4], in which 100 kHz frequency with a 10VPP voltage was used to distinguish the PLTs from the RBCs. The experimental results of their study showed a very high separation rate of platelets alone 98.8% with less cell loss 2%. The below fig 5 shows the perfect isolation of three particles (RBCs, WBCs, PLTs) with maximum efficiency.

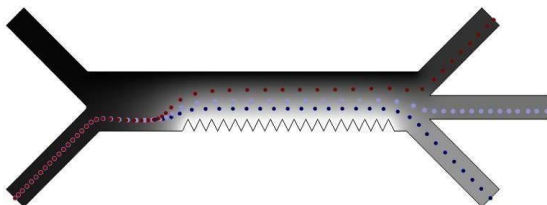


Fig. 5. The applied electrodes voltage is 9Vpp at 110 kHz, the RBCs are displayed in red, WBCs in light blue and the platelets in blue.

Diverse electric voltages were used to examine the efficiency of electric field on cells isolation from the samples (Table IV). The flow velocity used at the upper inlet is 700 $\mu\text{m/s}$ and the lower inlet is 150 $\mu\text{m/s}$ was computed using the cell paths. The 5VPP low voltage neglected creating suitable FDEP for platelet arrangement. Blood cells exhibit an illustrative flow at the blood inlet. Due to the smaller fDEP, RBCs were not properly redirected. The microfluidic system consequently failed to isolate the different blood cells.

The form of blood sorting using the electric voltage of 9VPP shows in Fig.5. A proper FDEP was developed to handle the PLTs, WBCs and RBCs productively, though the cells were closer to the separator walls but still included within their designated paths. Increasing electrical voltage to 25VPP increased the fDEP on the electrical field and the cell. The increase in FDEP caused the blood cells to divert in the vertical path from the electrodes. The PLTs thus joined the array outlet for the RBCs, and the RBCs cell trapped in the unit as shown in Fig. 6. These results mean that an electric voltage from 9VPP to 15VPP could be suitable to efficiently isolate RBCs, WBCs and PLTs from the existing microfluidic interface layout.

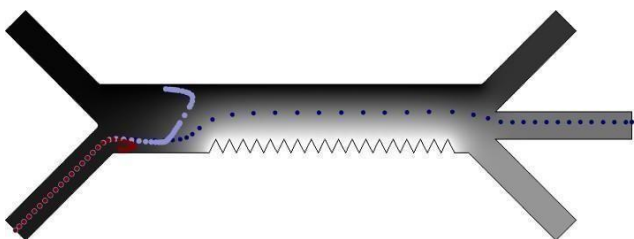


Fig. 6. The voltage applied between electrodes is 30Vpp. The particles followed a similar path, and the RBCs, WBCs were stuck in the device, the RBCs are displayed in red and the WBCs in light blue.

The effect of flow speed at the top and the bottom inlets on cell displacement was also examined. The results were processed utilizing 110 kHz frequency at an applied

potential of 9VPP (Table V). The increased flow speed used at the top inlet compared to the bottom inlet is to reduce the number of blood cells that have been arranged. The higher flow speed utilized at the top and the bottom inlet to increase the movement of the blood cells and the wall collisions region. The separation device is meant to provide an automatic diagnosis tool. In all cases, the FDEP did not properly reirrigate the blood cells that were circulating at high flow rate at the top and bottom inlet, and consequently decreased the number of segregated cells. Increasing the flow rates therefore substantially reduced the impact of FDEP on the blood cells, and consequently decreased the efficacy of the microfluidic device.

V. CONCLUSION

A channel design with new electrode arrangements is applied in this paper to separate RBCs, WBCs, and platelets from blood sample, using the fractionation of the field flow of dielectrophoresis. The channel and electrode arrangements with side flow inlet velocities specifically deflect the cells in different collections outlets depending on their size. With the generation of a non-uniform electric field and arranging the alternating polarity electrodes, the particle paths were altered. The 2D finite element model was used to test design parameter variations, including the applicable electrode potential, frequency, and flow rate. For this updated model, 9V electric voltage is highly appropriate for the effective separation of red blood cells, White blood cells and Platelets. This design will not only help to isolate Red Blood cells, White Blood Cells and Platelets from Blood mixture but also other cell types over the range of sizes can separated with little tuning of electrodes potentials with higher efficiency, increasing high purity and recovery levels by 100%. The technology of the system makes it particularly suitable for isolation of infected cells from the healthy cells in the blood samples of a patients resulting in fast diagnosis with high accuracy.

REFERENCES

- [1] Catarino, S. O., Rodrigues, R. O., Pinho, D., Miranda, J. M., Minas, G., & Lima, R.. "Blood Cells Separation and Sorting Techniques of Passive Microfluidic Devices: From Fabrication to Applications". *Micromachines*, vol 10 no.9, pp. 593, 2019
- [2] Ma, J., Yan, S., Miao, C., Li, L., Shi, W., Liu, X. Lu, Y. "Paper Microfluidics for Cell Analysis. *Advanced Healthcare Materials*", vol. 8, pp. 1-20, 2018
- [3] Ayat Nada, Mohamed Omar and Ahmed M Sayed. "Separation Modeling of Blood Cells using Dielectrophoretic Field Flow". *International Journal of Computer Applications* vol. 181 no. 33 pp.36 - 41, 2018
- [4] Iliescu, C., Tresset, G., & Xu, G. "Dielectrophoretic field-flow method for separating particle populations in a chip with asymmetric electrodes". *Biomicrofluidics*, vol. 3, no.4, pp.044104, 2009.
- [5] Lee, D., Hwang, B., & Kim, B. "The potential of a dielectrophoresis activated cell sorter (DACS) as a next generation cell sorter". *Micro and Nano Systems Letters*, vol 4, no. 2, pp 1-10 2016
- [6] K. Tatsumi, K. Kawano, H. Okui, H. Shintani, and K. Nakabe, "Analysis and measurement of dielectrophoretic manipulation of particles and lymphocytes using rail-type electrodes," *Med. Eng. Phys.*, vol. 38, no. 1, pp. 24–32, 2016.

- [7] Yao, J., Zhu, G., Zhao, T., & Takei, M. Microfluidic device embedding electrodes for dielectrophoretic manipulation of cells - A review, vol 40, no. 8 pp 1166-1177, 2018.
- [8] Jin, J., Ooi, C. H., Sreejith, K. R., Zhang, J., Nguyen, A. V., Evans, G. M., Nguyen, N.-T. "Accurate dielectrophoretic positioning of a floating liquid marble with a two-electrode configuration". *Microfluidics and Nanofluidics*, vol 23, no 85. 2019.
- [9] Zhao, K., Larasati, L., Duncker, B. P., & Li, D. (2019). "Continuous Cell Characterization and Separation by Microfluidic AC Dielectrophoresis". *Analytical Chemistry* vol. 91 no. 9 pp.6304-6314, 2019.
- [10] Yousuff, C.M.; Ho, E.T.W.; Hussain K., I.; Hamid, N.H.B. "Microfluidic Platform for Cell Isolation and Manipulation Based on Cell Properties". *Micromachines* vol. 8, no. 15, 2018.
- [11] C. M. Yousuff, N. H. B. Hamid, K. I. Hussain and E. T. W. Ho, "Output channel design for collecting closely-spaced particle streams from spiral inertial separation devices", *AIP Advances* vol. 7, pp. 085004, 2017.
- [12] C. M. Yousuff, N. H. B. Hamid, K. I. Hussain and E. T. W. Ho, "Numerical modelling and simulation of dielectrophoretic based WBC sorting using sidewall electrodes," 2016 6th International Conference on Intelligent and Advanced Systems (ICIAS), Kuala Lumpur, pp 1-6, 2016
- [13] Punjiya, M., Nejad, H.R., Mathews, J. et al. "A flow through device for simultaneous dielectrophoretic cell trapping and AC electroporation". *Sci Rep* vol. 9, pp. 11988, 2019.

Smart Health Monitoring System using IOT and Machine Learning Techniques

Honey Pandey

Department of ECE

Hindustan Institute of Technology and Science

honeypandeyhp37@gmail.com

S. Prabha

Department of ECE

Hindustan Institute of Technology and Science

sprabha@hindustanuniv.ac.in

Abstract— Coronary illness is that the principle purpose for death around the world. Human services field contains a tremendous measure of information, for handling those information certain methods are utilized. Handling or processing is one in all methods regularly utilized. This strategy predicts the emerging potential outcomes of cardiovascular ailment. The results of this strategy are to foresee the previous cardiovascular malady. The task manages IOT using sensor (pulse sensor to watch pulse) with Arduino and furthermore the outcome can be checked in sequential screen. With the use of IFTTT the readings of sensor are perused in google sheet which is then changed over into csv go looking like data. The datasets utilized are grouped as far as therapeutic parameters which are additionally utilized for preparing and testing the information. This strategy assesses those parameters utilizing information preparing order method. With the work of AI calculations and classification. Initially, the dataset is dissected, watched and screened, at that point the obtained information is handled in python programming utilizing Machine Learning Algorithm to be specific Decision Tree Algorithm and Random backwoods classifier Algorithm. SVM (Support vector machine) shows the higher outcome as far as exactness for identifying heart illness. Henceforth the proposed framework is demonstrated to be solid one for foreseeing prior heart disease. The proposed hardware as well as software system helps patient to predict heart disease in early stages. It will be helpful for mass screening system in villages where hospital facilities are not available, i.e., rural areas.

Keywords—Health Care System, IOT, Machine Learning Techniques, SVM Classifier

I. INTRODUCTION

Healthcare plays a vital role in our daily life. Health diseases can be diagonalized and prevented at the early stages with proper treatment. The abnormalities present inside our body or under the skin can be easily identified by using various curing equipment like CT, MRI, PET etc. Also, certain uncommon diseases like heart attack, heart stroke can be easily prevented at the early stages as they occur. Due to the tremendous increase in the population of the world, there is an unpredictable spread of degenerative illness in huge number which have created a trouble on modern health care systems, and the demand for funding from hospital beds to doctors and nurses is exceedingly high. To maintain the standard and quality of the health care provided at its most favourable level, there is a need to reduce the burden on healthcare systems. The Internet of Things (IoT) is a potential solution to decrease the pressures on healthcare systems. Prior, the incidental checking of patients with diabetics is nitty gritty in and furthermore observing of patients with explicit infection, for example, Parkinson ailment is portrayed in. Researchers are looking forward to serve specific purposes for curing diseases at the early stage, so various rehabilitation technique such as aiding rehabilitation are done so as to monitor the patients progress continuously. Since huge amount of data is present in today's era, data preprocessing, storage and analysis should be taken in consideration, with little mention of adding those into a

system and should be utilised. A scope of wearable frameworks is proposed to supply dependable remote transmission of information. Both the medical clinic administrators and IT are made a fuss over information security and IoT gadget the executives. AI might be a field which might be a subset of man-made reasoning (AI). Applying man-made reasoning, we will manufacture better a higher future. AI might be a mastermind to pick up from points of reference and information, without being explicitly altered. Instead of composing code, the data is bolstered to the conventional calculation, and rationale is given dependent on the data. AI is drilled in web look, spam sifting, advertisement position, stock exchanging, etc. Despite the fact that gaining from this abundant information is foreseen to bring significant science and designing advances together with upgrades in nature of our life, it brings huge experiences at the indistinguishable time. A report from McKinsey Global Institute confirm that AI will be the driver of the resulting huge influx of development Internet of Things (IoT) conceptualizes the possibility of remotely partner and checking true articles (things) through the Internet. These days Health-care Environment has explained science and information dependent on Wireless-Sensing hub Technology arranged. Patients are confronting an unsure circumstance of prevision end because of the particular explanation of heart issues and assault which is a direct result of nonexistence of good therapeutic upkeep to patients at the required time. This is for uniquely identifying the mature age patients, youngsters and illuminating specialists and friends and family. So, we are thinking of an imaginative undertaking to gadget such unexpected passing rates by utilizing Patient Health Monitoring that utilizations sensor innovation and utilizations web to impart to the friends and family if there should be an occurrence of issues. We have additionally observed ML procedures being utilized in ongoing improvements in different territories of the Internet of Things (IoT). AI is broadly utilized these days in numerous business applications like web-based business and some more. Information preparing is removing data and information from immense measure of data. Data mining is a basic advance in finding information from database or constant information. Information preparing is basically used to separate the concealed data from a lot of database. Expectation is one of the regions where this AI is utilized, our subject is about forecast of coronary illness by handling patient's dataset and an information of patients to whom we have to anticipate the opportunity of presence of a coronary illness.

II. MATERIALS AND METHODS

A. Heartbeat rate sensor:

Pulse Sensor is an effective fitting and attachment play beat sensor for Arduino. The sensor cuts onto a fingertip and expansion straightforwardly into Arduino. It furthermore joins an open-source watching application that diagrams your pulse in certified time. The front of the sensor is that is verified with the heart shape logo. This is routinely the side

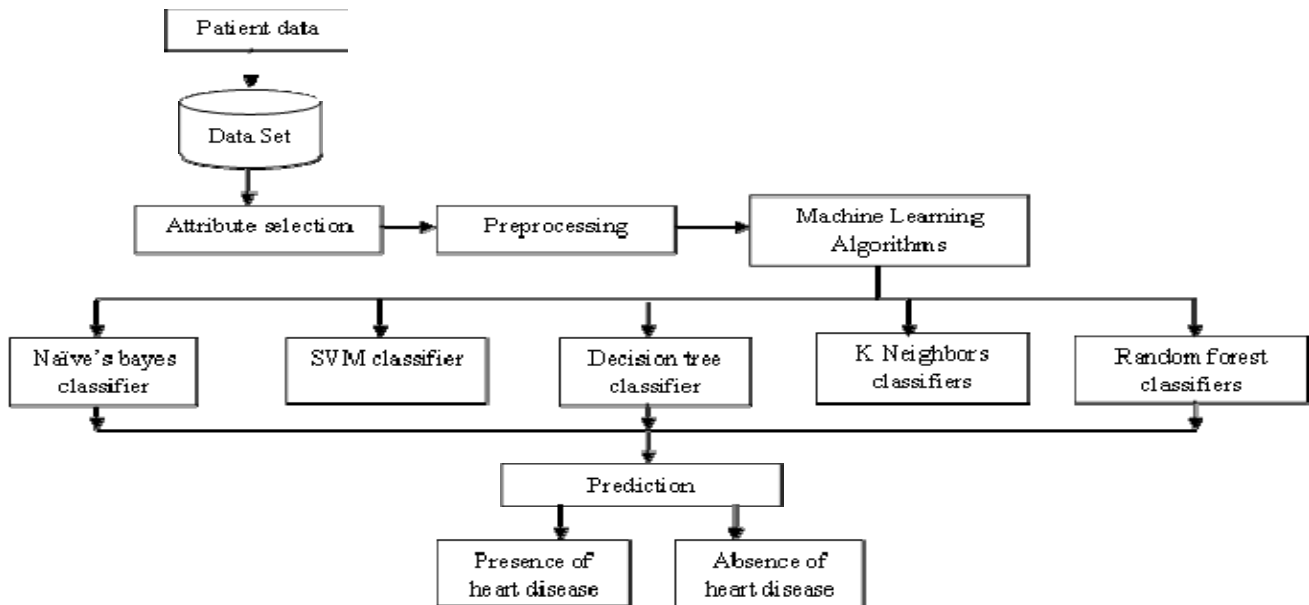


Figure 1: A Smart Intelligent System Framework Predicting Heart Disease

that produces contact with the skin. On the front you see a little low round hole, which is the spot the LED emanates through from the back, and there is moreover to some degree square imperceptibly underneath the LED. The LED gleam light into the fingertip or ear ligament, or other thin tissue, and sensor scrutinizes the proportion of light that bounces back. That is the manner in which it learns the beat. The opposite side of the sensor is the spot the remaining of the parts are mounted. 2.2. Dataset: An informational index (or dataset) is a lot of information. An individual column of information is called an example. It is a perception from the space. An assortment of examples is a dataset and when working with AI techniques we ordinarily need a couple datasets for various purposes. The information is then prepared and tried utilizing AI calculations. A dataset that we feed into our AI calculation to prepare our model and the dataset that we use to approve the exactness of our model however isn't utilized to prepare the model.

B. Information Preprocessing:

Pre-processing deals with recommends the movements applied to our information before supporting it to the figuring. Information Pre-processing is a structure that changes over the grungy information into an impeccable educational record. Some defined AI model needs data in a predefined position, for instance, Random Forest calculation doesn't fortify invalid attributes, therefore to execute flighty backwoods check invalid qualities must be administered from the chief unpleasant educational record. Another perspective is that enlightening assortment should be organized with the goal that more than one Machine Learning and Deep Learning estimations are executed in one instructive record, and best out of them is picked

C. Machine learning classifiers:

In request to investigate the heart patients and sound individuals, AI arrangement calculations are utilized. Some well-known characterization calculations talked about quickly right now are utilized in machine learning:

(1) Logistic regression: it is a characterization calculation. For combined gathering issue, so as to anticipate the estimation of insightful variable y when $y \in [0, 1]$, 0 is negative class and 1 is sure class. It in like manner practices multiclassification to envision the estimation of y when $y \in [0, 1, 2, 3]$. To describe two classes 0 and 1, a theory $h(\theta) = \theta^T X$ will be planned and edge classifier yield is $h(\theta(x))$ at 0.5. In the event that the value of speculation $h(\theta(x)) \geq 0.5$, it will foresee $y = 1$ which imply that the individual has coronary illness and on the off chance that estimation of $h(\theta(x)) < 0.5$, at that point anticipate $y = 0$ which shows that the individual is healthy. Hence, the expectation of strategic relapse under the condition $0 \leq h(\theta(x)) \leq 1$ is finished. Strategic relapse sigmoid capacity is frequently composed as follows:

$$h(\theta(x)) = g(\theta^T X),$$

where $g(z) = 1 / (1 + e^{-z})$ and

$$h(\theta(x)) = 1 / (1 + e^{-z}). \quad \text{eq. (1)}$$

(2) Support Vector Machine: The SVM is an AI characterization calculation which has been for the most part utilized for arrangement issues. Because of the high achievement of SVM in arrangement, different applications generally applied it. In a twofold characterization issue, the occurrences are isolated with a hyper plane $w^T x + b = 0$, where w and b are dimensional coefficient vectors, which are standard to the surface, b is adjusted a motivator from the earliest starting point stage, and x is enlightening assortment regards.

(3) Naive Bayes: The Naïve's Bayes is a grouping regulated learning calculation. It depends on restrictive likelihood hypothesis to decide the class of another component vector. The NB utilizes the preparation dataset to discover the restrictive likelihood esteem of vectors for a given class. In the wake processing the likelihood restrictive estimation of every vector, the new vectors class is made sense of dependent on its contingency likelihood. NB is utilized for content concerned issue characterization.

(4) Decision Tree Classifier: A Decision tree is an overseen AI computation. A Decision tree shape is just a tree where every handle is a leaf center point or decision center point. The techniques for the Decision tree are immediate and suitably reasonable for how to take the decision. A decision tree contained inside and outer focus focuses related with one another.

$$P(W/Q) = \frac{P(Q/W)P(W)}{P(Q)}$$

$$= \frac{P(Q/W)P(W)}{P(Q/W)P(W) + P(Q/M)P(M)}$$

$$P(A/B) = \frac{P(B/A)P(A)}{P(B)} \quad \text{eq. (2)}$$

(5) K-Nearest Neighbor: K-NN is an overseen learning game plan computation. K-NN estimation predicts the class name of another data; K-NN utilizes the correspondence of new commitment to its wellsprings of information tests in the readiness set. If the new data is same as the models in the arrangement set. The K-NN gathering execution isn't worthy. Let (x, y) be the readiness discernments and the learning limit h: X Y, with the objective that given recognition x, h(x) can choose y regard. The overall framework has been represented in figure 1.

III RESULTS

Thus, health disease which is the death cause all around the world can be reduced by the proper treatment and early diagnosis. This project deals with internet of things which helps to record the real time (patient) data using pulse rate sensor and arduino and is recorded using thing speak. Thus, machine learning algorithms were used to make prediction of heart disease in humans.



Figure 2 Pulse rate in bpm

Thus 40 sample data of patients were collected and is used for machine learning algorithms. I have mainly focused on algorithms such as support vector machine (SVM), K- Nearest Neighbors (KNN). classifier, decision tree, random forest classifier and naïve's bayes algorithm. after comparing all algorithms using real time. Hence, the

waveform in thing speak is obtained for pulse rate and body temperature are represented in figure 2 and figure 3.



Figure 3: Body Temperature in F

The observation of patient's data shows that support vector machine algorithms gives the greater accuracy and prediction. The results of the following algorithms are shown in Figure 4.

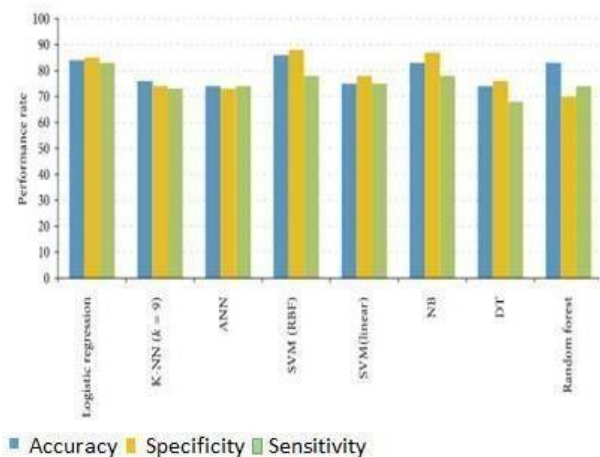


Figure 4: Comparison of all Algorithms

KNN algorithm – 75%
 Support Vector Machine – 86% Naïve Bayes – 83%

A	B	C	D
DATE AND TIME	PATIENT INFO	PULSE RATE (BPM)	BODY TEMP (F)
12/19/2019 at 11.00 A.M	Patient_Info	82	100
12/19/2019 at 11.15 A.M	Patient_Info	85	99
12/19/2019 at 11.25 A.M	Patient_Info	100	98
12/19/2019 at 11.33 A.M	Patient_Info	97	97
12/19/2019 at 11.47 A.M	Patient_Info	170	90
12/19/2019 at 12.04 P.M	Patient_Info	150	88
12/19/2019 at 12.13 P.M	Patient_Info	98	97
12/19/2019 at 12.33 P.M	Patient_Info	84	98
12/19/2019 at 03.04 P.M	Patient_Info	70	81
12/19/2019 at 03.17 P.M	Patient_Info	60	82
12/19/2019 at 03.38 P.M	Patient_Info	88	99

Figure 5: Data Obtained from Sensor
 Decision Tree – 74% Random Forest – 83%

Thus, support vector machine gives the highest rate of accuracy and prediction when compared to other algorithms.

IV CONCLUSIONS

Since coronary illness is that the principle purpose for death around the world. Human services field contains a tremendous measure of information, for handling those information certain methods are utilized. Handling or processing is one in all methods regularly utilized. Thus, this paper focuses on the real time data for more accurate prediction and accuracy using IOT & machine learning. The data is observed in the google sheet and further used in machine algorithms. So, I observed that when all algorithms are compared with each other, it is obtained that KNN algorithm gives 78% accuracy, support vector machine gives 86% accuracy, random forest classifier gives 83% accuracy, decision tree gives 74% accuracy and naïve's bayes gives 83% accuracy. Thus, support vector machine (SVM) gives highest accuracy when compared to all algorithms. The proposed hardware as well as software system helps patient to predict heart disease in early stages. It will be helpful for mass screening system in villages where hospital facilities are not available, i.e., rural areas.

REFERENCES

- [1] Monika Gandhi, Shailendra Narayan Singh, "Predictions in heart disease using techniques of data mining", In 2015 International Conference on Futuristic Trends on Computational Analysis and Knowledge Management (ABLAZE), pp. 520-525, IEEE 2015.
- [2] A.Rairikar, V. Kulkarni, V. Sabale, H. Kale, A. Lamgunde, "Heart disease prediction using data mining techniques", In 2017 International Conference on Intelligent Computing and Control (I2C2), pp. 1-8, 2017, IEEE, June 2017.
- [3] Santhana Krishnan J, Geetha S., "Prediction of Heart Disease Using Machine Learning Algorithms", In 2019 1st International Conference on Innovations in Information and Communication Technology (ICIICT), IEEE 2019.
- [4] Hlaudi Masethe, Mosima Masethe, "Prediction of Heart Disease using Classification Algorithms", pp. 11994-12000, IEEE 2009.
- [5] Z. Zhiao, Chnaowei, z. Nakdahira, "Healthcare application based on Internet of Things", Proc. IEET Int. ConfE. on Technolgy. Application, pp. 661-662, IEEE Nov. 2013.
- [6] Shiva Rama Krishnan, Subhash Chand Gupta, Tanupriya Choudhury, "An IoT based Patient Health Monitoring System", IEEE August 2018.
- [7] Aditi Gavhane ; Gouthami Kokkula ; Isha Pandya ; Prof. Kailas Devadkar, "Prediction of Heart Disease Using Machine Learning", In 2018 Second International Conference on Electronics, Communication and Aerospace Technology (ICECA), IEEE October 2018.
- [8] IoT", In 2017 International Conference on Big Data, IoT and Data Science (BID), IEEE April 2018.
- [9] Z. Zhiao, Chnaowei, z. Nakdahira, "Healthcare application based on Internet of Things", Proc. IEET Int. ConfE. on Technolgy. Application, pp. 661-662, Nov. 2013.
- [10] S. Pradeep Kumar, Vemuri Richard Ranjan Samson, U. Bharath Sai, P L S D. Malleswara Rao, K. Kedar Eswar, "From Smart Health Monitoring System of Patient Through IoT", International conference on I-SMAC, pp. 551-556, 2017.
- [11] S. Ananth, P. Sathya, P. Madhan Mohan, "Smart Health Monitoring System through IOT", In 2019 International Conference on Communication and Signal Processing (ICCSP), IEEE April 2019.
- [12] M.S. Uddin, J.B. Alam, S. Banu, "Real time patient monitoring system based on Internet of Things", 4th International Conference on Advances in Electrical Engineering, pp. 516-521, 2017.
- [13] R.T. Hameed, O.A. Mohamad, O.T. Hamid, N. Tãpuş, "Patient monitoring system based on e-health sensors and web services", 8th International Conference on Electronics Computers and Artificial Intelligence, pp. 1-6, 2016.
- [14] B. Priya, S. Rajendran, R. Bala, R. Gobbi, "Remote wireless health monitoring systems", Innovative Technologies in Intelligent Systems and Industrial Applications Monash, pp. 383-388, 2009.
- [15] Alvee Rahman, Tahsinur Rahman, Nawab Haider Ghani, Sazzad Hossain, Jia Uddin, "IoT Based Patient Monitoring System Using ECG Sensor", 2019 International Conference on Robotics, Electrical and Signal Processing Techniques (ICREST), february 2009..

2020 IEEE Sixth International Conference
on Bio signals, Images and
Instrumentation (ICBSII 2020)

SESSION II
RESEARCH PAPERS

A Deep Learning Approach on Segmentation of Bone for BMD Measurement from DEXA Scan Images

S.M.Nazia Fathima
Dept. of Electronics and
Communication Engineering,
Sethu Institute of
Technology,
Virudhunagar, India
naziafathimasm@gmail.com

R.Tamilselvi
Dept. of Electronics and
Communication Engineering,
Sethu Institute of
Technology,
Virudhunagar, India
tamilselvi@sethu.ac.in

M.Parisa Beham
Dept. of Electronics and
Communication Engineering,
Sethu Institute of
Technology,
Virudhunagar, India
parisaphd2011@gmail.com

A.Nagaraj
Dept. of Electronics and
Communication Engineering,
Sethu Institute of
Technology,
Virudhunagar, India
nagaraj.sa@gmail.com

Abstract— Osteoporosis is a silent disease which increases fracture risk condition in the body. The disease is noticed more in women, but can affect both men and women in all ages. The disease is alarmed by means of a parameter called Bone Mineral Density (BMD). BMD is estimated in both X-ray and DEXA images by means of various image processing algorithms and machine learning algorithms. Lot of literature also exists for the detection of osteoporosis condition. In recent years, deep learning methods show its face for the measurement of BMD. The paper focusses with the measurement of BMD and segmentation of bone region in DEXA image using U net architecture. The parameters used in the architecture shown better results in terms of Dice, F1 score.

Keywords—DEXA images, DEXSIT, U-net, Deep learning, Dice

I. INTRODUCTION

Loss in the strength of the bone results in a disease called as osteoporosis, which defines the porous nature of the bone. Porous nature of the bone is measured by a parameter called as Bone Mineral Density (BMD). The impacts are noticed in various developed countries like Europe, United States, India and other Asian Countries. The osteoporosis increases the fracture risk condition in both genders of people. But commonly it is noticed in women. Lot of methods are used to measure BMD and identify the osteoporosis condition. They are SPA (Single Photon Absorptiometry), DPA (Dual Photon Absorptiometry), SEXA (Single Energy X-ray Absorptiometry) were used to measure Bone Mineral Density (BMD). Currently, DEXA (Dual Energy X-ray Absorptiometry), QCT (Quantitative Computed Tomography), QUS (Quantitative Ultra Sound) and RA (Radiographic absorptiometry). Among these methods, DEXA is considered as a gold standard method for measuring BMD, but cost is very high compared with conventional methods. There are different manufacturers for DEXA machines. Osteoporosis may be detected in early stage and prevents fracture risk condition. In initial stages, measurement of BMD is done by image processing algorithms. Image processing involves lot of process like preprocessing, segmentation and BMD measurement. Unlike other diseases detection, still an effective algorithm is not proposed for measurement of BMD in DEXA images. Diagnostic approaches employs texture analysis of radiographs. but the selection of Region of Interest (ROI) is made manually by physicians. Segmentation by humans is a

long process for segmentation and Machine learning algorithms also didn't show its entire face for detection of osteoporosis condition. Manual segmentation involves human intervention for classification of bone condition. This leads to more false positives. With the development of algorithms based on deep learning, it helps in diagnosis of diseases more accurately than the traditional methods. Segmentation of ROI is crucial for the accurate diagnosis of disease. So there is a need to propose an accurate automatic segmentation methods for segmentation of bone region and improves the accuracy for calculation of Bone Mineral Density (BMD) [1].

Based on the above said issues, in this paper, a deep learning approach based on the U Net architecture is proposed for segmentation of the bone region from soft tissue, thereby to evaluate the value of BMD more efficiently, thereby to show that osteoporosis can be detected from the images. As there is no standard database to validate our algorithms for the measurement of BMD, our developed DEXSIT dataset is used, to train, validate and test the proposed method.

The organization of the paper is portrayed: few papers as existing literature in Section 2, proposed dataset and the details about the images are discussed in Section 3. U-NET architecture is discussed in Section 4. Training and testing stages, the results of the network are discussed in Section 5. Section 6 concludes the effectiveness of the architecture and the accuracy.

II. RELATED WORKS

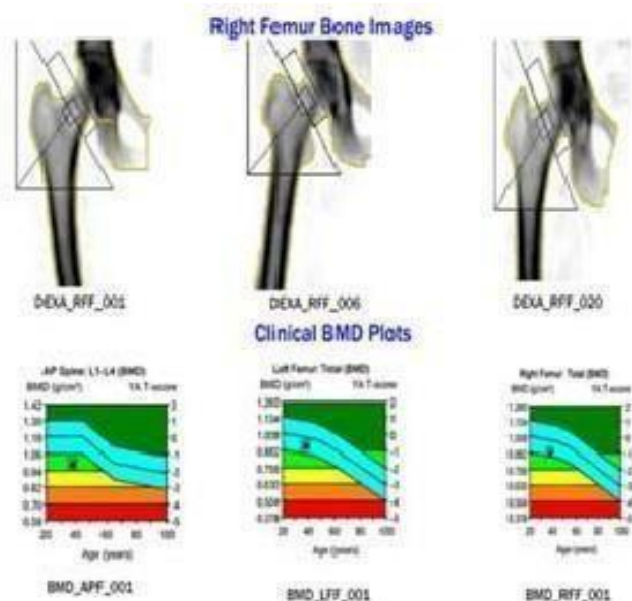
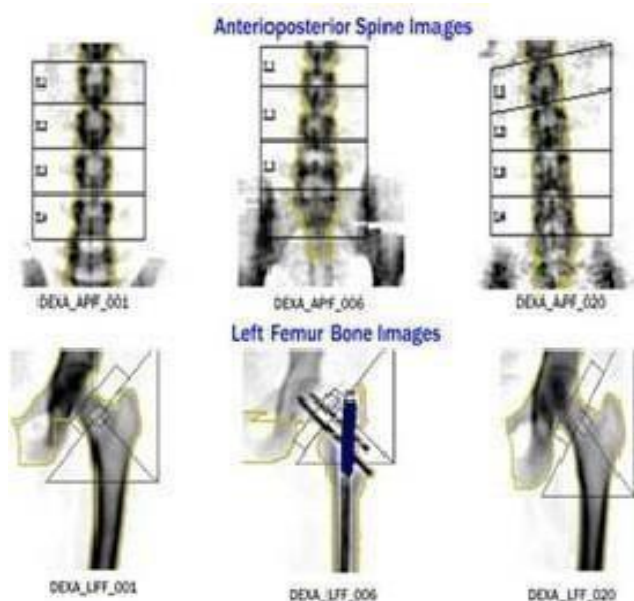
Segmentation and classification methods in DEXA images are a high end research in medical image processing. There are various research challenges exists in BMD measurement. Much previous work focuses on using classical image processing techniques. Machine learning had made a great impact in the medical field. Indeed, due to the large amount of information encoded in X-Ray and DEXA images, lot of solutions exist in determining bone fracture risk condition.

Arun Krishnaraj et al [2] analysed sagittal view of CT spine images using deep learning methods. Multiclass segmentation approach is based on cascaded two U-nets. Specificity, Sensitivity, and Accuracy of the networks are measured. The values for accuracy, Sensitivity and specificity for the detection of osteoporosis state or osteopenia state are 82% , 84.4% and 72.7%.

Steffen R ger et al [3] proposed deep convolutional neural networks (DCNNs) for the analysis of DEXA images. The proposed method involves detection of bone splinters in DEXA phantom images. 47 phantoms image dataset is used

The classification accuracy results with 90 % and

without 99 % bone splinters.



Li Chen et al [4] proposed a new parameter to measure the T score and Z-score and BMD based on the connectivity between the components. A scalar value is estimated which defines the connectivity between the components. The value calculates the T and Z values which defines the quality and intensity value. Dildar Hussain et al [5], proposed a method called Pixel Label Decision Tree (PLDT), which uses high and low energy features for segmentation procedure. The PLDT method is compared with various methods.

Nicolas Roussel [6], in his thesis explained image enhancement in terms of filters and among various filters, adaptive filter showed better signal to noise ratio. A deep convolutional neural network is used for the segmentation on DXA images. Even though a lot of works are there in BMD measurement for detection of osteoporosis condition, still lot of research challenges exists in the osteoporotic research. Based on the above research challenges, U net architecture is used for segmentation and measured BMD to detect the osteoporosis condition.

III. DATASET OVERVIEW

There is no proper dataset is publically available for the measurement of BMD and detection of osteoporosis condition. Thus we motivated and proposed two dataset DEXSIT and XSITRAY for the osteoporosis condition detection in DEXA images and X-Ray images. DEXSIT is a benchmark database, as to our knowledge no such database is available so far. The images in the annotated dataset are clearly with age, gender and a unique id for the subject along with the BMD plot. All the images are resized to 512 x 512.

A. DEXSIT Database

DEXSIT is a collection of DEXA images of three different regions. This database is collected from 42 subjects of

which 38 are female and 4 are male. There are total of 126 DEXA images. Samples images are shown in Fig.1.

IV. PROPOSED METHOD

The proposed method involves four important phases. Image enhancement, Data augmentation, U-net architecture for the segmentation of bone region to measure BMD and classification. The phases are shown in Fig.2.

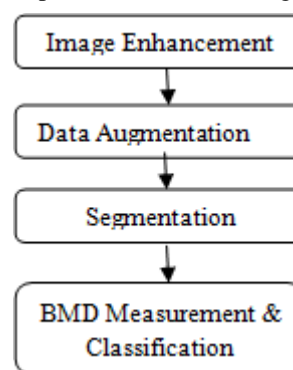


Fig.2 Phases involved in BMD measurement

A. Image Enhancement

Preprocessing involves enhancement of the images that is helpful for the further processing of the images. Preprocessing improves efficiency of the algorithm and reliability of the segmentation. Various filters are used for image enhancement and noise suppression. The best appropriate filter is chosen which is dependent on the value of Peak Signal to Noise Ratio (PSNR). PSNR value must be greater when applied to the Images. The higher PSNR value represents low noise level. Many filters like Gaussian filter, filter, shock filter, median filter were applied to the images

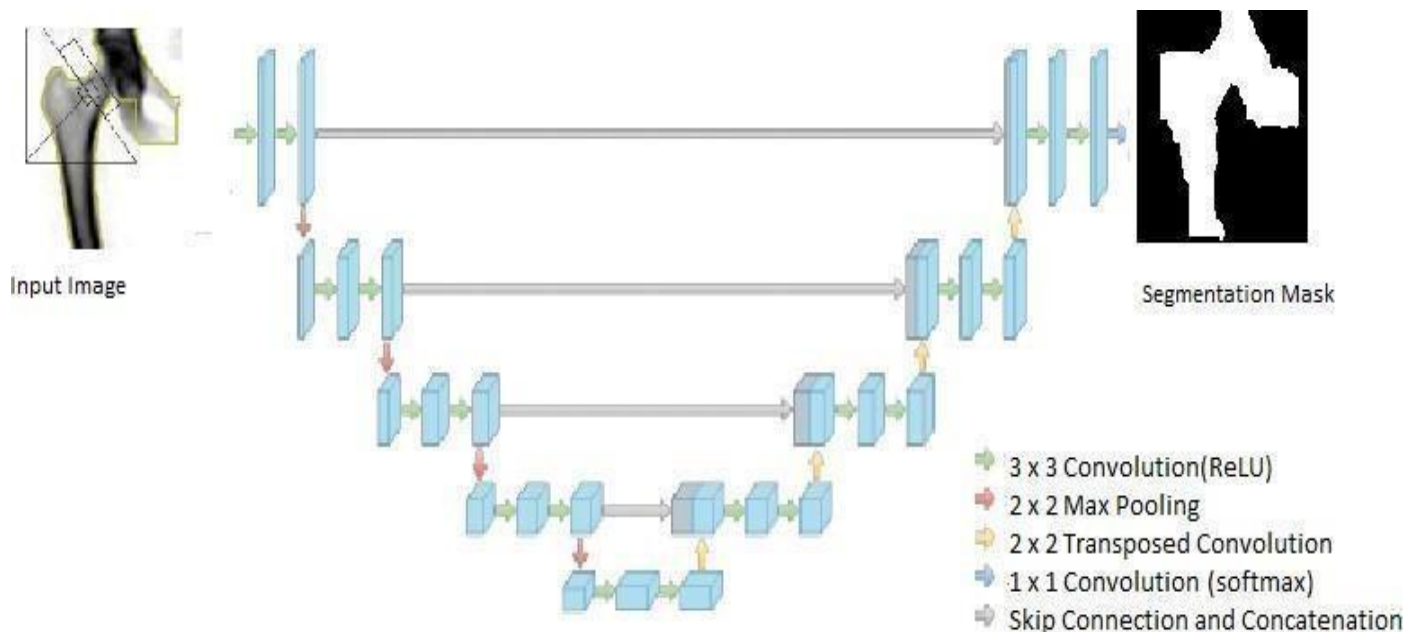


Fig.3 The U-NET Architecture

to get a clear image for segmentation in image processing[7]. In this proposed work, normalization is done to enhance the intensity of the images.

B. Data Augmentation

In deep learning concepts, data augmentation plays very major role to improve the accuracy in image segmentation. As in medical dataset, the collection of images is difficult and with few datasets better results need to be obtained, thus, data augmentation increases the size of dataset by creating different versions of images. After experimenting with a variety of filters, for generating realistic augmented images, all the images are rotated at various degrees. The images are either horizontally flipped or vertically flipped. Also shear transformation are performed over the images with the range of 0.5.

C. U-Net Architecture

U-net architecture is used for segmentation. U-Net is a Fully Convolutional Network (FCN) that does image segmentation which predicts each pixel's class. It works with very few training images yet generates more precise segmentations. The network architecture is demonstrated in Figure 3. The architecture has two paths namely contraction path and expansion path. The contraction path is also known as encoder that captures the features from the image. Encoder consists of convolutional and max pooling layers. A continuous two 3x3 convolution operations is involved. Then one max pooling operation with the pooling size of 2x2 and stride of 2 is used. The expansion path is also known as decoder. Decoder upsamples the feature map by a 2x2 transposed convolutions. Then sequence of two 3x3 convolution operation is done. The sequence is repeated four times. At halves the number of filters in each stage. At

the end, one 1x1 convolution operation is performed to generate the final segmentation map. All the convolution layer in the architecture uses ReLU (Rectified Linear Unit) activation function, but the final convolutional layer uses a softmax activation function. Later, these feature maps are linked with the output of the up sampling operation, which is passed on to succeeding layers. He-normal weight initialization method is used to initialize the convolution kernel weights.

1) Training

The U net architecture model is trained based on the input images and its ground truth images after augmentation process. Numbers of images are increased because of augmentation procedure. After augmentation, 326 images were used for training. For testing and validation rest of the images are divided equally.

The output of the softmax layer from the CNN defines a loss function. The loss function reduces the error between the actual and prior defined images. For the proposed work, a negative log-probability of a target label is defined.

V. RESULTS & DISCUSSION

A. Evaluation

The performance of U-NET architecture is evaluated using Dice, DSC metric, also known as F1-score, Jaccard similarity and IOU (Intersection over Union). The network performance is evaluated by the above said parameters. The bone segmentation using U net architecture shows the F1 score of 0.97 during training and 0.90 during testing phase. The images in the left column are the original images. It is managed to locate the boundary and segment the bone region accurately. Figure 4 shows the input image, ground Truth image, predicted output and the original output for sample set of images. The values of evaluation of metrics of segmentation n results of DEXA images are given in Table.1.

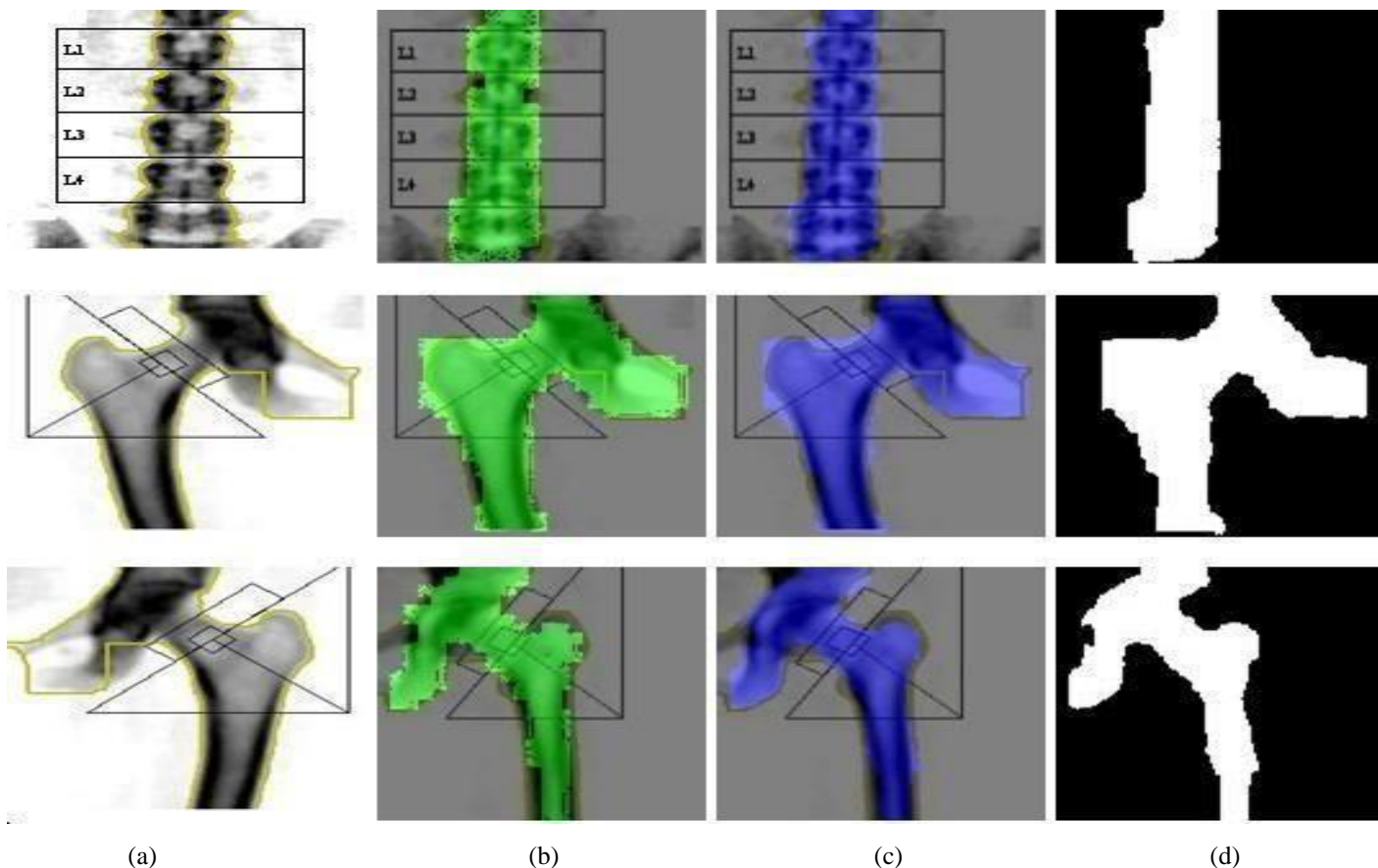


Fig.4. (a) Sample Input Image (b) Ground Truth image (c) Predicted Image (d) Segmented Image

B. BMD Measurement

After segmentation, BMD is measured to classify the risk condition of the bone. A mathematical model is defined to measure BMD from the segmented image. Using Bone Mineral Content (BMC) and standard deviation [8], BMD is measured. From the BMD, T-score value is calculated to detect the fracture risk condition; T-Score of the Sample images along with the clinical report is shown in Table 2.

TABLE 1. OUTPUT PARAMETERS BASED ON U NET ARCHITECTURE FOR DEXA IMAGES

Parameters	Training	Validation
Number of images	323	139
Dice	0.939312	0.941328728
Jaccard Index	0.88585975	0.889623967
F1 Score	0.9746632	0.9030798
IOU	0.97026689	0.904197299

TABLE 2. T-SCORE OF THE SAMPLE IMAGES ALONG WITH THE CLINICAL REPORT

Sample Images	rated score	T-	Clinical T-score
Image 1	1.1		1.3
Image 2	1.2		1.24
Image 3	0.8		0.7
Image 4	0.9		0.9
Image 5	1		1

VI. CONCLUSION

No previous works has been done on DEXA images with deep learning approach for segmentation of bone and non-bone regions. Automatic image segmentation is performed using the deep convolutional neural network is used in the proposed work. Thus, overcomes the limitations of earlier methods such as histogram threshold algorithms and fuzzy c-means (FCM). Proposed method reduces the processing time and improves accuracy, with limited datasets. With U-Net architecture we obtained more accurate results in less amount of time compared to manual and semiautomatic segmentation. The network is trained on a

dataset of DEXA images consisting of 126 images, artificially augmented to generate more training images of DXA images. Evaluating the network performance we find F1 score of 0.97, with an IOU of 0.97, for DEXA images. Hence, this work helps to diagnose osteoporosis more accurately with better improved segmentation.

REFERENCES

- [1] S.M.Nazia Fathima, R.Tamilselvi and M.Parisa Beham, "Estimation of t-score and BMD values from X-ray images for detection of osteoporosis", ACM Digital Library, 2019.
- [2]. Arun Krishnaraj, Spencer Barrett, Orna Bregman-Amitai, Michael Cohen-Sfady, Amir Bar, David Chetrit, Mila Orlovsky, dad Elnekave, "Simulating Dual-Energy X-Ray Absorptiometry in CT Using Deep- Learning Segmentation Cascade", J Am Coll Radiol 2019.
- [3] Steffen Rüger, Markus Firsching, Julija Lucic, Alexander Ennen, Norman Uhlmann, and Thomas Wittenberg, "Automated detection of bone splinters in DEXA phantoms using deep neural networks", Current Directions in Biomedical Engineering , Volume::5, Issue:1,pp.281–284, 2019.
- [4] Li Chen and V. B. Surya Prasath, "Measuring Bone Density Connectivity Using Dual Energy X-Ray Absorptiometry Images", International Journal of Fuzzy Logic and Intelligent Systems, Volume: 17, Issue: 4, pp. 235-244, December2017.
- [5]. Dildar Hussain, Mugahed A. Al-antari, Mohammed A. Al-masni, Seung-Moo Han* and Tae-Seong Kim, "Femur segmentation in DXA imaging using a machine learning decision tree", Journal of X-Ray Science and Technology,2018.
- [6]. Nicolas Roussel "Denoising of Dual Energy X-ray Absorptiometry Images and Vertebra Segmentation", thesis Stockholm, Sweden 2018.
- [7]. S.M.Nazia Fathima, R.Tamilselvi and M.Parisa Beham, "Comparison of Various Filters on Dexa Images", Proceedings of ETICT 18, 2018.
- [8]. S.M.Nazia Fathima, R.Tamilselvi and M.Parisa Beham, "Evaluation of Fracture Risk Condition using Bone Mineral Content and Standard Deviation", International Journal of Innovative Technology and Exploring Engineering (IJITEE)ISSN:, Volume-8 Issue-8, 2278-3075, June, 2019.

MAMMSIT: A Database For The diagnosis and detection of Breast Cancer in Mammography images

M. Parisa Beham
Department of
ECE

Sethu Institute of
Technology
kariapatti,India
parisaphd2011@g.mail.com

N. Kayalvizhi
Department of
ECE

Sethu Institute
of Technology
kariapatti,India
kayalvizhi@sethu.a.c.in

R.Tamilselvi
Department of
ECE

Sethu Institute of
Technology
kariapatti,India
tamilselvi@sethu.a.c.in

A. Nagaraj
Department of

ECE
Sethu Institute of
Technology kariapatti,India
nagaraj.sa@gmail.com

Abstract

In recent days Mammography is most widely used techniques to detect the Breast cancer. Masses and calcifications are the abnormalities indicate the breast cancer. Breast cancer is the leading cause of cancer deaths in women. Advanced technologies with existing imaging modalities improve breast cancer screening. Most of the Mammographic image data sets are not easily available. The Mammographic Image Analysis Society (MIAS) and Digital Database for Screening Mammography (DDSM) are the most easily available data set for Mammographic images. MAMMSIT is another data set for the mammographic image analysis. The mammogram data set is named as MAMMSIT and it contains Normal and Malignant group images of mammography. Our proposed data set provided with appropriate annotations details such as age, background tissue, ultra sound screen position (i.e., left and right) and BIRADS level are included in the database.

Keywords: Mammogram, Database, Malignant, Mammographic images.

I. INTRODUCTION

In the medical image processing filed, specialized methods such as Mammography is used to visualize the low X-ray system of breasts. Breast cancer is the leading cause of cancer deaths in women. In Recent medical technology field Mammograms takes an very important role and also supports for early detection and diagnosis of breast cancer. Mammography is adapted for screening or for diagnostic purposes. Screening mammography is one of methods used to detect breast changes in women who have no signs or symptoms or new breast abnormalities.

At the age of 40, every women must undergo mammogram test atleast once in a year [2]. Image compression method of mammogram imaging, breasts is compressed between two firm surfaces to spread out the breast tissue. Reviewed by a doctor who looks for symptoms of cancer using an X- ray captures black-and-white images of breasts that are displayed on a computer screen. The objective is to detect cancer before clinical signs are markable. In diagnostic mammography method is analyzing suspicious breast changes such as breast pain, an unusual skin appearance, nipple thickening or nipple

discharge. It's also used to find out abnormal images on a screening mammogram. In additional mammogram images are appending to the diagnostic mammogram. Breast cancer detection and diagnosis is currently questioning method of digital mammography. Separation of image acquisition and image display method using the development of imaging modality and it's allowing examination of both.

A mammogram of white area occurs on lump or tumor. Tumors can be cancerous or benign. If a tumor is benign, it is not a health risk and is unlikely to grow or change shape. Most tumors found in the breasts are non-cancerous. Small white specks are usually harmless. Sometimes occurring symptoms of cancer; the radiologist will check their finding areas of white, high density tissue, shape and pattern. A mammogram can also give person information about character of back ground tissue such as Fatty, Fatty - glandular, dense -glandular. The higher risk of breast cancer has a dense breast. Abnormalities of classes in dense breast on mammogram finding are very difficult. If a person has had breast cancer, Mammograms are still possible surgery or implants. However, it may be necessary to take more images of each breast, and it might take longer to check the images [1].

In imaging science, image processing is any form of signal processing for which an image as an input, such as a photograph or video and the output of image processing may be either an image or a set of characteristics or parameters related to the image [3]. In medical image processing system mammographic images are processed and it's used to convert an image signal, either digital or analog, converted into a physical image. As a result, very suitable differences between abnormal and normal but dense tissue can be made more obvious.

There are few Mammogram databases are publically available such as Digital Database for Screening Mammography (DDSM) ,DDSM data base contains 10480 image files in LJPEG format ,more than available all other databases[5][8] . LJPEG format is a non-standard version of the free format DDSM and finding the regions of interest of each image. Mammographic Image Analysis Society Digital Mammogram Database (MIAS) database consists of low quality 8 bit 320 mammogram images and compare among those databases required a greater

variety of images with different spatial and contrast resolutions. Computer Assisted Library for Mammography (CALMa)[6] and LLNL/UCSF database [7] consists of 3000 and 198 respectively.

Inspired by the above issues, in this work we proposed to build a database of mammography scan images which we named it as ‘MAMMSIT Database’, for the benefit of biomedical engineering research community. The important pitfall in the research and development of this community is that, unavailability of clinical interpretation. In the creation of database our key contributions in this work are:

- Create a new MAMMSIT database, involves 398 (normal and malignant) mammogram scan images.
- Present the annotation for the entire 398 subject’s biological data.
- Provide clinical report as per WHO standard with suggestions of the health care provider.

III. MAMMSIT DATABASE

The MAMMSIT database is deliberated through subsequent stages:

- 1) Structure Details
- 2) Labeling the Images
- 3) Classifications

TABLE I. BIRADS SCORE

BIRADS (in Lesion)	Status
0	Incomplete
I	Negative
II	benign findings
III	probably benign
IV	suspicious abnormality
V	highly suspicious of malignancy
VI	known biopsy with proven malignancy

A. Structure Details

MAMMSIT dataset involves 398 mammogram scan images collected from various subjects. Each subject includes reference number, age, background tissue, abnormality classes and abnormality of severity in

scan images. The samples of mammogram normal scan images of two subjects are shown in Figure. 1. Similarly, the samples mammogram and malignant images of 5 subjects are shown in Figure. 2. Table 1 shows the interpretation of malignant images.

B. Labeling the Images

In this proposed database of all the images are labelled perfectly for the ease understanding and interpretation for researchers. From the label itself one can easily identify the reference number, background tissue. For each subject, two samples are obtained viz., left screen image and right screen image. For example, labeling of left and right mammography scan image is given as MAMMSIT-L-001.jpg for a subject ID 001 and MAMMSIT-R-004.jpg for a subject ID 004 respectively. Here, in the first case MAMM refers to mammography scan image, 001L is the subject reference number of left screen image. In the next case 004R is the subject reference number of right screen image.

The list of annotations provided in the MAMMSIT database is as follows:

1. Database reference number
2. Age
3. Character of background tissue: F: Fatty
G: Fatty-glandular D: Dense-glandular
3. Classes of abnormality present as CALC: Calcification
CIRC : Well-defined/circumscribed masses
SPIC : Speculated masses MISC : Other, ill-defined masses
ARCH : Architectural distortion ASYM : Asymmetry
NORM : Normal
4. Severity of abnormality
5. BIRADS (Breast Imaging Reporting and Data System) score

C. Classifications

The MAMMSIT dataset is classified into two types: Normal and Malignant. The classification performance was analyzed by using the complete set of abnormality presents report classified the following character presents in background tissue are calcification, well-defined circumscribed masses, speculated masses, ill-defined masses, architectural distortion, and asymmetry.

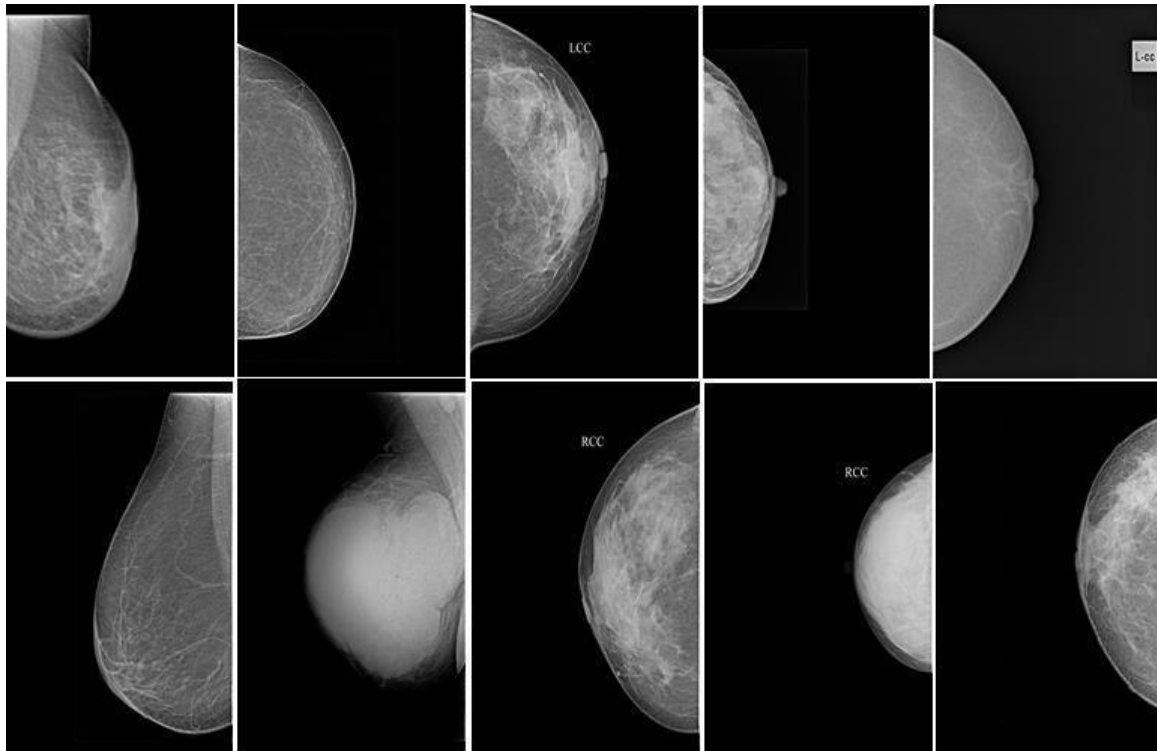


FIGURE 1. SAMPLES OF NORMAL AND ABNORMAL IMAGES

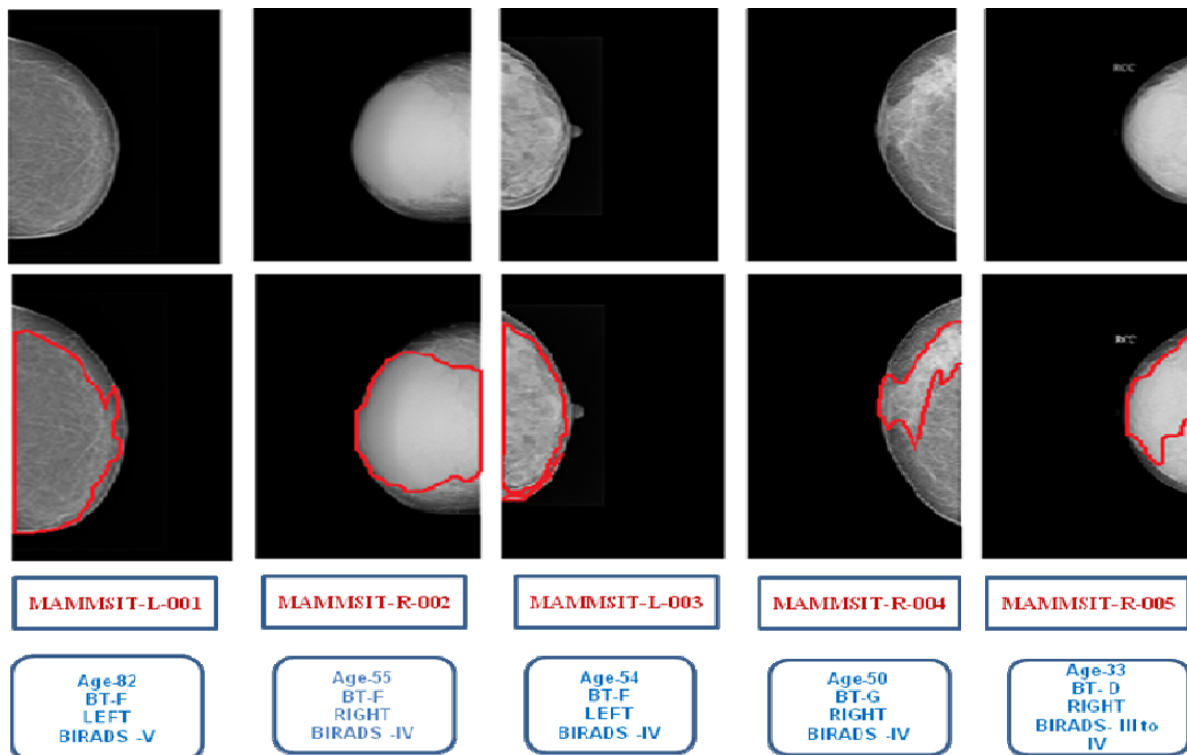


FIGURE 2. SAMPLES OF MALIGNANT IMAGES WITH GROUND TRUTH AND ANNOTATION

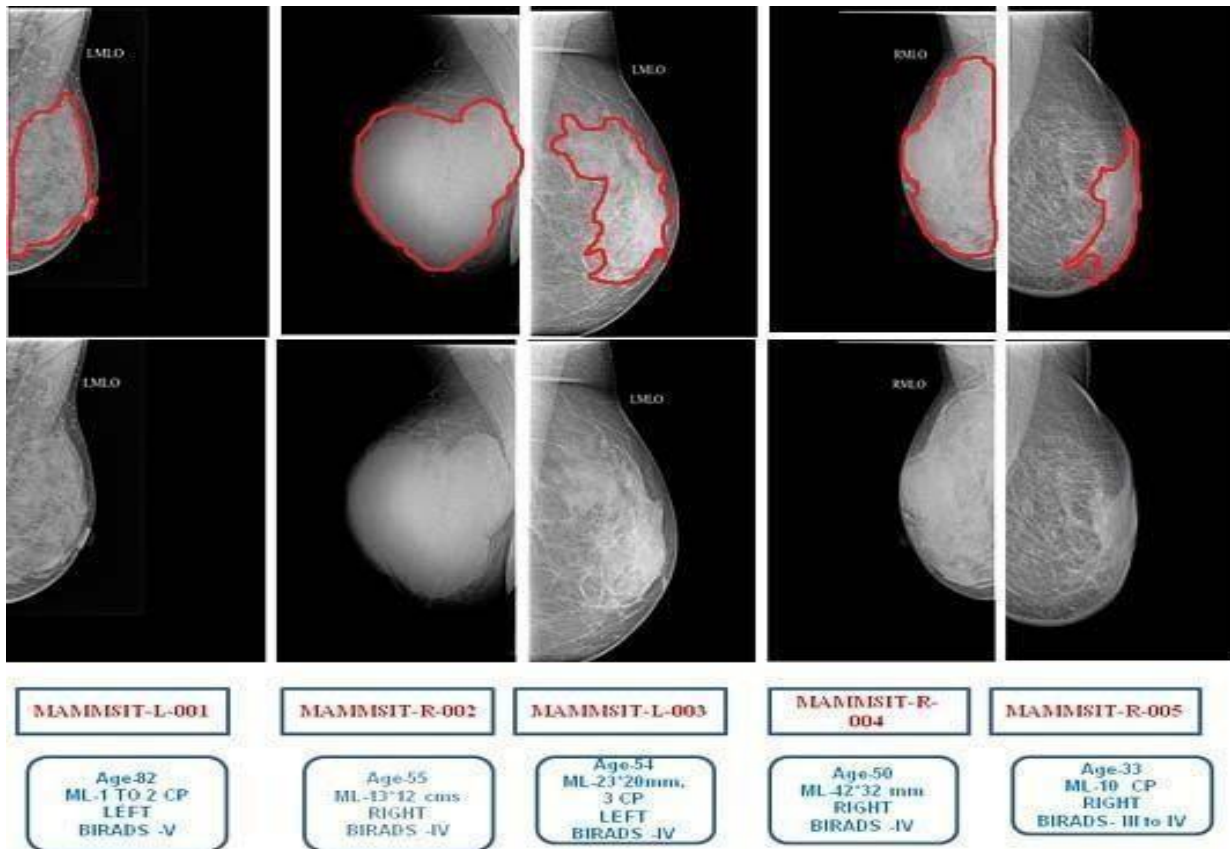


FIGURE 3. SAMPLES OF MALIGNANT IMAGES WITH GROUND TRUTH AND ANNOTATION BASED ON CLOCK POSITION

TABLE.2. CLASSIFICATION DETAILS OF MALIGNANT IMAGES

Ref. No	BT	Classes of abnormality	AGE	Malignant	BIRAD S
MAMMSIT-L-001	F	NORM	82	L	V
MAMMSIT-R-002	F	NORM	55	R	IV
MAMMSIT-L-003	F	ASYM	54	L	IV
MAMMSIT-R-004	D	CALC	50	R	IV
MAMMSIT-R-005	G	ARCH	33	R	III to IV

BIRADS classifications method is very useful in monitoring breast cancer treatment and supporting breast cancer research again by making statistics easier to calculate using BIRADS score as shown in Table 1. Figure 1 shows the sample normal and abnormal mammography images of 10 subjects. Figure 2 shows samples of malignant images with ground truth and annotation. Figure 3 depicts the samples of malignant images with ground truth and annotation based on clock position/mass lesions. Table 2 represents the examples of five subjects with the respective classification details.

III. CONCLUSION

The paper describes recent database for Screening Mammography. It acts as a resource of mammogram image analysis researchers. The database now contains substantial numbers of “normal” and “malignant” cases. The main characteristics of this MAMMSIT database are a) 398 mammogram images

b) Marking the entire subject’s biological data. By providing this database available to the biomedical research community, we hope to promote the analysis of many uncertain problems.

ACKNOWLEDGEMENT

The authors thank to Dr. Rajkumar, Radiologist, Government Hospital, Ramnad, India for his help and suggestions in building this database. The authors also immensely thank Dr. Ilayaraja Venkatachalam, Radiologist, Pixel Scans, Trichirappalli, India for providing images with all clinical interpretation to create this database.

ETHICAL APPROVAL

The mammogram database used in this paper is provided by Pixel scans, Trichy. The ethical committee of Pixel scans has reviewed and approved to conduct research using this mammogram database and publish papers based on the results using those biomedical images.

REFERENCES

- [1] Syed Jamal Safdar Gardezi Ahmed Elazab , “Breast Cancer Detection and Diagnosis Using Mammographic Data: Systematic Review”, Journal of medical internet research , Vol.21,No 7,2019
- [2] Giger “ML: Machine Learning in Medical Imaging.” J Am Coll Radiol 15(3 Pt B),pp:512–520,2018
- [3] Karin Dembrower , Peter Lindholm , Fredrik Strand “A Multi- million Mammography Image Dataset and Population-Based Screening Cohort for the Training and Evaluation of Deep Neural Networks the Cohort of Screen-Aged Women”, Journal of Digital Imaging ,ISSN: 0897-1889
- [4] Bruno Roberto ,Nepomuceno Matheus, and Homero Schiabel “Online Mammographic Images Database for Development and Comparison of CAD Schemes” Journal of Digital Imaging, Vol 24, No 3 (June), 2011: pp500-506.
- [5] Heath M, et al: The digital database for screening mammography. Proceedings of the Fifth International Workshop on Digital Mammography, 2001, pp 212–218
- [6] Amendolia SR, et al: The CALMA project. Nucl Instrum Methods Phys Res, Sect A, Accel Spectrom Detect Assoc Equip 461(1-3):428–429,2001
- [7] Lawrence Livermore National Library/UCSF Digital Mammogram Database. Centre for Health Care Technologies Livermore. Livermore, CA, USA
- 8) Kallergi M: Computer-aided diagnosis of mammographic microcalcification clusters. Med Phys 31(2):314–326,2004

Shape Description of FDG uptakes in Pre and Postoperative fused PET/CT Images

J. Angelin Jeba
Department of ECE,
Anna University, CEG Campus,
Chennai-600025, Tamilnadu, India.
E-mail: jebaangelin@gmail.com

S. Nirmala Devi
Department of ECE,
Anna University, CEG Campus,
Chennai-600025, Tamilnadu, India.
E-mail:nirmala_1969@hotmail.com.

Abstract— Automatic object recognition with shape descriptors help to interact with the real-time environment. This paper describes the shape analysis of radioactivity Fluoro Deoxy Glucose (FDG) uptakes present in pre and postoperative stages of Fused PET/CT images using shape feature extraction approach. Shape features are invariant to various affine transformations such as translation, rotational, flipped, scale, etc., are more robust for shape analysis. Geometrical properties of the FDG uptakes are extracted at various levels of spatial resolution by hierarchical Ka abstraction from the segmented PET/CT images. Rotational invariants considered are the Zernike moments magnitudes and the shape signatures of Fourier descriptors are investigated. The discrimination power of features between pre and post-operative images is examined and evaluated.

Keywords— Shape descriptor, Geometric Moment Invariant, Rotational Invariants, Shape signatures, Zernike descriptor

I. INTRODUCTION

Medical imaging plays an important role in clinical events and their applications include preoperative planning, diagnosis, radiotherapy treatment, surgical guidance, and postoperative assessment [1]. The requirement for functional characterization of diseases leads to the advancement of Positron Emission Tomography (PET) scanners. The multimodality technique of combining PET with Computerized Tomography (CT) or Magnetic Resonance Imaging (MRI) utilizes the biological and structural capability of imaging. This provides higher accuracy, sensitivity, robustness, and specificity than realizable with a single modality examination [2]. Even though the sensitivity and specificity of FDG-PET images are higher than the structural images such as CT or MRI, the PET images have low resolution as its limitations. Hence for diagnosis purposes, PET image depends on information about anatomy from another modality for localizing the FDG uptake regions [3].

Positron Emission Tomography / Computerized Tomography (PET/CT) fusion is a multimodality imaging technology that combines both the metabolic information of PET and spatial information of CT. PET/CT fusion imaging is capable to detect the disease with accurate staging at an earlier stage of diagnosis. It is also helpful in localizing even small areas of FDG radiotracer activity which is not possible with a single modality diagnosis. Fused PET/CT imaging has its wide applications in treatment planning, staging, therapy follow-up, and diagnosis of disease in the field of oncology [4].

The shape is a visual feature prominent for region or boundary based analysis of an image. Shape descriptors are of two types such as contour based shape descriptors, and region

based shape descriptors. The shape based object recognition with moment invariants is the task in computer vision for detecting and examining the objects in images. In medical images, it leads to complex problems due to variations in pose, occlusion, scaling, poor illuminations, rotations, etc., [5]. Hence, the descriptor should be capable to express the information residing on the shape boundary and also the inside region. The whole pixels of the FDG uptakes are included for the assessment of progression between pre and postoperative stages.

The organization of the paper is: Section II briefs the previous study related to this work, Section III deals with the shape descriptors applied for region based analysis, Section IV discusses the experimental setup and results, and Section V deals with the conclusion, and future enhancement.

II. RELATED WORKS

Shape description is an efficient method to describe the content of an image since the shape is the prominent feature of an image. Boundary based and region based descriptors were the two different shape descriptors investigated by the authors in the literature. Boundary based descriptors are not suited for complex shapes that include disjoint regions. Hu in [6] derived the geometric invariant moments to describe the Region Of Interest (ROI). Region based moment descriptors are reliable since they include the pixels inside the region along with the boundary pixels. Lo et al. [7] investigated the geometric moment invariants with group-theoretic technique and complex moments. Suk et al. in [8] considered the affine transformation and specified the method to eliminate dependent and reducible invariants by extracting moment invariants with graphs. Various types of moments such as regular moments, Zernike moments, Legendre moments, complex moments, and pseudo-Zernike moments were stated by Teh et al. in [9]. These moment features are widely used for shape description, reconstruction, and image compression.

This work aims to define the shape of an object thereby to perform the analysis at pre and post-operative stages comparatively. The automatic comparative analysis is clinically important to analyze the progression of the disease during the intermediate stages. In this paper, we have discussed the geometric invariant moments, stepwise recursive decomposition, rotational Zernike invariant moments and shape signatures for the segmented fused PET/CT images.

III. SHAPE DESCRIPTORS

The shape analysis using region based descriptors related to moments that are invariant under transformation is elaborated in this paper.

A. Geometric Invariant Moment

The Geometric Moment (GM) Descriptors is a technique widely used in shape recognition that is based on moment invariants representation of shape and similarity measure. Regular moment invariants are the numerical feature defined from the probability theory, and the algebraic invariants to describe the image [10, 11]. The features generated using the GM technique are Rotation Scale Translation (RST) invariants. In an image, the gray level values of each pixel represent as $f(x,y)$, with size $M \times N$, the $(p+q)$ th order of geometric moment in a discrete domain is given in equation 1.

$$m_{pq} = \sum_{x=1}^M \sum_{y=1}^N x^p y^q f(x, y) \quad (1)$$

Where, $f(x,y)$ gives the pixel value at x^{th} row and y^{th} column of the gray level image. The extracted moments describe the characteristics of the ROI in an image. It is affected by coordinate transformation [11]. Thus, the center moment for an image at $(p+q)$ th order is defined as,

$$\mu_{pq} = \sum_{x=1}^M \sum_{y=1}^N (x-x_0)^p (y-y_0)^q f(x, y) \quad (2)$$

Where, the center of the image x_0, y_0 is defined by,

$$\begin{aligned} x_0 &= \mu_{10} / \mu_{00} \\ y_0 &= \mu_{01} / \mu_{00} \end{aligned} \quad (3)$$

The normalized center moment of an image at $(p+q)$ th order is given by

$$\eta_{pq} = \mu_{pq} / \mu_{00}^{1+(p+q)/2} \quad (4)$$

The normalized center moment η_{pq} are translational and scaled invariants, but do not possess rotational invariant property. The set of moment invariants obtained by Hu considering the translational invariance, scaled invariance, and rotational invariance. The features are obtained by the linear combination of lower order normalized center moments. The equations obtained are:

$$\begin{aligned} N1: & \eta_{20} + \eta_{02} \\ N2: & (\eta_{20} - \eta_{02})^2 + 4\eta_{11}^2 \\ N3: & (\eta_{30} - 3\eta_{12})^2 + (3\eta_{21} - \eta_{03})^2 \\ N4: & (\eta_{30} + \eta_{12})^2 + (\eta_{21} + \eta_{03})^2 \\ N5: & (\eta_{30} - 3\eta_{12})(\eta_{21} + \eta_{03}) \left[(\eta_{30} + \eta_{12})^2 - 3(\eta_{21} + \eta_{03})^2 \right] + \\ & (3\eta_{21} - \eta_{03})(\eta_{30} + \eta_{12}) \left[3(\eta_{30} + \eta_{12})^2 - (\eta_{21} + \eta_{03})^2 \right] \\ N6: & (\eta_{30} - \eta_{03}) \left[(\eta_{30} + \eta_{12})^2 - (\eta_{21} + \eta_{03})^2 \right] + \\ & 4\eta_{11}(\eta_{30} + \eta_{12})(\eta_{21} + \eta_{03}) \\ N7: & (3\eta_{21} - \eta_{03})(\eta_{30} + \eta_{12}) \left[(\eta_{30} + \eta_{12})^2 - 3(\eta_{21} + \eta_{03})^2 \right] + \\ & (\eta_{30} - \eta_{03})(\eta_{21} + \eta_{03}) \left[3(\eta_{30} + \eta_{12})^2 - (\eta_{21} + \eta_{03})^2 \right] \end{aligned} \quad (5)$$

B. K_d Decomposition

The K_d creates an abstraction by dividing the data according to the shape of the region contained in the binary image. This method corresponds to the decomposition of the image successively into quadrants blocks considering its complexity. If the sub-image is not homogeneous, then it is further decomposed into four equal sized sub-images. The processes are repeated until all the sub-images blocks are homogeneous [12]. The difference between the maximum value, and the minimum value of the block elements are calculated. If the value is greater than its threshold, then the sub-image is said to be homogeneous. The coordinates of the centroids at the particular level yields a feature vector that evaluates the image similarity using a distance metric formula.

Recursive Subdivision Method [13] for a binary image is explained in the following steps,

- The function calculates the x coordinates of an image.
- The function decomposes the image into two using the calculated coordinates and step 1 is repeated.
- The output vector is these coordinates and it is of length $2d-1$.

The problem of empty sub-images is removed entirely, with K_d decomposition so that at each level the region is divided equally between 2 sub-images based on K_d -tree splitting strategy. The complexity of an image is computed by calculating the homogenous number of blocks at every level.

Distance Metric

The Euclidean distance between two normalized feature vectors p_i^j and q_i^j in K level decomposition is calculated. The distance metric is measured as,

$$d(p, q) = \sqrt{\sum_{j=1}^{n(c(j))} \sum_{i=1}^2 (p_i^j - q_i^j)^2} \quad (6)$$

The normalized distance metric is given as,

$$d(p, q) = \frac{1}{\sqrt{\frac{n(c(j))}{n} \sum_{j=1}^2 (p_i^j - q_i^j)^2 \sum_{k=1}^n c(k)}} \quad (7)$$

There is $c(k)$ number of components at the K^{th} level. As we increase the level of image decomposition, we extract increasingly higher resolution feature but it is likely to be affected by noise or distortion than 6th level features. So, the normalized metrics that give decreasing precedence to successive levels of the features were considered. It applies equal weighting to each level of decomposition [14], i.e. in this case, each level of features is normalized between 0 and $1/k$, where k is the depth of decomposition.

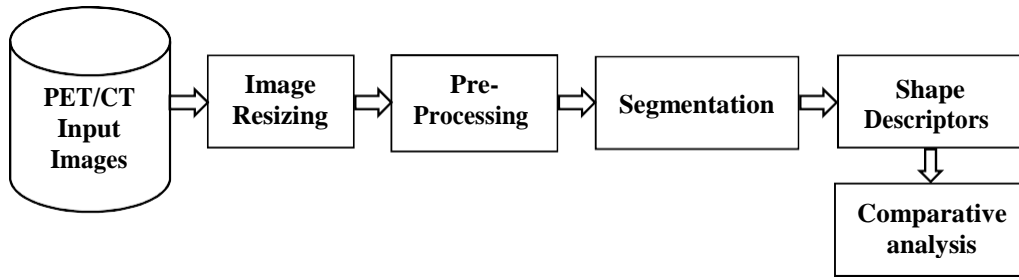


Fig. 1. Block Diagram of the Experimental Setup.

C. Zernike Moment

Zernike moments describe the magnitudes that exhibit the rotational invariance property defined in the polar domain. Zernike basis functions determine the complete orthogonal set inside the unit circle.

$$x^2 + y^2 = 1 \quad (8)$$

The complex Zernike polynomials are represented in Cartesian coordinates as $V_{nm}(x, y)$ and in polar coordinates as $V_{nm}(\rho, \theta)$. The polynomial is decomposed into the product of a radial polynomial $R_{nm}(\rho)$, and phase term $e^{-im\theta}$ depending on the value of θ .

$$V_{nm}(\rho, \theta) = R_{nm}(\rho) e^{-im\theta} = R_{nm}(\rho) e^{-im\theta}$$

The Zernike moment of an image is given by,

$$A_{nm} = \frac{n+1}{\pi} \sum_{x,y} V_{nm}(\rho, \theta) f(x, y) \quad (10)$$

The phases of Zernike moments are the rotational angle estimates that computes the representation for an object directionally [15]. The Zernike moments magnitudes are invariant to the changes in image rotation [15, 16]. Let φ_{nm} denotes the phase/argument of the complex Zernike moment A_{nm} , and φ_{nm}^α denotes the phase rotated counterclockwise by an angle α , then the equation follows

$$\varphi_{nm}^\alpha = \varphi_{nm} - m\alpha$$

The compatible representation of the phase can capture object shape that exhibits the variation directionally. Directional information of the object in an image is useful for applications like shape analysis, image compression, and textural analysis.

Shape Signatures

Shape signatures are the one-dimensional function derived from the circumference coordinates of the shape. The shape signature acquires the persistent features of the shape of an object [17, 18]. Centroid distance function, Complex coordinates, tangent angle, curvature function, chord length function, area function, and triangle-area representation are frequently used as shape signatures. Signatures describe the shape all alone since it is rotational and translational invariant.

Shape signatures are very sensitive to changes that exist in the boundary because it leads to matching errors [18].

IV. EXPERIMENTAL RESULTS

Preoperative and Postoperative stages of fused PET/CT images at different planes such as coronal, axial, and sagittal are considered for experimentation. The images with uptakes acquired from different regions such as lungs, breast, bone, liver, etc., are collected from the imaging center. Fig. 1 shows the block diagram of the shape recognition process. The input images are resized to the resolution of 227 x 227. It is then preprocessed in order to remove the artifacts present. The images are filtered and contrast enhanced in HSI space to remove the additive Gaussian noise. The performance results of which are evaluated in [19]. Then, the image segmentation is carried out using a hybrid kernelization of the graph cut partitioning algorithm. The segmented results are evaluated and compared in [20]. The segmentation is followed by shape analysis using region based descriptors. The segmented image saved in .jpeg format is the input to the system.

A. Shape analysis

Shape based features such as area, irregularity, circularity, Shape Index (SI), and perimeter are extracted from the segmented regions of the image. Circularity is the two dimensional feature measure of an object's shape resemblance to that of the circle. Circularity indicates the shape's large-scale features than its corners and edges sharpness or its surface roughness alternatively. A smooth ellipse has low circularity if the eccentricity is large. Regular polygons with sharp edges increase their circularity value with increasing numbers of sides. Irregularity is the feature measure of irregular shape. The area of the region in an image corresponds to the number of pixels including the boundary region of the segmented or extracted image. The perimeter of the segmented region is described as the pixels count in the boundaryline of the region. Shape Index [21] is a quantitative statistical measure of the shape in a particular unit of area. It can be expressed as

$$SI = 1.27 * A * L \quad (12)$$

Where A is the area of the shape and L is the length of the longest axis in the region. If the value is 1.0, it is of maximum compaction and the shape is circular. If the shape is elongated, then the compaction of the slope is less and results in a lower value of SI. The shape features showing the progression

between the preoperative and postoperative stages are shown in Table I.

TABLE I
SHAPE FEATURES SHOWING PROGRESSION

Shape Features	Coronal view		Sagittal view		Axial view	
	Pre	Post	Pre	Post	Pre	Post
Perimeter	116.592	330.005	60.926	243.87	138.532	140.651
Area	862	3333	253	2134	914	1297
Solidities	0.950	0.922	0.923	0.955	0.847	0.928
Circularities	1.255	1.381	1.168	1.143	1.923	1.214
Centroid	175.425	183.306	146.016	154.467	133.000	142.993
Bounding Box	154.500	142.000	136.500	127.500	128.000	120.500
Major Axis	45.025	61.564	19.611	52.187	48.302	46.006
Minor Axis	25.080	48.389	17.282	41.518	26.080	37.336
Eccentricity	0.5570	0.587	0.8810	0.670	0.540	0.812
Roundness	0.7969	0.791	0.8560	0.875	0.520	0.824

B. Geometric Moment Descriptors

The segmented images are feature extracted to describe the shape geometrically. The geometric moments invariant are the features of order $n=7$ generated for the pre and post-operative images at all the planes. The scaling and translational moment feature vector for $n=7$ is described in Table II

TABLE II
GEOMETRIC MOMENT INVARIANTS

Order	Coronal view		Sagittal view		Axial view	
	Pre	Post	Pre	Post	Pre	Post
N1	0.6015	0.5192	0.5787	0.5495	0.7998	0.6708
N2	0.0041	0.0109	0.0104	0.0101	0.0099	0.0088
N3	0.0117	0.0025	0.0004	0.0004	0.0003	0.0019
N4	0.0044	0.0007	0.0005	0.0001	0.0064	0.0155
N5	0.0000	0.0000	-0.0000	0.0000	0.0000	0.0001
N6	0.0001	0.0001	0.0000	-0.0000	-0.0003	0.0013
N7	-0.0000	0.0000	0.0000	-0.0000	-0.0000	-0.0003

C. Rotational Moment Invariants

The image is mapped onto a unit disc, and the desired value of 'n' order moments computes the real and imaginary parts of the Zernike moment using Radial polynomials. The Zernike

rotational moments upto order $n=4$ for the repeated values of m are tabulated in Table III. The rotational invariants are the phase features at different angle points A_{nm} of the segmented region is tabulated in Table IV. The rotational invariant phase features for order $n=4$ are calculated as follows:

$$\begin{aligned}
 \phi_1 &= A_{11} \\
 \phi_2 &= A_{21} * A_{12} \\
 \phi_3 &= (A_{20} * A_{12})^2 \\
 \phi_4 &= (A_{30} * A_{12})^3 \\
 \phi_5 &= A_{22} \\
 \phi_6 &= (A_{31} * A_{12})^2 \\
 \phi_7 &= (A_{40} * A_{12})^4
 \end{aligned} \tag{13}$$

TABLE III
ROTATIONAL MOMENTS UPTO N=4

Order n	A_{nm}
1	A_{11}, A_{12}
2	A_{20}, A_{21}, A_{22}
3	A_{30}, A_{31}
4	A_{40}

D. Successive K_d tree Decomposition for $k=6$ levels

For six levels of K_d tree decomposition performed on the extracted binary image of size 227×227 total of 124 features are obtained. These feature vectors are used to calculate the distance between the preoperative and postoperative images at all planes. The calculated distance for the images considered in this paper are given below:

For Coronal plane, $d = 7.415$

For Sagittal plane, $d = 16.013$

For Axial plane, $d = 0.031$

The segmented image and its K level decomposition along with its shape signatures for all the three reference planes at pre and postoperative stages are shown in Fig. 2 and Fig. 3 respectively. For the axial plane, the progression of the tumor between stages is less and hence the calculated difference between the centroid points is less. When the progression is severe then the comparative distance between stages is high.

TABLE IV
ROTATIONAL INVARIANT MOMENTS

Angle Points	Coronal view		Sagittal view		Axial view	
	Preoperative	Postoperative	Preoperative	Postoperative	Preoperative	Postoperative
ϕ_1	0.5333	0.9645	1.1374	1.0814	1.7542	1.6809
ϕ_2	0.3138	0.1734	0.3713	0.2674	1.2395	0.6497
ϕ_3	0.2686-0.0051j	0.1361-0.0001j	0.3451-0.0003j	0.2357+0.0070j	1.8183-0.0466j	0.9319-0.0711j
ϕ_4	0.0950-0.0092j	0.0287-0.0008j	0.1351-0.0015j	0.0695+0.0002j	1.5486-0.0253j	0.4376-0.0278j
ϕ_5	2.1055	1.6733	2.3556	2.0860	5.4742	4.7438
ϕ_6	0.5897-0.0098j	0.2576+0.0028j	0.7789+0.0147j	0.4950+0.0162j	6.1027-0.1630j	2.7849-0.2232j
ϕ_7	0.1336-0.0034j	0.0315+0.0021j	0.2050+0.0101j	0.0927+0.0077j	5.5359-0.3193j	1.3426-0.2290j

Image Plane	Input Image	Segmented Image	Binary Image	K=6 Decomposition	Shape Signatures
Coronal					
Sagittal					
Axial					

Fig. 2. Pre-Operative fused PET/CT image shape description at allplanes.

Image Plane	Input Image	Segmented Image	Binary Image	K=6 Decomposition	Shape Signatures
Coronal					
Sagittal					
Axial					

Fig. 3. Post-Operative fused PET/CT image shape description at allplanes.

V. CONCLUSION

This paper explains the shape description for the comparison of FDG uptakes at pre and post-operative stages in fused PET/CT images. The shape features such as centroid, perimeter, circularity, eccentricity, bounding box, and area are extracted from the segmented image. The centroid points are used for the extraction of geometric invariant moments and rotational invariant Zernike moments. The shape signature describes the one dimensional Fourier description of the segmented image. The x coordinates of the segmented image are investigated using K_d tree decomposition for six levels and comparative distance between the pre and post-operative stages is attained. The obtained shape features can be used to classify the distribution of FDG uptakes in the future.

REFERENCES

- [1] J. B. Antoine Maintz and Max A. Viergever, "A survey of medical image registration," *Medical Image Analysis* volume 2, number 1, pp 1–36 Oxford University Press at Elsevier journal, 1998.
- [2] Brent Foster, UlasBagci n, AwaisMansoor, Ziyue Xu, and Daniel J. Mollura. "A review on segmentation of positron emission tomography images," *Computers in Biology and Medicine* 50, an Elsevier Journal, pp 76–96, 2014.
- [3] S. Basu, T. Kwee, S. Surti, E. Akin, D. Yoo, and A. Alavi, "Fundamentals of PET and PET/CT imaging," *Ann. NY Acad. Sci.* 1228 (1) pp 1–18, 2011.
- [4] David Jakobsson, Fredrik Olofsson, Anders Ericsson, and Johan Karlsson, "Decision Support System for Lung Cancer using PET/CT Images," Lung Institute of Technology Andreas Jarund, WeAidU in Europe AB7th October 2004.
- [5] Raja Tanveer Iqbal, Costin Barbu, and Fred Petry, "Fuzzy component based object detection," *International Journal of Approximate reasoning* 45(3), an Elsevier Journal, pp 545-563, 2007.
- [6] Hu, M.K., "Visual pattern recognition by moments invariants," *IRE Trans. Information Theory* (8) pp 179- 87,1962.
- [7] C.-H. Lo, and H.-S. Don, "3-D moment forms: their construction and application to object identification and positioning," *IEEE Trans. Pattern Anal. Machine Intell.* 11, pp 1053–1064,1989.
- [8] T. Suk, and J. Flusser, "Graph method for generating affine moment invariants," *The 17th International Conference on Pattern Recognition*, Cambridge, UK, pp 192–195, 2004.
- [9] C.-H. Teh, and R.T. Chin, "On image analysis by the methods of moments," *IEEE Trans. Pattern Anal. Mach. Intell.* 10, pp 496–513, 1988.
- [10] Zhongliang Fu, Liang Fan, IZhiqiang Yu, and Kaichun Zhou, "A Moment- Based Shape Similarity Measurement for Areal Entities in Geographical Vector Data," *International Journal of Geo-Information* 7(6):208, pp 1- 19, 2018
- [11] Mohamed Rizon, Haniza Yazid, Puteh Saad, Ali Yeon Md Shakaff, Abdul Rahman Saad, Mohd Rozailan Mamat, Sazali Yaacob, Hazri Desa and M. Karthigayan, "Object Detection using Geometric Invariant Moment," *American Journal of Applied Sciences* 2 (6): pp 1876-1878,2006.
- [12] A. Sexton, A. Todman, and K. Woodward, "Font recognition using shape- based quad-tree and kd-tree decomposition," In *Proceedings of the Joint Conference on Information Sciences*, volume 5, pages212–215,2000.
- [13] Georgios Vamvakas, Basilis Gatos, and Stavros J. Perantonis, "Handwritten character recognition through two-stageforeground sub- sampling," *Pattern Recognition*, 43(8) pp 2807–2816,2010.
- [14] Sh.Tseng, Zh.Yang, W.Huang, Ch.Liu and Y.Lin, "Object feature extraction for Image Retrieval based on Quadtree segmented Blocks," *csie*, vol. 6, pp.401-405, 2009.
- [15] Naveen Kumar, Adam C. Lammert, Brendan Englot, Franz S. Hover, and Shrikanth S. Narayanan, "Directional Descriptors Using Zernike Moment Phases For Object Orientation Estimation In Underwater Sonar Images," *IEEE conference - ICASSP*, PP 1025 -1028,2011.
- [16] Khotanzad, A., and Y.H. Hong, "Invariant image recognition by zernike moments," *IEEE Trans. Pattern Analysis and Machine Intelligence*, 12: 489-497,1990.
- [17] Pooja Gudodagi, Dr. Jagadeesh. Pujari, and Prof. J. C. Karur, "Analysis of Shape Signature Using Centroid based Local Features," *International Journal of Engineering Research & Technology (IJERT)*, pp 1-4, 2018.
- [18] Vittoria Bruni, Lorenzo Della Cioppa, and Domenico Vitulano, "An entropy-based approach for shape description," *26th European Signal Processing Conference (EUSIPCO)* pp 608 -612, 2018.
- [19] J.Angelin Jeba and S.Nirmala Devi, "Performance Evaluation of Contrast Enhancement Technique for PET-CT Images in HSI Color Space," *Advances in Engineering Research (AER)*, vol. 142, pp.222 226, Feb 2018.
- [20] J.Angelin Jeba and S.Nirmala Devi, "Efficient graph cut optimization using hybrid kernel functions for segmentation of FDG uptakes in fused PET/CT images," *Applied Soft Computing* 85, an Elsevier Journal, pp 1- 10,2019.
- [21] Sun Hyung Kim, Vladimir Fonov, D. Louis Collins, Guido Gerig, The IBIS Network, and Martin A. Styner, "Shape index distribution based local surface complexity applied to the human cortex," *Proc SPIE Int Soc Opt Eng.*, pp 1-11,2015.

BRAMSIT: A Database for Brain Tumor Diagnosis and Detection

R.Tamilselvi
Department of
ECE Sethu
Institute of
Technology
kariapatti,India
tamilselvi@sethu.
ac.in

A.Nagaraj
Department of
ECE Sethu
Institute of
Technology
kariapatti,India
nagaraj.sa@gmail
.com

M. Parisa Beham
Department of ECE
Sethu Institute of
Technology
kariapatti,India
parisaphd2011@
gmail.com

M.Bharkavi Sandhiya
Department of ECE
Sethu Institute of
Technology
kariapatti,India

Abstract

MRI is the most frequently used imaging technique to detect brain tumor. The brain is composed of nerve cells and supportive tissues such as glial cells and meninges. A brain tumor is a collection, or mass, of the brain in abnormal cells. Primary brain tumors can be either malignant or benign . A primary brain tumor is a tumor located in the brain tissue. New technologies in supplement to existing imaging modalities improve brain tumor screening. Most brain tumor databases are not publicly available. BRAMSIT is a resource for possible use by the MRI image analysis research community. The projected MRI database is a termed BRAMSIT, characterized by an attempt to offer a group of normal and malignant brain tumor images. The details such as age, and the MRI axial position (i.e., trans-axial, coronal and sagittal) of the patient are interpreted in the database.

Keywords: Brain tumor, Database, Malignant, Benign

I. INTRODUCTION AND RELATED WORKS

Brain tumor is a life- threatening disease. Brain tumors can be malignant or benign. When tumor cells grow it cause pressure inside the skull, this leads to brain damage. Two types of Brain tumor namely Primary and secondary. Primary brain tumors are benign and that are originates in brain. Secondary brain tumors occur when cancer cells spread over the brain from other organ such as lung or breast. It is also called as metastatic brain tumor. Brain tumor can be occurred in any ages. If brain tumor detected early stage it is treatable. Brain tumor cause more death in children and adults under the age of 40 than any other cancer. In India the tumors ranges from 5 to 10 per 100,000 populations with an increasing trend.

Diagnosing brain tumor is a tedious process. Computer Tomography scan (CT scan), Magnetic Resonance Imaging(MRI), tests like an Angiogram, Spinal tab and Biopsy are used to diagnosis brain tumors. CT scan uses x-ray to produce images. CT scan expose patients to ionizing radiation .High radiation are involved in CT scan . A new study in the Journal of the National Cancer Institute suggests that CT scans, commonly used in medical imaging, may increase the risk of brain tumors.

Magnetic Resonance Imaging (MRI) plays an important role in the medical era. It is noninvasive method to detect Brain tumor. MRI uses Magnetic field and Radio waves to produce Brain images. MRIs create more detailed pictures than CT scans. MRI is the preferred screening examination for brain tumor. The goal is to detect brain tumor before clinical signs are noticeable. The size of the tumor can be measured by MRI. A special dye called contrast medium is injected into the patient's vein or given as a pill or fluid to swallow before an MRI scan.

Any area with abnormal tissue can cause for cancer. The abnormalities will be examined by radiologist. A focused white area on MRI can be a lump or tumor. Tumors can be cancerous or benign. If a tumor is benign, it is not a risky and is unlikely to grow or change shape. The radiologist will check its shape and pattern, as they can sometimes be a sign of cancer.

Medical image processing system used to process MRI images. Image processing converting physical image into equivalent digital image and extract the details from the digital image. Image processing is any form of signal processing in which input as an image like photograph or video and the output may be either an image or a set of characteristics or parameters related to the image. As a result, very suitable differences between abnormal and normal but dense tissue can be made more obvious. BRAMSIT images need to be combined with a regular database of young bud researchers to accurately examine the clinical results of the images.

In order to detect tumors and validate the results, a few databases available publically and help the research community to come up with better algorithms. Among those BRATS dataset, Fig share and kaggle plays a major role with huge image dataset. Fig share[5] consisting of 3064 T1-weighted contrast-enhanced images with three kinds of brain tumor such as normal, benign and malignant. The images can be down loaded along with their ground truth images in BLACK & WHITE (BW) format. The dataset consists of tumor mask, tumor border, and original image in .MAT file. The space occupied by the database is more. Some of the sample dataset images are shown in Figure 1

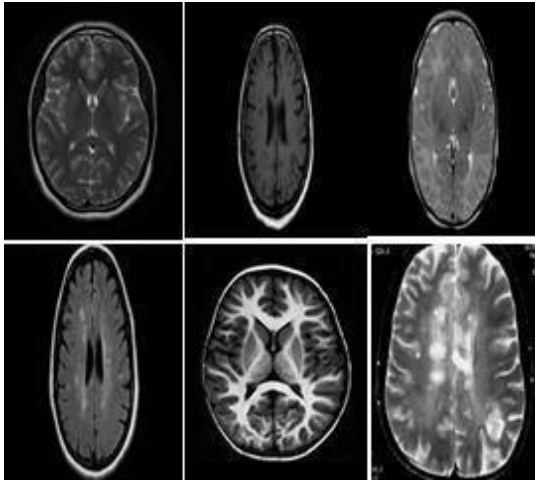


Fig.1. Sample Figshare Dataset Images along with its ground truth Images[5]

Brats dataset[6] is a dataset used for many researchers for their work. The numbers of images along with their ground truth are . The images consist of normal benign and malignant images. Lot of versions exist in Brats dataset. All the proposed algorithms for tumor detection in various survey papers are normally validated in BRATS dataset only. Figure 2 shows the sample Dataset images.

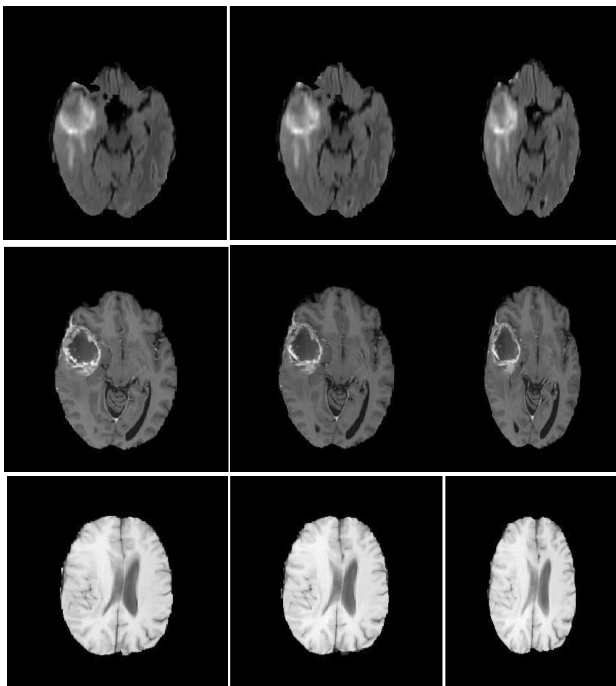


Fig.2. Sample Brats Dataset Images and its ground truth Images[6] Kaggle dataset [7] involves the images for brain tumor detection. It is developed by Navoneel Chakrabarty in the year 2019. These datasets involves original images only. Few images are available for analysis. samples are An example of images from Kaggle dataset are shown in Figure 3.

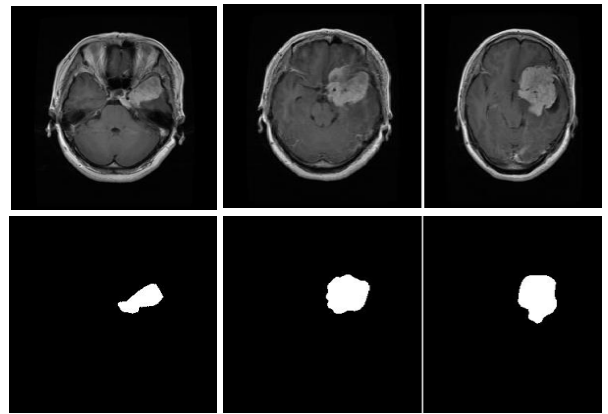


Fig.3. Sample Kaggle Dataset Images[7]

In [1], the authors discussed about the method to produce local volumes of the tumor databases. The authors analyzed numerical and quality parameter of the images using changes in morphological variations. In [2], the authors discussed a new method with a large number of CNNs with the information in overlapping regions. The authors used the OASIS dataset for validation of the results. V.P.Gladis Pushpa Rathi et al[3] proposed a tumor classification method based on feature extraction, features selection, PCA analysis and LDA analysis. The classification accuracy for the proposed method is 98.87%. The authors Amit Kumar Rohit et al.,[4], discussed a single query system based on Content Based Image Retrieval System(CBIR).The proposed system involves preprocessing, feature extraction and detection of tumors. The accuracy of the proposed method is 98.33%. Based on above said survey, many of the works still didn't follow a simple user friendly and accessible database. In this work, we proposed to create a database of MRI scan images, which we named as 'BRAMSIT Database' for the benefit of the biomedical engineering research community. An important risk in the research and development of this community is the lack of medical explanation and the plane for the tumor identification. Although some relevant papers have discussed localization issues, they do not provide such databases friendly to researchers.

Thus motivated by these factors, our main contributions in this work are:

- Create a new BRAMSIT database which involves 319 MRI scan images along with its ground truth images.
- Present the annotation of all the 319 subject's biological data along with their axial position

II. BRAMSIT DATABASE

The BRAMSITdatabase is deliberated through subsequent stages:

- 1) Structure Details along with their axial position
- 2) Labelling the Images
- 3) ManualAnnotation

These are explained step by step

A. Structure Details

This dataset involves of 319 MRI scan images collected from various subjects. BRAMSIT consist of 319 images of different subjects. Each subjects includes reference number, age and their axial. The samples of BRAMSIT normal scan images of some subjects are shown in Figure 4. Similarly, the samples MRI abnormal and ground truth images of 5 subjects are shown in Figure 5.

The salient features of the database are:

- Creation of database along with its clinic statistics for better use of images for research.
- Abnormal Images with the Ground truth for easy classification.

The sample images along with the ground truth images are used for better segmentation and classification. All the ground truth images are developed from the experts opinion.

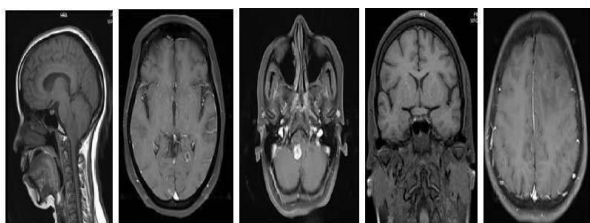


FIGURE 4 SAMPLE OF MRI NORMAL SCAN IMAGES

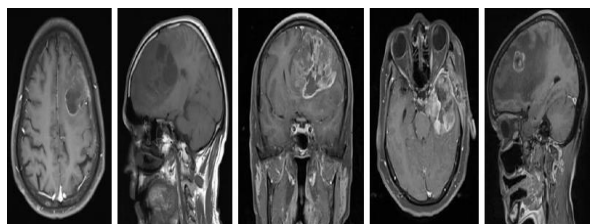


FIGURE 5 SAMPLE OF MRI ABNORMAL SCAN IMAGES

B. Labelling the Images

In the proposed database all the images are labeled perfectly for the purpose of understanding and interpreting. From the label itself one can easily identify the Subject ID, age and axial position. For example for a image with any abnormality suspect, the images are taken in three planes such as Sagittal, Transaxial, and coronal View or Transaxial, Coronal and Sagittal View or Coronal, Sagittal View and Transaxial view. Based on that, some abnormal suspected images are three in number based on their plane. Some normal images are single image with single view. Considering these factors,

if Sub1 has three view images then it is labelled as Sub_1_STC, Sub_1_TCS, Sub_1_CST. This indicates subject1's STC means Sagittal, Transaxial, and coronal View, Sub_1_TCS means subject1's Transaxial, Coronal and Sagittal View and Sub_1_CST means subject1's Coronal, Sagittal View and Transaxial view. In normal cases, the images are labelled as Sub_2_N_TCS, Sub_2_N_STC and Sub_2_N_CST view.

TABLE 1. DETAILS OF THE SUBJECT IN THE DATABASE.

Ref.No	Age	Gender	Axial
Sub_1_TCS	40	Male	Transaxial
Sub_2_STC	51	Male	Sagittal
Sub_2_CTS	51	Male	Coronal
Sub_3_TCS	55	Female	Trans axial
Sub_4_STC	58	Female	Sagittal

C. Manual Annotation

BRAMSIT provides a detailed analysis of each and every MRI scan image. Each MRI scan images for the following attributes we manually annotated.

- Unique ID of the subject- Based on the axial Position
- Age
- Axial position –Transaxial, Sagittal and Coronal
- Gender- Male or Female

From the database, the table 1 shows the details of the images. The manual annotation is represented below: The age of the subject, gender, subject Id and the axial position is annotated. A sample subject shown in the annotation box below. Sample MRI images and the ground truth images are shown in Figure.6.

Age:40
Gender: Male
Id: Sub_1_TCS
Tru>Cor>Sag_2

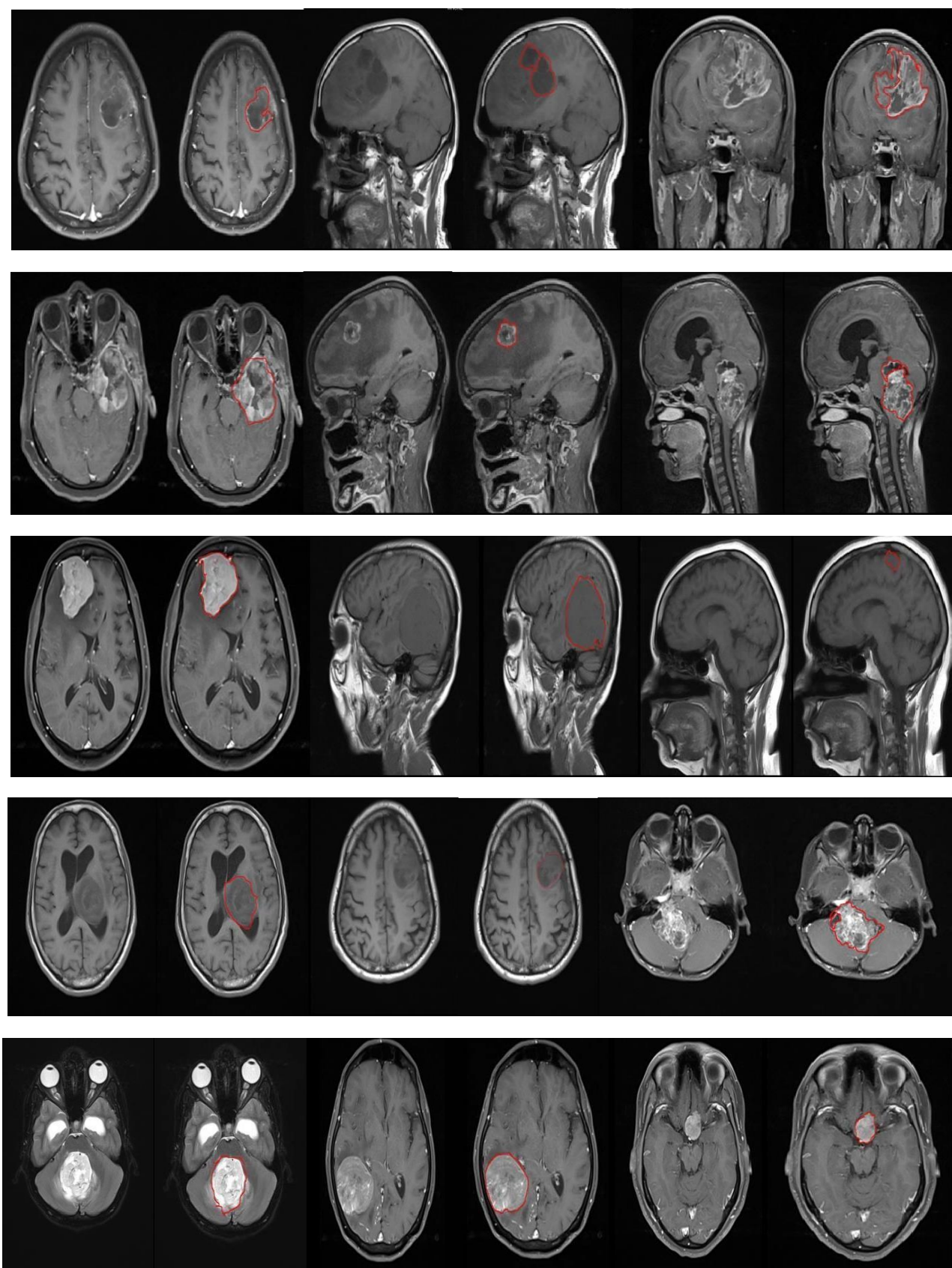


FIGURE 6. SAMPLE OF MRI ABNORMAL SCAN IMAGES AND THEIR GROUND TRUTH IMAGES

III. COMPLEXITY OF THE DATABASE

As said earlier, many databases are there for analysis of brain tumor in MRI imaging modality. As this dataset is also created for the same research outcome when compared with the other databases, one main feature of the proposed dataset is the ease of access and the speed in processing or analysis of the images. When compared with the BRATS dataset, Figshare and Kaggle, the proposed BRAMSIT processing time and accessing time is very less during some benchmark image processing algorithms.

TABLE.2. ACCESS TIME AND PROCESSING TIME FOR VARIOUS DATASET AND PROPOSED BRAMSIT DATABASE

S.No	Dataset	AccessTime	Processing Time
1	BRATS	2.35ms	4.2ms
2	Figshare	2.01ms	3.52ms
3	Kaggle	2.45ms	3.87ms
4	BRAMSIT	0.2ns	1.5ns

As shown in table 2, the access time and processing time for the proposed dataset is very less when compared with other datasets.

IV. CONCLUSION

The paper describes Screening Brain Tumor for the most recent database. Investigating brain tumor image analysis by using it as a resource. The "abnormal" and "ground truth" images. The main characteristics of this BRAMSIT database are a) 319 MRI images b) Marking the entire subjects biological data. The biomedical research community provides the brain tumor of many uncertain research problems.

REFERENCES

- [1] Alexandre Guimondy, Gérard Subsol, Jean-Philippe Thirion, "Automatic MRI Database Exploration and Applications", International Journal on Pattern Recognition and Artificial Intelligence, Volume 11, number 8, December 1997.
- [2] Pierrick Coupé, Boris Mansencal, Michaël Clément, Rémi Giraud, Baudouin Denis de Senneville, Vinh-Thong Ta, Vincent Lepetit and José V. Manjon, "AssemblyNet: A Novel Deep Decision-Making Process for Whole Brain MRI Segmentation", arXiv:1906.01862.
- [3] V.P.Gladis Pushpa Rathi and Dr.S.Palani, "Brain Tumor MRI Image Classification With Feature Selection and Extraction Using Linear Discriminant Analysis", International Journal of Information Sciences and Techniques (IJIST) Vol.2, No.4, July 2012.
- [4] Amit Kumar Rohit, N. G. Chitaliya "Novel Approach for Content based MRI Brain Image Retrieval", International Journal of Soft Computing and Engineering (IJSCE) ISSN: 2231-2307, Volume-4, No. 3 July 2014.
- [5] Pareek, Meenakshi & Jha, CK & Mukherjee, Saurabh & Joshi, Chandani, "Brain Tumor Detection Using Watershed Segmentation Techniques and Area Calculation", International Journal of Informatics and Communication Technology (IJ-ICT). Vol.7, No.71, pp71-76, 2018.

[6] Shaoguo Cui, Lei Mao, Jingfeng Jiang, Chang Liu, and Shuyu Xiong "Automatic Semantic Segmentation of Brain Gliomas from MR Images Using a Deep Cascaded Neural Network", Journal of Healthcare Engineering, 2018.

[7] Chakrabarty, Navoneel, "Brain MRI Images for Brain Tumor Detection", <https://www.kaggle.com/navoneel/brain-mri-images-for-brain-tumor-detection>, 2019.

Molecular Docking Analysis Of CFTR Inhibitors

M.Brindha
Junior Research Fellow,
Department of Instrumentation
& Control Engineering,NIT,
Trichy, Tamilnadu
yatra.kumar@gmail.com

R. Shelishiyah
Assistant Professor,
Biomedical Engineering
Department, Vel Tech
Chennai, Tamilnadu
shelishiyah.raymond@gma il.com

S. Vasanthavalli
Biomedical Engineer, Adayar Cancer
Institute,
Chennai, Tamilnadu
vasanthavalli186@gmail.com

Abstract— Lung inflammations is the phenotypic exhibition of Cystic Fibrosis (CF) - a genetic disease of the secretory glands which mainly affecting respiratory, digestive and urogenital system. Although anti-inflammatory drugs fro synthetic compounds are effective, they show adverse side effects. This study is a novel approach to screen the most effective natural compound (s) from plant and marine sources to provide treatment for Cystic Fibrosis related causes with minimal effects. The emergence of Computational techniques and Insilico methods are associated with low investment Drug Discovery and promising results providing a narrow way to find the leadmolecule.

Keywords: Cystic Fibrosis, Insilico methods, computational techniques, drug discovery

I. INTRODUCTION

Bioinformatics – a database management system speaks of biology in terms of molecules applying mathematics, computer science and, statistics, to understand and analyze molecules in structural and molecular levels. They are largely applied in sequence alignment, gene finding, genome assembly, prediction and alignment of protein structures, predicting gene expression and protein-protein interactions, genome-wide association studies and the modeling evolution.

A. Cystic Fibrosis

Cystic fibrosis (CF) or mucoviscidosis is a genetic disease – a defective Cystic Fibrosis Transmembrane Conductance Regulator (CFTR) gene, inherited from parents who, themselves are not affected by the disease. Although congenial, the disease is distinct only if two faulty genes are inherited from the parents. The CFTR protein controls the salt and water movements in cells. A defective CFTR gene causes cystic fibrosis (CF).

B. Cystic Fibrosis Inherited

Two CFTR genes are inherited - one from each parent, and inheriting a faulty CFTR gene from parents causes CF. CF carriers inherit one faulty CFTR gene and one normal CFTR gene and live normal lives with no CF symptoms. However, their offspring tends to get affected. Figure 1 shows the detailed inheritance pattern of Cystic Fibrosis.

C. Cystic Fibrosis Symptoms & Diagnosis

The faulty CFTR gene makes the mucus thick and salty. It increases viscosity and airway resistance. This causes critical infections in respiratory, digestive and urogenital tracts and sinusoidal linings. The phenotypic hallmark of CF chronic lung infection and associated inflammation from opportunistic microbes such as Pseudomonas aeruginosa (PA), Haemophilus influenza, and

Staphylococcus aureus. This eventually leads to deterioration of lung function and death in most CF patients. Besides these infections, vitamin deficiency and malnutrition also join in, as the sticky and viscous mucus blocks the ducts of pancreas preventing the enzymes from reaching the intestines and there by disturbing

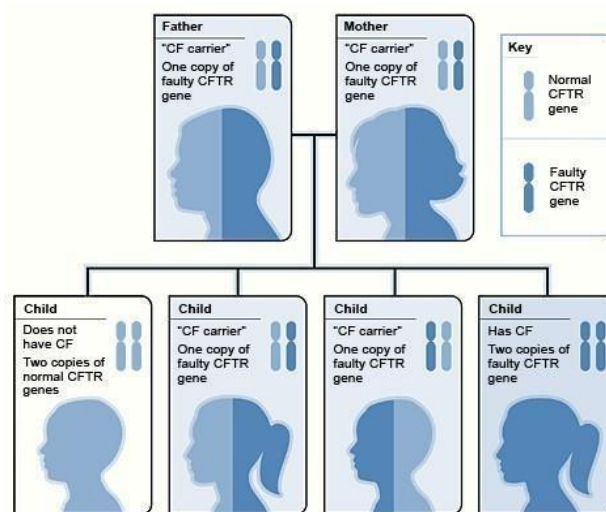


Figure 1: Inheritance pattern for cystic fibrosis.

digestion. This deprives the body of getting the necessary nutrients, leading to malnutrition. CF also disturbs hemostasis – by excreting excess salts through sweat, causes osteoporosis, infertility in men and meager fertility in females. All these symptoms vary with individuals, not all symptoms are expressed in the same person. The aforesaid abnormalities start in early childhood and get critical with age. This makes it incumbent to treat the disease in the early stages to increase the lifespan of the patient.

D. Cystic Fibrosis Diagnosis & Treatment

Cystic Fibrosis can be diagnosed from a newborn screening test, sweat test, lung function test, and sputum culture test. The main treatments for respiratory problems in people who have cystic fibrosis are chest physical therapy (CPT), exercise, and medicines. Cystic fibrosis causes several digestive problems, including poor growth and development, bulky stools, intestinal gas, a swollen belly, severe constipation, and pain or discomfort. Hence nutritional therapy can improve physical strength to stay active and also resist some types of pleural infections. Cystic fibrosis (CF) lung disease is characterized by persistent inflammation in the respiratory tract. Anti-inflammatory drugs, such as corticosteroids and ibuprofen, have proved to slow the decline of pulmonary function although their use is limited because of frequent adverse events [6]. Inhaled dry powder mannitol is well established for use in bronchial provocation testing but an international Phase III trial has

dry powder mannitol is well established for use in bronchial provocation testing but an international Phase III trial has suggested the use of regular inhaled mannitol increases lung function and reduces exacerbation frequency in cystic fibrosis [7]. At present synthetic drug Ivacaftor (also known as Kalydeco or VX-770) used for the treatment of cystic fibrosis developed by Vertex Pharmaceuticals and the Cystic Fibrosis Foundation. This drug is taken two times a day with fat-containing food, helps the protein made by the CFTR gene function better and as a result, improves lung function and other aspects of CF. Ivacaftor drug increases chloride transport by potentiating the channel-open probability (or gating) of the G551D- CFTR protein. The main disadvantage of this synthetic drug cannot be given to children under the age of 6 and also causes serious side effects like respiratory tract infection, abdominal pain, etc. To overcome the synthetic drug disadvantages, chemical extracts from the plant and marine compounds can be used for drug development which causes minimal effects.

II. METHODOLOGY

A. Databases used for the selection of chemical compound

A detailed study about the CF was done using NCBI and Pubmed databases. The following are the databases used for the structural analysis of the CFTR protein and their interactions with the inhibitors.

1) Protein Data Bank

The Protein Data Bank (PDB) database informs on 3-D structural data of macromolecules, like proteins and nucleic acids obtained from NMR spectroscopy and X-ray crystallography.

2) Drug Bank

The Drug Bank combines drug data with drug target (i.e. sequence, structure, and pathway) information. It has been widely used *In silico* drug target discovery, drug design, drug docking or screening, drug metabolism prediction, drug interaction prediction, and general pharmaceutical education.

B. Software Used

The following are the softwares involved for selecting the target protein for the CFTR gene.

1) Open Babel Software

OpenBabel is open software, mainly used for converting chemical file formats suitable for molecular modeling

2) ARGUS Lab Software

This ARGUS Lab software contains a graphical representation of molecular models. By using this we will be able to design our molecular structure for a chemical compound by combining various elements. This software can be used for simplifying the chemical compound structure and if needed atoms like hydrogen, nitrogen, oxygen, chlorine, and fluorine can be added accordingly.

3) GEMDOCK-Molecular Docking Tool

The interactions between a receptor and a ligand are fundamental for drug discovery. A common

technique central to receptor-ligand interactions was molecular docking. GEMDOCK was found to be an accurate tool for docking and it is an automatic system that generates all related docking variables, such as atom formal charge, atom type, and the ligand-binding site of a protein. This tool was developed by Jinn-Moon Yan, a professor of the Institute of Bioinformatics, National Chiao Tung University mainly used for computing a ligand interaction and orientation to the active site of a target protein.

4) ADME Suite

ADME Suite provide information on pharmacokinetic profiling of compounds, namely Absorption, Distribution, Metabolism, and Excretion properties. It predicts oral bioavailability, P-gp specificity, passive absorption, P450 inhibitors, blood-brain barrier permeation, distribution, substrates and inhibitors, daily dose. It also describes the drug effect.

MOLECULAR DOCKING ANALYSIS

Most biological and pharmacological reactions are triggered when a small molecular ligand binds to its receptor - usually a protein. These receptor-ligand binding interactions can be studied using Molecular Docking, hence the understanding of binding sites of ligands to their receptors. CFTR and tyrosine kinase 2 are the two proteins of functional importance in Cystic Fibrosis. The crystallographic protein structures available in PDB was used to investigate the molecular action of the protein towards the plant and marine-based natural compounds. The table 1&2 shows the hydrogen bonding and energy affinity between the two selected proteins and plant compounds.

TABLE 1. DOCKED PLANT COMPOUNDS

Ligand	Total Energy	VDW	H-Bond
Colchicine	-98.8504	-78.5359	-20.3144
Forskolin	-90.8536	-51.3214	-39.5322
Tomatidine	-91.2824	-81.7824	-9.5
Withaferin	-97.3994	-81.0177	-16.3817

TABLE 2. DOCKED PLANT COMPOUNDS WITH PROTEIN TYROSINE KINASE2

Ligand	Total Energy	VDW	H-Bond
Colchicine	-96.9424	-69.9558	-28.9866
Forskolin	-93.0522	-63.109	-29.9432
Tomatidine	-95.4505	-78.1175	-17.333
Withaferin	-104.829	-85.621	-19.2077

The table 3&4 shows the hydrogen bonding and energy affinity

between the two selected proteins and marine plant based compounds.

TABLE 10.3 DOCKED MARINE COMPOUNDS WITH CFTR PROTEIN

Ligand	Total Energy	VDW	H-Bond
Saxitoxin	-97.6673	-38.1603	-58.1137
Sceptrin	-127.837	-103.562	-24.2753
Tetrodotoxin	-99.2198	-47.0956	-52.1242

TABLE 10.4 DOCKED MARINE COMPOUNDS

WITH PROTEIN TYROSINE KINASE2

Ligand	Total Energy	VDW	H-Bond
Saxitoxin	-82.0161	-57.8453	-24.1708
Sceptrin	-119.265	-97.46	-21.805
Tetrodotoxin	-80.3597	-48.4047	-31.955

IV. RESULTS AND DISCUSSIONS

The emergence of Computational techniques and Insilico methods are useful in Drug Discovery with promising results and also provide a narrow way to find the lead molecule. To overcome the disadvantages of KALYDECO(synthetic drug) we suggest that drugs made from sceptrin(marine compound), withaferin and colchicines(plant compounds) will be effective and fewer side effects when compared to the synthetic drug, as well as it triggers the chloride channels. From the

Figure 2. 3D Structure view of protein tyrosine kinase2 binded with plant based compounds

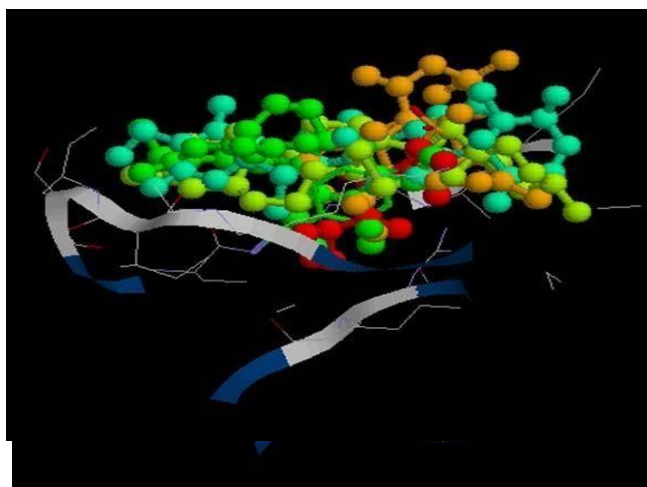


Figure 3. 3D structure view of protein TYROSINE KINASE2 binded with marine based compounds

v.

CONCLUSION

The investigation of protein– ligand docking experiment provided us with the best ligand to be chosen from the observed results. The obtained results show Colchicine plant-based compound ranks highest in binding affinity towards both the proteins; it has shown -98.8504 – Cystic fibrosis and - 96.9424 - tyrosine kinase2. With this, Sceptrin a marine compound has shown a good binding affinity towards the proteins, it has shown -127.837- Cystic fibrosis and - 119.265- tyrosine kinase2. This has been concluded that the comparative evaluation of the plant and marine compounds for its inhibitory efficacy towards the protein responsible for Cystic fibrosis, Colchicine and Sceptrin plant based and marine-based both are ranking good in inhibitory action towards the proteins, the remaining compounds have shown positive effect but possess some non-drug properties like higher molecular weight, number of Hydrogen bond donors, acceptors and Log P-value. Further studies can be carried out in the future to design these as a potent drug for treating the disease.

REFERENCES

1. Lihua Liang, Owen M. Woodward, Zhaohui Chen, Robert Cotter, William B. Guggino."A Novel Role of Protein Tyrosine Kinase2 in Mediating Chloride Secretion in Human Airway Epithelial Cells", PLoS ONE-July 2011, issue 7, volume 6.
1. Lipkind G M; Fozzard H A, A structural model of the tetrodotoxin and saxitoxin binding site of the Na⁺ channel. Biophysical journal, 1994
2. Collin FS."Cystic fibrosis: molecular biology and therapeutic implications", Science 1992, 256(5058):774-9, PMID:1375392[PubMed- indexed for MEDLINE].
3. Fan S, Harfoot N, Bartolo RC, Butt AG J, "CFTR is restricted to a small population of high expresser cells that provide a forskolin-sensitive transepithelial Cl⁻ conductance in the

- proximal colon of the possum”, *Trichosurus Vulpecula. Exp Biol.* 2012 Apr 1, 215(Pt 7):1218-30. PMID: 22399668 [PubMed - in process].
4. Kerem B, Rommens JM, Buchanan JA, Markiewicz D, Cox TK, Chakravarti A, Buchwald M, Tsui LC, "Identification of the cystic fibrosis gene: genetic analysis". *Science.* 1989, PMID: 2570460 [PubMed - indexed for MEDLINE].
 5. Sermet-Gaudelus I, Stoven V, Annereau JP, Witko-Sarsat V, Reinert P, Guyot M, Descamps-Latscha B, Lallemand JY, Lenoir G, "Interest of colchicine for the treatment of cystic fibrosis patients", *Mediators Inflamm.* 1999;8(1):13-5 PMID: PMC1781779 PMID: 10704084 [PubMed - indexed for MEDLINE].
 6. Hurt K, Bilton D "Inhaled mannitol for the treatment of cystic fibrosis", *Expert Rev Respir Med.* 2012 Feb;6(1):19-26 PMID: 22283575.
 7. Maitra R, Porter MA, Huang S, Gilmour BP, "Inhibition of NFkappaB by the natural product docking analysis, we found that protein TYROSINE KINASE2 is an efficient target protein inhibitor than CFTR protein. Our study can be divided into two cycles, inhibitory profile analysis of the plant and marine compounds with Cystic fibrosis and the same with tyrosine kinase2. In this present study, we have used iGEMDOCK software to map the interaction points of the proteins and compounds
Withaferin A in cellular models of Cystic Fibrosis inflammation", *J.Inflamm (Lond).* 2009 May 13; 6:15, PMID: PMC2689213 PMID: 19439083.
 8. Guggino WB, Banks-Schlegel. "Macromolecular interactions and ion transport in cystic fibrosis", *SP m J Respir Crit Care Med.* 2004 Oct 1;170(7):815-20.. PMID: 15447951.
 9. Drumm ML, Collins FS, "Molecular biology of cystic fibrosis", *Mol Genet Med.* 1993; 3:33-68. PMID: 7693108.
 10. Mitchell G, Gattuso M, Grondin G, Marsault É, Bouarab K, Malouin F, "Tomatidine inhibits replication of *Staphylococcus aureus* small-colony variants in cystic fibrosis airway epithelial cells.", *Antimicrob Agents Chemother.* 2011 May;55(5):1937-45. Epub 2011 Feb 28. PMID: PMC3088192 PMID: 21357296 [PubMed - indexed for MEDLINE].
 11. Joseph F. Hoffman, Alicia Dodson, Amittha Wickrema, and Sulayman D. Dib- Hajj "Tetrodotoxin-sensitive Na⁺ channels and muscarinic and purinergic receptors identified in human erythroid progenitor cells and red blood cell ghosts", *Proc Natl Acad Sci USA.* 2004 August 17, pp 12370-12374. PMID: PMC514482

Analysis of Histogram Distance Measures for Change Detection In Brain Symmetry

K.Suresh

*Department of Information Technology,
St. Joseph's College of Engineering,
Chennai-600119, India,
sureshk@stjosephs.ac.in*

U. Sakthi

*Department of Computer Science and
Engineering,
St. Joseph's Institute of Technology,
Chennai-600119, India.
sakthi.ulaganathan@gmail.com*

N. Sri Madhava Raja*

*Department of Electronics and
Instrumentation Engineering,
St. Joseph's College of Engineering,
Chennai-600119, India
nsrimadharaja@stjosephs.ac.in*

R. Prabhu

*Department of Electronics and
Communication Engineering,
St. Joseph's College of Engineering,
Chennai-600119, India,
prabhutcece@gmail.com*

Abstract— It is important to analyze and quantify the spatial relationship between the brain symmetry planes (BSP) on radiological images. The unsupervised change detection problem is taken to detect the abnormalities based on brain symmetry assuming the left and right part of brain is roughly symmetric. The input to the problem is symmetrical axial MR slices, and its output is to place axis-parallel boxes that circumscribe the tumor part. This change detection process uses a score function based on histogram distance measure computed with gray level intensity histograms. In this work histogram distance measures is analyzed for the change detection problem. Several image databases are utilized to test the performance of Bhattacharyya, Chi-Square, Correlation, Intersection distance measures. From the experimental results, Chi-Square distance metric seems effective in localizing brain abnormalities than the other distance metrics for the change detection problem.

Keywords— Brain symmetry planes, MR Images, Histogram Distance Measures, Brain abnormalities

I. INTRODUCTION

The advances in medical sciences had resulted in reducing fatalities and shown positive signs in treating complex diseases. Magnetic brain (MR) surgery can be effectively applied in the detection of brain tumors by identifying the tumor's position, area and other required information [1]. Detection precision can be further enhanced by applying effective computations and segmenting the tumor from the MR data [2-3]. The history of medical diagnosis observed over the years had pointed out a few lapses in the treatment being afforded and more often than not had resulted in fatality due to incorrect or timely diagnosis. Physicians and radiologists treating brain tumor patients have been highly benefitted by the MRI technology that aids them in charting out further treatment options. Interpretation of MRI data is done visually and specific to the type of patient which can be applied for the detection of several brain related abnormalities like disorders, tumors, cysts, stroke and issues pertaining to blood vessels of brain [4-6].

Change detection methods can be applied for detecting the irregularities in a test image by comparing it with some reference image [7]. Change detection can be applied in a variety of applications like video surveillance, segmentation of medical images and inspecting the industrial process. A recent survey on change detection

had been carried out in [8] to justify its necessity in several fields. Tumor in brain can be identified by rightfully spotting the changes on the right and left sections of the brain. The proposed research is based on the critical observation that is found to be exhibited by the normal brain whose left and right halves can be segmented through an axis of symmetry (LOS) [9]. Even then a point to point comparison between the right and left halves yields only less significant details. This is due to the fact that the symmetric structure exhibited by the brain structure is uneven.

A score function is used in the change detection process that is based upon histogram similarity metrics that are assessed using grey level intensity histograms. Regional similarities between symmetrical regions can be compared using histogram like representations [10, 11]. Distance measures like Bhattacharyya coefficient (BC) [12], Chi-Square Distance Metric [13], histogram intersection are discussed in few literatures portraying their applications in the comparison of regional similarities between histograms. These distance measures are also applied for several computer vision applications like object tracking [14], edge detection [15], and registration [16]. Albeit all these a robust and reliable region based change detection technique is required for precisely capturing the changes between brain symmetry.

The region based segmentation methods [17 – 19] may be of supervised or non-supervised types. The process of detecting tumors from brain MRI in a more precise way through automatic means is cumbersome and yet to be realized. Incorporating global region based features although may be important but requires rigorous computational effort. Widely applied global region based methods like intensity thresholding [20, 21] and region growing can be applied. But the results pertaining to detection and segmentation of tumor after applying these methods are far from being precise.

In this work, axial slices of the MR brain scan is divided with respect to vertical LOS and detects the changes. The LOS taken up splits the head MRI into two sections that are nothing but a mirror replica of each other. The change in the observed region is detected by tracking the change in intensity over the region identified by the tumor coordinates. After the tumor coordinates are obtained, a box boundary can be fixed over the identified region exhibiting dissimilarity. This work employs a

region based similarity metrics that allows user specified parameters for comparing the histograms of two symmetry regions. This can be followed by forming a boundary over the tumor region resulting in the isolation of the tumor with high precision. The symmetry technique is employed for comparing the upper right and upper left sections for dissimilarity and the same process is repeated for lower sections too [22]. Empirical results obtained from the proposed approach that employed the novel region based Chi-square test that takes in user regulated parameters had shown considerable improvements with respect to the dice similarity measure.

II. LOCATING BOUNDING BOXES USING CHANGE DETECTION

A. Selecting a Template (Heading 2)

An image with a height h and width w that is divided into two sections - Left Reference Image and Right Test Image - based on LOS is considered. The anomaly A , seen from the two samples of the image. While sweeping vertically, y_1 and y_2 have been found. Likewise, the coordinates x_1 , x_2 are obtained while sweeping horizontally. The anomaly 'A' in the test image 'T' is detected from the reference image 'R', this is depicted in Fig. 1.

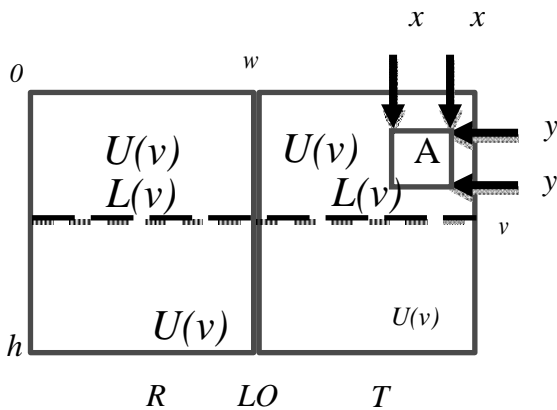


Fig 1. Finding abnormality A from test image T using reference image R.

The anomaly 'A' is detected in two rapid searches using histogram metrics. First, the vertical sweep is done where the search traverses in top-down direction ($v = 0 \dots h$) of the image followed by the horizontal sweep in left-right direction ($v = 0 \dots w$) where the search is halved compared to vertical direction.

The score function used to detect region based dissimilarity is given as,

$$E(v) = Ss(P_T^{U(v)}, P_R^{U(v)}) - Ss(P_T^{L(v)}, P_R^{L(v)}) \quad (1)$$

$v=0 \dots h$

Where, Ss denotes the normalized intensity histograms of T and R across the region $U(v)$. Similarly the definition for the region $L(v)$, the histograms and are done accordingly. The similarity score between two normalized histograms 'a' and 'b' is denoted by $Ss(a, b) \in [0, 1]$.

The usage of the score function $E(v)$ enables a quicker localization of the bounding box containing the anomalous

brain region. Fig. 2 shows that the score plot increases initially, then continues to decrease and the finally begins to increase again after crossing the anomaly 'A'. The start of the decreasing of the score plot denotes the beginning of the anomaly while the resumption of increase shows the end region of the anomaly. At y_1 and y_2 , the intersection of the increasing and decreasing segments can be seen, which are the lower bound and upper bound of anomaly A. Similarly, x_1 (left bound) and x_2 (right bound) of the bounding box can be identified using the plot found from the score function of the horizontal sweep.

III. HISTOGRAM DISTANCE METRICS

Bhattacharya Coefficient

Bhattacharya suggested ways that can be used to measure the similarity between two probability distributions having computational complexity of $O(n)$ [23]. The Bhattacharya distance measures the degree to which two normalized distributed data samples overlap and this is depicted in the following equation. This coefficient can be used to find the relative closeness of two samples that are considered.

$$BC(a, b) = \sum_{x \in X} \sqrt{a(x)b(x)} \quad (2)$$

This highlights the similarity features of two probability distribution functions. When the two PDFs are found to possess disjoint supports, the measure of BC is seen to be 0 while the two PDFs are equal, BC becomes 1.

Modified Chi-Square Distance Metric

χ^2 (Chi-Square) distance metric is a type of weighted Euclidean distance measure that measure the similarity between two samples when their relative difference are emphasized [24]. The correspondence of distribution

between the bins is given by χ^2 which measure the distance between $a=[a_1, \dots, a_n]$ and $b=[b_1, \dots, b_n]$ both of which are histograms having n bins. Additionally, the entries of both the histograms sum up to one, i.e. they are normalized.

$$\chi^2(a, b) = \frac{1}{2} \sum_{i=1}^n \frac{(a_i - b_i)^2}{(a_i + b_i) + \alpha} \quad (3)$$

Where 'a' and 'b' indicates the observed and expected histogram distributions to test the goodness of fit. The custom parameter α value is taken based on application specific. The denominator $(a_i + b_i)$ implies large differences in the bins should contribute less weight.

Correlation

Correlation is a measure of the statistical relationship between two entities that involve dependence. It's computational complexity is $O(n)$. If the features of two objects are highly correlated, even if the observed values are far apart in terms of Euclidean distance, the Correlation based distance considers the two objects to be similar. If the correlation coefficient is +1 (positive relationship) or -1

(negative relationship) then it is a perfect linear relationship on the other hand, there is no linear relationship if the correlation coefficient is found to be 0. Same number of elements must be present in both the variables.

$$CR(a, b) = \frac{\sum^n (a_i - \bar{a})(b_i - \bar{b})}{\sqrt{\sum_{i=1}^n (a_i - \bar{a})^2 \sum_{i=1}^n (b_i - \bar{b})^2}} \quad (4)$$

Intersection

Intersection, as the name suggests is a measure based on the intersection of two histograms. It's computational complexity is $O(n)$. Histogram intersection is not symmetric and helps in checking the occurrence of a specific object over a region. It demonstrates the ability to handle partial matches when the areas of two histograms are different. The similarity of two discretized histograms are calculated using histogram intersection while also calculating possible values of the intersection lying between the identical distributions as 1 and non-overlapping distributions as 0.

$$I(a, b) = \sum_{i=1}^n \min(a_i, b_i) \quad (5)$$

IV. RESULTS AND DISCUSSIONS

In this study four distance measures are utilized to detect the region of change in symmetrical brain images. The image samples utilised in this study are obtained from BRATs dataset contains axial slices of brain images of different width and height. Also, clinical DICOM axial brain series is employed to assess the region of change for the different similarity measures considered in this work. The considered images for evaluation is shown in Figure 3.

For the change detection process the brain MR slice in axial view of a subject is divided into four quadrants as shown in Figure 4. The vertical separation indicates the approximate symmetrical line (SL) through the centroid of the Brain Symmetry Plane (BSP). Thereby the brain slice is divided into two approximately equal regions: the right side of the fragment is considered as the test image T which consists of the tumor region and the other side of SL is represented as R is considered as reference image of the same slice which not contains tumor. The image splits 'T' and 'R' are there by almost symmetric after obtaining a reflection of one another.

The vertical score function is obtained from Eq. (1) is calculated by going across image for top of each row in vertical direction till bottom. In the considered image in Figure 4, the horizontal line divides HSP at position $v=180$. The maximum dissimilarity is obtained with that of the top quadrants than that of the bottom quadrants. The presence of tumor information in the top right quadrant provides a lesser similarity in the bottom quadrants. The dissimilarities increases when the sweep start progressing towards the tumor part, hence the score plot increases to a maximum point. Once the anomaly A is reached the score plot starts decreasing and reaches the minimum point then increases after overpassing A (as in Figure 2).

During the vertical sweep, significant values $y1$ and $y2$ are obtained from the pair of symmetrical image. Similarly, horizontal sweep procedure provides the values $x1$ and $x2$ based on Eq. (1). The focus of the work is locating the tumor and it is implementing a bounding box technique. This is successful after both the sweeps. Figure

6 depicts the integrated histogram bin comparison of both top and the bottom quadrants.

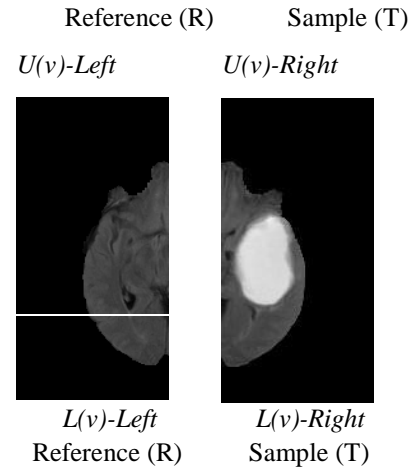


Figure 4. Vertical line represents geometric axis of symmetry. Horizontal line ($v=180$) divides the skull into four quadrants

During the vertical sweep, significant values $y1$ and $y2$ are obtained from the pair of symmetrical image. Similarly, horizontal sweep procedure provides the values $x1$ and $x2$ based on Eq. (1). The focus of the work is locating the tumor and it is implementing a bounding box technique. This is successful after both the sweeps. Figure 6 depicts the integrated histogram bin comparison of both top and the bottom quadrants.

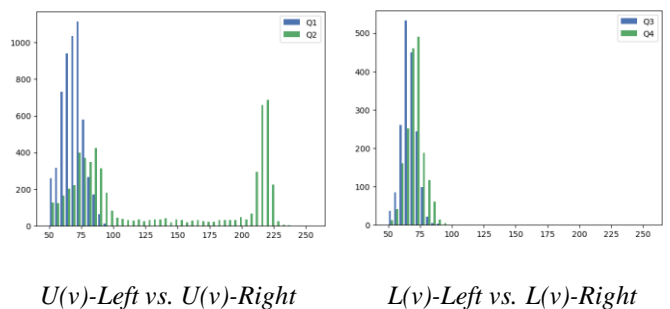


Figure 5. Histogram Comparison of top and bottom quadrants

The change detection process thus utilizes distance measures to find similarity and to detect the region of change. The four distance measures for finding histogram similarity is applied to the score function depicted in Eq (1). The score plots for the distance measures is shown in Figure 6.

The change detection process thus utilizes distance measures to find similarity and to detect the region of change. The four distance measures for finding histogram similarity is applied to the score function depicted in Eq (1). The score plots for the distance measures is shown in Figure 6.

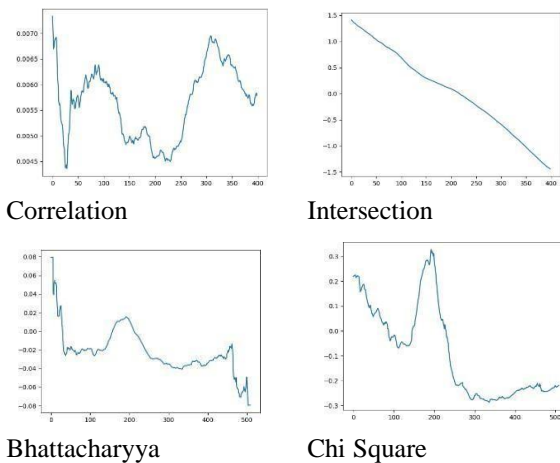
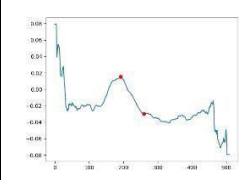
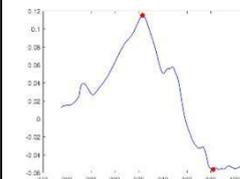
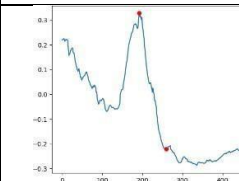
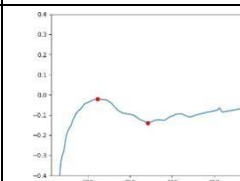


Figure 6. Sample Change Detection score plots for histogram distance measures (Vertical Sweep) For Slice 10

From the score plots of the considered distance measures shown in Figure 6, evidently indicates that Bhattacharyya and Chi-Square measures clearly depicts the increasing-decreasing-increasing nature of the score plot $E(v)$ and thus detects the change in the vertical sweep. The plots of BC and CS also given some reasonable assumptions regarding the reference image (R), sample test image (T) and the anomaly 'A'. The score plots of other distance measures not provides any equitable assumptions in detecting the region of change.

Table 1. Score Plots for DICOM Series

	VERTICAL	HORIZONTAL
BC		
CS		

The detected change is identified by the top and bottom values (y1, y2) along the y axis through the vertical sweep.

Further, the distance measures BC and CS are employed to identify the change along horizontal direction to obtain (x1, x2), so that a bounding box is placed along the region of change. The custom parameter value for is chosen as 0.0001 for tumor detection. Table 1 and Table 2 shows the score plots of both horizontal and vertical sweep generated by the BC and CS distance measures of clinical MRI dataset and BRATs dataset respectively.

The points (y1, y2) corresponding to the top and bottom bounds and (x1, x2) corresponding to left and right

bounds of the bounding box are shown as red dots. In order to determine whether the reference (R) or test image (T) contains the tumor, the average intensity is computed between the bounding boxes on both sides. The bounding box with higher mean image intensity is supposed to contain the anomaly. The box coordinates values (y1, y2) and (x1, x2) for the images considered for the similarity metrics BC and CS are shown in Table 3 and Table 4 respectively. Based on the coordinates of Table 3 and Table 4 bounding box is plotted on each respective slice over the tumor area, and is shown in Fig 7 and Fig8.

Table 2. Score Plots for Skull Stripped MR Images

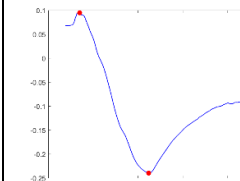
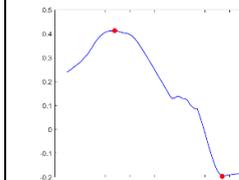
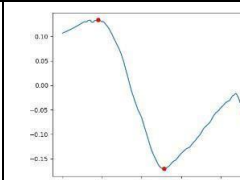
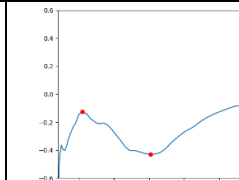
	VERTICAL	HORIZONTAL
BS		
CS		

Table 3 Skull Encircled Images

Slice No	CS				BC			
	Y1	Y2	X1	X2	Y1	Y2	X1	X2
S 10	194	258	311	371	183	263	323	382
S 11	175	274	322	386	182	282	358	386
S 12	163	280	311	371	162	282	329	363
S 13	169	298	319	374	168	292	344	386
S 14	173	312	313	368	172	261	324	376

Table 4 Skull Stripped Images

Slice No	CS				BC			
	Y1	Y2	X1	X2	Y1	Y2	X1	X2
S1: (256x256)	47	131	142	184	35	112	154	197
S2: (256x256)	119	241	57	93	98	167	58	80
S3: (176x216)	117	182	102	132	150	186	100	144
S4: (160x216)	147	197	37	75	149	200	47	65
S5: (256x256)	108	158	149	185	104	156	173	203

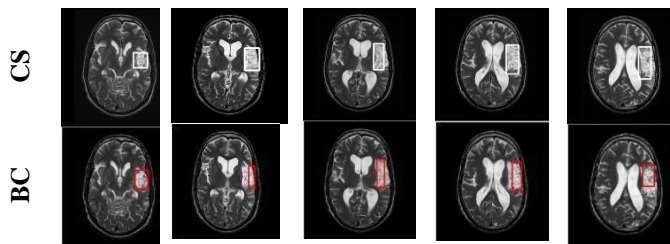


Figure 7. Bounding Box results for Clinical MRI Slices:
 Row 1, Chi-Square distance metric (CS);
 Row 2, Bhattacharya Coefficient (BC)

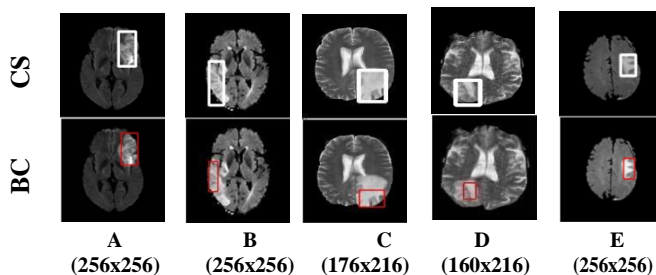


Figure 8. MRI slices (BRATs): Row 1, Chi-Square distance metric (CS); Row 2, Bhattacharya Coefficient (BC)

Figure 7 and Figure 8 portrays placement of bounding boxes over tumor detected area on clinical MR slices and benchmark slices respectively. From these figures the placement of bounding box boundary using CS holds maximum tumor intensities than the results of BC. From the results of Fig 7 and Fig 8 visually shows inclusion of custom parameter with chi-square distance metric outperforms Bhattacharyya measure in both the chosen dataset.

V. CONCLUSION

The proposed study analyses the bin to bin histogram measures for the change detection problem. An approach to automatically detect brain anomaly, from axial MR slices is reflected. The score function for detecting the dissimilar region is computed using the histogram similarity measures. Different image databases are utilized to test the performance of Bhattacharyya, Chi-Square, Correlation, Intersection distance measures. The generated score plots for the distance metrics are compared and analyzed for the change detection problem. From the results obtained from the generated score plots, it affirms that Chi-Square distance metric seems effective in obtaining lower and upper bounds of bounding box coordinates for the change detection problem.

REFERENCES

- [1] G Karaa WB, editor. Biomedical image analysis and mining techniques for improved health outcomes. IGI Global; 2015 Nov3.
- [2] El-Dahshan ES, Mohsen HM, Revett K, et al. Computer-aided diagnosis of human brain tumor through MRI: A survey and a new algorithm. *Expert systems with Applications*. 2014 Sep 1;41(11):5526-45.
- [3] El-Dahshan, E. S. A., Mohsen, H. M., Revett, K., & Salem, A. B. M. (2014). Computer-aided diagnosis of human brain tumor through MRI: A survey and a new algorithm. *Expert systems with Applications*, 41(11), 5526-5545.

- [4] Grover, V. P., Tognarelli, J. M., Crossey, M. M., Cox, I. J., Taylor-Robinson, S. D., & McPhail, M. J. (2015). Magnetic resonance imaging: principles and techniques: lessons for clinicians. *Journal of clinical and experimental hepatology*, 5(3), 246-255.
- [5] Suresh, K.; Sakthi, U. (in press). Object tracking based 3D modelling and quantification of abnormal contours in brain MRI DICOM study. *Journal of Engineering Science & Technology (JESTEC)*.
- [6] Suresh, K.; Sakthi, U. A soft-computing based hybrid tool to extract the tumour section from brain MRI. *Multimed. Tools Appl.* 2019, 1–5, doi: 10.1007/s11042-019-07934-1
- [7] Sri Madhava Raja, N., Vishnupriya, R, Kapur's Entropy and Cuckoo Search Algorithm Assisted Segmentation and Analysis of RGB Images. *Indian Journal of Science and Technology*, DOI: 10.17485/ijst/2016/v9i17/89936.
- [8] Manjula, B. & Godweena, A. & Raja, N. & Satapathy, Suresh. (2020). A Study on Mining of Tumor Pixel Group in Flair Modality Brain MRI. 10.1007/978-981-13-9282-5_71.
- [9] Hu Q, Nowinski WL. Radiological symmetry of brain and head images: comparison and applications. *International Journal of Computer Assisted Radiology and Surgery*. 2006 Aug 1;1(2):75-81.
- [10] N. Naik, S. Patil, and M. Joshi. A scale adaptive tracker using hybrid color histogram matching scheme. In *Emerging Trends in Engineering and Technology (ICETET)*, 2009 2nd International Conference on, pages 279–284, Dec 2009.
- [11] Q. Zhang and R. L. Canosa. A comparison of histogram distance metrics for content-based image retrieval, 2014.
- [12] Comanicu D, Ramesh V, Meer P. Real-time tracking of non-rigid objects using mean shift. *Proceeding of CVPR2000*;2:142–9.
- [13] Gagunashvili, N. D. (2006). χ^2 Test For The Comparison Of Weighted And Unweighted Histograms. In *Statistical Problems In Particle Physics, Astrophysics And Cosmology* (pp. 43-44).
- [14] Kaushal, M., Khehra, B. S., & Sharma, A. (2018). Soft Computing based object detection and tracking approaches: State-of-the-Art survey. *Applied Soft Computing*.
- [15] Konishi S, Yuille A, Coughlan J, Zhu S. Fundamental bounds on edge detection: an information theoretic evaluation of different edge cues. *IEEE CVPR 1999*:573–9.
- [16] Viola P, Wells W. Alignment by maximization of mutual information. *International Journal of Computer Vision* 1997;24(2):137–54.
- [17] Niu, S., Chen, Q., De Sisternes, L., Ji, Z., Zhou, Z., & Rubin, D. L. (2017). Robust noise region-based active contour model via local similarity factor for image segmentation. *Pattern Recognition*, 61, 104-119.
- [18] Raja NSM, Fernandes SL, Dey N, Satapathy SC, Rajinikanth V (2018) Contrast enhanced medical MRI evaluation using Tsallis entropy and region growing segmentation. *Journal of Ambient Intelligence and Humanized Computing*: 1-12. Doi: 10.1007/s12652-018-0854-8
- [19] S, Madhavanthi & K, Madhumathi & P, Dr.Deepa & Raja, N.. (2017). A Soft-computing Assisted Tool to Detect and Analyse Brain Tumor. *International Journal of Engineering and Technology*. 9. 1341-1348. 10.21817/ijet/2017/v9i2/170902260.
- [20] Suresh, K., & Sakthi, U. (2018). Robust multi-thresholding in noisy grayscale images using Otsu's function and harmony search optimization algorithm. In *Advances in Electronics, Communication and Computing* (pp. 491-499). Springer, Singapore.
- [21] Suresh, K., & Sakthi, U. (2019). Analysis of heuristic-based multilevel thresholding methods for image segmentation using R programming. *International Journal of Reasoning-based Intelligent Systems*, 11(2), 151-160.
- [22] K. Revanth, T. D. Varsha shree, N. S. Madhava Raja and V. Rajinikanth, "Computational Investigation of Stroke Lesion Segmentation from Flair/DW Modality MRI," 2018 Fourth International Conference on Biosignals, Images and Instrumentation (ICBSII), Chennai, 2018, pp.206-212.
- [23] S.-H. Cha and S. N. Srihari. On measuring the distance between histograms. *Pattern Recognition*, 35(6):1355 – 1370,2002.

- [24] Asha, V., Bhajantri, N. U., & Nagabhushan, P. (2012). GLCM-based chi-square histogram distance for automatic detection of defects on patterned textures. arXiv preprint arXiv:1212.0383.

2020 IEEE Sixth International
Conference on Biosignals, Images
and Instrumentation(ICBSII 2020)

SESSION III
RESEARCH PAPERS

Delay and Power Efficient FIR Architecture for Noise Suppression of EOG Signal

Gundugonti Kishore Kumar

*Dept. of Electronics and
Communication Engineering*

V R Siddartha Engineering College

Vijayawada, India

gkishorekumar@vrsiddartha.ac.in

Balaji Narayanam

*Dept. of Electronics and
Communication Engineering*

JNTUK University College of

Engineering

Kakinada, India

prof.balaji.ece@gmail.com

D Hema Malini

*Dept. of Electronics and
Communication Engineering*

V R Siddartha Engineering College

Vijayawada, India

hemamalini.m9@gmail.com

Abstract—In this paper, we proposed a modified FIR filter using Canonical signed digit (CSD) technique for de-noising the Electro-Oculography (EOG) signal. A dipole was formed between cornea and retina in an eye, resulting in voltage difference with occurrence of eye movement, which in turn generates an electrical signal. These signals are called as EOG and are useful in many medical and bioelectrical applications. To remove the noise in EOG signal an enhanced 16-bit FIR filter was used. The proposed FIR architecture uses CSD based multipliers, unlike the conventional shift-add the proposed architecture provide greater improvement in power and delay. CSD is used in order to reduce the design complexity of the multiplication by representing the filter coefficients in CSD format. The proposed approach was implemented on Xilinx FPGA development kit. By comparing the synthesis results for existing and proposed methods, which has achieved an improvement of 12.60% and 11.76% in Power Delay Product (PDP) and Area Delay Product (ADP) respectively

Keywords—*Electro-Oculography (EOG), Canonical signed Digit (CSD), FIR Filter, FPGA, Power Delay Product (PDP), Area Delay Product (ADP)*

I. INTRODUCTION

Electro-Oculography (EOG) is one of bio-signals that can be measured and monitored and it measures the cornea-retinal standing potential of front and rear ends of the human eye. Resulting signal is called Electro-Oculogram. The EOG provides corresponding voltage generated by the eye movement. It can be used to study the eye movement pattern and related aspects [1] [2]. The signal amplitude will be in (50, 3500) μ V range. Signal frequency range will be 0 to 30 Hz [3]. Some of the applications are in ophthalmological diagnosis, recording eye movement and in many Human Computer Interface [4]. EOG has wide range of applications in medical diagnosis, study of different eye movements and Human Machine Interface (HMI). In [5], a wearable EOG for recording eye movements of people in transit in an everyday environment was analyzed. EOG signal consists of some impulsive noises, which are canceled by using Median filter [6]. Many noise suppression techniques for EOG signals are implemented, out of them bandpass FIR filter has accuracy and best processing speed [7]. Multipliers are important and basic

building blocks in Digital Signal Processing and Digital Image Processing [8]. Hence to reduce the complexity in multiplication and to reduce path delays, area of the existing conventional methods, CSD based representation is very effective [9]. CSD representation will be useful for many design-implementation of digital filters and CSD based filter architecture for image conversion [10]. This paper describes the denoising of EOG signal using FIR filtering techniques.

The principle of EOG signal was mentioned in section II. Section III focuses on conventional shift-add method of multiplication. Proposed method and its implementation in FPGA along with Software/Hardware co-simulation was discussed in sections IV and V. Synthesis Results of proposed architectures are mentioned in sections VI. Conclusion and Future Work was discussed in last section.

II. FIR FILTER

In Digital Signal Processing (DSP) one of the important block is Digital filter. Some of the applications of filters are noise reduction and noise suppression. Impulse response of FIR filter has finite duration, as it gets resolved to zero in a finite time. The equation of FIR filter is stated by [11], which is shown below,

$$y(n) = \sum_{k=0}^{N-1} h(k) * x(n-k) \quad (1)$$

Where $x(n)$ is input sample, $Y(n)$ is output sample, $h(k)$ is filter coefficient, N is filter order. Equation (1) represents FIR filter of order N as each value of output is weighted sum of most recent input values. The term $x(n-k)$ in (1) represents the input with delay of multiplication process which is also called as taps which define filter order in different forms of FIR filter structures. FIR filter Transpose form is having more advantages than direct form [12]. Multipliers and adders along with delay elements are the basic building blocks of FIR filter, which is shown in Fig. 1. In order to improve the overall throughput fast multiplication techniques are required. Combination of adders were used instead of multipliers and to store the sample value in memory for each sample per clock cycle, delay elements are used.

Filter coefficients are obtained by MATLAB FDA tool by designing the 16-bit low pass Equiripple FIR filter with frequency range of 5-30Hz. The obtained filter coefficients are : [-192, -288, -352, 224, 864, 1696, 2624, 3552, 4256, 4640]. The designed filter is of 24-order, hence we get 24 filter coefficients in which 12 are mentioned above [h_0-h_{11}], remaining coefficients are symmetric in nature.

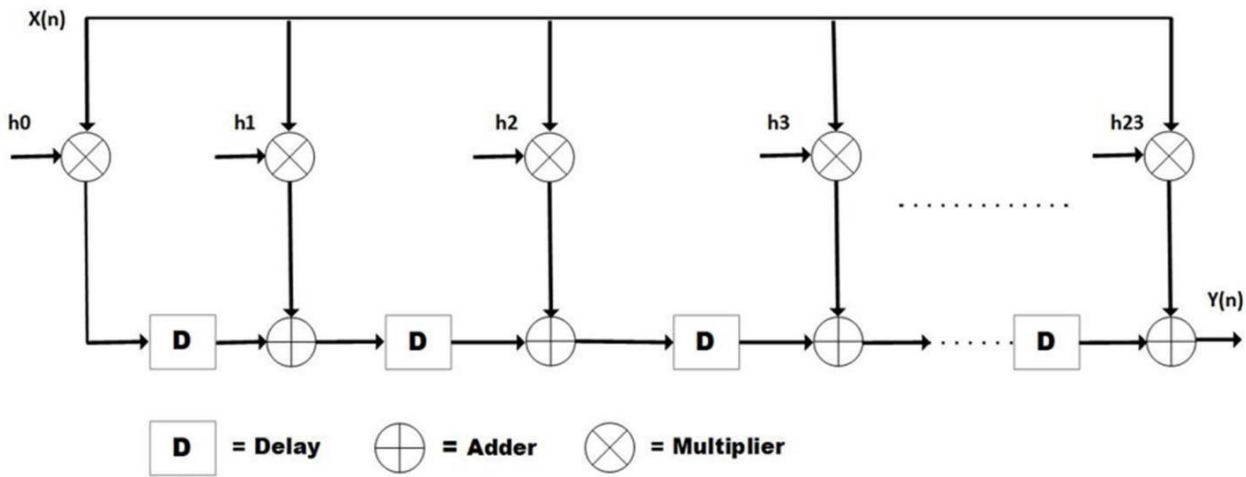


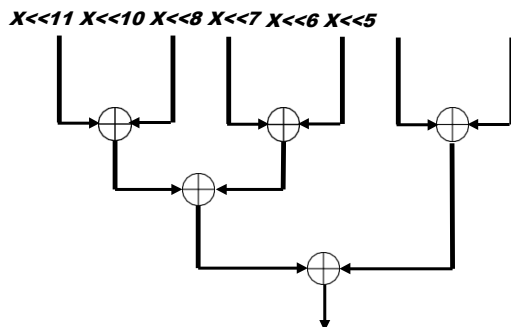
Fig. 1. FIR Filter Architecture

III. CONVENTIONAL SHIFT-ADD MULTIPLIER

From the literature survey, we conclude that FIR filter optimization can be done in multiplier block. By using shifting operation, binary multiplication will be achieved. Here, the multiplication with 0 bits are neglected, which in turn reduces the computations and complexity, which leads to a great reduction in number of logic devices and their switching activities, which reduces the area and power. In order to obtain the multiplication by 2^n , simply left shift the number (binary bits) by n -bit. Shift-Add multiplication on each coefficient was done by simply shifting the binary number by obtained shift values and adding all the results by using an Ripple Carry Adder (RCA). Filter coefficient 3552 (i.e., h_9 and h_{14}) has maximum path delay, hence representing the coefficient 3552 in binary form as:

0000 1101 1110 0000, which can also be represented as follows: $2^{11} + 2^{10} + 2^8 + 2^7 + 2^6 + 2^5$.

Here input sample is shifted and added, instead of performing binary multiplication. Maximum number of RCAs required for this implementation was for the coefficient h_9 and number of adders required are 3. Maximum delay was shown in Fig. 2.



IV.



Fig. 2. Shift-Add representation for maximum path delay coefficient in Filter

PROPOSED CSD MULTIPLIER

To further optimize filter area and delay, in Shift and Add technique the filter coefficients were represented in CSD form instead of normal binary representation. In CSD representation, we get a minimal non-zero terms than binary representation. Instead of binary digit set (0, 1) which is used by Shift and Add method, CSD representation uses ternary number system with digit set of (-1, 0, 1). The digit -1 is denoted as "1 bar". In this CSD, two consecutive non-zero digits are not allowed, which means that "11" or "1-1" is invalid. Hence, we achieve lesser number of adders in this implementation. Hence, hardware can be efficiently implemented using CSD representation, instead of binary representation [13]. Filter Coefficients in CSD are represented as shown in equation (2)

$$y(n) = \sum_{r=0}^{B-1} x_r 2^r \quad (2)$$

Where $x_r = 0, 1, -1$ (represented as 1 bar)

As Shift-Add, multiplication has 3 RCA's, which takes long time for computation, hence to reduce number of RCA's filter coefficients are represented in CSD format. For CSD representation, the critical path or the maximum delay is for coefficient h_7 and maximum number of Ripple carry Adders (RCA) required for this is shown in Fig. 3: From the above, we get to know that minimum required number of RCA's for multiplication in FIR filter designed using shift-add method is 3 RCA. Where each RCA consists of one Half Adder (HA) and (N + 1) Full Adders (FA) [14]. Minimum required RCA's for CSD based representation was 2 RCA's. The proposed multiplier uses less number of RCA's compared to conventional multiplier, and it consumes less area, power and delay than the conventional method.

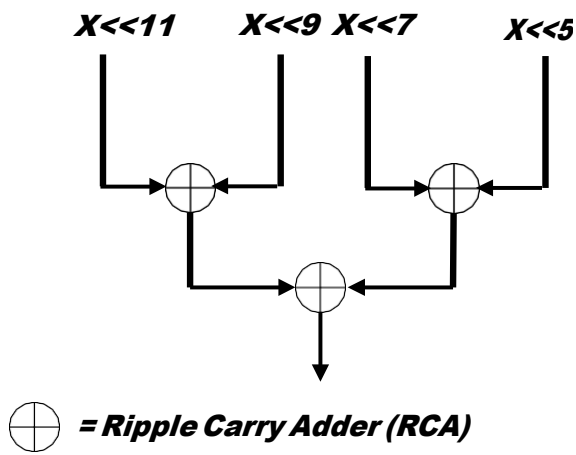


Fig. 3. CSD based Representation for critical path delay coefficients in filter

V. IMPLEMENTATION OF FIR FILTER WITH PROPOSED METHOD

The setup for removing noise in EOG signal using proposed method is implemented using Verilog HDL and Matlab, hardware/software co-simulation was used. Initially simulation results are verified and then functionality was implemented in hardware/software co-simulation block. In proposed model the test EOG signal was obtained from [15], this was generated from workspace and was given to FPGA block. Final Filtered signal was observed on scope. The proposed model was implemented and verified on FPGA Zed Board Zynq evaluation and development kit xc7z020c1g4841 using Xilinx System Generator (XSG) 2016.2. The hardware/software co-simulation setup shown in Fig. 4.

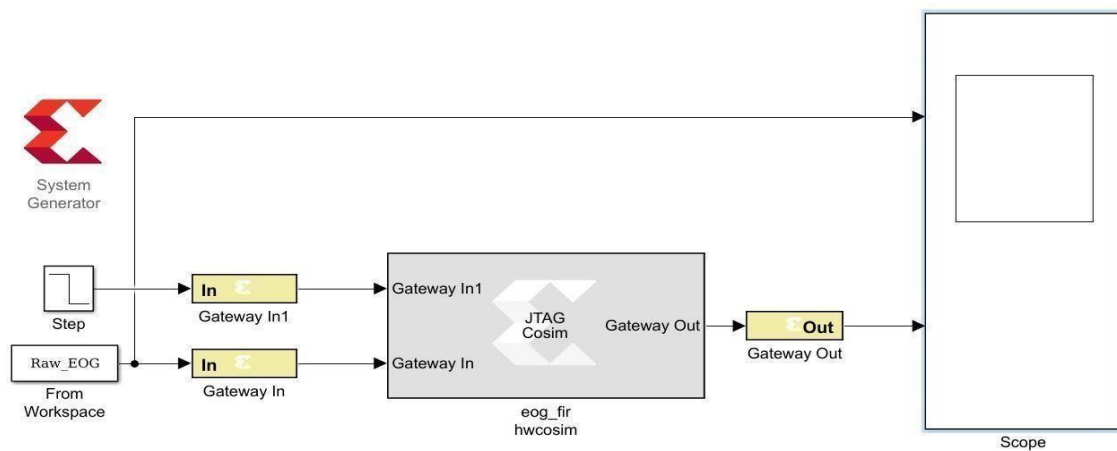


Fig. 4. Hardware/Software Co-Simulation setup for noise removal in EOG

The applied raw EOG signal and its filtered output signal will be observed on the scope in XSG. The JTAG co-simulation in XSG generates the Xilinx block set required for the hardware zed board. The output waveform of raw EOG and noise removed EOG signal was mentioned in Fig. 5.

VI. SYNTHESIS RESULTS

In this section, synthesis results of proposed and conventional filter are shown, by comparing their area, power and delays. The results were obtained from cadence 90nm technology design tool. Other computations like Area Delay Product (ADP), Power Delay Product (PDP), and increase in delay (D %) was also listed in Table I. Compared to the conventional method; proposed architecture has shown a reduction in delay by 9.45%. Similarly, an improvement of 12.60% and 11.76% was achieved for PDP and ADP respectively. The comparison of Area, Delay and Power was shown in Fig. 6. The improvements in percentages of area, power and delay for both methods were obtained as 2.55%, 9.45% and 3.47%

respectively. The proposed architecture occupies less area, power efficient and reduced delay compared to conventional methods.

TABLE I
 SYNTHESIS RESULTS OF CSD BASED FIR ARCHITECTURE FOR SUPPRESSING NOISE IN EOG

Method	Conv	Proposed
Area (um)	30795	30009
Power (uW)	5212.67	5031.60
Delay (nS)	7.94	7.19
D (-)%	-	9.45
PDP	41409.47	36192.31
ADP	244635.5	215854.7

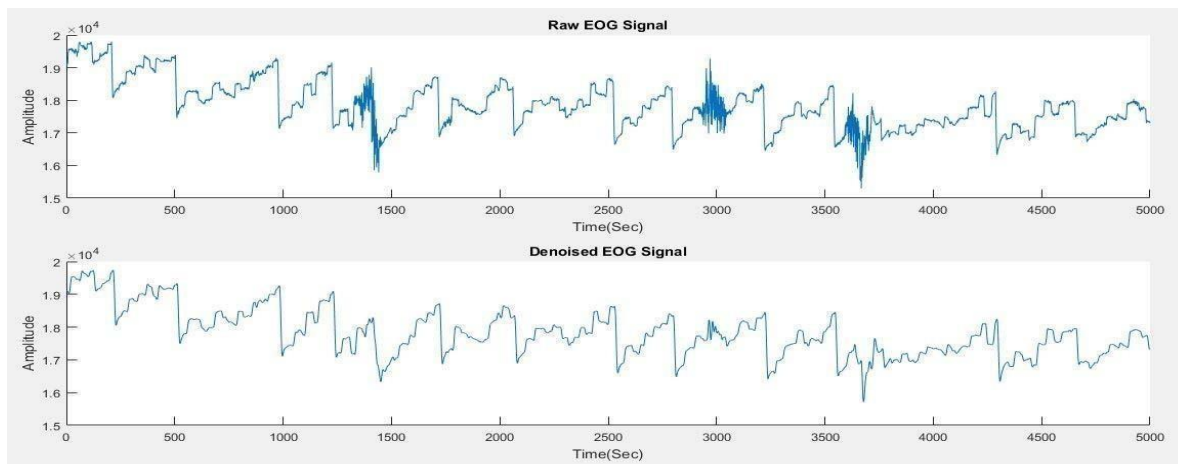


Fig. 5. Waveform of Raw EOG signal and Denoised EOG signal



Fig. 6. Power, Area and Delay Comparisons

CONCLUSION AND FUTURE WORK

In this, we have proposed a modified FIR filter for denoising the EOG signal. In this proposed modified architecture, uses CSD based representation for minimizing the multiplication. The proposed architecture was compared with the conventional method of shift-add and improvement was shown in terms of area, power and delay. The filters have been synthesized and implemented in Zynq development kit using Vivado Design suit to target the device xc7z020c1g4841. Results prove a good improvement in PDP & ADP for this filter. While the proposed architecture model was implemented using a RCA, we are currently exploring the possibility to extend it to a carry-save (CSA) realization, which are used for high-speed applications. Further, an adaptive algorithm can be implemented for detecting the saccadic eye movements for wearable devices.

REFERENCES

- [1] W. B. W. Daud and R. Sudirman, "Time frequency analysis of electrooculograph (eog) signal of eye movement potentials based on wavelet energy distribution," in 2011 Fifth Asia Modelling Symposium. IEEE, 2011, pp. 81–86.
- [2] Y. Lu, C. Zhang, B.-Y. Zhou, X.-P. Gao, and Z. Lv, "A dual model approach to eog-based human activity recognition," *Biomedical Signal Processing and Control*, vol. 45, pp. 50–57, 2018.
- [3] M. Merino, O. Rivera, I. G´omez, A. Molina, and E. Dorronzoro, "A method of eog signal processing to detect the direction of eye movements," in 2010 First International Conference on Sensor Device Technologies and Applications. IEEE, 2010, pp. 100–105.
- [4] S. Soltani and A. Mahnam, "A practical efficient human computer interface based on saccadic eye movements for people with disabilities," *Computers in biology and medicine*, vol. 70, pp. 163–173, 2016.
- [5] A. Bulling, J. Ward, H. Gellersen, and G. Troster, "Robust recognition of reading activity in transit using wearable electrooculography," vol. 5013, 05 2008, pp. 19–37.
- [6] A. Roy, J. Singha, L. Manam, and R. H. Laskar, "Combination of adaptive vector median filter and weighted mean filter for removal of high-density impulse noise from colour images," *IET Image Processing*, vol. 11, no. 6, pp. 352–361, 2017.
- [7] A. Dasgupta, S. Chakraborty, A. Chaudhuri, and A. Routray, "Evaluation of denoising techniques for eog signals based on snr estimation," in 2016 International Conference on Systems in Medicine and Biology (ICSMB). IEEE, 2016, pp. 152–156.
- [8] M. L. Kiran and K. Ramanaiah, "Design and implementation of high speed radix-2 csd based floating point multiplier," *International Journal of scientific research in multidisciplinary studies*, vol. 3, no. 7, pp. 17–22, 2017.

- [9] G. A. Ruiz and M. Granda, "Efficient canonic signed digit recoding," *Microelectronics journal*, vol. 42, no. 9, pp. 1090–1097, 2011.
- [10] H. Lee and G. E. Sobelman, "Fpga-based digit-serial csd fir filter for image signal format conversion," *Microelectronics journal*, vol. 33, no. 5-6, pp. 501–508, 2002.
- [11] M. B. Trimale et al., "A review: Fir filter implementation," in 2017 2nd IEEE International Conference on Recent Trends in Electronics, Information & Communication Technology (RTEICT). IEEE, 2017, pp. 137–141.
- [12] K. N. Parvin and M. Z. Hussain, "Multiplication techniques for an efficient fir filter design for hearing aid applications," in 2018 2nd International Conference on Inventive Systems and Control (ICISC). IEEE, 2018, pp. 964–968.
- [13] A. Sharma and T. K. Rawat, "Design and fpga implementation of lattice wave fractional order digital differentiator," *Microelectronics Journal*, vol. 88, pp. 67–78, 2019.
- [14] K. Paldurai, K. Hariharan, G. Karthikeyan, and K. Lakshmanan, "Implementation of mac using area efficient and reduced delay vedic multiplier targeted at fpga architectures," in 2014 International Conference on Communication and Network Technologies. IEEE, 2014, pp. 238–242.
- [15] A. Bulling, J. A. Ward, H. Gellersen, and G. Troster, "Eye movement analysis for activity recognition using electrooculography," *IEEE transactionson pattern analysis and machine intelligence*, vol. 33, no. 4, pp. 741–753, 2010.

Analysis of Obstructive Sleep Apnea using ECG Signals

A.K.Jayanthy
Dept. of Biomedical Engineering
SRM Institute of Science and
Technology
Chennai, India
jayanthk2@srmist.edu.in

Subhiksha Somanathan
Dept. of Biomedical Engineering
SRM Institute of Science and
Technology
Chennai, India
subhiksha.somanathan@gmail.com

Shivani Yeshwant
Dept. of Biomedical Engineering
SRM Institute of Science and
Technology
Chennai, India
shivaniyeshwant21@gmail.com

Abstract — Sleep is an important component in one's daily life and comprises about one-third of one's day. Sleep loss and disorders effect one's productivity thereby causing a significant impact on the economy. Polysomnography (PSG), which is considered the gold standard for sleep diagnosis, contains recording of multiple physiological signals Electroencephalogram (EEG), Electrooculogram (EOG), Electrocardiogram (ECG), Electromyogram (EMG), blood oxygen levels (oximetry). It has been observed that the PSG recordings obtained from the patients suffering from Obstructive Sleep Apnea (OSA) contain consistent, often repetitive, episodes of breathing pauses. However, PSG recordings are very expensive thus limiting its accessibility by the financially weaker section of the society. They are also at a greater risk of human error as over 7-8 hours recording is visually evaluated by a neurologist. The aim of this paper is to simplify the tools used for the analysis of sleep apnea. The signals procured via ECG for the analysis of OSA were explored and the accuracy for the same was analyzed. Three parameters of the signals namely Power Spectral Density, Correlation and R-R peak interval were analyzed.

Keywords—*sleep disorders, Obstructive Sleep Apnea, ECG*

I. INTRODUCTION

Sleep comprises about one-third of one's daily routine and a good sleep cycle with adequate amount of sleep is absolutely important for good health and maximum productivity. Sleep is essential for the quality of one's daily activities. It removes toxins that accumulate in the brain and helps one concentrate and respond quickly. Poor quality sleep, chronic lack of sleep or other sleep disorders lead to wide range of health, economic and social consequences. They are also known to be a leading cause of serious conditions like hypertension, cardiovascular disorders and depression.

A. Sleep Disorders

It has been well established that poor sleep quality, sleep loss and sleep disorders hamper not only the health of an individual but also affect the economy of the country. With the growing glorification of busy lives and hustle culture, a large section of the population is known to suffer from sleep disorders. Statistics are evident that 60% of the population have never been asked about their sleep quality. The importance of sleep is still under-recognized.

B. Sleep Diagnostics

Polysomnography is considered the gold standard of sleep diagnosis. [1] It consists of recording of various electro-physiological signals: brain waves (EEG), eye movements (EOG), heart rate and rhythm, chest and abdominal activity, chin muscle activity and leg movements (EMG) and oxygen saturation levels in blood. To determine if the person is asleep or awake, EEG, EOG and chin movements are evaluated. It is an expensive procedure and is performed in a sleep laboratory in the presence of a sleep technician. The fact that it is performed in a sleep laboratory, in an environment that the patient is not familiar with, the procedure is at a greater risk of being inaccurate as unnecessary patient movements are also recorded. The 7-8 hours of recordings are visually evaluated by a neurologist and are thus prone to human error. Therefore, there is a growing need to shift from manual evaluation of recordings of multiple signals to a more automated and simpler procedure.

C. Proposed System

In this paper, we hope to simplify the diagnosis process of sleep apnea by analysing just one easily obtainable signal – namely, ECG. The complexity of obtaining an ECG signal is far lesser than that of PSG signals. Further, ECG can even be obtained using a single lead system which minimizes the complexity of the equipment used and the number of potential machineries that will hinder or cause discomfort to the patient. This will also minimize the cost needed to procure signals and hence the diagnosis procedure. This in turn will encourage more people to opt for a sleep study in order to successfully diagnose and treat the disease

II. LITERATURE REVIEW

J. N. McNames [2] illustrated the use of spectrograms for recognizing sleep apnea patterns in ECG signals. This was done with the help of visual inspection of the spectrogram patterns for various features of the ECG.

J. Cheborova [3] highlighted the difficulties and limitations of feature extraction in PSG signals and attempted to come up with a simple classification algorithm for detection of sleep apnea.

Liali Almazaydeh [4] presented new techniques for sleep apnea classification that are being developed by bioengineers for most comfortable and timely detection. According to the paper short duration epochs from the ECG database is processed by an automated classification algorithm. The algorithm was based on Support Vector Machine classification. Recordings from subjects both with and without OSA were used to train and test the algorithm. The proposed algorithm has a high degree of accuracy, approximately 96.5%.

Atri R [5] proposed an algorithm which considered a wide range of features dependent on heart rate variability (HRV) and ECG- derived respiratory. It employs bi-spectralanalysis of the acquired signals to demonstrate quadratic phase coupling that can be observed among signal components having different frequencies.

T Penzel [6] compares thirteen algorithms proposed for classifying sleep apnea using ECG signals.

C Varon [7] demonstrated the use of serial correlation coefficients of RR interval time series and standard deviation for detection of sleep apnea using single lead ECG system. M Schrader [8] used ECG signals from the Physionet database to classify sleep apnea signals using three variables.

A.B Ramli [9] determined the efficiency of using cross correlation techniques for abnormal feature extraction from ECG.

Fook Joo Chin [10] proposed an algorithm that employs peak valley detector and cross correlation technique for automatic identification of features in ECG signals. Sivarajni V [11] explores the use of ECG signals for detection of sleep apnea as opposed to PSG signals. Ahnaf Rashik Hassan [12] studies the performs of eight-well known classifiers for feature extraction scheme of ECG signals for sleep apnea detection and determines theaccuracy of the same.

III. METHODOLOGY

A. ECG Database

The OSA Database was available as a part of public library available in Physionet. It was used as the main dataset in the project. The entire database was divided into two sets, ‘training set’ and ‘test set’. The database consists a set of 35 recordings, which contains a single ECG signal per subject digitized at 100 Hz with 12-bit resolution. The recording is of approximately 8 hours (individual recordings vary in length from slightly less than 7 hours to nearly 10 hours). Each recording includes a set of reference annotations. The reference annotation is used to indicate the presence or absence of apnea during that minute. Raw signal obtained from Physionet for subject 1 is shown in Fig. 1.

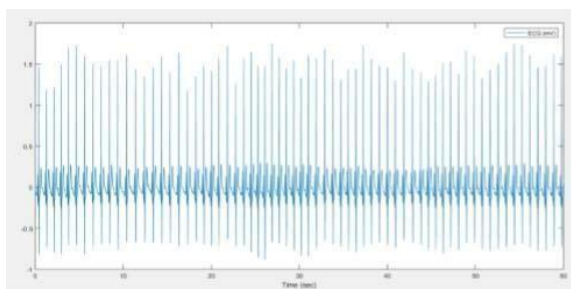


Fig 1: Raw ECG signal of subject

For the purpose of this paper, we have processed over 25 raw signals of 5 different subjects to studythe patterns of OSA and its descriptive markers in the ECGsignal.

B. Data Preprocessing

All data processing and analysis was performed in MATLAB R2018b environment. About 5 subsets of ECG recordings of 1-minute duration per subject of has beenselected. In the next step the raw data has been transformed into usable form using the MATLABenvironment.

The data needs to be pre-processed in order to obtain comparable results for automatic signal analysis. Many artifacts occur due to interference of other physiological signals. Data pre-processing includes removing as much noise as possible, detecting and removing artifacts, outliers, o sets, and preferably normalizing the amplitude range. Thus, in the first part of preprocessing, any portion of signal that presented itself as an outlier was removed effectively. The signal was then effectively low pass filtered at the rate of 200 samples per minute. DC drift was then eliminated followed by normalization. These steps were carried out on the rawsignal Fig 1 and the resulting signal is shown in Fig 2. This helps eliminate the drift caused due to DC voltage and high frequency noise, thus reducing computation required to estimate spectrogram over the frequency rangeof interest.

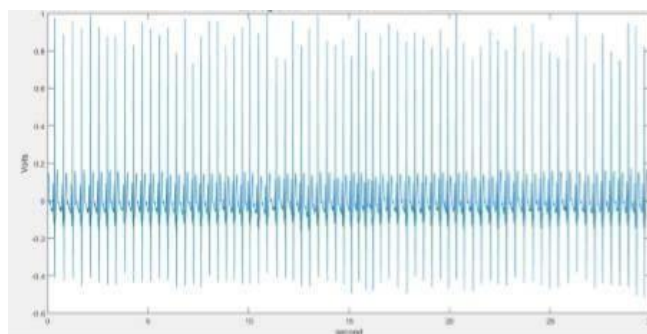


Fig 2: ECG signal after cancellation of DC drift and normalization

C. Feature Extraction

In this step, the descriptive parameters are extracted fromthe signal and are made available for easier visual inspection. A set of ECG signals were obtained for each subject. These signals of one-minute duration were chosen randomly. Some of these were ECG signals obtained during an episode of sleep apnea (Apnea signals) and the normal ECG signals where an episode of sleep apnea was absent were considered as reference signals for that corresponding subject. The annotations present on Physionet helped us make this distinction.

1) R-R Peak Detection

As a first step in the analysis, QRS detection has been implemented using Pan-Tompkins algorithm. Derivative filtering was done, followed by squaring of the waveform. Moving Window Integration was performed on the signal and a delay of 15 seconds was introduced in the samples and the corresponding waveform was plotted. ECG signal after averaging was obtained. The maximum and mean value of the peak points was calculated and a suitable threshold was selected. Further, the QRS points which were different from the Pan-Tompkins algorithm was also obtained and plotted. Finally, R-R interval was obtained by using difference operation method on the obtained results. The obtained result is shown in Fig 3. A number of false peaks were obtained while performing this algorithm as shown in Fig 4. Hence, visual inspection of the R-R peaks proved to be a more accurate method for R-R peak interval estimation.

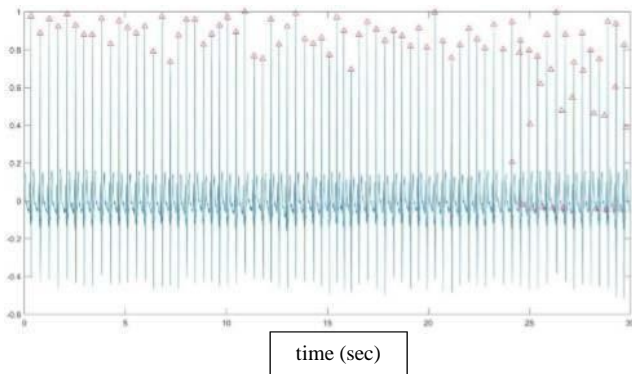


Fig 3: Final output obtained after the R-R peak detection.

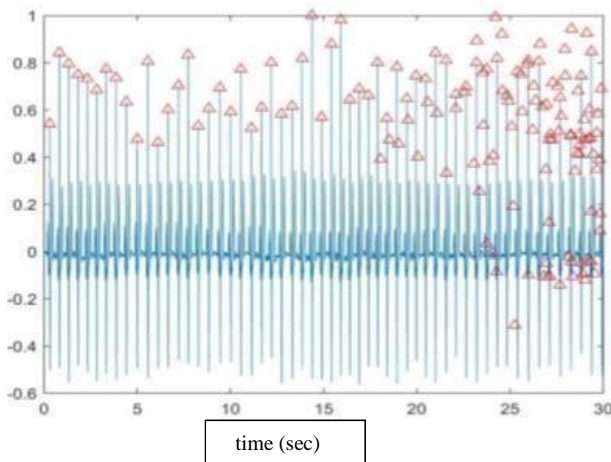


Fig 4: False peaks obtained during R-R peak detection.

2) Frequency Space Features

Spectral powers in the ECG signals (absolute or relative) are expected to be the key information extracted from the datasets. Based on the literature review, almost each normal/apneic stage should be characterized by a typical pattern of some frequency change.

The spectrograms were estimated by applying FFT to a series of signal segments extracted from the dataset. The estimates of the signal energy were also calculated in order to find the average weighted energy used to estimate the power spectral density. The sampling frequency was set as 1000 Hz. From the Power Spectral Density (PSD) plot, energy was obtained using equation 1:

$$\text{Energy (E)} = \sum \text{abs(PSD frequency)}^2 \quad (1)$$

Fig 5 illustrates the result obtained after performing PSD analysis. The power of the signal was then obtained by using equation 2. The FFT signal was obtained and the PSD was calculated. The obtained PSD was 11.4779

$$\text{Power (P)} = E/N \quad (2)$$

where N is the length of the signal. The reference waveform is shown in fig 6. The FFT signal was obtained and the PSD was calculated. The obtained PSD was 97.4911W/Hz (ref.value)

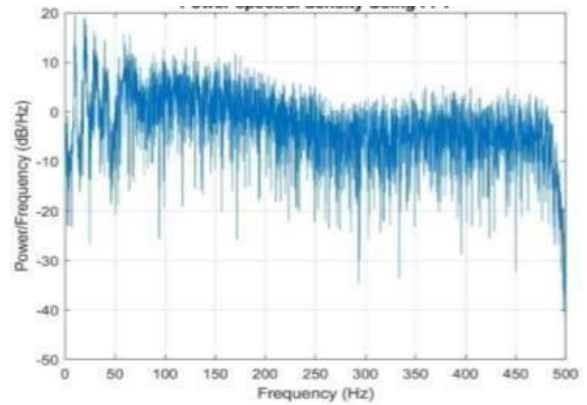


Fig 5: PSD waveform for apnea signal of subject 2

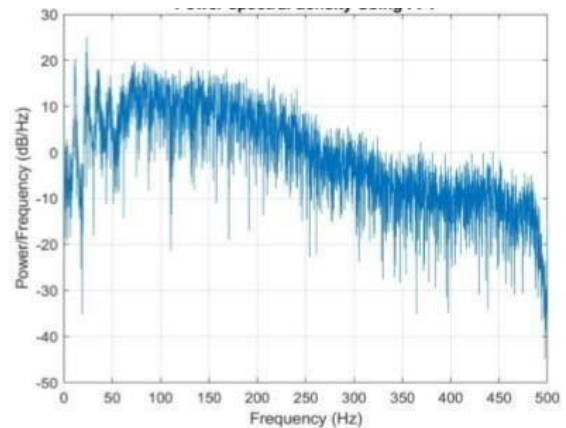


Fig 6: PSD waveform for reference signal

3) Correlation Coefficient

Based on literature review, it has been proved that calculating the cross correlation coefficient is an effective method of calculating the similarity (or the lack of it) between a reference ECG signal and an abnormal signal. The sleep apnea ECG signal was correlated with the reference ECG signal obtained from the same data set. Corresponding correlation plot was obtained on MATLAB as shown in Fig 7. The correlation coefficient was then calculated on MS Excel using equation 3:

$$R(k) = 1/N \sum x(n)y(n-k) \quad (3)$$

where x(n) is the reference ECG signal, y(n) is the sleep apnea ECG signal, which was delayed by an arbitrary factor k, N is the number of samples in a sequence, The limits of the summation were taken to vary from n=0 to n=N-1

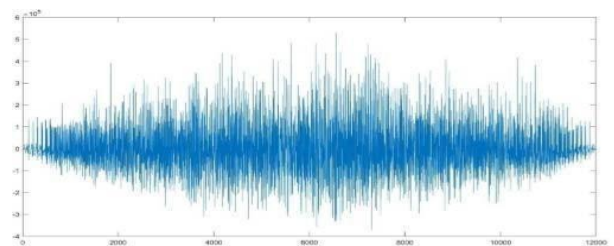


Fig 7: Signal obtained after correlating a reference ECG signal with an apnea ECG signal

IV. RESULTS

A. R-R Peak Detection

The results of R peak detection (avg R-R values) for a signal in each dataset have been tabulated below. The average RR intervals were visually inspected and calculated in mV. A significant drop in the values has been observed with respect to the normal ECG values.

Table 1: Result obtained after R-R peak detection (* reference ECG signal)

Subject	Signal	Avg R-R values(mV)
1	1.1*	0.9307
1	1.2	0.70
2	2.1	0.8105
3	3.2	0.5265
4	4.3	0.425
5	5.1	0.79

B. Spectrogram Estimation

The PSD values that were calculated are recorded below. A significant variation in the PSD values has been observed in apnea signals, when compared with the normal ECG signals from the same set. In table 2, The PSD values of the corresponding signals are mentioned. The reference value of each dataset has been highlighted. Values for dataset 4 and 5 weren't in accordance with the findings as the variation in the PSD values in these cases weren't significant.

Table 2: PSD values of signals as obtained. (*Reference ECG signal)

Subject	Signal	PSD values(W/Hz)
1	1.1*	97.4911
	1.2	56.9404
	1.3	39.5574
	1.4	52.75
	1.5	59.8955
	1.6	44.3509
2	2.1	199.3743
	2.2	658.3998
	2.3	176.4574
	2.4	239.8916
	2.5*	1.1236e+0.3
3	3.1	1.9585e+0.3
	3.2	1.7789e+0.4
	3.3	1.3181e+0.3
4	3.4*	739.921
	4.1*	4.5204
	4.2	11.8785
	4.3	11.4779
5	4.4	16.474
	5.1	3.8202e+0.3
	5.2*	1.2168e+0.6
	5.3*	1.7092e+0.6
	5.4*	1.0229e+0.4
	5.5	3.442e+0.3

C. C

Co
lin
coe
coe
coe
A
coe
the
and

strength of
correlation
Positive
negative
negative
als w.r.t to
indicated

Table 3: The correlation coefficient obtained after correlation. (* Reference ECG signal)

Subject	Signal	Correlation coefficient
1	1.1*	1
	1.2	-0.00329
	1.3	-0.001179
	1.4	-0.02437
	1.5	-0.02466
	1.5	-0.01218
2	2.1	0.001523
	2.2	0.008316
	2.3	0.04923
	2.4	-0.03871
	2.5*	0.043639
3	3.1	0.017326
	3.2	0.22221
	3.3	0.001869
	3.4*	-0.00611
4	4.1*	0.004783
	4.2	-0.02594
	4.3	-0.02548
	4.4	-0.0028
5	5.1	0.01127
	5.2*	0.052309
	5.3*	0.003375
	5.4*	0.007733
	5.5	-0.00658

V. CONCLUSION

It was found that the mathematical calculation of average RR intervals to indicate OSA episodes, had very low accuracy. Due to complexity of the patterns, it was found that we could manually (by visual inspection) classify the ECG more accurately. The accuracy was calculated manually using a simple mathematical formula.

$$\text{Accuracy} = (\text{Test/Reference}) \times 100 \quad - (4)$$

The spectrogram estimation method had an accuracy of over 90% and was is considered as the most accuratemethod of classifying ECG signals.

The correlation technique has an accuracy of over 75% in detecting OSA episodes. However, it doesn't deliver a quantitative value for representing the similarity or difference between the test signal and reference ECGsignal.

ACKNOWLEDGEMENT

The OSA Database was available as a part of public library available in Physionet. It was used as the main dataset in the project. The entire database was divided into two sets, 'training set' and 'test set'. The database consists a set of 35 recordings, which contains a single ECG signal digitized at 100 Hz with 12-bit resolution. The recording is of approximately 8 hours (individual recordings vary in length from slightly less than 7 hours to nearly 10 hours). Each recording includes a set of reference annotations. The reference annotation is used to indicate the presence or absence of apnea during that minute.

REFERENCES

- [1] "New guideline for sleep apnea diagnosis." *Medscape*, 11 August, 2014
- [2] JN McNames, A M Fraser, "Obstructive Sleep Apnea Classification Based on Spectrogram Patterns in Electrocardiogram," *Computers in Cardiology 2000*, Volume 27 (Cat. 00CH37163), Cambridge MA, 2000, pp 749-752
- [3] J. Cheborova, "Analysis of Sleep Polysomnography Data using Advanced Signal Processing Algorithms," MS Thesis, Faculty of Electrical Engineering, Department of Cybernetics, Czech Technical University, Prague, January 2017
- [4] L. Almazaydeh, K. Elleithy, M. Faezipour, "Detection of Obstructive Sleep Apnea Through ECG Signal Features," 2012 IEEE Conference on Electro/Information Technology, Indianapolis, IN, 2012, pp 1-6
- [5] R. Atri , Mohebbi M, "Obstructive sleep apnea detection using spectrum and bispectrum analysis of single-lead ECG signal," *Institute of Physics and Engineering in Medicine*, Volume 36, number 9, 10 August 2015
- [6] T. Penzel, J. McNames, P. Chazal, "Systematic Comparison of Different Algorithms for Apnea Detection based on Electrocardiogram Recordings," *Medical and Biological Engineering and Computing 2002*, Volume 40, Number 4, page 402
- [7] C Varon, A Caicedo, D Testelmans, "A novel algorithm for the Automatic Detection of Sleep Apnea from Single Lead ECG," *IEEE Transactions on Biomedical Engineering*, Volume 62, Issue 9, September 2015
- [8] M Schrader, C Zywietz, V. Von Einem, "Detection of sleep apnea in single channel ECGs from the Physionet database," *Computers in Cardiology 2000*, Volume 27 (Cat. 00CH37163), 24 September 2002
- [9] A.B Ramli, P.A Ahmed, "Correlation Analysis for abnormal ECG signals feature extraction," 4th National Conference of Telecommunication Technology, 2003. NCTT 2003 Proceedings. 14 January 2003
- [10] Fook Joo Chin, Qiang Fang, Irena Cosic, "A computationally light-weight real-time classification method to identify different ECG signals", *Bioelectronics and Bioinformatics (ISBB) 2011 International Symposium on*, pp. 287-290, 2011.
- [11] Sivaranjni V, Rammohan T, "Detection of sleep apnea through ECG signal features", *Advances in Electrical Electronics Information Communication and Bio-Informatics (AEEICB) 20162nd International Conference on*, pp. 322- 326, 2016.
- [12] Ahnaf Rashik Hassan, Md. Aynal Haque, "Identification of Sleep Apnea from Single-Lead Electrocardiogram", *Computational Science and Engineering (CSE) and IEEE Intl Conference on Embedded and Ubiquitous Computing (EUC) and 15th Intl Symposium on Distributed Computing and Applications for Business Engineering (DCABES)*, 24 August 2016

Fractal Characterization of Auditory Evoked Potentials

Suman Paria

School of Bioscience and Engineering
Final Year Student of Master of Biomedical Engineering,
Jadavpur University,
Kolkata, India.
sparia1996@gmail.com

Nilotpal Das

School of Bioscience and Engineering
Final Year Student of Master of Biomedical Engineering,
Jadavpur University,
Kolkata, India.
nilotpal.das@outlook.com

Uttaran Bhattacharjee

School of Bioscience and Engineering
Final Year Student of Master of Biomedical Engineering,
Jadavpur University,
Kolkata, India.
uttaranb417@gmail.com

Dr Monisha Chakraborty

School of Bioscience and Engineering
Associate Professor,
Jadavpur University,
Kolkata, India.
monishachakraborty@rediffmail.com

Abstract— Evoked potentials has the ability to signify electrical fluctuations in various zones of the human brain. The electrical fluctuations are generated by thresholding specific sensory neural pathways response. These evoked potential tests along with other diagnostic tests in synergy are used for pin point diagnosis of neurological pathologies. The basic concept of evoked potential test is to determine the time taken by a sensory pathway to deliver the threshold stimulus to the brain. Evoked potentials play a crucial role as they can highlight the anomalies in the neural pathway, which are not diagnosed during neurological examinations. The neural mechanisms in brain are non-linear in nature therefore along with analysis of linear in nature, Very few studies have been conducted in field of non- linear analysis of AEP. Non-linear analysis of AEP will provide information regarding neural mechanism. In this study we are using Higuchi fractal dimension analysis, which is an efficient algorithm for calculating fractal dimension, to study hearing complexity of human brain.

Keywords— *Higuchi Fractal, AEP, Evoke Potential., ABR.*

I. INTRODUCTION

When stimulation is applied to the human brain it generates the work-specific potential that is the Event Related Potential cause specific spatiotemporal patterns. Due to synchronization of specific stimulus, the brain reaches into a regular state results ERP [1, 2].ERP reveals a very important pathway for studying cognitive state with clinical significance of brain responses that is memory, attention and hearing. Auditory evoked potentials (AEP) is an ERP response evoked from the auditory sensors' pathway of the brain when an audio stimulus is applied using an earphone.

AEP signal originate with consistent either positive or negative tips, latency, amplitude and behavioral reciprocity [3, 4]. To measure the fluctuations in temporal mechanics [5] and feedback onset of brainstem auditory evoke responses of natural hearing in various intensity of

acoustic stimulus the features of fractal dimension were pulled out. This work reflects a meaningful difference among the fractal dimensional values of natural hearing in various decibels. Here in this paper about the fractal analysis of AEP data to validate non-invasive study [6] of auditory sensors organ is thus performed. Brainstem auditory evoked responses describe the bio-potential fluctuations within the auditory sensory pathway in reply to acoustic stimulus [7]. Brain stem evoked response audiometry (BERA) is the most common test. Brainstem evoked response illustrates post receptor role of the cochlea, and working of brainstem with auditory neurons [8].

II. EQUIPMENTS AND METHOD USED

A. THE ABR ACQUISITION SETUP

For this study five subjects without any hearing defects were studied. For AEP data acquisition 2/4 Channel Portable EMG Aleron 201/401 (RMS) in fig 1. For data analysis and computational purpose the MATLAB platform was used.



Figure.1.AEP Data acquisition setup

B. ABR ACQUISITION

During the experiment the electrodes are placed in

subjects' scalp. Each active electrode on mastoid position. The ground electrode on the forehead and the reference electrode on the C_z position of the head [9]

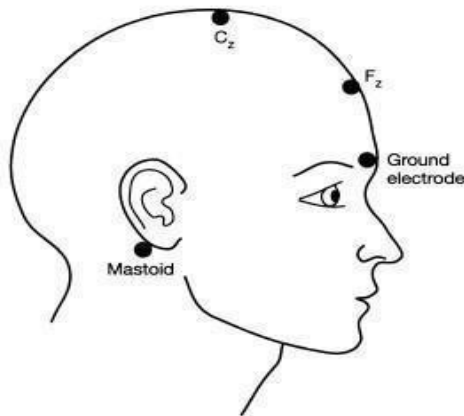


Figure.2. Electrode positions AEP data acquisition

Through the headphone the acoustic stimuli were applied. The stimulus is in tone burst nature. As output the live average response of auditory neural pathway with respect to the applied auditory stimulus is captured and saved for both ear for further analysis.

C. The method for calculating Higuchi's fractal dimension

Higuchi in 1988 proposed a process for obtaining the fractal dimensions of curves in an unbounded two dimensional shape [10]. For time-dependent phenomena the fractal dimension quantify the non-linearity of a wave illustrated graphically by plotting the values of the period quantity against time and its complexity.

Discrete responses could be evaluated as chronological sequences $x(1), x(2), x(3), \dots, x(N)$ generated from the original sequence of discrete-time data. This method creates new time series. This new sequence of discrete-time data are X_N^k .

X_N^k is defined as:

$$x(N), x(N+k), \dots, x(N + \text{int}[\frac{N-k}{k}]) \quad m=1,2,3 \dots k \quad (1)$$

So, the length of the curve X_N^k is described as:

$$L_N^k = \frac{1}{k} \sum_{i=1}^{\text{int}[\frac{N-k}{k}]} |x(N+ik) - x(N+(i-1)k)| \quad (2)$$

Where N = volume of the input time-sequence discrete data X and $\frac{(N-1)}{(\text{int}[\frac{N-k}{k}])}$ is considered as normalization

factor. $L_N(k)$ Average value for all m consisting the mean value of the curve length $L(k)$ for each $k = 1,2,3, \dots, k_{NAS}$ as:

$$L(k) = \frac{\sum_{N=1}^k L_N(k)}{k} \quad (3)$$

Where the initial time m and interval time k . An align of mean points $L(k)$ was calculated. The gradient of least squares linear best fit measured as HFD by plotting of $\ln(L(k))$ with $\ln(k)$:

$$\text{Higuchi Fractal Dimension} = \frac{\ln(L(k))}{\ln(k)} \quad (4)$$

In general, the real response plot can be shredded into littler parts with overlapping or without overlapping that is called the signal is divided into smaller windows. Taking window length N this process is applied for calculating HFD values. Either overlapping or non-overlapping condition of every window, HFD values are obtained. For entire region the specific FD values are averaged. Here signal complexness is approached with the help of mean HFD values. For low frequency sinusoidal signal or linear less complex curve the HFD value assumed to be 1 to ease the clarification about HFD values. Similarly it is assumed 2 for stochastic light disturbance or higher complex curve but in reality it is lightly greater than 2 due to mathematical rough estimation.

For HFD calculation the factor k_{NAS} selection has a great importance. On the other hand Higuchi not explained much details during his own writing [11]. But he clarified the details for greater values of k_{NAS}

Such that $k_{NAS} = 2^{11}$ for $N = 2^{17}$. A few analysis have been addressed for choosing k_{NAS} . In past to find out the perfect k_{NAS} and N , k_{NAS} has been taken 3 to 10 for signal parts of variable N varying from 50 to 1000. Taking $k_{NAS} = 6$; the most fit HFD derived from 1 to 1.5 [12].

III. RESULTS AND DISCUSSION

In figure 3, the points I, II, III, IV, and V are five wave shapes.

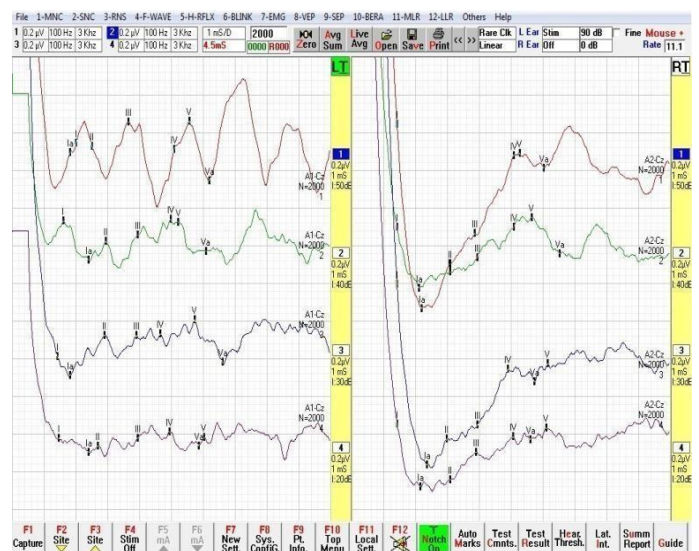


Figure.3. AEP data acquisition result in Aleron201/401(RMS)

Wave shape V has highest magnitude. It denotes the threshold of the signal. This address the electric response developed in particular anatomical position of inferior colliculi wave shape I for cochlear nerve and II for nuclei. Wave III and IV superior olivary nucleus and lateral lemniscuses respectively [11].

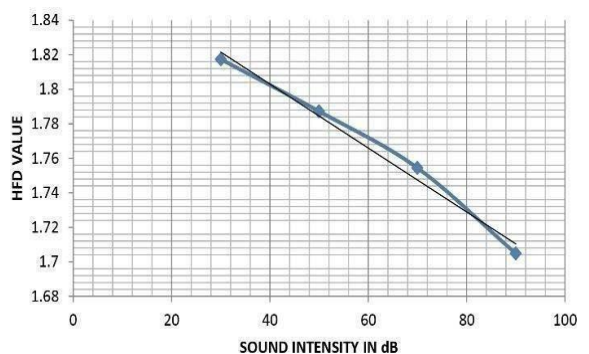


Figure.4a.variation of HFD value and sound level in right ear

In differential symptomatic dissonant induced hearing loss the ABR assigned for differentiate cochlear with retro- cochlear site for lesion. In natural hearing the structure of the wave shape and inter-waveform latencies is in general pattern. The latencies of all wave shapes are greater for conductive hearing loss but inter-wave latencies are in typical nature. For central conduction time delay the basic structure of the waveforms may be abnormal expect the wave shape I. Inter-wave latencies between (I-V) and (III-V) are extended [11]. Here from five subjects using various level of intensity in descending order using earphones (i.e. mainly Audiometry purpose) the sound was applied. The subject were asked to laydown in a comfortable bed and the surface electrodes were placed accordingly. The whole data set was acquired in csv format and for processing purposes it was converted in excel format and Higuchi fractal dimensions were obtained and plotted.

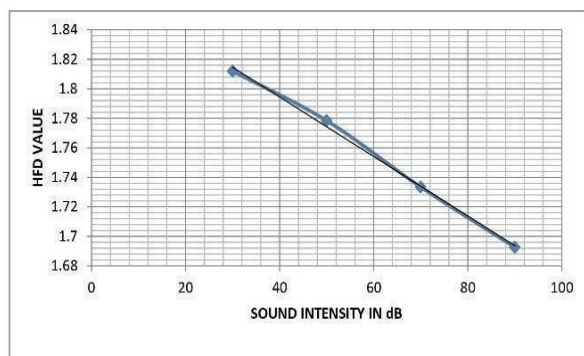


Figure.4b. variation of HFD values with sound level in left ear

For this study we have chosen five subjects and we applied the sound stimulus in various dB that is 90dB, 70dB, 50dB, 30dB in both ear. The AEP data was 481 samples and their subsequent fractal values were calculated. The standard deviations also shown here that the data points are very consistent in nature. Two graphical plots (fig 4a and 4b) also drawn here

for visualizing the characteristic of hearing threshold level in various sound intensity.

IV. CONCLUSION

The auditory evoked potential (AEP) components with latencies less than 10ms, commonly called brainstem auditory evoked potentials (BAEPs), are the most useful AEPs for intra operative monitoring. BAEPs are captured using surface electrodes. This responses represent electric fluctuations delivered from the nerve and auditory relay of brainstem by inducing an auditory stimulus with in 10ms. In this work, the fractal attributes have been drawn from the captured BAEPs responses. The FD values of natural hearing subjects from both ear in various intensity were recorded. The acquired attributes were related to their hearing threshold levels. From the output, it was observed that average FD value of hearing in lower intensity (decibel) is meaningfully higher than fractal dimension values hearing in higher intensity. So there is a linear relationship between HFD and decibel. The HFD value decrease is somewhat linear in nature with higher decibel.

In addition, it was observed that the concerned fractal features can clearly diversify the hearing threshold scale perception of normal subject in various sound intensity it was observed that in lower sound intensity there is more complexity in hearing. Fractal dimension is to figure out of the physiological complexity of a signal. FD values are used to draw conclusions regarding the underlying physiological phenomenon. It is clearly seen here that when the stimulus is higher, complexity is less. It can be concluded that at due to greater amplitude of the stimulus, greater number of neurons work synchronously in the transmission of the neural impulse, thereby reducing the complexity of the phenomenon. Whereas when the impulse is less, lesser neurons are involved in the transmission of the neural signal, and the degree of asynchrony is greater. This maybe the physiological explanation of the above observations. However, brain being a non-linear system, other parameters might influence the neural workings. Therefore, further analysis involving other non-linear tools and greater number of data is required, which is a part of our future work.

REFERENCES

- [1] M. Emre Cek, M. Ozgoren and Acar Savaci, "Continuous time wavelet entropy of auditory evoked potentials," J. Comp. in Bio and Med, vol. 40, pp. 90-96, 2009.
- [2] D. Puthankattil Subha, P. K. Joseph, and U. Rajendra Acharya, "EEG signal analysis: A survey," J. Medical Sys., vol. 34, pp. 195-212, 2008
- [3] G. Plourde, "Auditory evoked potentials," Journal Best Practice. and Research clinical Anaesthesia, vol. 20, pp. 129-139, 2006.
- [4] E. Delgada and Ozcan ozdamar, "Automated auditory brainstem response interpretation," IEEE Engineering in Medicine and Biology, vol. 13, pp. 227-237, 1994.
- [5] M. P. Paulraj, S. B. Yacob, A. Hamid, B. Adom, K. Subramaniam and C. R. Hema, "EEG based hearing threshold classification using fractal feature and neural network," 2012 IEEE Student Conference on Research and Development (SCORED), Pulau Pinang, 2012, pp. 38-41. doi: 10.1109/SCORED.2012.6518607.
- [6] Sheila R. Pratt, John D. Durrant, in Handbook of Clinical Neurophysiology, 2013.
- [7] EDWARD GOLDSON, DESMOND P. KELLY, in Developmental- Behavioral Pediatrics, 2008.
- [8] Harvey L. Edmonds Jr. PhD, Warren J. Levy MD, in Kaplan's Essentials of Cardiac Anesthesia (Second Edition), 2018.
- [9] S. L. Bell^{1*}, D. C. Smith², R. Allen¹ and M. E. Lutman¹ Recording the middle latency response of the auditory evoked potential as a measure of depth of anaesthesia. A technical note.
- [10] T. Higuchi, Approach to an irregular time series on the basis of the fractal theory, Physica D 31 (2) (1988) 277-283. Mariola Sliwinska-kowalska, in Handbook of Clinical Neurology, 2015.
- [12] Srdjan Kesić, Sladjana Z. Spasić. "Application of Higuchi's fractal dimension from basic to clinical neurophysiology: A review", Computer Methods and Programs in Biomedicine, 2016.

Optimal Filtering of Single Channel EEG Data using Linear Filters

Ashmita Bera
Final Year M.E student

Nilotpal Das
Phd Scholar

Dr. Monisha Chakraborty
Associate Professor

School of Bioscience and Engineering
Jadavpur University
Kolkata, India
ashmitabera95@gmail.com

School of Bioscience and Engineering
Jadavpur University
Kolkata, India
nilotpal.das@outlook.com

School of Bioscience and Engineering
Jadavpur University
Kolkata, India
monishachakraborty@rediffmail.com

— **Electroencephalogram (EEG) is a flexible diagnostic tool used to study the underlying neural activities of the brain. However, these EEG datasets are often contaminated by artefacts that reduce the quality of these acquired bio-signals and are difficult to remove and cause misinterpretation of the underlying neural information. Moreover, no universally applicable denoising technique exists nor is there any set standard for comparison of denoising methods. A method to compare denoising methods based on Signal to Noise Ratio (SNR) and Cross-Correlation analysis using an ideally filtered signal was proposed in this paper. The ideally filtered signal was achieved using Blind Source Separation (BSS) technique. BSS techniques are computationally intensive, require greater number of EEG channels and require manual supervision for appreciable performance. Thus, in order to achieve comparable denoising performance on single-channel EEG data simple universally applicable linear filters were used. Filter order optimization was performed for various linear filters for maximal SNR performance. Signals filtered using linear filters were compared to BSS filtered signal using Cross-Correlation Analysis. It is seen that for most filters, their performances correlates to that of the optimal signal achieved by BSS, at their least orders, hereby overcoming the limitations of BSS.**

Keywords—EEG, filters, blind source separation, SNR.

I. INTRODUCTION

Electroencephalogram (EEG) is a flexible diagnostic tool used to study the underlying neural activities of the brain in high time resolution. However, EEG being a very weak bio- signal with amplitude ranging from $0.5\mu\text{V}$ to $100\mu\text{V}$ is often contaminated by noise and artifacts with sources other than the brain, such as, muscular, ocular and environmental artifacts which reduces the quality of these acquired bio signals substantially. These artifacts are not only difficult to eliminate, but also lead to misinterpretation of the underlying neural information processes [1,2]. Presence of such artifacts may lead to false alarms in epilepsy detection, [13] misinterpretation in critical care units [12], affect the detection of Event-Related Potentials (ERP) and correspondingly affect related Brain-Computer Interfaces, [14] and affect diagnosis of diseases such as Alzheimer's. [15] Hence, it is very important to pre-process and denoise EEG data for proper analysis and interpretation.

Till date various EEG denoising techniques have been developed each having their own set of

advantages and disadvantages. Some of the common EEG denoising techniques include linear filtering [2], regression analysis [17], blind source separation (BSS) techniques which include Canonical Correlation Analysis (CCA) wavelet-based techniques, Principal Component Analysis (PCA), Independent Component Analysis (ICA), Empirical Mode Decomposition (EMD), adaptive filtering, etc. Recent studies have used a combination of two or more of these techniques to achieve proper denoising or artifact removal performances. Despite the presence of a plethora of EEG noise removal techniques, no such algorithm has proved to be universally applicable for all data acquisition protocols. Moreover, there is no universally accepted standard or protocol to compare the denoising performance of these techniques.

The aim of this paper is to initially propose a technique for comparison of denoising methods and achieve maximal EEG denoising performance with minimal computational complexity. BSS based EEG denoising techniques like ICA and CCA are quite commonly used and achieve appreciable artifact removal performance, but require manual supervision and are computationally intensive [3]. Moreover, these techniques require a greater number of EEG data channels for optimal performance, though recently single channel BSS based techniques have been studied.

Thus, in this paper we try to achieve the efficiency and denoising performance of BSS based denoising techniques on single channel EEG data using simple linear filters. Infinite Impulse Response (IIR) and Digital Finite Impulse Response (FIR) filters effectively remove artefacts with little computational complexity and are suitable for real time use [5]. The choice of filters depends on the type of analysis one is performing with the EEG data. For this we initially denoise EEG data collected under controlled lab environment using BSS based denoising technique with manual supervision and obtain an ideally denoised signal. We then try to achieve a similar denoising performance using digital FIR and IIR filters. We also find out the filter order at which each filter performs best using a filter order optimisation technique [18].

METHODOLOGY

The methodology used in this work can be represented using simple flowcharts –

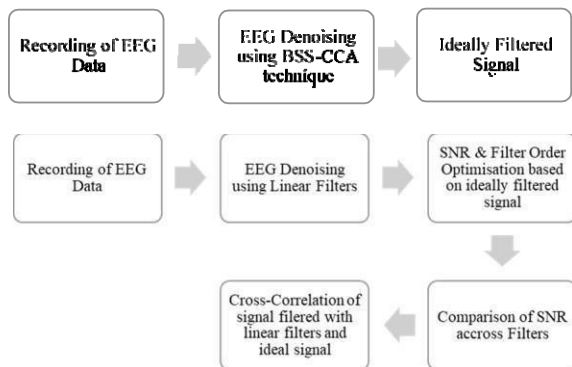


FIG. 01: Methodology for the presented study

A. Recording EEG Data

EEG was recorded on 21 channel EEG recorder (RMS). Electrodes placement was according to the International 10–20 System. Sampling frequency was 256 Hz and an average reference montage was used. EEG data was recorded in an air-conditioned dark room with subject's eyes closed condition so as to eliminate EOG artefacts and specifically focus on other environmental noise sources and EMG noises. It was then loaded in MATLAB to perform pre-processing steps. An Intel Core i5 processor and 8 GB memory computer was used for this study. The program took approximately 2 minutes to execute on one dataset.

B. EEG Denoising using BSS based technique

1) Blind Source Separation

Since most of the artifacts present in the raw EEG dataset is in both spectral and temporal domains, ordinary linear filters are unable to extract these artifacts without the knowledge of their sources or signal characteristics. The BSS is an effective denoising technique that extracts individual unknown source sig from mixture and estimates the unknown mixing channel [7]. When surface EEG electrodes acquire raw EEG datasets, they are usually contaminated with muscle artifacts or ocular artefacts. The BSS technique identifies these unknown sources other than the EEG montages, without much knowledge about these sources. In BSS, the main assumption is that the sources possess little correlation and that number of sources is either equal or lower than that of the observed channels or they are independent.

Let X be the observed signals in multichannel recording, of a linear mixture of sources S , along with additive white noise vector N . Thus,

$$X = AS + N$$

The objective of BSS is to estimate of this linear mixture matrix A , such that W is a set of iterations that leads back to the source signals S .

$$S' = WX$$

2) Canonical Cross Correlation Analysis (CCA)

CCA is a method in BSS that separates a number of mixed signals by second order statistics (SOS) for generation of components derived from their uncorrelated nature. CCA addresses the problem by finding uncorrelated components, after which it finds a set of ordered components from lowest to highest auto correlation, where the most auto correlated component comprises of maximum artifacts.

3) Denoising EEG Data using BSS-CCA

EEG data is first loaded in MATLAB and then imported in EEGLAB plugin [17]. Artefact removal based on BSS-CCA technique is implemented using Automatic Artifact Removal Toolbox 1.3 which contains several well-established artefact removal techniques. The performance of the algorithm is monitored, and the results are highly appreciable, as observed in

Figure 03. The wealth of EEG signal

after implementing BSS-CCA, in Figure 04, shows the spectral density of the signal.

C. EEG Denoising using Linear Filters

Two categories of digital filters are considered, as shown in Figure 05: IIR and FIR. Impulse response in FIR is exactly the same as the sequence of filter coefficients which depends only on the inputs, so it is called feed forward. The IIR filter, on the other hand, is recursive and the output depends on both current and previous inputs as well as previous outputs. The basic parameters of the filter design are as follows:

1. Order of filter – 1 to 100
2. Cut-off Frequency – 70Hz
3. Sampling frequency- 256 Hz
4. window length in all the windows is order+1

IIR and FIR filters were designed in MATLAB program.

The denoising process of the EEG signal is shown in Figure 1.

The IIR filters used in this study are:

1. Butterworth
2. Elliptic
3. Chebyshev type I
4. Chebyshev type II

The FIR filters used in this study are:

1. Equiripple
2. Least Square
3. Constrained Least Square
4. Window Method
 - Rectangular Window
 - Blackman Window
 - Bartlett Window
 - Hanning Window
 - Hamming Window
 - Kaiser Window

The need to work over a single channel of data with minimum computational complexity is achieved by use of linear filters. Rousselet [9] found that there were no effects of low-pass filtering on the ERP onsets on his data, but rather that high-pass filtering was more problematic, suggesting the use of a causal high-pass filter.

D. Calculation of Signal to Noise Ratio (SNR)

The objective of initially obtaining an ideally filtered EEG signal is to establish a basis for comparison of filters. SNR is simply defined as signal power over noise power.

$$SNR = \frac{P_{signal}}{P_{noise}} = \left(\frac{A_{signal}}{noise} \right)^2$$

To compare various denoising techniques based on SNR, noise power is made constant for each set of data. This is done by defining the noise signal as—

Noise = Raw EEG Signal – Ideally Filtered Signal.

Thus, Noise power for a single data set becomes constant, and hence filtering performance of digital filters can be effectively compared [18].

E. Filter Order Optimisation

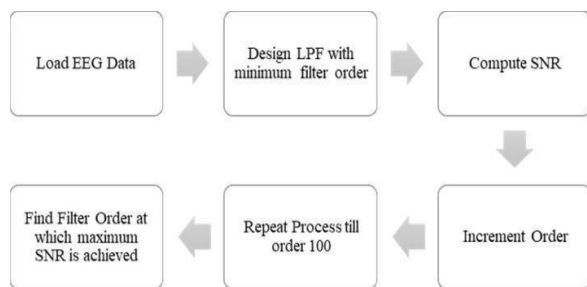


FIG 02: Steps for filter optimisation

The filter optimization process consists of 5 steps, as shown in Figure 02:

1. Loading optimally achieved EEG data
 2. Designing IIR and FIR filters using the MATLAB program.
 3. Implementing designed IIR and FIR filters on the optimally achieved EEG data for orders 1-100.
 4. Evaluating SNR – Quantification of filters for every order is done by calculating the SNR of the filter with respect to the reference signal
- $$SNR = \frac{\text{Signal power}}{\text{noise power}}$$
5. Incrementing filter order and redesigning the filter up to order 100.
 6. Filter order at which maximum SNR is obtained is selected.

F. Cross-Correlation Analysis

Correlation is the degree of similarity between two time signals as a function or indicates. When two independent indicates are compared, the procedure is called cross- correlation. It's importance in measurement of relationship between test signal and

other measure of performance is an indication of the working capacity of a system. We use cross- correlation in our study to compare the closest filter performance to the optimal signal.

The strength of a linear relationship between two variables is quantified by Correlation. When two variables are highly correlated, increase in one variable will result in increase in the other variable. Two uncorrelated variables are not necessarily independent, i.e they do not have a tendency to increase or decrease in tandem, however, they might show a nonlinear relationship. [19]

The population correlation coefficient $\rho_{X,Y}$ between two random variables X and Y with expected values μ_X and μ_Y and standard deviations σ_X and σ_Y is defined as

$$\rho_{X,Y} = \text{corr}(X, Y) = \frac{\text{cov}(X, Y)}{\sigma_X \sigma_Y} = \frac{E[(X - \mu_X)(Y - \mu_Y)]}{\sigma_X \sigma_Y}$$

where E is the expected value operator, cov means covariance, and corr is a widely used alternative notation for the correlation coefficient.

In our study, we measured the cross-correlation coefficient between filtered signal and ideal signal. The cross-correlation coefficient is a marker of similarity between the filtered and ideal signal, thereby quantifies how closely the filtered signal resembles the ideal signal created using BSS-CCA algorithm.

III.RESULT

A. EEG Signal Denoising using BSS-CCA



FIG 03: TOP: Raw EEG signal before filtering as obtained from EEG acquisition system. BOTTOM: The same EEG signal after denoising using BSS-CCA algorithm.

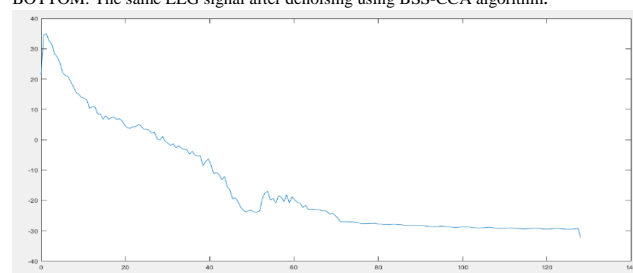


FIG 04: Welch of EEG signal after BSS-CCA denoising

B. Filter Order Optimisation

TABLE 01: Filter order and their corresponding SNR

SR NO	Filter Name	Max SNR	Corresponding Order
1	Butterworth	4.1964	2
2	Chebyshev 1	4.1696	1
3	Chebyshev 2	4.1694	2
4	Elliptic	4.1694	2
5	Equiripple	7.4434	3
6	Least squared	5.6444	2
7	Constr.least sq	4.3891	13
8	Rectangular	4.1918	6
9	Bartlett	4.1688	2

In the above Table 01, it can be observed that Equiripple filters have the highest SNR compared to other filtering techniques. Difference in SNR between various filters is not that significant. Another important observation is the variation of SNR with filter order for different filters, as shown in Figure: 06. In a previous study based on ECG data, a similar trend was observed, that is, after a particular optimal filter order, SNR decreased with increasing filter order. A similar phenomenon is observed here too. The maximum performance of most filters is realized in around filter order 2-3, with a few being exceptions. SNR is a quantitative evaluation of denoising performance [18], thus visual inspection of is important. It is seen that BSS-CCA provides cleanest output data while retaining neurological information. Interestingly, other filtering techniques are able to achieve appreciable denoising performance without affecting neural information

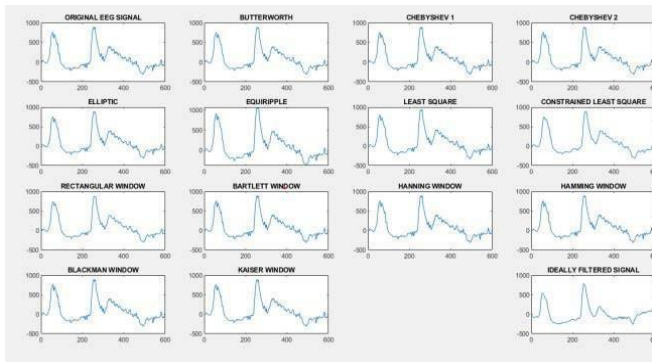


FIG 05: Denoising by various filters

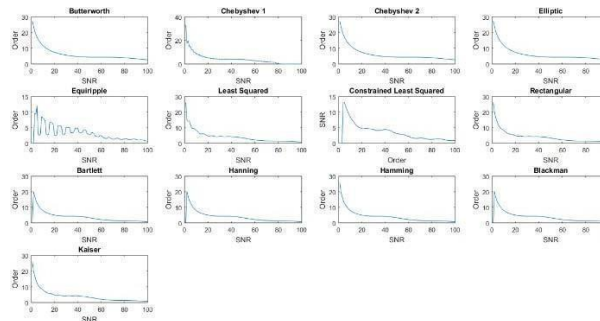


FIG 06: SNR vs Filter order for Denoising filters

C. Cross-Correlation Analysis

SR NO.	Filter Name	Correlation Coefficient	Corresponding Order
1	Butterworth	0.8830	2
2	Chebyshev 1	0.8894	1
3	Chebyshev 2	0.8830	2
4	Elliptic	0.8830	2
5	Equiripple	0.8838	3

TABLE 02: Cross Correlation Analysis data

In the above Table 02, the results of correlation analysis have been tabulated. Correlation coefficient is a marker of similarity between the filtered signal and ideal signal. There is negligible differences between the performance of the linear filters and the high correlation coefficient indicates the filtered signals closely resemble ideally filtered BSS-CCA signal.

CONCLUSION

EEG is a very important tool in the study of neurophysiological conditions in both research and clinical setups. EEG being a very weak bio-signal is easily corrupted by various forms of noise. Even though many denoising techniques exists, each technique has its own advantages and disadvantages, hence no universally applicable EEG denoising technique is present. Moreover, there is no set standard for the comparison of various denoising techniques.

In this paper we have initially proposed a method for the performance comparison of linear filters based on SNR and compared the performance of linear filters against BSS-CCA denoising technique. BSS-CCA is a highly effective artifact removal algorithm but has the downsides of being computationally intensive and its performance depends on the number of channels present in the data. We evaluated simple digital linear filters to achieve similar denoising performance working on single channel data, thereby alleviating the downsides of BSS-CCA. As this study comprises of a part of an EEG visual study protocol of the author, the channel selected in this study is O1, as most of the visual pathway terminates in the Occipital lobe of the brain.

An algorithm to aid in selection of an optimum filter with its corresponding order for a desirable output is presented here. An algorithm selects the best performing linear filter, closest to the performance of a BSS implemented signal, hereby overcoming the limitations of the said technique. The presented algorithm has a universal approach and can work across dataset acquisition protocols and applications. SNR acts as a reliable quantifier and analyses the ratios of these filters to the optimally achieved signal, i.e., BSS signal, while, correlation analysis measures how closely the denoised signal relates to the ideal signal. The filter orders when studied against their respective SNRs showed a similar trend for every filter under study. Such a trend was also observed in our previous work using ECG signals [18]. The SNR varied inversely to the order of the filter. It was also observed that the IIR filters showed better performance with respect to the optimally achieved signal, than the FIR filters. It

was seen that EEG denoised using linear filters closely resembled the ideal signal thus linear filters can be used for EEG denoising where fast performance is a requirement. Thus, this algorithm will help in detecting artifacts and then aid in denoising them effectively.

REFERENCES

- [1] M.kahle, G.Wilson, C.Russel, 'Removal of ocular
- [2] artefacts from EEG : A comparison of adaptive filtering method and regression method using simulated data', IEEE, Engineering in Medicine and Biology,
- [3] Vivek Singh, Karan Veer, Reecha Sharma, Sanjeev Kumar, 'Comparative study of FIR and IIR filters for the removal of 50 Hz noise from EEG signal', International Journal of Biomedical Engineering and Technology, 2016 Vol.22 No.3, pp.250 – 257. Md Kafiul Islam, Amir Rastegarnia, 'Methods for artifact detection and removal from scalp EEG: A review', Neurophysiology Clinical Neurophysiology (2016) 46, 287—305.
- [2] Pun, Carson KS, S. C. Chan, K. S. Yeung, and K. L. Ho, 'On the design and implementation of FIR and IIR digital filters with variable frequency characteristics', Circuits and Systems II: Analog and Digital Signal Processing, IEEE Transactions, vol.49(11), 689-703, 2002.
- [3] Proakis, John G, 'Digital signal processing: principles algorithms and applications', Pearson Education India, 2001.
- [4] Niedermeyer, Ernst and FH Lopes da Silva, 'Electroencephalography: basic principles, clinical applications, and related fields', Lippincott Williams & Wilkins, 2005.
- [5] Fitzgibbon, S. P, D. MW Powers, K. J. Pope and C. R. Clark, 'Removal of EEG noise and artifact using blind source separation', Journal of Clinical Neurophysiology, vol.24(3), pp. 232-243, 2007.
- [6] Anneleen Vergult, Wim De Clercq, 'Improving the Interpretation of Ictal Scalp EEG: BSS-CCA: Algorithm for Muscle Artifact Removal', Epilepsia, 48(5):950– 958, 2007 Blackwell Publishing, Inc.
- [7] Rousset, G. A., Gaspar, (2010), 'Healthy aging delays scalp EEG sensitivity to noise in a face discrimination task', Front Psychol. 1:19, doi:10.3389/fpsyg.2010.00019.
- [8] Andreas Widmann, Erich Schröger, 'Filter Effects and Filter Artifacts in the Analysis of Electrophysiological Data', Front Psychol. 2012; 3: 233.
- [9] M.E. Daviesa, C.J. James, 'Source separation using single channel ICA', Signal Processing and Control Group, ISVR, University of Southampton, UK Signal
- [10] Seneviratne U, Mohamed A, Cook M, D'Souza W, 'The utility of ambulatory electroencephalography in routine clinical practice: a critical review', Epilepsy Res 2013;105:1—12.
- [11] Fisher RS, Vickrey BG, Gibson P, Hermann B, Penovich P, Scherer A, et al. 'The impact of epilepsy from the patient's perspective I. Descriptions and subjective perceptions', Epilepsy Res 2000;41:39—51.
- [12] Vaughan TM, Heetderks W, Trejo L, Rymer W, Weinrich M, Moore M, et al. 'Brain-computer interface technology: a review of the second international meeting', IEEE Trans Neural Syst Rehabil 2003;11:94—109.
- [13] Cassani R, Falk TH, Fraga FJ, Kanda PA, Anghinah R. 'The effects of automated artifact removal algorithms on electroencephalography-based Alzheimer's disease diagnosis', Front Aging Neurosci 2014;6:55.
- [14] A. Jain, B. Abbas, O. Farooq and S. K. Garg, 'Fatigue detection and estimation using auto-regression analysis in EEG', 2016 International Conference on Advances in Computing, Communications and Informatics (ICACCI), Jaipur, 2016, pp. 1092-1095, doi: 10.1109/ICACCI.2016.7732190
- [15] Arnaud Delorme, Scott Makeig, 'EEGLAB: an open source toolbox for analysis of single-trial EEG dynamics including independent component analysis', Journal of Neuroscience Methods 134 (2004) 9–21
- [16] Nilotpall Das, Monisha Chakraborty, 'Performance Analysis of FIR and IIR Filters for ECG Signal Denoising based on SNR', 978-1-5386-1931-5/17/\$31.00 ©2017 IEEE
- [17] Rödel, E, Fisher RA, 'Statistical Methods for Research Workers', Oliver & Boyd, Edinburgh, London. XIII, 12, 429-30.

Fractal Characterization of ECG signals: Indian Classical Music as stimulus

Nilotpal Das
PhD Scholar,
School of Bioscience and Engineering
Jadavpur University
Kolkata, India
nilotpal.das@outlook.com

Dr Monisha Chakraborty,
Associate Professor,
School of Bioscience and Engineering
Jadavpur University
Kolkata, India
monishachakraborty@rediffmail.com

Abstract— Music elicits a wide range of effects on human physiology. The diverse effects of musical stimuli on cardiovascular and autonomic nervous-system dynamics are characterized by the analysis of Electrocardiography (ECG) signals. ECG reflects the electrical activity of the heart. Studies suggest that human heart and ECG is non-linear and chaotic in nature, therefore needs to be studied using non-linear methods. In this paper, monofractal Detrended Fluctuation Analysis or DFA method will be first used, followed by subsequent multifractal method – Multifractal Detrended Fluctuation Analysis (MFDFA). Using these methods, we will be studying the non-linear characteristics of ECG while listening to Indian Classical Music. Very few studies have been performed to characterize how Indian Classical Music affects the non-linear nature of ECG signals using multifractal tools. In our experiment, the presence of long-range scale-invariant structure in ECG signals is initially studied using DFA. The scaling behaviour of ECG signals is characterized by more than one scaling exponent, suggesting the multifractal nature of ECG. MFDFA is performed to study the multifractal nature of ECG. Width of multifractal spectrum while listening to music is compared with resting condition. Results show that the range of multifractality increases while listening to music.

Keywords—ECG, DFA, MFDFA, music, multifractal

I. INTRODUCTION

The effects of music on human mind and body are apparent and realizable even though difficult to quantify. The effects of music on the cardiovascular system have been studied with a greater focus on the analysis of pulse dynamics or heart rate variability (HRV). Studies on HRV revealed that listening to music reduces stress and causes relaxation [1,2]. It is believed that every music has a specific musical signature which might resonate with the rhythm of the body (heart rate) [3]. Such an observation confirmed the observed individual response specificity of heart rate while listening to music, that is, different individuals respond differently to different music [4, 5]. It was also seen that repeated exposure to self-selected music caused a significant reduction in heart rate, thereby suggesting the stress-reducing property of music [4].

The above-cited studies have used HRV to understand the effects of music on heart. HRV is a highly effective tool to understand the working of the autonomous nervous system and reflects the level of stress and emotions [6,7,8,9]. HRV studies have also been conducted to study the effect of music on cancer survivors [10]. Even though HRV studies have been commonly used in the analysis of the effects of music, it only reflects the variation of heart rate and does not reflect other morphological changes in the electrical activity of the heart.

Electrocardiography (ECG) studies while listening to music have revealed increase in the amplitude of QRS complex and reduced amplitude in the T-wave [11].

of ECG have been performed to quantify emotions generated while listening to music and automated emotion recognition algorithm was developed [12].

Recent studies have stressed the use of non-linear tools to analyse the underground physiological response of human system [13, 14, 15, 16]. It is now known that biological signals are irregular, non-stationary and autocorrelated and thus non-linear properties of signals are used to measure the correlational properties [17]. Fractal analysis is commonly used to study the non-linear properties of signals. Fractal signals are long-memory processes characterized by slow decay in the autocorrelation function. Fractal structures are self-similar and scale-invariant in nature and are characterized by power-law exponents. If the signal is characterized by a single power-law exponent then the signal is monofractal in nature, and if there exists a range of scaling exponents then the signal is multifractal in nature [18]. Biological systems are generally multifractal in nature and require multifractal analysis. Multifractal Characterization of ECG signals have been widely studied and are better in detecting irregularities not detected by other linear analyses [19]. It has been seen that the multifractal nature of the heart varies with its health. Multifractality studies can be used to differentiate between healthy and diseased subjects [13,20]. In diseased conditions, multifractality of ECG signal decreases. Multifractality of ECG is greater in young subjects compared to older subjects. [19,21]

Fractal nature of HRV was analysed while listening to music which showed changes in complexity in HRV with music [22] but very few studies have been conducted on the fractal characterization of ECG signals while listening to music. In this paper, we will study the fractal nature of ECG while using Indian Classical music as a stimulus. We will perform both monofractal and multifractal characterization of ECG signals. Monofractal characterization will be performed using Detrended Fluctuation Analysis (DFA) with and without music stimulus. To further extend the study, multifractal characterization will be performed using Multifractal DFA (MFDFA) technique on ECG signals with and without music stimulus [23].

II. METHODOLOGY

The methodology followed in this study is simple and is represented with the help of a flowchart:

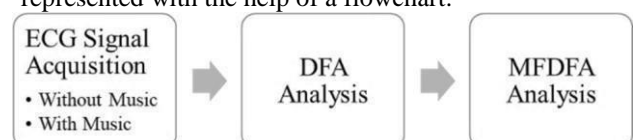


Fig. 1. Block Diagram of Methodology followed.

A. Data Acquisition

ECG signal was acquired using RMS Vesta ECG machine. Electrodes were placed according to Einthoven Triangle and Lead 2 was selected for ECG analysis. The sampling frequency of the signal acquisition system is 500Hz.

8 healthy subjects of age between 22-27 years, without any cardiovascular conditions or medication at the time of the experiment, were randomly selected. Out of the 8 subjects 5 were male and 3 were females. Subjects were seated in a relaxed position in an air-conditioned room and music was played using over-the-ear headphones.

The experimental protocol involved an initial resting period of 5 minutes without any auditory impulse. This is the rest phase or no-music phase. After the resting period, Indian Classical Music recordings were played for 5 minutes. This is called the Music phase. The music phase was followed by a 5- minute no-music phase or rest phase. The whole cycle is repeated 3 times, in each cycle, a different music recording was played. The music recordings used were from archived recordings of Late Pandit Ravi Shankar, sampled at a frequency of 44100Hz. The Ragas used in this study were – Ahir Bhairav, Bhimpalasi and Yaman Kalyan.

B. Detrended Fluctuation Analysis

In 1994 Peng introduced the method called Detrended Fluctuation Analysis to study the long-range correlations in DNA [24]. DFA is used to study the scaling nature present in fractal structures. It has several advantages in detecting correlations present in non-stationary signals all the while being insensitive to long-range correlations which are due to the non-stationary nature of the signal (artefacts)

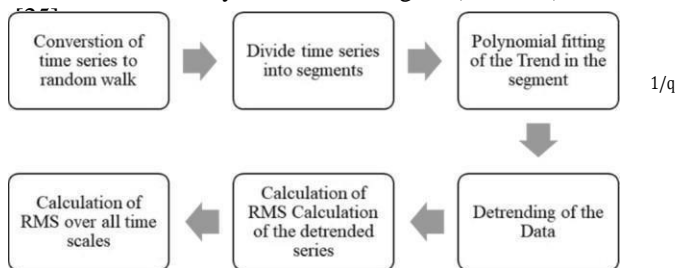


Fig. 2. Block diagram of steps followed in DFA.

In the DFA algorithm, the signal of length N is first integrated. The signal is integrated to convert the noise-like signal into a random walk like signal. After integration, the signal is divided into smaller segments, each of length n. Subsequently, the signal in each of the segments is fit to a polynomial curve which represents the trend in the segment. Detrending of the signal is performed by subtracting the local trend $y_n(k)$ in the segments of the signal from the integrated signal $y(k)$. The fluctuation of this detrended signal is quantified by calculating the Root Mean Square (RMS) fluctuation using the formula –

$$F(n) = \sqrt{\frac{1}{N} \sum_{k=1}^N [y(k) - y_n(k)]^2} \quad (1)$$

The calculation of RMS fluctuation is done over various time scales. The logarithmic plot of $F(n)$ and (n) gives a linear relationship. The slope of the line is the scaling exponent α . This obtained scaling exponent is a generalization of the Hurst exponent [26].

Hurst exponent (H) is a marker of the monofractal nature of the signal and defines how fast fluctuations grow with increasing scale [26]. It gives a measure of long-term memory of a signal and is related to the autocorrelations embedded in a signal. H is also directly linked to the fractal dimension (D) which is a measure of the complexity of a signal. For self-similar time series, the relation between H and D

$$H + D = d + 1 \quad (2)$$

Where, d is the dimension in which the object is embedded (d = 2 for time-varying signals) [27,28].

By calculating the scaling exponent, we can understand the type of correlation present in the signal. If α or H is less than 0.5, the signal is anti-persistent and anti-correlated in nature. Values of α or H greater than 0.5 reflect persistent and correlated nature [23].

DFA is used to study the monofractal nature of a signal and gives a single power-law exponent α which is the slope of $\log F(n)$ plotted against $\log n$. For monofractal signals, the relationship is linear in nature. If the relationship is non-linear in nature and contains irregularities, it means the signal is not monofractal but multifractal in nature and has a spectrum of scaling exponents. Therefore, the signal needs to be analysed using multifractal methods.

C. Multifractal Detrended Fluctuation Analysis

Monofractal methods in the analysis of bio-signals assume that scale-invariant nature of the signal is independent of time and space. But that is rarely the case [26]. The conventional DFA method developed by Peng was extended by Kantelhardt to include multifractal analysis [29]. In MFDFA a q-order exponent is introduced, and the resulting equation is -

$$F(n) = \left\{ \frac{1}{N} \sum_{k=1}^N [y(k) - y_n(k)]^{q/2} \right\}^{1/q} \quad (3)$$

The q-order exponent can take values from any negative integer to any positive integer, except zero. Equation (3) is the same as (1) when, $q = 2$, which is the case of monofractal DFA. But in MFDFA, Hurst Exponents are calculated for a range of q. The significance of q-order exponent is that when q takes negative values, periods with small fluctuations are detected, and when q takes positive values, periods with large fluctuations are detected. MFDFA generates a range of scaling exponents $h(q)$ representing the scaling exponent of q^{th} order. The range of multifractality or the multifractal spectrum is the difference between the maximum value of $h(q)$ and the minimum value of $h(q)$.

In the experiment, q values were taken from -5 to +5 [30]. Values of scale were taken up to $1/10^{\text{th}}$ of sample size [26].

IV. RESULTS

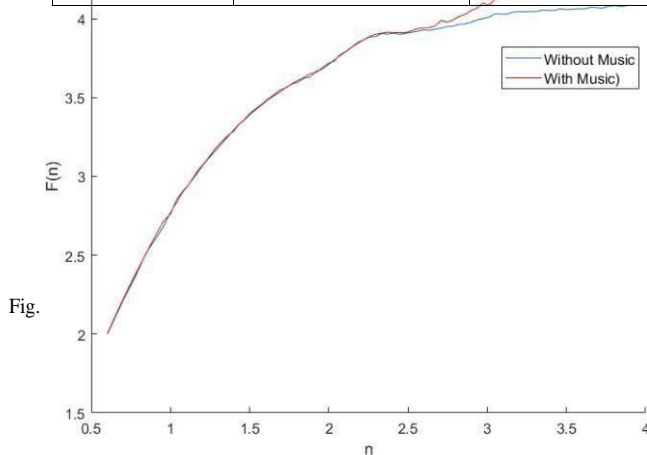
A. Detrended Fluctuation Analysis of ECGsignals

TABLE I. DFA ANALYSIS OF ECG SIGNALS

DF A	Average α	Standard Deviation
Without music	0.718	0.138
With music	0.586	0.065

It is seen that α values when listening to music is lesser than α values without music. The consistency in this result means that when the subject is listening to Indian Classical music the correlated nature of ECG signal reduces, that is the signal becomes more uncorrelated. The relation between scaling exponent and complex nature of a signal is established in (2), decrease in Hurst exponent will cause an increase in fractal dimension, meaning increased complex nature of the signal. Thus, we can say that an increase in the uncorrelated nature of ECG implies a more complex nature of ECG or simply we can say the complexity of ECG increases while listening to music. It is well known that music affects the sinus rhythm of the heart [3]. The complexity in the ECG signal is found to increase when the person is subjected to listening to music. This is due to the irregularities in heartbeat pattern arising while listening to music. The structural variations, rhythm changes and other variations present in music induce changes in rhythmic activity of the heart, thereby increasing the complexity in the beating pattern of the heart. This might be the physiological reasoning behind the consistent increase in the complex nature of ECG while listening to music.

MFD FA m = 3	Average Spectrum width	Standard Deviation
Without music	1.58	0.249



ECG is greater, but when music stimulus is applied, in all subjects and all cases, the scaling exponent tends to concentrate towards a particular value. A possible explanation for this might be the dependence of the correlated nature of ECG on the music signal applied.

Figure 3 shows the plot of $\log F(n)$ versus $\log n$. It can be seen that the curve is non-linear nature with irregularities. This suggests the multifractal nature of the signal, that is ECG is multifractal in nature and needs subsequent multifractal analysis.

B. Multifractal Detrended Fluctuation Analysis of ECG signals

TABLE II. MFDFA ANALYSIS OF ECG SIGNALS M=1

MFD FA m = 1	Average Spectrum width	Standard Deviation
Without music	1.27	0.222
With music	1.29	0.174

TABLE III. MFDFA ANALYSIS OF ECG SIGNALS M=2

MFD FA m = 2	Average Spectrum width	Standard Deviation
Without music	1.54	0.298
With music	1.59	0.267

TABLE IV. MFDFA ANALYSIS OF ECG SIGNALS M=3

The results of MFDA shows that ECG is indeed multifractal in nature and the width of the multifractal spectrum varies with music stimulus. MFDFA of ECG signals gives the width of the spectrum of scaling exponents which indicates the degree of multifractality. It is seen that when listening to music, the degree of multifractality of ECG signals increases. Most MFDFA analysis of biosignals only includes only linear trend fitting ($m=1$) whereas analysis of multifractal for $m=1$ to 3 is recommended, where $m=2$ refers to quadratic polynomial fit and $m=3$ refers to cubic polynomial fit [26]. This is done to consider both linear and non-linear trends. It is seen that the width of multifractality spectrum increases with increase in the degree of polynomial fitting.

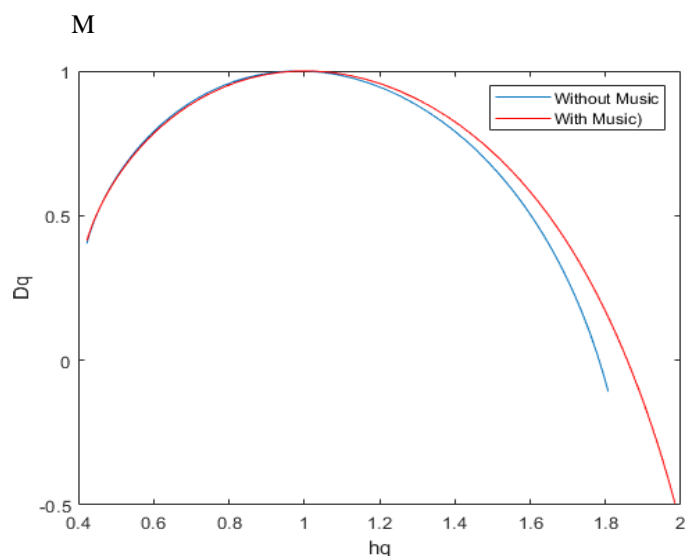


Fig. 4. Multifractality spectrum of ECG signals with and without Music.

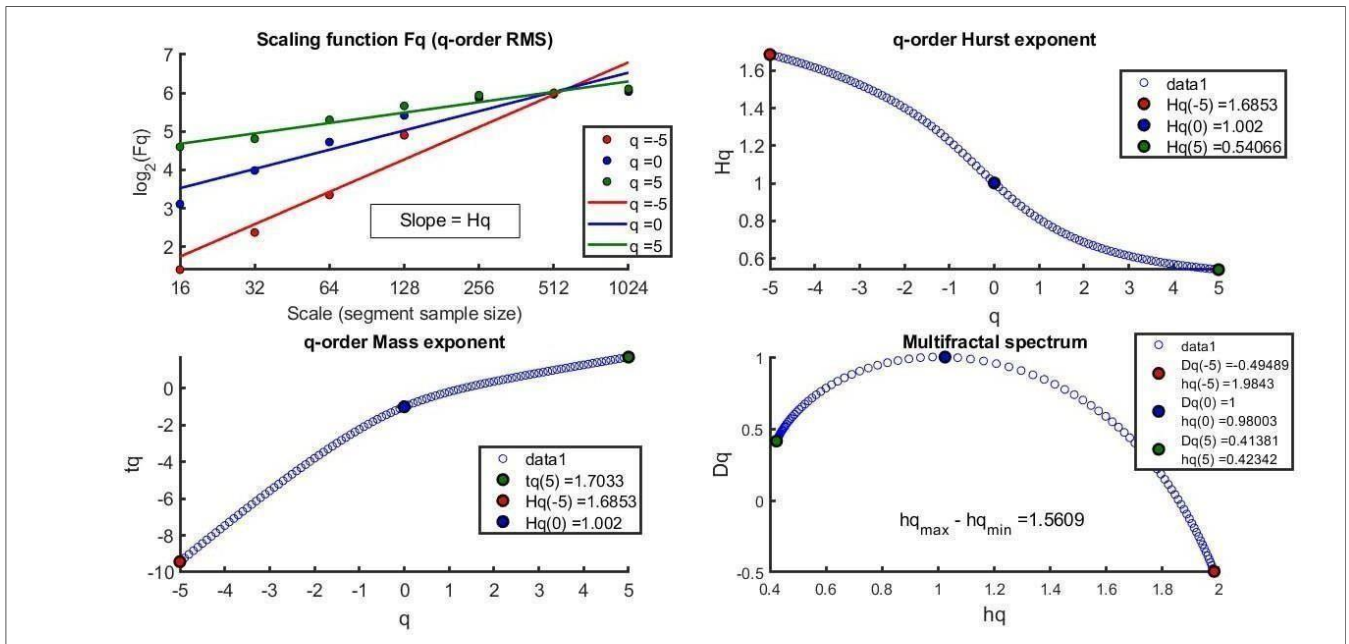


Fig 5. Results of MFDFA algorithm when applied on ECG signals of Music phase.

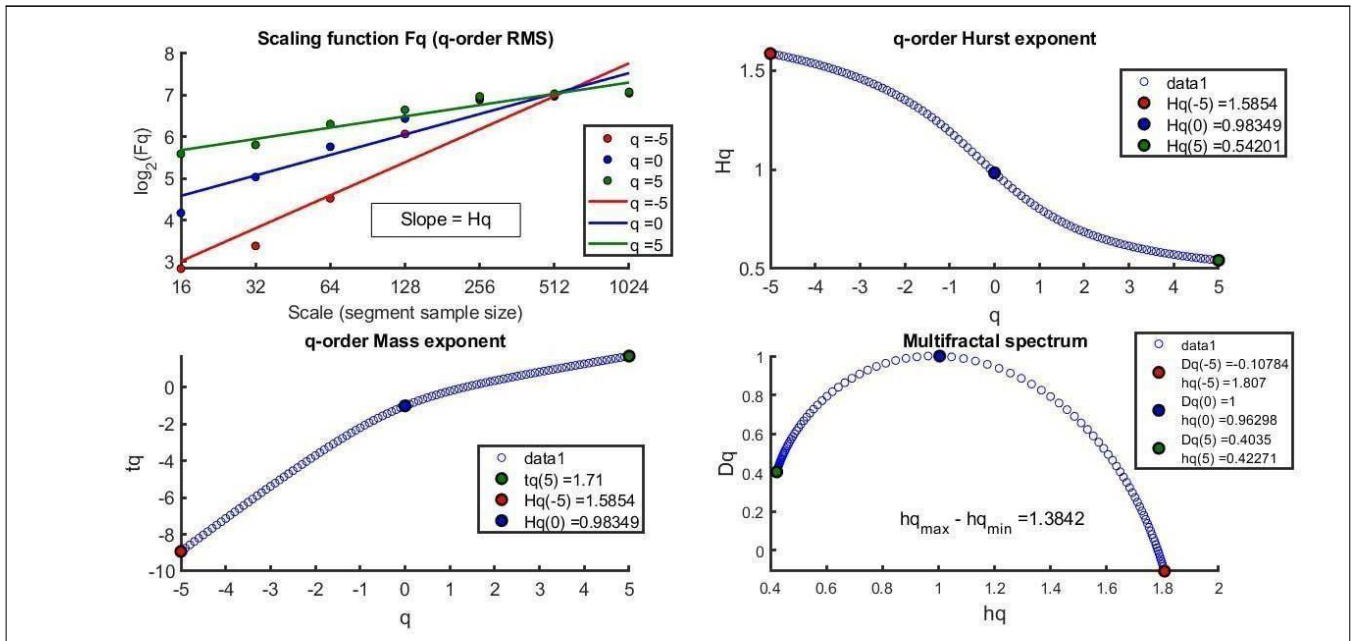


Fig 6. Results of MFDFA algorithm when applied on ECG signals of Resting Phase.

The increase in multifractality spectrum indicates an increase in the fluctuations of the fractal structure of ECG when listening to music. Such an observation is consistent over linear, quadratic and cubic polynomial trend fitting.

Figure 5 and 6 show the results of the MFDFA algorithm when applied on ECG signals with and without music stimulus. The non-linear relationship between H_q (q -order Hurst Exponent) and q reinstates the multifractal nature of the ECG signal. Similar non-linear nature is seen in the variation of t_q (q -order mass exponent) with q . It can be seen that H_q decreases with increasing values of q . When $q=2$, it can be seen that the value of H_q is greater 0.5. It is greater in case of without music condition. This is the exact same result of DFA as when $q=2$ in MFDFA, the algorithm is the same as DFA.

CONCLUSION

ECG is multifractal in nature [19,21]. The nature and range of multifractality vary with music stimulus. Very few studies have been performed to study the non-linear characteristics of the ECG signal with music as a stimulus. In our study, we used Indian Classical Music as a stimulus. To study the non-linear and chaotic nature of ECG signals, DFA and MFDFA have been used. DFA considers the signal has a singular scaling exponent, and that the fractal structures within the signal are independent of space and time. But, in reality, bio-signals are multifractal in nature and the fractal structures vary with time and space. Thereby multifractal analyses are required.

The results of DFA outputs a scaling exponent α which is the measure of correlated nature of the signal. It was seen that,

when the subject listens to music, the scaling exponent α decreases, indicating an increase in the complexity of cardiovascular dynamics. The synchrony of ECG signal reduces compared to resting condition and the effects of music are reflected in greater uncorrelated nature of ECG. The regular varying nature of the heart is disturbed, and it tends towards a particular degree of non-linearity as reflected by the low standard deviation of α values as compared to high standard deviation of α values during nomusic condition.

The results of DFA exhibits a non-linear relationship between RMS fluctuation and scale, suggesting the signal is supposedly multifractal in nature. MFDFA is an efficient tool to analyse the range of multifractality in a signal. MFDFA is a modification of conventional DFA to include a q-order exponent which characterizes small and large variations occurring in the signal.

The non-linear relationship between H_q and q and the width of the multifractal spectrum confirms the multifractality of ECG signals. It is seen that multifractality increases while listening to music. The effects of music induce changes in the complexity of the electrical activity of the heart. Heart being a non-linear system are perturbed by the musical structures and features and thereby its complex and chaotic nature increases.

Various studies on the multifractality of ECG have shown that healthy functioning of heart corresponds to the increased width of the multifractal spectrum compared to in diseased conditions [19,21]. A study on the effects of meditation on multifractal nature of ECG reported an increase of multifractality in ECG during meditation, and it was concluded that increase in multifractality is due to the feeling of well-being in subjects [31]. We have currently performed our experiment on healthy subjects and studied the non-linearity of ECG while listening to music. Increase in complexity and uncorrelated nature of ECG was observed in DFA. Increase in multifractality of ECG was observed in MFDFA. The increased range of multifractality while listening to music indicates a positive effect of Indian Classical Music on heart.

REFERENCES

- [1] N. Das and D. M. Chakraborty, "Effects on Indian Classical Music on Heart Rate Variability," presented at the 5th International Conference for Convergence In Technology, Pune, 2019.
- [2] Y. Z. Tan, S. Ozdemir, A. Temiz, and F. Celik, "The effect of relaxing music on heart rate and heart rate variability during ECG GATED-myocardial perfusion scintigraphy," *Complementary Therapies in Clinical Practice*, vol. 21, no. 2, pp. 137–140, May 2015.
- [3] A. Banerjee *et al.*, "Study on Brain Dynamics by Non Linear Analysis of Music Induced EEG Signals," *Physica A: Statistical Mechanics and its Applications*, vol. 444, pp. 110–120, Feb. 2016.
- [4] M. Iwanaga, A. Kobayashi, and C. Kawasaki, "Heart rate variability with repetitive exposure to music," *Biological Psychology*, vol. 70, no. 1, pp. 61–66, Sep. 2005.
- [5] M. Dosty, S. Daneshvar, and M. Haghjoo, "The effects of sedative music, arousal music, and silence on electrocardiography signals," *Journal of Electrocardiology*, vol. 44, no. 3, pp. 396.e1-396.e6, May 2011.
- [6] H. J. Trappe, "[Music and health--what kind of music is helpful for whom? What music not?]," *Dtsch Med Wochenschr*, vol. 134, no. 51– 52, pp. 2601–2606, Dec. 2009.
- [7] H. Nakahara, S. Furuya, S. Obata, T. Masuko, and H. Kinoshita, "Emotion-related changes in heart rate and its variability during performance and perception of music," *Ann. N. Y. Acad. Sci.*, vol. 1169, pp. 359–362, Jul. 2009.
- [8] R. J. Ellis and J. F. Thayer, "Music and Autonomic Nervous System (Dys)Function," *MUSIC PERCEPT*, vol. 27, no. 4, pp. 317–326, Apr. 2010.
- [9] M. Orini, R. Bailón, R. Enk, S. Koelsch, L. Mainardi, and P. Laguna, "A method for continuously assessing the autonomic response to music-induced emotions through HRV analysis," *Med Biol Eng Comput*, vol. 48, no. 5, pp. 423–433, May 2010.
- [10] C.-Y. Chuang, W.-R. Han, P.-C. Li, and S.-T. Young, "Effects of music therapy on subjective sensations and heart rate variability in treated cancer survivors: A pilot study," *Complementary Therapies in Medicine*, vol. 18, no. 5, pp. 224–226, Oct. 2010.
- [11] G. C. Ray, A. Ya Kaplan, and E. Jovanov, "Morphological variations in ECG during music-induced change in consciousness," presented at the 19th Ann. Int. Conf. IEEE/EMBS., 1997.
- [12] Y.-L. Hsu, J.-S. Wang, W.-C. Chiang, and C.-H. Hung, "Automatic ECG-Based Emotion Recognition in Music Listening," *IEEE Transactions on Affective Computing*, pp. 1–1, 2017.
- [13] P. Ch. Ivanov *et al.*, "Multifractality in human heartbeat dynamics," *Nature*, vol. 399, no. 6735, pp. 461–465, Jun. 1999.
- [14] Y. Zheng, J. Gao, J. C. Sanchez, J. C. Principe, and M. S. Okun, "Multiplicative multifractal modeling and discrimination of human neuronal activity," *Physics Letters A*, vol. 344, no. 2–4, pp. 253–264, Sep. 2005.
- [15] J. M. Hausdorff, "Gait dynamics, fractals and falls: Finding meaning in the stride-to-stride fluctuations of human walking," *Human Movement Science*, vol. 26, no. 4, pp. 555–589, Aug. 2007.
- [16] A. L. Goldberger, L. A. N. Amaral, J. M. Hausdorff, P. Ch. Ivanov, C.-K. Peng, and H. E. Stanley, "Fractal dynamics in physiology: Alterations with disease and aging," *Proceedings of the National Academy of Sciences*, vol. 99, no. Supplement 1, pp. 2466–2472, Feb. 2002.
- [17] R. Galaska *et al.*, "Comparison of Wavelet Transform Modulus Maxima and Multifractal Detrended Fluctuation Analysis of Heart Rate in Patients with Systolic Dysfunction of Left Ventricle," *Annals of Noninvasive Electrocardiology*, vol. 13, no. 2, pp. 155–164, 2008.
- [18] A. Fielding, "Applications of fractal geometry to biology," *Bioinformatics*, vol. 8, no. 4, pp. 359–366, Aug. 1992.
- [19] S. Dutta, "Multifractal properties of ECG patterns of patients suffering from congestive heart failure," *J. Stat. Mech.*, vol. 2010, no. 12, p. P12021, Dec. 2010.
- [20] G. Wang, H. Huang, H. Xie, Z. Wang, and X. Hu, "Multifractal analysis of ventricular fibrillation and ventricular tachycardia," *Medical Engineering & Physics*, vol. 29, no. 3, pp. 375–379, Apr. 2007, doi: 10.1016/j.medengphy.2006.05.007.
- [21] J. Wang, X. Ning, and Y. Chen, "Multifractal analysis of electronic cardiogram taken from healthy and unhealthy adult subjects," *Physica A: Statistical Mechanics and its Applications*, vol. 323, pp. 561–568, May 2003, doi:10.1016/S0378-4371(03)00045-1.
- [22] A. Dey, S. Chakraborty, S. K. Palit, D. K. Bhattacharya, D. N. Tibarewala, and M. Roy, "Study the effect of music on HRV impulse using multifractal DFA analysis," in *2014 International Conference on Communication and Signal Processing*, 2014, pp. 1338–1342.
- [23] C. K. Peng, S. Havlin, H. E. Stanley, and A. L. Goldberger, "Quantification of scaling exponents and crossover phenomena in nonstationary heartbeat time series," *Chaos*, vol. 5, no. 1, pp. 82–87, Mar. 1995.
- [24] C.-K. Peng, S. V. Buldyrev, S. Havlin, M. Simons, H. E. Stanley, and A. L. Goldberger, "Mosaic organization of DNA nucleotides," *Phys. Rev. E*, vol. 49, no. 2, pp. 1685–1689, Feb. 1994.
- [25] J. Wang and K. Cheng, "Scale invariance analysis of the premature ECG signals," *Physica A: Statistical Mechanics and its Applications*, vol. 391, no. 11, pp. 3227–3233, Jun. 2012.
- [26] E. A. F. Ihlen, "Introduction to Multifractal Detrended Fluctuation Analysis in Matlab," *Front Physiol*, vol. 3, Jun. 2012.
- [27] B. B. Mandelbrot, "Self-Affine Fractals and Fractal Dimension," *Phys. Scr.*, vol. 32, no. 4, pp. 257–260, Oct. 1985, doi: 10.1088/0031-8949/32/4/001.
- [28] R. M. Bryce and K. B. Sprague, "Revisiting detrended fluctuation analysis," *Scientific Reports*, vol. 2, no. 1, pp. 1–6, Mar. 2012, doi: 10.1038/srep00315.

- [29] J. W. Kantelhardt, S. A. Zschiegner, E. Koscielny-Bunde, S. Havlin, A. Bunde, and H. E. Stanley, "Multifractal detrended fluctuation analysis of nonstationary time series," *Physica A: Statistical Mechanics and its Applications*, vol. 316, no. 1, pp. 87–114, Dec. 2002.
- [30] M. Chakraborty, T. Das, and D. Ghosh, "Non-linear fractal analysis of ECG signal collected from Maternal and normal sinus women," in *2016 3rd International Conference on Recent Advances in Information Technology (RAIT)*, 2016, pp. 123–127.
- [31] A. Bhaduri and D. Ghosh, "Quantitative Assessment of Heart Rate Dynamics during Meditation: An ECG Based Study with Multi-Fractality and Visibility Graph," *Front. Physiol.*, vol. 7, 2016, doi: 10.3389/fphys.2016.00044.

FPGA Implementation of Epileptic Seizure Detection Using ELM Classifier

J Prabin Jose
Assistant Professor

Electronics and Communication
Kamaraj College of Engineering
Madurai
prabinjose@gmail.com

M.Sundaram
Professor

Electronics and Communication
VSB Engineering College,
Karur
cm.sundaram2011@gmail.com

G.Jaffino

Assistant Professor
Electronics and Communication
Aditya College of Engineering
Surampalem
jaffino22@yahoo.com

Abstract— Electroencephalography (EEG) Signals are widely used to determine the brain disorders. The Electrical activity of human brain is recorded in the form of EEG signal. The abnormal Electrical activity of the human brain is called as epileptic seizure. In epilepsy patients, the seizure occurs at unpredictable times and it causes sudden death. Detection and Prediction of Epileptic seizure is performed by analyzing the EEG signal. The EEG signal of human brain is random in nature, hence detection of seizure in EEG signal is challenging task. Hardware implementation of Epileptic seizure detection system is necessary for real time applications. In this work an accurate approach is used to identify the Epileptic seizure and that is implemented in FPGA (Field Programmable Gate Array). The hardware implementation of epileptic seizure detection algorithm is done using Xilinx System generator tool. In the first step the EEG signal is extracted from the human brain and it is filtered by using Finite Impulse response (FIR) band pass filter. The band pass filter separates the EEG signal into delta, theta, alpha, beta and gamma brain rhythms. The band separated brain signal is modeled by linear prediction theory. In the next step features are extracted from the modeled EEG signal and the classification of normal or seizure signal is done by using Extreme Learning Machine (ELM) classifier. The EEG signals used in this paper were obtained from Epilepsy Center at the University of Bonn, Germany. The hardware architecture, Look up tables, resource utilization, Accuracy and power consumption of the algorithm is analyzed using xilinx zynq-7000 all programmable soc.

Keywords— *Electroencephalography EEG; Epileptic; Linear prediction; FPGA; ELM*

I. INTRODUCTION (HEADING 1)

The abrupt, irregular and frequent reactions of human brain are termed as epileptic seizure disease. In the world 70 million people are facing trouble because of epileptic seizure diseases. The EEG signal is measured from human brain by placing electrodes in the scalp. The EEG signal has strong affinity with the activity of the brain. So EEG signal is generally used for seizure detection and diagnosis. Commonly optic investigation is used by EEG professional in EEG signal for seizure identification. This approach takes more time for detection and prediction. This problem can be conquered by designing automatic seizure detection device. The seizures arise due to accidental condition's and disturb the normal behaviour of the brain. [1].

Selvathi et al proposed an approach based on EEG signal amplitude and frequency, which is implemented in FPGA [2]. In this method 82% of LUTs and 14% registers were utilized to implement

the algorithm. The time required to implement the algorithm is 13.568ns. The major drawback of this work is that the complexity of the algorithm is high in terms of LUTs used. Sreethu Raj et al proposed a system for FPGA Implementation of EEG Feature Extraction and Seizure Detection [3]. This approach

uses FIR filtering method and wavelet based feature extraction technique. The classification of the signal is performed by using Support vector machines. Verilog hardware description language is used to implement the proposed system. John mosses et al [4] described the concept of interpolation algorithms and its hardware architecture. The performance of the algorithm is analysed based on the gate count, frequency, and power and memory buffer.

In recent years, a few experiments have been implemented for seizure detection with the help of two different mechanisms. The first mechanism use the preictal EEG signal to determine the modification of brain behaviour such as spikes [5]. The second mechanism is based on investigate the non-linear progression of the EEG signal based on dominant rule and determine seizure free state[6]. Few approaches has also been reported using artificial neural networks [7] based on wavelet transform [8].

Markos G. Tsipouras, and Dimitrios have demonstrated energy circulation of EEG signal with the help of time frequency approach[9]. This approach produces extreme classification accuracy of segments based on artificial neural network. Lina Wang et al proposed a system which is based on several realm feature extraction signals [10]. The artifacts in the EEG signal is removed by using wavelet threshold method. Information theory techniques are used to extract the nonlinear features and time-frequency domain features. Principal Component analysis is used to select optimum features for the classifier. The classification of the features is performed by using support vector machine Classifier. Shantha et al [11] evaluate the EEG signal using wavelet approach and the detection was performed by using support vector machine classifier. Most of the research articles for seizure detection are based on algorithmic and not hardware based approach. This work aims to implement the algorithms in FPGA hardware for real time detection of seizure.

METHOD USED

The schema of proposed method used in this paper is shown in Fig1. The input EEG signal is filtered by using band pass filter to eliminate the undesirable parameters present in the signal. The band pass filter is used to separate the EEG signal into five EEG subbands: delta (0–4 Hz), theta (4–8 Hz), alpha (8–12 Hz), beta (13–30 Hz), and gamma (>30Hz). The bandpass filter is designed by using Xilinx Sysgen block set. The segmented band signal is further modeled by using linear prediction theory which is used to estimate the random quantity from certain available data.

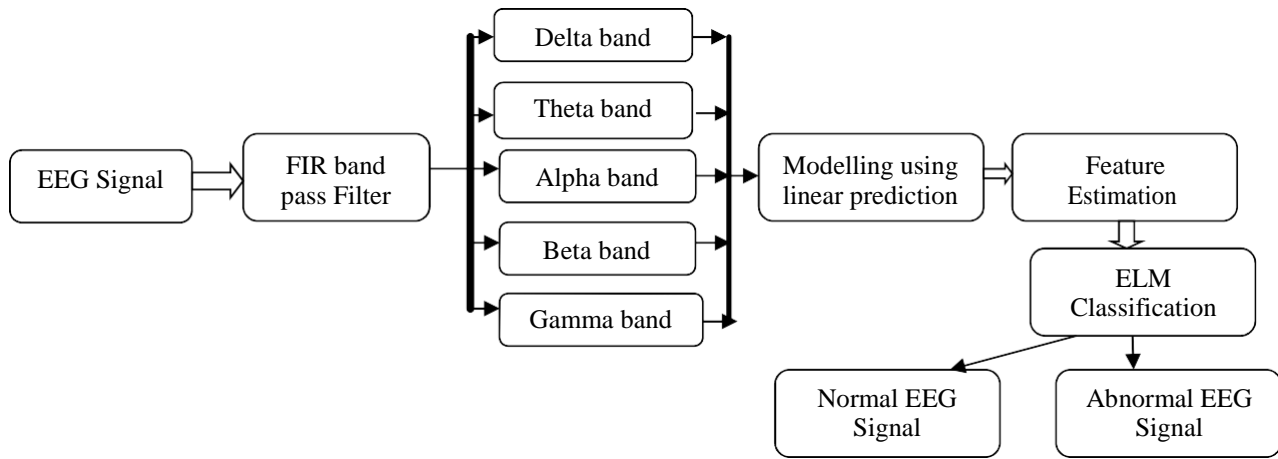


Fig1: Flow chart of the Proposed Approach

The numerical features are derived from each sub band and form a feature vector. The ELM classifier is used to classify if seizure is present or absent in the given signal. The feature extraction process and ELM classifier algorithm is designed by using Xilinx System block set.

A. Dataset Used

The data set evaluated in this work is attained from University of Bonn, Germany .It includes both normal and abnormal EEG signal. The dataset contains 100 normal EEG signal (denoted as Z) and 100 Epileptic seizure EEG Signals (denoted as S). The duration of each signal is 23.6 seconds. The sample EEG signal available in the dataset is shown in the Fig2

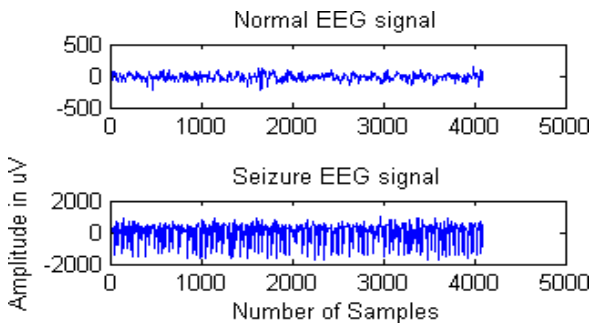


Fig 2 Sample EEG Signals

B. Filtering of EEG Signal

The individual EEG subband signals are obtained by using band pass FIR filter. The FIR filter has the advantages of linear phase, high stability and scale space analysis. The primary EEG signal contains five subbands: *delta*, *theta*, *alpha*, *beta*, and *gamma*. The sampling frequency of the EEG dataset used in this work is 173.61 Hz. Based on Nyquist sampling theorem, the maximum convenient frequency is half of the sampling frequency (ie 86.81 Hz). In the band pass filter, the pass band cut of frequency is based on different subband frequency. The filter coefficient for the required filter is designed using FDA tool which is available in the Xilinx System block set. The complete setup of the blocks used to implement the proposed work is shown in Fig3. The Verilog code for xilinx vivado zynq-7000 is developed from the block design using system generator module.

C. Modeling of sub band signal using Linear Prediction

The concept of Linear prediction approach is based on probabilistic theory .This modelling is used for the estimation of random brain signal parameters from the available brain waves. In this modelling the prediction of a sampled value is based on the past sample values. Consider the sample value $x(n)$ has to be predicted from its past

sample value $x(n-1)$. The predicted $\hat{x}(n)$ is sample value given by first order predictor equation

$$\hat{x}(n) = ax(n-1) \text{ ----- (1)}$$

where a is a real constant

The prediction error is expressed as $e(n)$ and is given by the equation

$$e(n) = x(n) - \hat{x}(n) \\ e(n) = x(n) - ax(n-1) \text{ -----(2)}$$

the mean square error is given by the equation

$$\mathcal{E} = E[e^2(n)] = E[(x(n) - ax(n-1))^2] .$$

The condition for minimum error is given by

$$\frac{\partial}{\partial a} [E(e^2(n))] = 0$$

$\frac{\partial}{\partial a}$

Substituting for $e(n)$ from equation (2) yields the orthogonally relation equation and is given by

$$E[e(n)x(n-1)] = 0 \\ E[(x(n) - ax(n-1))x(n-1)] = 0 \text{ -----(3)}$$

The autocorrelation $R_{xx}(\cdot)$ expression based on equation (3) is given by

$$R_{xx}(1) = aR_{xx}(0)$$

The optimum value of a is given by

$$a = \frac{R_{xx}(1)}{R_{xx}(0)}$$

Based on the optimum value of ‘ a ’ the minimized error value is estimated and is given by

$$\xi_{\min} = (1 - a^2)R_{xx}(0)$$

II. FEATURE EXTRACTION

The feature extraction step scale down the original signal complexity by considering selective features that discriminate normal signal and abnormal signal. The EEG signal is very large for processing. Feature extraction process remodel the complex EEG signal into reduce feature sample model. The extracted features in this work are explained below.

A. Energy

The energy feature describes the strength of the signal. It is extracted by using sum of squared modulus value. The energy of the EEG signal is indicated as

$$E = \sum_{n=0}^{N-1} |X_n|^2$$

Where X_n is the sample values in each subbands and N is the total number of samples in the given EEG signal.

B. Spectral Entropies

The probability of variability within the signal is described by spectral entropies. The Entropy of different frequency band is estimated to reveal more information about the signal. The entropy feature is used to represent the dynamical characteristics of nonlinear signals. The entropy feature of the EEG signal is estimated using the following equation

$$Entropy = -\sum_{n=0}^{N-1} P_n \log P_n$$

P_n represent the relative power of the signal

C. Power Spectral Density (PSD)

The Power Spectral Density (PSD) shows the circulation of the energy of the EEG signal in terms of time frequency axis. It refers to the amount of power per unit (density) frequency (spectral) as a function of frequency. The mean power of the EEG signed is derived by integrating the power spectral density over the frequency band. The algorithm for

measuring the PSD is explained in the below step.

- 1) Fast Fourier transform (FFT) is enumerate for each decomposed EEG signal $X(i)$
- 2) PSD is measured by using the equation

$$P(\omega_i) = \frac{1}{N} |X(\omega_i)|^2$$

Where N is the total number of samples present in the spectrum of the band.

- 3) The maximum value is estimated from the PSD of each subbands and is considered as third feature vector.

III. EXTREME LEARNING MACHINE CLASSIFIER

Traditional gradient-approach learning methods are widely used for training the multilayer feed forward neural networks. The learning speed of these methods are moderate than required and it has been consider as a major drawback. The two main reasons for this drawback are due to slow gradient learning algorithms which are used to train the neural networks and the parameters for the networks are

needed to be tuned iteratively by using these algorithms. To overcome this problem an efficient learning algorithm for single-hidden-layer feed forward neural networks (SLFNs) called Extreme learning machine (ELM) was proposed by Huang, et al.. SLFNs consist of single layer of hidden nodes (neurons), input nodes and output nodes. The structure of SLFNs is shown in the Fig 3. In ELM algorithm the input weights (linking the input layer to the hidden layer) and hidden biases (for hidden layers) are randomly chosen, and the output weights (linking the hidden layer to the output layer) are analytically determined by using Moore–Penrose (MP) generalized inverse. The weights and biases are randomly generated and then fixed based on best performance. ELM classifier provides better generalization performance and the learning speed is thousand times than other neural network algorithms. (at higher learning speed).

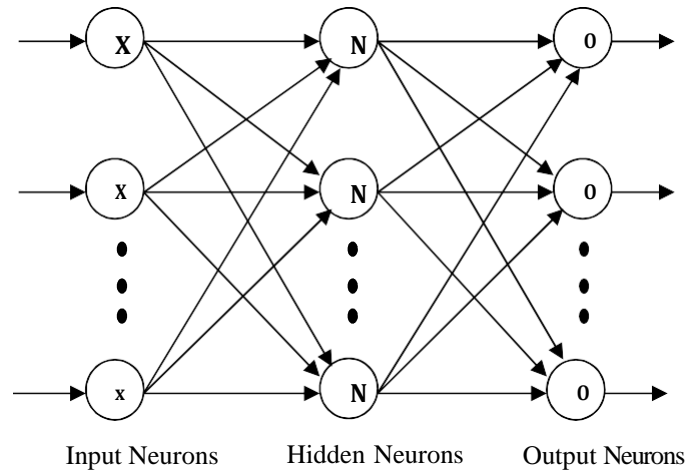


Fig. 3 Structure of SLFNs

Let us Consider the feature set as $\{x_i, t_i\}$, where $x_i = [x_{i1}, x_{i2}, \dots, x_{im}]^T$ be the feature values of the signals and $t_i = [t_{i1}, t_{i2}, \dots, t_{im}]^T$ be the class label values for target class. The Standard mathematical model for SLFNs with N hidden neurons (nodes) and activation function $g(x)$ is modelled as

$$\sum_{j=1}^N \beta_j g(w_j x_i + b_j) = 0, \quad i=1, \dots, n$$

Where n is the total number of features and m is the total number of training signals where $w_j = [w_{j1}, w_{j2}, \dots, w_{jn}]^T$ is the weight vector connecting the j^{th} hidden nodes (neurons) and their input neurons, $b_j = [\beta_{j1}, \beta_{j2}, \dots, \beta_{jm}]^T$ is the weight vector connecting the j^{th} hidden neuron and the output neurons and b_i is the bias value for the j^{th} hidden neurons. In the equation $w_j \cdot x_i$ is the inner product of the feature values and the input weight matrix.

The above equation (4) can be rewritten as

$$H\beta = O$$

Where $H = g(w_j \cdot x_i + b_j)$ is the hidden layer output matrix which is given by

$$H = \begin{bmatrix} g(w_1 \cdot x_1 + b_1) & \dots & g(w_N \cdot x_1 + b_N) \\ \vdots & \ddots & \vdots \\ Lg(w_1 \cdot x_N + b_1) & \dots & Lg(w_N \cdot x_N + b_N) \end{bmatrix} \quad 1$$

$$\beta = \begin{bmatrix} b_1^T \\ \vdots \\ b_N^T \end{bmatrix} \quad \text{and} \quad O = \begin{bmatrix} 1 \\ \vdots \\ k^T \end{bmatrix}$$

A. ELM Algorithm

In machine learning classifier, the learning algorithms use a finite number of feature samples for training. For the given training feature set $\{x_i, t_i\}$, input parameters for the ELM algorithm is described below

- (i) The number of input neurons (nodes) selected is equal to the total number of features used for an individual signal.
- (ii) The number of hidden neurons N which is much less than the number of training samplesm.
- (iii) The activation function is $g(x)$. The various activation functions available are sigmoidal function, polynomial function, hard-line function, etc... In this work the activation function used is Gaussian function.
- (iv) The total number of output neurons (nodes) which is equal to the total number of output class required to classify

IV. EXPERIMENTAL RESULTS AND DISCUSSION

The proposed method is implemented using Xilinx Vivado design suite and Matlab Sysgen tool box. The proposed method is synthesized using Xilinx Vivado synthesizer. In this paper 100 non-seizure and 100 seizures EEG signal is used to test the performance of the system. Each EEG signal is sampled at 173.6Hz. EEG signal is decomposed using FIR bandpass filter to form delta, theta, alpha, beta, gamma subbands. The Sysgen block contains Finite Impulse Response (FIR) band pass filter, Feature extraction block and ELM Classifier. The Simulink System Generator Model for Epileptic seizure detection is shown in Fig3. The device utilization summary of epileptic seizure detection system is shown in Table 1. The Verilog code for xilinx vivado zynq-7000 SOC is generated from the proposed model using system generator module. The generated verilog code is synthesized and implemented in xilinx vivado design suite. The device utilization summary of epileptic seizure detection is tabulated in table 1. The device utilization summary provides the information about number of registers, LUTs and IO required to implement the proposed model in FPGA

Table1: Device utilization Summary

Resource	Utilization	Available	Utilization %
Slice LUTs	243	203800	1
Slice Registers	1084	407600	1
DSP	16	840	2
IO	33	442	7

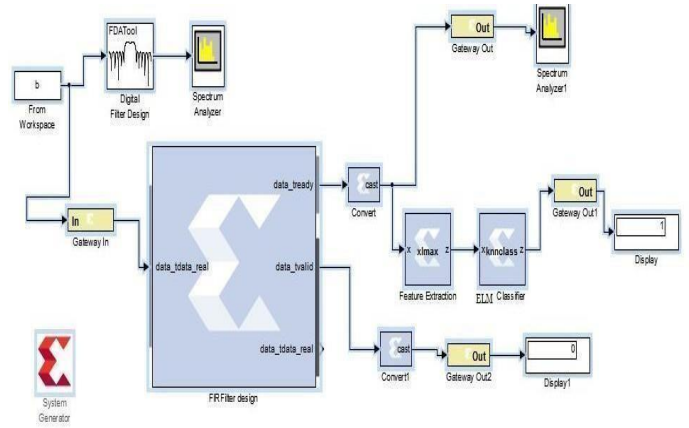
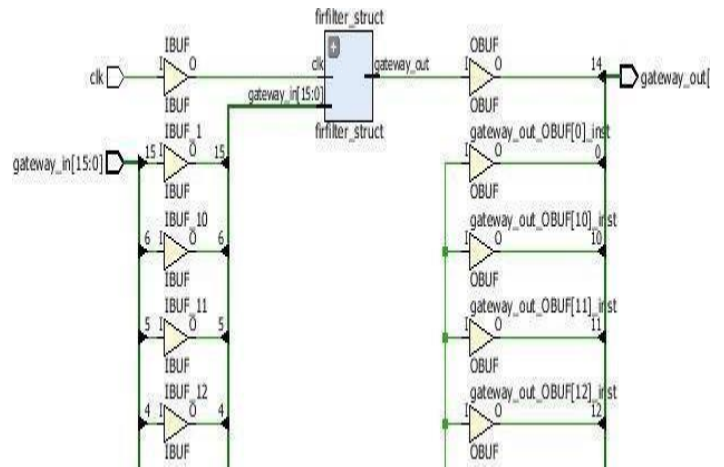


Fig3. Simulink System Generator Model for Epileptic seizure detection

The synthesized hardware architecture of the algorithm generated by using Xilinx vivado design suite is shown in the Fig4



The power analysis report of the proposed algorithm is mentioned in the belowtable2.

Table2.Power AnalysisReport

SINo	Parameter	Value(W)
1	Total On-Chip Power	0.16
2	Dynamic power	0.001
3	Device Static	0.158
4	Junction Temperature	25.3
5	Confidence Level	high

The summary of power analysis of the algorithm derived from constraints files, simulation files is shown in Fig 5

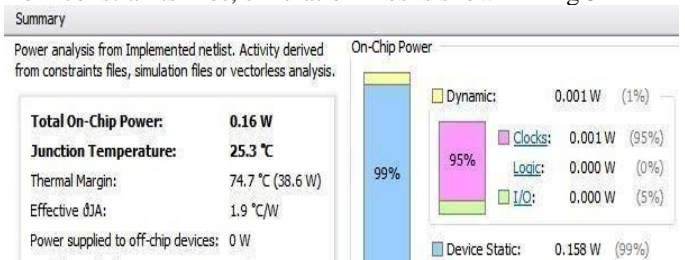


Fig5: Power Analysis summary

The table 2 explains the power analysis of total on chip power, dynamic power, device static, confidence level of the Algorithm. The power requirement of the proposed algorithm is very less when compared to other existing works in the literature. The total On-Chip Power and Dynamic Power of the algorithm is very less when compared to the other works. The Confidence level of the work is high for real time implementation.

The performance of the system is measured in terms of accuracy. The accuracy is given by

$$\text{Accuracy} = \frac{\text{correctly detected pattern} / \text{total number of patterns}}{\text{total number of patterns} / \text{total number of patterns}}$$

In the classification problem 160 signals feature values are considered as training features and 40 signals features are used for testing the classifier. Out of 160 training signals 157 signals are correctly classified and the 40 testing signals used for testing are correctly classified without error. So the accuracy obtained by this method is 98.5%.

A. Comparison with others works

There are many other methods proposed for the epileptic seizure detection in Literature. The comparison accuracy of the results obtained by this method and other methods are described in the table 3. In the existing methods real time implementation of the system was not analyzed. This method analyzed the performance of the system with respect to hardware complexity of the algorithm. The Slice LUTs and registers used by this ELM classifier is less when compared to existing methods. The detailed comparison between the algorithms related to epileptic seizure detection is tabulated in Table 3. From the table it is absorbed that Zynq Soc of FPGA family kit perform better than other FPGA kits. The speed of detection of Zynq Soc is very less when compared to other existing systems. So this method is very useful for real time detection of seizure in EEG signal.

Table 3: Analysis of Algorithms

Algorithm used	Devices	Speed	Number of LUTs	Power (W)
Amplitude and Frequency Analysis of EEG Signals	Virtex-5 kit	13.56 ns	82%	0.58
DFT based Search Algorithm v	Virtex-5kit	30.56 ns	10%	0.48
Mutual information based algorithm	Altera Stratix	20.32 ns	3%	0.21
Proposed method	Zynq-Soc	1ps	1%	0.16

filtered by using FIR band pass filter. The model of the system is synthesized implemented using Xilinx Vivado design suite. The resource utilization and power analysis report of the algorithms are analyzed. Accuracy of the classifier is computed. The speed of execution of the algorithm is also computed. The implementation results provided the timing summary of the method and the timing resolution is 1ps. Complex feature extraction process and deep learning neural network model can also be used to evaluate the performance of the method.

V. CONCLUSION

The epileptic seizure detection was performed by analyzing the features of the EEG signal and classification is performed by using ELM algorithm. The EEG signal is

REFERENCES

- [1]. EEG SIGNAL PROCESSING Saeid Sanei and J.A. Chambers Centre of Digital Signal Processing Cardiff University, UK
- [2]. D. Selvathi, Henry Selvaraj, "FPGA Implementation for Epileptic Seizure Detection using Amplitude and Frequency Analysis of EEG Signals", 25th International Conference on Systems Engineering, ISBN: 978-1-5386-0610-0, 2017
- [3]. Sreethu Raj, Anuja George, "FPGA Implementation of EEG Feature Extraction and Seizure Detection", International Journal of Innovative Research in Science, Engineering and Technology Vol. 5, Issue 9, September 2016, pp 16347-16352
- [4]. C. John Moses, D. Selvathi, and V.M. Anne Sophia, "VLSI Architectures for Image Interpolation: A Survey", Hindawi Publishing Corporation, VLSI Design, Volume 2014, Article ID 872501, 10 pages
- [5]. lasemidis, L. D., 'Epileptic seizure prediction and control', IEEE Trans. Biomed. Engng., **50**, 2003, 549-558.
- [6]. Annegers, J. F., 'The epidemiology of epilepsy', in The Treatment of Epilepsy, Ed. E. Wyllie, Lea and Febiger, Philadelphia, Pennsylvania: 1993, pp. 157-164.
- [7]. Engel, Jr, J. and Pedley, T. A., Epilepsy: A Comprehensive Textbook, Lippincott-Raven, Philadelphia, Pennsylvania, 1997.
- [8]. H. Adeli, Z. Zhou, and N. Dadmehr, "Analysis of EEG records in an epileptic patient using wavelet transform," J. Neurosci. Meth., vol. 123, no. 1, pp. 69-87, 2003.
- [9]. Tzallas A, Tsipouras M, Fotiadis D. Automatic seizure detection based on time-frequency analysis and artificial neural networks. Computational Intelligence and Neuroscience vol:13, article ID 80510, 2007.
- [10]. Lina Wang, Weining Xue, "Automatic Epileptic Seizure Detection in EEG Signals Using Multi-Domain Feature Extraction and Nonlinear Analysis", MDPI, March 2017
- [11]. Dr. R. Shantha Selva Kumari, J. Prabin Jose, "Seizure Detection in EEG Using Time Frequency Analysis and SVM", 2011 IEEE International Conference on Emerging Trends in Electrical and Computer Technology.

2020 IEEE Sixth International Conference
on Biosignals, Images and
Instrumentation(ICBSII 2020)

SESSION IV
RESEARCH PAPERS

Machine Learning techniques for Prediction from various Breast Cancer Datasets

Shalini M
 Research Scholar, Dept. of Computer
 Science and Engineering,
 Sathayabama Institute of Science and
 Technology
 Chennai, India
 shalini.mathi@gmail.com

Dr. S. Radhika Assistant Professor,
 Dept. of Electricals and Electronics Engineering
 Sathayabama Institute of Science and Technology
 Chennai,
 India radhikachandru79@gmail.com

Abstract— Cancer has become very common disease among Indians. Breast cancer occurs 14% of all cancers in women. One in every 28 women is getting affected by breast cancer [2]. Breast cancer detection and identification are done from gene expression and large datasets. Due to the increase in the generation of large datasets of medical data we can analyze specialized patterns that are hidden inside. To analyze the pattern from datasets machine learning techniques such as SVM, KNN, Decision tree are applied. In this paper, we tried to apply some Deep learning techniques to identify the patterns resides in a reoccurrence of breast cancer datasets, Mammogram datasets and to identify the patterns.

Keywords — Machine Learning, Data Preprocessing, Decision tree, Random Forest.

I. INTRODUCTION

According to NICPR (National Institute of Cancer Prevention and Research), Cancer is become very common disease among Indians. Around 2.25 million of people are living with the disease and every year 1157294 lakhs people are newly register. Development of Cancer before 75 years for male and female are less than 10% and risk of dying before their 75 years for male is 7.34% and 6.28% for female. In the year 2018, Total death due to cancer in 2018 is 7,84,821, in which 4,13,519 male and 3,71,302 female[1].

TABLE I. CANCER TYPES

Top Five Cancer commonly occurring in Men and Women		
	Men	Women
1	Lip cancer , Oral Cavity Cancer	Breast Cancer
2	Lung Cancer	Lip cancer, Oral Cavity
3	Stomach Cancer	Cervix Cancer
4	Colorectal Cancer	Lung Cancer
5	Esophagus Cancer	Gastric Cancer
25% of men and women are affected by first two cancer [7]		

Breast cancer occurs 14% of all Cancers in women. From Globocan 2018 data, newly registered cases are 162468 and death due to breast cancer in 2018 is 87090. For Women the Breast cancer is the second most commonly affecting cancers. Even men's are affected by this cancer. Cause of Breast cancer may be due to age factor, BRCA1, BRAC2 and TP53 gene mutation in women's cell, recurrence of Breast cancer, Dense Breast, increase in estrogen due to early stage, obesity after menopause, intake of alcohol, treatments for Hormonal imbalance, etc.,

Breast cancer was ranked in terms of age adjusted rate, Regional wise and mortality. They referred it from PCBR report from (1982 – 2014) [2].

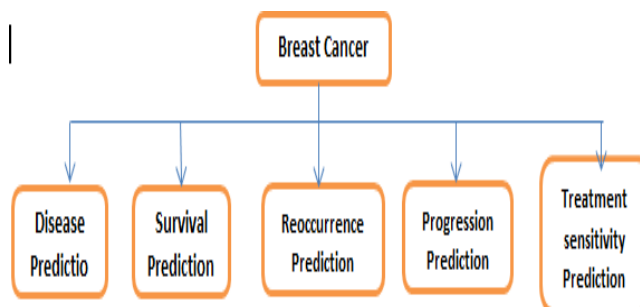
TABLE II. REGIONALLY AFFECTED WOMENS

Region	Affected Women per 100000 Women	Age adjusted rate of PBCRs (1982 to 2014)
Delhi	41%	1.44%
Chennai	37.9%	2.44%
Bangalore	34.4%	2.84%
Thiruvananthapuram	33.7%	
Breast cancer patients for India during 2020 will be as high as 1797900.		

Breast cancer detection and identification can be done from gene expression and large datasets. In gene expression, BRAC1, BRAC2 and TP53 are gene entail of breast cancer. Hereditary cancer is due to mutation of BRAC1 and BRAC2 gene. Gene mutation predictions are done Blood Sampling extraction, DNA extraction, Sample preparation from DNA or RNA extraction, Sequencing, Analysis of Sequence Data, Identification of any sequence mutation, perform the Cross checking and final result will generated. Disadvantages of gene expression for prediction is won't use to identify at early stage and difficult to differentiate benign from the Malignant tumor.

Machine learning algorithms are used in prediction of Breast cancer. Machine learning is a technique where model are created from given input and predict new input using that model. The Machine learning techniques are categorized into supervised learning, Unsupervised Learning and Reinforcement Learning.

In Supervised learning, the input and what to derive from the input is known formerly. Examples of Supervised learning are classification and regression. In Classification techniques, the given input is classified into given labels (either belongs to malignant or benign). In regression technique, the output derived from model will be a real number (from weight derive a height of a person).



In Unsupervised learning, input is known but don't know the label to classify. Examples of Unsupervised learning are Clustering, Anomaly detection, Neural networks. In Clustering, the given inputs are grouped according to their properties. In Anomaly detection, identification of unusual events occurrence from the given data is done. In neural network, it is a collection of connected nodes and has input layer and Output layer, in between one or more hidden layers to process the classified output.

II. DATA COLLECTION

A. Data samples

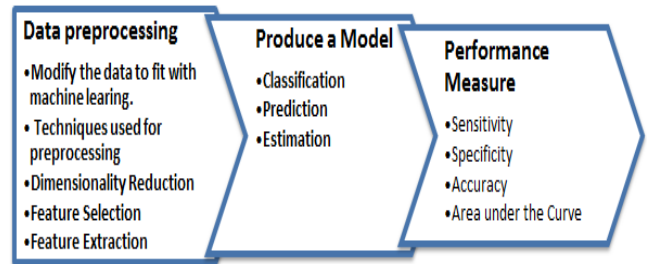
Datasets for breast cancer are available as open source. Datasets can be collected from TCGA, UCI Machine Learning Repository. Breast Cancer Wisconsin data set of UCI machine Learning repository is available with 10 attributes of 699 instances. In *Wisconsin datasets* focus on information about affected cell structures such as Thickness of cancer cell, consistency of Cell Size and Cell Shape, ticking property, Single Epithelial Cell Size, cell without cytoplasm coverage, rate of Bland Chromatin, check visibility of Nucleoli, Mitoses- cell production activity[10]. In *Mammographic Mass Data Set* from UCI machine Learning repository contains 6 attributes such as mammogram assessment (BI_RADS), age of the patient, shape of the cancer cell, mass margin, mass density, and identify whether benign or malignant of 961 instances are available[10]. In UCI Machine Learning repository, *Breast Cancer Coimbra Data Set* are freely available with 10 attributes such as Age of the patient , Body Mass Index, Glucose , Insulin level ,HOMA, Leptin, Adiponectin, Resistin, MCP-1 of 116 instances[10]. *Breast Tissue datasets* of UCI Machine Learning repository, have 10 attributes of IO Impedivity ,y, PA500 phase angle(500hz), HFS high-frequency slope of phase angle, DA impedance distance between spectral ends, AREA area under spectrum, A/DA area normalized by DA, MAX IP maximum of the spectrum, DR distance between IO and real part of the maximum frequency point, P length of the spectral curve, Class carcinoma, fibro-adenoma, mastopathy, glandular, connective, adipose of 106 instances. *Breast Cancer datasets of UCI Machine Learning repository*, have no-recurrence and recurrence of breast cancer was collected. Have 9 attributes such as age of the patient, menopause stage, size of the tumor, auxillary lymph nodes, diffusion of lymph node, degree of malignancy, which breast is affected, Affected breast quadrant, irradiation information of 286 instances.

B. Data Preprocessing

Initially, Data samples are collected with several features and different values. The collected data can have many issues such as noisy data, outliers, missing data, duplicate data and biased data. To overcome these data related issues data preprocessing should be done. The Data cleaning process include remove or reduce noise information and missing data. This missing data can be avoid by deleting that tuples itself, type the missing values, if it is numeric use fill with attribute mean and attribute mean of same class[4].

Data preprocessing techniques such as Dimensionality Reduction, Feature Selection and Feature Extraction, modifies collected data such that it can fit with Machine Learning techniques. Dimensionality reduction rejects

unrelated features and reduces noisy data. In feature selection, after dimensionality reduction is done the new features are selected from the old features. Embedded, Filter and wrapper are some techniques used for feature selection. The disadvantage of feature selection possibly will leads to variations in the prediction features. In feature extraction, select the data/ feature that can extract knowledge.

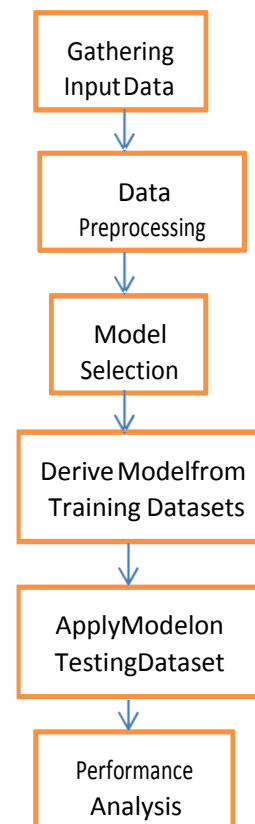


In the recurrence breast cancer dataset there is no missing values and noise.so directly can be used for model prediction.

In the Mammogram dataset, 2 missing values in BI_RADS assessment, 5 missing values in age, 31 in shape, 48 in margin, 76 in density. Missing values are replaced with mean of attribute values of same class.

TABLE III. MISSING VALUE DERIVATION

Class	BI_RADS assessment	Age	Shape	Margin	Density
0	3.957364	49.71318	2.065891	1.943798	2.899225
1	4.782022	61.55955	3.458427	3.723596	2.939326



MODEL FORMATION

A. Introduction

After the data preprocessing techniques, derive the model using any machine learning techniques such as classification, prediction and estimation. In Machine learning techniques, before deriving model, the datasets are separated as training sets and test sets. The models are created using training sets and test datasets are used to predict error of derived model. The various methods are used for prediction of Breast Cancer such as Artificial Neural Network, Decision tree, SVM and Bayesian networks.

Deep Learning techniques used for predictions are Unsupervised Pre- Training Networks, Convolutional Neural Networks, Recurrent Neural Networks, and Recursive Neural Networks. CNN used on images to identify Objects, and classify images. RNNs contains feedback loop used to process Languages. The various methods are used for evaluating the performance of a classifier. Some of them are Holdout method, Random sampling, Cross validation and Bootstrapping.

Hold out Method	Random Sampling	Cross-Validation	Bootstrap
<ul style="list-style-type: none"> Separation of Datasets into training and testing data Performance is estimated from testing data 	<ul style="list-style-type: none"> The Holdout method is repeated several times and choose randomly 	<ul style="list-style-type: none"> Each sample is used same number of times for training and only once for Testing 	<ul style="list-style-type: none"> The Samples are separated eith replacement into training and test sets

TABLE IV. MACHINE LEARNING TECHNIQUES

Methodology	Description	Advantage / Disadvantage
ANN	Output is generated from the combination of input layer and hidden layers.	Generic layered structure causes time consuming and poor performance
Decision Tree	A tree structured classification contains nodes(Variables) and leaves (Decision Outcomes)	Easy to infer and quick to learn
SVM	It works on high dimensional feature space and identifies many hyper plane and choose best hyper plane that classify the data points into two classes.	Feasible for smaller datasets and cannot handle larger datasets.
Bayesian Network	Probability estimations rather than prediction	Expensive

B. Apply Model on Mammogram datasets

By applying decision tree on mammogram datasets, predict the severity of mammogram based on BI_RADS_assessment, age of the patients, shape of the

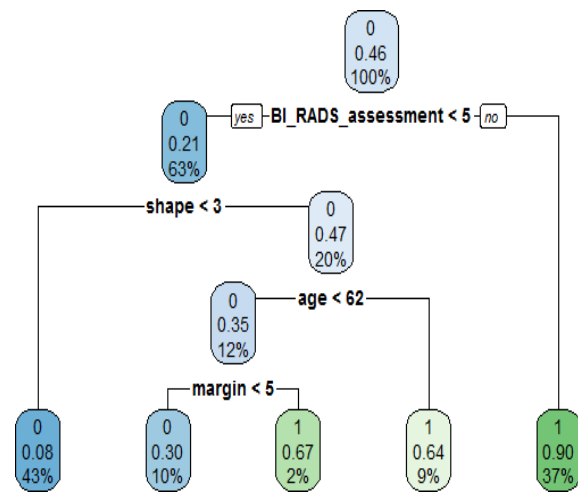
tumor, margin of the tumor, and density of the tumor. From 961 instances we took 80% of data as training data (786) and rest of them are testing data (193). In this Mammogram datasets, severity of patients not having breast cancer is 53% and severity of patients having breast cancer is 46%.

After applying Decision tree to the mammogram datasets, if BI_rads_assessment is greater than 5 then there is a 37% possibility of Breast cancer. If BI_rads_assesment is less than 5 and age of that person is greater than 62 then there is 9% of possibilities. Last condition is if BI_rads_assessment is less than 5, age less than 62 but if margin is greater than 5 then 2% possible of breast cancer

TABLE V. CONFUSION MATRIX FOR MAMMOGRAM DATASETS

	False	True
False	99	13
True	14	67

From Confusion Matrix, 99 members are exactly identified as not having cancer and 67 members are predicted as cancer patients. 13 patients are wrongly classified as cancer patient. 14 members are wrongly classified as not having cancer. Accuracy of the above DT is 86%.



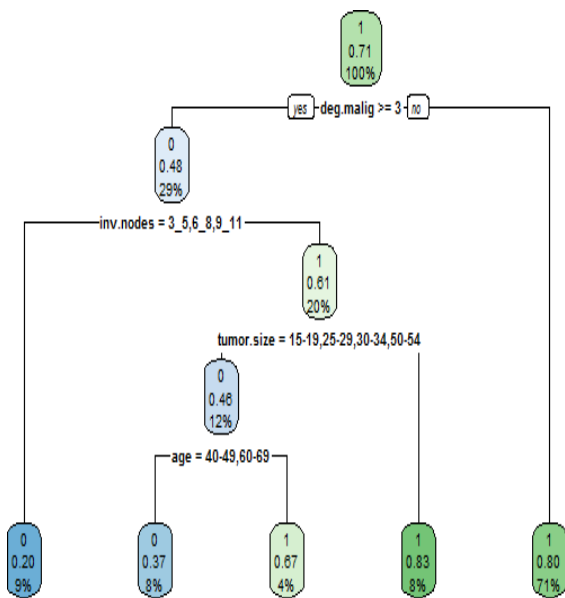
Random Forest Regression and Neural Network algorithms are applied on Mammogram datasets using COLAB. Severity in mammogram datasets can be predicted using Random forest algorithm and Neural Network algorithm both the algorithm had 0.41 and 0.38 mean squared prediction error.

```

0.41058297925970183
Train on 672 samples, validate on 288 samples
Epoch 1/10: loss: 0.4656 - mean_squared_error:
0.4656 - val_loss: 0.2690
val_mean_squared_error: 0.2690
Epoch 2/10: loss: 0.2086 - mean_squared_error:
0.2086 - val_loss: 0.1573 -
val_mean_squared_error: 0.1573
Epoch 3/10: loss: 0.1700 - mean_squared_error:
0.1700 - val_loss: 0.1580 -
val_mean_squared_error: 0.1580
Epoch 4/10: loss: 0.1517 - mean_squared_error:
0.1517 - val_loss: 0.1713 -
val_mean_squared_error: 0.1713
Epoch 5/10: loss: 0.1541 - mean_squared_error:
0.1541 - val_loss: 0.1561 -
val_mean_squared_error: 0.1561
Epoch 6/10: loss: 0.1489 - mean_squared_error:
    
```

C. Apply Model on Recurrence datasets

Decision tree is applied on Recurrence datasets, to predict re-occurrence of breast cancer based on age of the patient, menopause stage, size of the tumor, auxiliary lymph nodes, diffusion of lymph node, degree of malignancy, which breast is affected, Affected breast quadrant, irradiation information. The missing values are altered with frequent values. 80% of random data act as training data and 20 % act as testing data.



After applying Decision tree algorithm on Recurrence Datasets, Patterns derived are if degree of Malign is less than 3 then 71% of patient can have reoccurrence of Breast cancer. Suppose degree of malignant greater than or equal to 3 and inv_nodes are 3-5,6-8,9-11 and tumor size is 15-19,25-29,30-34,50-54 then possibility of recurrence is 8%.

TABLE VI. CONFUSION MATRIX FOR RECURRENCE DATASETS

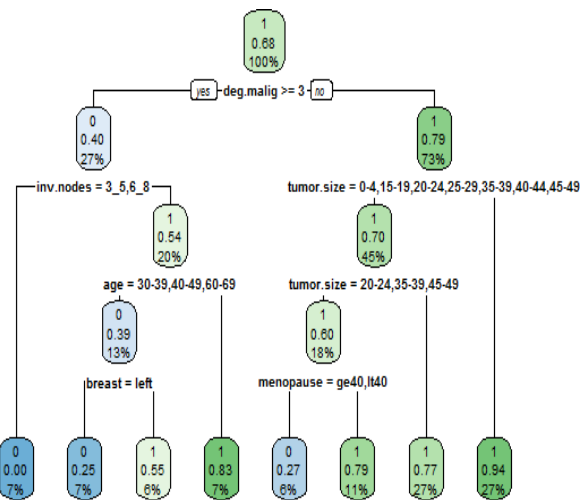
	False	True
False	8	11
True	5	34

From Confusion Matrix, 8 members are exactly identified as not having cancer and 34 members are predicted as recurrence of cancer. 8 patients are wrongly classified as cancer patient. 34 members are wrongly classified as not having cancer. Accuracy of the above DT is 72%.

Percentage of training and testing data taken for performing DT are 60% and 40%, in both the cases the common prediction is if degree of malignant is less than 3 then more possible of recurrence of Breast Cancer.

TABLE VII. PERFORMANCE

	Mammogram	Recurrence
Sensitivity	83.75%	75%
Specificity	87.61%	61%
Accuracy	86%	72%



III. PERFORMANCE

A. Performance Measure

The errors are classified into two such as training error and generalization error. Training error causes misclassification, this can be reduced by increases the complexity of Model because whenever the model complexity increases then training error rate decreases. The generalization error is testing error; this can be reduced using Bias - Variance Decomposition (Bias + Variance). Whenever Training error rate decreases test error rates increases is called as over fitting. Performance of each classification methodology can be measured using sensitivity, specificity, accuracy and Area under the curve (AUC).

TABLE VIII. PERFORMANCE

Methodology	Description
Sensitivity	The Proportion of which are exactly predicted as disease present with correctly observed both positive and negative results
Specificity	The proportion of which no. of patient exactly predicted as not having disease with total no. of exact both positive and negative prediction.
AUC	A measure of the models performance which is based on the ROC curve that plots the tradeoffs between Sensitivity and (1 – Specificity)
Accuracy	A measure related to the total no. of correct prediction

IV. CONCLUSION

There are tremendous amount of medical datasets are available now. Analysis of data can give new pattern that can be used as new clinical traits, drug discovery, early prediction of disease, personalized medicine, side effects of any treatment and change food intake. Gathering of data from health care will leads to some security issues and need some ethical clearance to access those data. After Collection of data, Data preprocessing techniques are used to clean noisy data and avoid redundant data. Machine Learning techniques are used to identify the hidden patterns. Deep Learning techniques will have automatic feature selection. Prediction of Breast cancer can be done using machine learning and deep learning techniques.

V. REFERENCE

- [1] Shreshtha Malvia, et.al., “Epidemiology of breast cancer in Indian Women: Breast Cancer epidemiology” in Asian-Pacific Journal of Clinical Oncology 2017;13:289 – 295
- [2] O. L. Mangasarian and W. H. Wolberg: "Cancer diagnosis via linear programming", SIAM News, Volume 23, Number 5, September 1990, pp 1 & 18.)
- [3] M. Elter, R. Schulz-Wendtland and T. Wittenberg (2007), “The prediction of breast cancer biopsy outcomes using two CAD approaches that both emphasize an intelligible decision process”.
- [4] Medical Physics 34(11), pp. 4164-4172 I. S. Jacobs and C. P. Bean, “Fine particles, thin films and exchange anisotropy,” in Magnetism, vol. III, G. T. Rado and H. Suhl, Eds. New York: Academic, 1963, pp. 271–350.
- [5] Suad. A. Alasadi and Wesam S. Bhaya, “ Review of Data preprocessing Techniques in Datamining”, Journal of Engineering and Applied Science 12(16); 4102 – 4107, 2017.
- [6] By Michael K. K. Leung, Andrew Delong, Babak Alipanahi, and Brendan J. Frey, “Machine Learning in Genomic Medicine: A Review of Computational Problems and Data Sets”, IEEE. Translations and content mining are permitted for academic research only,
- [7] [<http://cancerindia.org.in/>]
- [8] Fabio Vandin, Eli Upfal, and Benjamin J. Raphael, Algorithms and Genome Sequencing: Identifying Driver Pathways in Cancer, © IEEE, 0018-9162/12 (2012), 39-46.
- [9] Boiculescu LV1, Dimitriu G., Multi-valued logic in breast cancer detection, Rev Med Chir Soc Med Nat Iasi. 2003 Apr-Jun;107(2):425-8.
- [10] Dua, D. and Graff, C. (2019). UCI Machine Learning Repository [<http://archive.ics.uci.edu/ml>]. Irvine, CA: University of California, School of Information and Computer Science

A Review on Image Processing Approaches for Glioma Grading

Seema P.D.
Department of Electronics and Communication
M S Ramaiah University of Applied Sciences
Bangalore, India
seema.biomedical@gmail.com

Christy Bobby T.
Department of Electronics and Communication
M S Ramaiah University of Applied Sciences
Bangalore, India
christy.ec.et@msruas.ac.in

Abstract— In recent years, brain tumour cases have been on the rise and late diagnosis leads to high morbidity and mortality. According to the World Health Organization (WHO), brain tumours occur in around 250,000 people throughout the world. To detect the tumour at an early stage, appropriate usage of imaging modality yielding high resolution images play a vital role. Also, accurate grading of tumours is important to find the severity of the disease and the clinical condition of the patient. This paper reviews the types of brain tumours, modalities used for imaging and the already developed algorithms and their respective results.

Keywords—Brain tumour, Brain tumour imaging, Glioma grading.

I. INTRODUCTION

Brain tumour is defined as the neoplasm (unusual growth of tissues) in any part of the brain with degrees of aggressiveness ranging from benign to malignant [1]. According to the World Health Organization (WHO), brain tumours occur in around 250,000 people throughout the world [2]. The main causes of brain tumours are genetically linked and in most cases, the causes are unknown [3]. The methods of diagnosing brain tumour play a pivotal role in terminating the tumour growth in the early stages of onset – the earlier the better. Hence, the need of the hour is to establish or develop an algorithm that would automatically and accurately detect the stages or grades of brain tumour without much human intervention.

II. BRAIN TUMOUR

Brain tumour is the abnormal growth of brain cells and the primary brain tumours can be generally graded as benign (does not consist of cancer cells) and malignant (consists of cancer cells). The type of primary brain tumours is determined on the basis of the type of cells involved in the tumour growth as well as the location of the tumour. The two types of primary brain tumour are Glioma and Meningioma. Glioma is a type of brain tumour that occurs in the glial cells that are responsible for the propagation of neural signals and also form a support and insulation to the neurons. The second type is meningioma, it originates in the meninges present in the exterior part of the brain below the skull. According to a survey in India, the common type of brain tumour is the Glioma accounting for 34.7% and is also the most frequently occurring tumour accounting for 47.3% [4]. Since it is the most common and frequently occurring type of brain tumour, extensive research and studies have been carried out on the same. Therefore, more details have been covered pertaining to glioma in this paper.

A. Glioma

Glioma is an umbrella term used for the type of brain tumour that occurs in specific cells called the glial cells. The types of gliomas based on the cell type and its origin are [5]:

- i) Ependymoma: It occurs in the ependymal cells situated in the cerebrospinal fluid(CSF)-filled space of the spinal cord [6]. Of all brain tumours, this type occurs less than 2% among adults and less than 10% among children. It does not spread or affect the normal brain tissue. Their occurrence is recurrent and hence considered as malignant.
- ii) Astrocytoma: This occurs in the brain cells known as astrocytes. They spread and affect the normal brain tissues, hence it is difficult to completely cure it.
- iii) Oligodendroglioma: This type of glioma spreads in a similar pattern as that as astrocytoma. They can sometimes be cured as it may be spreading slowly to the healthy tissues in the vicinity.
- iv) Brainstem glioma: This occurs in the brainstem located in the posterior part of the brain, it accounts to less than 2% among adults [7].
- v) Optic nerve glioma: It occurs in the optic nerve located behind the eyes and accounts to 1.7-7% of gliomas in adults [8].

Based on the intensity and rate of spreading, the gliomas are widely categorized as low grade glioma (LGG) and high grade glioma (HGG). The less intense cells that do not spread sporadically are LGG. The highly intense cells that spread rapidly by disrupting the healthy tissues in the vicinity of the tumour is called HGG. According to WHO, the classification of glioma are grade I, II, III and IV [9]. Grades I and II fall under the low grade glioma while grades III and IV fall under high grade glioma.

Fig.1 shows Magnetic Resonance Imaging(MRI) images of LGG and HGG. The latter is very distinct and evident (high intensity) while the former is in its initial stage.

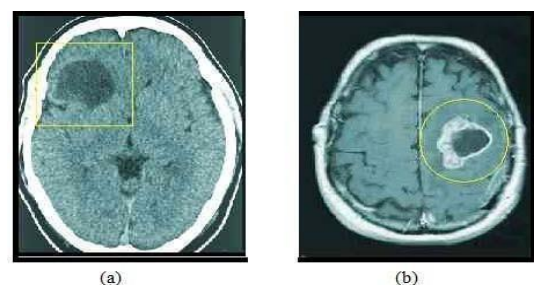


Fig. 1. MRI scans of a) LGG and b) HGG

III. DIAGNOSIS : IMAGING OF BRAINTUMOURS

The most significant and commonly used imaging modalities for brain tumour detection are Computed Tomography (CT) and Magnetic Resonance Imaging (MRI). These techniques aid in locating the brain tumour as well as determining its size and shape. The major advancement in these technologies is the introduction of iodine based contrast agents for CT and gadolinium based contrast agents for MRI [10]. They provide a greater visibility of the tumour and improved tumour detection. Since CT and MRI are the most commonly used imaging modalities, a detailed review of the same has been explicated further.

A. Computed Tomography

CT is a computerized X-ray imaging procedure that produces signals processed by the computer which is interfaced with the CT machine. These signals are processed to obtain tomographic images or slices which are digitally stacked together to form three dimensional (3D) images. The information obtained from these 3D images of the patient help in identifying possible tumours or any abnormalities. The contrast agent used in CT is iodine based which is injected intravenously and it helps in illuminating the blood vessels and also aids in detecting tumours easily. Even though MRI is the main diagnostic tool for central nervous system diseases, CT is still considered as a valuable imaging modality. CT is usually not preferred because of its low resolution, specificity and sensitivity compared to MRI [10]. Table I gives the advantages and disadvantages of CT.

Table I. Advantages and disadvantages of CT [36]

Advantages of CT	Disadvantages of CT
1. It shows the acute bleeding conditions	1. During CT process, the patient is exposed to ionizing radiation
2. It is most preferred for bony and calcified lesions	2. The resolution of the CT scanned images are relatively poor
3. It is a non-invasive, quick and painless	3. The injection of the contrast agent can cause kidney problems or allergic reactions
4. Good spatial resolution	4. It may require the patient to be under anaesthesia
5. Global view of veins	5. Cannot be performed without contrast
6. Distinguished by small differences in physical density	6. Less contrast resolution where soft tissue contrast is low
7. Avoids the invasive insertion of an arterial catheter and guidewire	

B. Magnetic Resonance Imaging

MRI is the most effective choice of imaging modality for diagnosing the brain tumour in those patients who exhibit the signs and symptoms. The important properties of MRI are its multiplanar capability and high contrast resolution. These factors help in the assessment of tumour location, directing biopsies, planning of proper therapy to be given and in the evaluation of therapeutic results. The different types of MRI images are spin-echo T1-weighted image (T1WI), T2-

weighted image (T2WI), and fluid attenuated inversion recovery (FLAIR). In T1WI, the CSF, air, water and inflammations are dark, fat is bright and the white matter is light in colour. The white matter and air are dark in T2WI whereas the inflammation and CSF are bright. The CSF and white matter appear dark in FLAIR images while the inflammation is bright [10]. Fig. 2 shows T1WI, T2WI and FLAIR images.

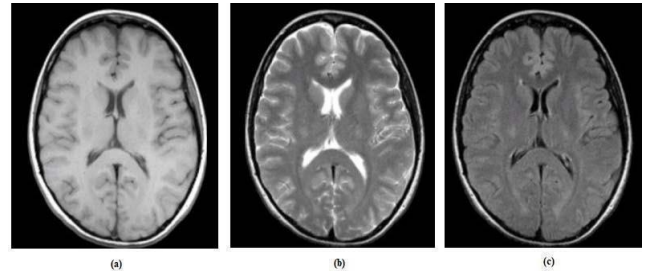


Fig. 2. MRI scans of a) T1WI b) T2WI c) FLAIR

During the process of acquiring MRI scans, the patient may be administered with a gadolinium based contrast agent to enhance the image. Gadolinium is a paramagnetic contrast agent which causes no harm to the patient as it is non-toxic.

The MRI possesses many advantages when compared to CT. The main advantage is that MRI has a high spatial resolution and does not need ionizing radiation. The advantages and disadvantages of MRI are tabulated in Table II. Considering these factors, it is appropriate to incorporate MRI imaging for the diagnosis of brain tumours.

Table II. Advantages and disadvantages of MRI [36]

Advantages of MRI	Disadvantages of MRI
1. The patient is not subjected to any radiation exposure	1. Patients with pacemakers or metal implants in their bodies are not eligible to undergo MRI
2. Provides a good resolution of images	2. People who are claustrophobic are slightly at a risk
3. Reconstruction of 3-D images is possible	3. The MRI procedure is lengthy and noisy
4. Good differentiation between the grey and white pixels	
5. The contrast agent used is Gadolinium which is relatively non toxic	

In order to view the vasculature of the brain and the haemodynamic factors, perfusion imaging is done. Perfusion imaging is an imaging technique that provides detailed information pertaining to the physiology of the tumour and the dynamics of the blood flow. The haemodynamic information such as blood volume, blood flow and capillary permeability aid in assessing and characterizing the gliomas more effectively [11-13]. The types of perfusion imaging are Dynamic Susceptibility Contrast (DSC) and Dynamic Contrast Enhanced (DCE). They are most commonly done in MRI than in CT. Hence, DSC-MRI and DCE-MRI are explicated further in detail.

1) *DSC MRI*

DSC-MRI is also known as bolus tracking MRI. It is the most common and robust quantitative method used to derive the relative cerebral blood volume (rCBV). The value of rCBV help in determining the glioma grade. The mean of rCBV is high in HGG and low in LGG [14].

DSC perfusion imaging method involves an intravenously injected gadolinium followed by the acquisition of gradient or spin echo images over the target organ. When the gadolinium passes through the path towards the target organ, it creates a magnetic field distortion around it [15-19]. This results in T2 dephasing and the loss of signal as the gadolinium passes. Perfusion parameters such as blood volume, capillary permeability, blood flow and mean transit time can be calculated by measuring the obtained signals. The image acquisition time in DSC-MRI is around 2minutes which is relativelyshort.

2) *DCE MRI*

Dynamic contrast enhanced (DCE) perfusion imaging is also known as permeability MRI. It requires intravenous administration of gadolinium to calculate the perfusion parameters from the regional increased signal (T1 shortening). The T1-weighted images are repeatedly acquired over 5-10 minute interval. The gadolinium gets accumulated during this time windowat a rate determined by perfusion, capillary permeability and surface area. The quantification of the image is obtained by applying a compartmental model. Several physiological parameters such as the transfer constant, fractional plasma volume and fractional volume of the tissue extracellular space are derived from this model [15-19]. Table III provides the differences between DSC and DCE methods.

Table III. Differences between DSC and DCE [16]

Imaging method	Dynamic Susceptibility Contrast (DSC)	Dynamic Contrast Enhanced(DCE)
Imaging sequence	T2 weighted	T1 weighted
Acquisition time	Short (1-2 minutes)	Long (5-10 minutes)
Clinical use	Brain stroke or tumours and heart ischemia	Brain/Breast/ pelvis tumours

IV. GRADING OF GLIOMA

Textural analysis, Machine Learning(ML) and Deep Learning (DL) algorithms have been developed in order to grade the glioma based on its stages. There have been very few studies on glioma grading using texture analysis of imaging data. The basics steps carried out for grading of glioma are image acquisition, pre-processing, feature extraction and selection, classification. Table IV shows the various tools used for feature parameter calculation and perfusion analysis for grading of the glioma.

Many research works have been carried out to grade gliomas using various textural feature extraction methods and ML and DL tools - these have been discussed further.

Table IV. Tools for feature parameter calculation and perfusion analysis [37]

	MaZda	RocketShip[37]	MITK
Languages	C++,Delp hi	Matlab	C++
Models - available	Texture features	Tofts, Extended Tofts, Fast Exchange Regime, 2CXM, Tissue uptake, Nested-model selection, Patlak, Semi-quantitative metrics	Tofts, Extended Tofts, Brix, Three-step linear (3SL), Semi-quantitative metrics
Input-Output	DICOM, Raw data	DICOM, Analyze, NIFTI, Raw data, Matlab data	DICOM, Analyze, NIFTI, NRRD, VTK, Raw data
GUI	yes	yes	yes
Source	http://www.elel.p.lodz.pl/progr amy-mazda/	https://github.com/petmri-ROCKETSHIP	http://www.mitk.org/download/releases/MITK-2018.04.2-Windows/

A. *Approaches for glioma grading*

The approaches for grading the glioma discussed are texture and statistics based, transform based, ML and DL. The research work and studies carried out pertaining to these approaches have been explained further.

1) *Texture and Statistics based approaches*

The statistical approach sees an image texture as a quantitative measure of the arrangement of intensities in a region. The texture of an image represents the intensityof the image, the distribution of the pixels and their correlation with respect to each other. Texture analysis is a method for quantifying the spatial distributions of intensities in images. It is a great aiding tool for quantification as it non-invasively processes the heterogeneity of the tumour through statistical parameters such as mean, median, kurtosis, energy, entropy and also help in aiding in the prediction of tumour occurrence [15-16].

A study by Karoline et al. [20] demonstrated the texture analysis in quantifying tumour heterogeneity and grade. Also, Ananda et al. [21] showed that textural features of T2WI were highly discriminant between grade I and grade III gliomas. This study also showed that first order statistics and Gray Level Co-occurrence Matrix (GLCM) based second order statistics were considered. The first order statistics descriptors were contrast, intensity, entropy, kurtosis, and spectral energy. For HGG, the ranges of the aforementioned first order statistics descriptors were

40.5±20, 170±20, 5.445±0.5405, 175±50, (8.5 ±0.08)*10¹¹ respectively. For LGG, the ranges of these descriptors were 11.5±0.5, 220±5.64, 6.5±0.422, 5.5±1.5, (5.5 ±0.08)*10¹¹ respectively. It was concluded that these ranges were highly differentiable between LGG and HGG.

Various studies [22-25] have indicated that histogram parameters, including the mean, minimum, maximum intensity value of a Voxel of Interest (VOI) or Region of Interest (ROI), were effective in differentiating glioma grades. In one study [26], the 3D Haralick features were derived from VOI intensity image, GLCM and the Gray-Level Gradient Co-occurrence Matrix (GLGCM). From 10 VOI, 420 texture and 90 histogram parameters were derived. The accuracy was 96.8% and the study concluded that texture features were effective compared to the histogram parameters for glioma grading.

The objective of the study carried out by Austin Ditmer et al. [27] was to determine the diagnostic accuracy of radiomic based filtration histogram to differentiate HGG from LGG by assessing tumour heterogeneity. The histogram parameters including mean, standard deviation, entropy, mean of the positive pixels (MPP), skewness, and kurtosis were analyzed. These features for LGG and HGG showed significant differences. The sensitivity and specificity obtained were 93% and 86% respectively.

2) Transform Based Approaches

A study carried out by Qijian Chen et al. [28] was based on scattering wavelet transform using multimodal MRI images. The radiomic features and the features based on wavelet scattering were extracted. The Support Vector Machine (SVM), Logistic Regression (LR) and Random Forest (RF) were trained for glioma grading. The result of this study was that the prediction of glioma grading was 99%.

In the study carried out by Manu Gupta et al. [29], a combination of Discrete Wavelet Transform (DWT) and Local Binary Pattern (LBP) techniques were used for feature extraction from glioma images. From this combination of DWT-LBP transformed images, skewness, kurtosis, and entropy were calculated. This study concluded that HGG has more structural complexity than LGG. The grading accuracy, sensitivity and specificity were 96%, 97% and 95% using Naive Bayes classifier.

In Nilesh et al. [30], Berkeley Wavelet Transformation (BWT) based brain tumour segmentation and the SVM based classifier were incorporated. The experimental results achieved 96.51% accuracy, 94.2% specificity and 97.72% sensitivity.

The major limitation in the texture analysis is overfitting. The problem of overfitting occurs when the number of independent parameters exceed the number of sample size to be analyzed. In order to overcome the limitations, ML and DL approaches are incorporated to make the grading models more robust and relatively accurate.

3) Machine Learning and Deep Learning Algorithms

ML and DL methods are now not only trending but also yielding relatively better accuracy and results. The advantage of incorporating the deep learning neural networks methods is that it is capable of determining more abstract and higher-

order relationships between features and data unlike texture analysis [32]. Further, the different studies carried out using ML and DL algorithms are reviewed and briefly explained further.

The aim of study [31] was to train a Convolutional Neural Network (CNN) to classify HGG and LGG using MRI images. CNN architectures such as AlexNet, GoogLeNet and transfer learning from ImageNet were used. A performance comparison was made between all three and thereby concluded that GoogLeNet performed better than AlexNet and ImageNet. The validation and test accuracy of GoogLeNet were 86.7% and 90.9% respectively.

In the study carried out by Bum-Sup Jang et al. [33], the method of Hybrid deep and machine learning CNN Long Short-Term Memory (LSTM) of DL was used. The character assessed in this method is pseudo-progression. The accuracy obtained by this method was 83%. In another study carried out by Zeynettin Akkus et al. [34], multi-scale CNN method of DL was used. The accuracy obtained was 87.70%. ResNet50 of DL was used by Panagiotis Korfiatis et al. [35], an accuracy of 94.90% was obtained. In this study, ResNet 36 and ResNet18 were also used and they yielded an accuracy of 80.72% and 76.75% respectively.

V. CONCLUSION

An evolution of neuroimaging techniques to detect brain tumours has been witnessed over the years. The transition from purely anatomy based approach to the latest perfusion imaging has been crucial in detecting glioma. The various approaches incorporated in order to grade brain tumours are still evolving. Initially, statistical approaches and texture analysis were considered to differentiate the various grades of brain tumours. Though these methods yielded satisfactory results and accuracy, the limitation of over-fitting had occurred. Nowadays, ML and DL algorithms are a first choice for the analysis and grading of glioma. These algorithms provide relatively greater accuracy and detailed information and also eliminate discrepancies encountered in the previous methods of grading. Still, there is a need to develop an exclusive clinical application that would yield a maximum accuracy of glioma grading. This would greatly help the radiologists and doctors in carrying out proper diagnosis and timely treatment. This will eventually decrease the morbidity and mortality rate related to glioma.

REFERENCES

- [1] P A McKinney "Brain Tumours: Incidence, Survival, And Aetiology" *J Neurol Neurosurg Psychiatry*;75(Suppl II):ii12-ii17. 2004
- [2] World Cancer Report. World Health Organization. 2014. ISBN 978-9283204299. 2014
- [3] "General Information About Adult Brain Tumors". NCI. 14 April 2014.
- [4] Dasgupta, Archya et al. "Indian data on central nervous tumors: A summary of published work." *South Asian journal of cancer* vol. 5,3:147-53. 2016
- [5] "Gliomas". *Johns Hopkins Medicine Health Library*. <https://www.hopkinsmedicine.org/health/conditions-and-diseases/gliomas>
- [6] M.Ross, *Histology, a text in atlas*, 6th edition 367, 2011
- [7] Hu J, Western S, Kesari S. "Brainstem Glioma in Adults" *Frontier of Oncology*; 6:180. 2016
- [8] Bhaker, Poonam et al. "Optic nerve glioma: A great mimicker." *Surgical neurology international* vol. 5 9., 23 Jan. 2014

- [9] WHO D. N. Louis et al., "The 2016 World Health Organization Classification of Tumors of the Central Nervous System: a summary," *Acta Neuropathol.*, vol. 131, no. 6, pp. 803–820, 2016
- [10] Hasebroock, K. M., & Serkova, N. J. "Toxicity of MRI and CT contrast agents. *Expert Opinion on Drug Metabolism & Toxicology*", 5(4), 403–416. 2009
- [11] Law M, Young RJ, Babb JS, et al. "Gliomas: predicting time to progression or survival with cerebral blood volume measurements at dynamic susceptibility-weighted contrast-enhanced perfusion MR imaging." *Radiology*2008;247:490–98
- [12] Roberts HC, Roberts TP, Brasch RC, et al. "Quantitative measurement of microvascular permeability in human brain tumors achieved using dynamic contrast-enhancedMR imaging: correlation with histologic grade". *AJNR American Journal Neuroradiology*, 21:891–99,2000
- [13] Law M, Yang S, Babb JS, et al. "Comparison of cerebral blood volume and vascular permeability from dynamic susceptibility contrast-enhanced perfusion MR imaging with glioma grade". *AJNR Am J Neuroradiol*,25:746–55,2004
- [14] J. H. Shin et al., "Using relative cerebral blood flow and volume to evaluate the histopathologic grade of cerebral gliomas: Preliminary results," *Am. J. Roentgenol.*, vol. 179, no. 3, pp.783–789,2002
- [15] Essig M, Shiroshi M S, Nguyen TB, et al. "Perfusion MRI: the five most frequently asked technical questions. *AJR Am JRoentgenol* ,200:24-34. 2013
- [16] Jahng G-H, Li K-L,Ostergaard, Calamante F. "Perfusion magnetic resonance imaging: a comprehensive update on principles and techniques." *Korean Journal of Radiology* 15:554-577.2014
- [17] McGehee BE, Pollock JM, MAldjian JA. "Brain perfusion imaging:how does it work and what should I use? *Journal of Magnetic Resonance Imaging*; 36:1257-1272.2012
- [18] Tofts P S. "T1- weighted DCE imaging concepts:modelling, acquisition and analysis." *MAGNETOM Flash*;3:30-35.2010
- [19] Zaharchuk G. "Theoretical basis of hemodynamic MR imaging techniques to measure cerebral blood volume, cerebral blood flow and permeability" *American Journal of Neuroradiology*; 28:1850-8.2007
- [20] Skogen K, Ganeshan B, Good C, Critchley G, Miles K "Measurements of heterogeneity in gliomas on computed tomography relationship to tumour grade" . *J Neurooncol* 111: 213–219,2013
- [21] S AR, Thomas T "Texture Description of low grade and high grade Glioma using Statistical features in Brain MRIs." *Int J of Recent Trends in Engineering and Technology*,2010
- [22] Shen N, Zhao L, Jiang J, et al. "Intravoxel incoherent motion diffusionweighted imaging analysis of diffusion and microperfusion in grading gliomas and comparison with arterial spin labeling for evaluation of tumor perfusion". *J Magn Reson Imaging*;44:620–632. 2016
- [23] Hu YC, Yan LF, Wu L, et al. "Intravoxel incoherent motion diffusionweighted MR imaging of gliomas: Efficacy in preoperative grading".*Sci Rep*;4:7208. 2014
- [24] Lin Y, Li J, Zhang Z, et al. Comparison of intravoxel incoherent motion diffusion-weighted MR imaging and arterial spin labeling MR imaging in gliomas. *Biomed Res Int*;2015:234245.2015
- [25] Bai Y, Lin Y, Tian J, et al. Grading of gliomas by using monoexponential, biexponential, and stretched exponential diffusion-weighted MR imaging and diffusion kurtosis MR imaging. *Radiology*;278:496. 2016
- [26] Tian, Q., Yan, L.-F., Zhang, X., Zhang, X., Hu, Y.-C., Han, Y.,Cui, G.-B. "Radiomics strategy for glioma grading using texture features from multiparametric MRI". *Journal of Magnetic Resonance Imaging*. doi:10.1002/jmri.26010, 2018
- [27] Austin Ditmer, Bin Zhang, Taimur Shujaat, Andrew Pavlina, Nicholas Luibrand, Mary Gaskill Shipley, Achala Vagal "Diagnostic accuracy of MRI texture analysis for grading gliomas" *Springer Nature Journal Of Neuro Oncology*,2018
- [28] Qijian Chen, Lihui Wang, Li Wang, Zeyu Deng, Jian Zhang and Yuemin Zhu "Glioma Grade Predictions using Scattering Wavelet Transform-Based Radiomics" *ArXiv*, 2019
- [29] Manu Gupta, Venkateswaran Rajagopalan and B. V. V. S. N. Prabhakar Rao "Glioma grade classification using wavelet transform-local binary pattern based statistical texture features and geometric measures extracted from MRI" *Pages 57-76*,2018
- [30] Nilesh Bhaskarrao Bahadure, Arun Kumar Ray, and Har Pal Thethi, "Image Analysis for MRI Based Brain Tumor Detection and Feature Extraction Using Biologically Inspired BWT and SVM" *International Journal of Biomedical Imaging Volume* , Article ID 9749108, 2017
- [31] Yang Yang, Lin-Feng Yan, Xin Zhang, Yu Han, Hai-Yan Nan, Yu-Chuan Hu1, Bo Hu1, Song-Lin Yan, Jin Zhang, Dong-Liang Cheng, Xiang-Wei Ge, Guang-Bin Cui Di Zhao and Wen Wang "Glioma Grading on Conventional MR Images: A Deep Learning Study With Transfer Learning" *Frontiers in Neuroscience*, 2018
- [32] Madeleine M. Shaver, et al "Optimizing Neuro-Oncology Imaging: A Review of Deep Learning Approaches for Glioma Imaging" *MDPI*, 2019
- [33] Jang, B. S., Jeon, S. H., Kim, I. H., & Kim, I. A. "Prediction of Pseudoprogression versus Progression using Machine Learning Algorithm in Glioblastoma". *Scientific reports*, 8(1), 12516. doi:10.1038/s41598-018-31007-2, 2018
- [34] Akkus, Z., Galimzianova, A., Hoogi, A., Rubin, D. L., & Erickson, B. J. "Deep Learning for Brain MRI Segmentation: State of the Art and Future Directions". *Journal of digital imaging*, 30(4), 449–459. doi:10.1007/s10278-017-9983-4, 2018
- [35] Ulas Baran Balogulu, Ozal Yildirim, U Rajendra Acharya. "Application of Deep Transfer Learning for Automated Brain Abnormality Classification Using MR Images" *Article in Cognitive Systems Research* · December 2018
- [36] Raymond Y. Kwong, E. Kent Yucel, "Computed Tomography Scan and Magnetic Resonance Imaging", *Cardiology Patient Page*, American Heart Association, 2003
- [37] Samuel R. Barnes, Thomas S. C. Ng, Naomi Santa-Maria, Axel Montagne, Berislav V. Zlokovic and Russell E. Jacobs "ROCKETSHIP: a flexible and modular software tool for the planning, processing and analysis of dynamic MRI studies" *BMC Medical Imaging*, 2015

Establishing Authenticity for DICOM images using ECC algorithm

Veena Suresh
Department of Computer Science
PES University
Bengaluru, India
veenasuresh@pes.edu

S Rajashree
Department of Computer Science
PES University Bengaluru, India
rajashrees@pes.edu

Abstract—Preserving medical data is of utmost importance to stake holders. There are not many laws in India about preservation, usability of patient records. When data is transmitted across the globe there are chances of data getting tampered intentionally or accidentally. Tampered data loses its authenticity for diagnostic purpose, research and various other reasons. This paper proposes an authenticity based ECDSA algorithm by signature verification to identify the tampering of medical image files and alerts by the rules of authenticity. The algorithm can be used by researchers, doctors or any other educated person in order to maintain the authenticity of the record. Presently it is applied on medical related image files like DICOM. However, it can support any other medical related image files and still preserve the authenticity.

Keywords—DICOM, MRI Brain images, Electronic Medical Records (EMR), Authenticity, ECDSA

I. INTRODUCTION

Preserving Electronic Medical Record (EMR) details is of utmost priority in every domain. The details are a welcome relief in case of emergencies for the person himself, for the immediate family, for the organisation in which he is employed, for insurance claim, for research labs etc. The medical data can be tampered for various issues like monetary benefits, ethical, social, psychological etc. Once the accuracy is lost, the accountability can be questioned leading to collapse of the entire system. The damage done could be unreasonable. The persons who can legally and socially authorise to access data can be categorised as Family physician, and doctors, care takers, researchers only upon getting proper prior permission. For protecting these private data the “Health Insurance Portability and Accountability Act” HIPAA[1] and “General Data Protection Regulation” GDPR[2] privacy rule are formulated.

Researchers in medical field domain are aware that they should be trustworthy else they may not get patients data for analysis. Patient’s or their guardian’s value research and are open to share the information with the hope of benefitting from scientific advances for themselves or their families. The task for the researcher is to protect privacy and to safeguard the data through security mechanisms at affordable cost.

Data collected from patient may contain sensitive information (like gender), habits (like smoking, alcohol, drugs consumption). Data may also include

information about patients communal, cultural, or financial status which will be helpful for analysing mental, physical health and stress parameter. Data have also been used by researchers to study genomic profile to gain insight into hereditary disease. [3]

This paper introduces one simple and effective practice for executing security control in a hospital data centre infrastructure (ISO27002) environment and describes the methodology for implementing the same by providing authenticity to data. In order to access and maintain health data from unauthorised users, this paper proposes the ECDSA algorithm. The methodology is applied to MRI brain image and the results are shown. As it is a simple and easily understandable approach the people who can use this can be a simple educated care giver, a medical professional, insurance agent or anybody who has specific credentials to access the file. The methodology can be extended to include the entire medical record.

II. LITERATURE SURVEY

HIPAA is standard by United States legislation designed for providing privacy of patient data and security related to medical personal information[1].

The GDPR is a standard set of rules that should be followed by those who share data of citizens of European Union designed for securing data of the EU citizens. The GDPR is formulated to provide control to individuals or organizations over their personal data there by sharing of data is done through consent of the person or organization to use the data for either study or any other purpose[2].

The Healthcare sector in India when compared with other few international standards has no perfect laws to govern the privacy of individuals with respect to diagnosis methods, treatment and the use of contemporary technology. Privacy and security with the healthcare sector includes

- Privacy, secrecy and confidentiality of information.
- Individual dignity (modesty, personal values)
- Associational privacy (sharing of death news, medical problems and cure).
- Proprietary privacy (information about personal assets, genetic data, and body tissues)
- Health care must also provide additional privacy on decision making (autonomy)[4].

Government laws which focus on access control which is a main feature in other countries about the healthcare information systems to protect the privacy and secrecy of patient’s data and to ensure secure access to information as required by healthcare

professionals needs still more strict laws.

In our nation with more than one billion individuals, data is inevitable to be distributed or strewn, especially healthcare data as it is not an organised sector. If the health care has not maintained the record of previous diagnosis or if patient does not have his old diagnosis report, then doctors may need to redo all or some of them as no other way will be available to retrieve the patient's data. The present law states that doctors must maintain the medical records of patients who is availing treatment or has undergone diagnosis in their centres for at least three years but the followers are less in number due to lack of infrastructure or lack of team who can maintain these data.

- **Format of a health record**

The data for any patient is stored in digital format as electronic health records (EHR). This EHR includes diagnosis done and medicines prescribed by doctors, for a patient admitted the recording of observations time to time and orders for the administration of drugs along with time and dosage and if any therapies are advised and who will be doing that, test results for each of investigations done, x-rays or MRI or any scans is prescribed. If prescribed, then that report must also be attached with EHR. The maintenance of all the above information which is complete and accurate should be the main concern of health care that needs to be fulfilled by healthcare which is a prerequisite for issue of licence for healthcare.

Traditionally health care providers used to maintain health data of patient but due to the development in technology to store data in cloud, (personal health records (PHR)) third-party websites whose security and privacy depends on the party who is providing the cloud storage[5].

- **Characteristics of DICOM (“Digital Imaging and Communications in Medicine”) Image**

DICOM is a form of digital image which is an example for medical record. DICOM images can be used for transmission, storage, retrieval, printing, processing, and displaying information of the patients who has undergone the MRI brain investigation[6]. The digital format has an advantage which makes patient data to be exchanged for emergency purpose easily. The capture of image requires integration of many devices like image-acquisition, picture archiving and communication system (PACS), workstations and printers which are designed and developed from different vendors. These devices are designed to meet different requirements of medical field using most efficient and advanced technologies.

EHR Information taken from patients or with health care providers can be grouped into data sets. The data set is a file consisting of a header and image. Data set stores information about patient analysis, and information about acquisition parameters which is required for imaging study. It also stores information about image parameters such as dimensions, size, colour space, and data needed by the system to show the medical image. After the header contents, single attribute (7FE0) that contains all the pixel

intensity data for the picture is present[6]. These data are stored in digital form as 0s and 1s, which can be used for reconstruction of picture by using the data present in the header. The qualities may contain ideas about a single or more points of a study depending on some parameter like methods that has created the image.

For security purposes to avoid tampering or misuse of data header, information of DICOM file is encoded such a way that separating images is not possible. But if the picture is separated from the original data, then computer cannot know the details of the patient on whom the current analysis has been done or for which patient it belongs which leads to incorrect image to be displayed.

- **Reading information present in the header**

The information contained within the header is organized as tags. The tags are organized in such a way that they are groups of data elements. The DICOM header has information that will be helpful in studying the DICOM image itself.

- **Magnetic Resonance Images (MRI)**

MRI is used in preparation of diagnostic medicine and in physiological studies. Spatial images are the details with physical and chemical data produced with an idea of uses of MRI scan [7].

III. METHODOLOGIES AVAILABLE TO AVOID TAMPERING

There are various ways in which digital data (images) can be tampered. For avoiding these damages to data, the following tasks are performed on the DICOM file.

- **Removing Patient personal Information from header:** The tags that indicate the patient identity which mostly include the information such as name, age, gender, DOB, hospital ID, religion, caste, creed, occupation, referring physician, institution name, study date, and DICOM Unique Identifiers (UIDs). The above said demographic information of the patient which is personal information is encoded within an image header. Anyone who has access to the DICOM file can extract information from the header even though data is not displayed on the screen.

- **Removing patient information during upload:** Creation of such files and accessing such electronic files which can be used for training often involve transmission digital data in the form of DICOM image over the Internet.

- **Converting to other file formats:**

Even for researcher's data privacy is beneficial as images are used when giving lectures, documentation purposes, paper presentations or even when research papers are published. This can be achieved by converting DICOM image to other formats such as JPEG or TIFF. The drawback of this method is header information is lost and patient identity cannot be obtained from the resultant image.

- **Anonymization:** The complete information belonging to the patient is removed from the DICOM header. This is achieved by using software's such as DICOM Works, or FP Image.[8]. All tags of the groups “0008” is the study information and “0010” is for patient information with respect to DICOM header could be eliminated and replaced during anonymization.

IV. DRAWBACKS OF SOME OF THE METHODS

- One main disadvantage of these file formats, as compared to DICOM image, is they have a user-determined window level and window width that is previously agreed at the time when image is created.[9] Because of this contrast between structures that is present within the image cannot be attuned and also the post processing cannot be implemented.

The Tiff format have very good quality of image but requires more space for storing these image files. Conversion of tiff image format to low jpg format is possible but regaining original image is impossible.

I. METHODOLOGY PROPOSED

(MRI) is a technique used in field of radiology of medicine to get pictures of the anatomy and the physiological processes of the body. If the MRI data is tampered by anyone for any reason then the patient whose data is tampered will be at risk of over or less dosage of medicine if we are not able to recognise the tampering of data. To know that data is valid and no manipulation is happened with the data file obtained by MRI scan is authenticated using digital signatures.

The MRI image shown in figure 1 is authenticated using the Elliptical curve digital signature[10]. ECDSA has 3 phases where first phase is the generation of public and private keys. This algorithm uses p192 curve parameters provided by NIST to generate keys along with current time as seed.

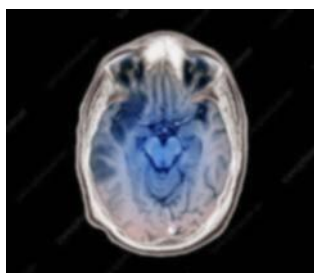


Fig 1: MRI Image of BRAIN

For implementation purpose here MIRACL crypto- library is used as it is in C language it can be easily ported to any platform.

The public key value which will be sent along with the original image and its signature for the above MRI brain image is shown in figure 2.

```

csestaff@pesu-G41MT-S2P:~/miracl$ ./ecsgen
Enter 9 digit random number seed = 764873264872
public key = 0 4267998241863427259524322983623348696746734598690349986127
csestaff@pesu-G41MT-S2P:~/miracl$ cat private.ecs
3305551966067723538228118357636382781514692838910233353370
csestaff@pesu-G41MT-S2P:~/miracl$
    
```

Fig 2: public and private key using seed as 764873264872

The private key which will be used for generating the signatures of the image and which is kept secret is shown in figure 2.

Once the keys are generated then the private key value along with hash value of the file (SHA 256 algorithm is used to find the hash value of the image file) are used to find the signature of image file that will be written to a output file

which will have same name as that of image file appended by .ecs extension. The signatures generated for image in figure 1 is shown in figure 3.

```

csestaff@pesu-G41MT-S2P:~/miracl$ ./ecsign
Enter 9 digit random number seed = 653275473622
file to be signed = MRI.jpeg
csestaff@pesu-G41MT-S2P:~/miracl$ cat MRI.ecs
1251561860110683510443080375983171541839281582923694008237
337751390293111843907952346389415241065218398872326406813
csestaff@pesu-G41MT-S2P:~/miracl$
    
```

Fig 3: Signatures of Image file stored in Image.ecs file

The verification phase uses the public key of the first phase and finds the hash value of the image received and compares it with the signature received. If both match then the image is not tampered and message “signature verified” is displayed. If signatures does not match then some manipulation is there in the image there by the image can be discarded and proper action can be taken against the one who is responsible for tampering of data. The figure 4 shows image verified value first and then after blurring the image using convert command from imagemagic package it shows “signature not verified” thereby showing the data is tampered.

```

csestaff@pesu-G41MT-S2P:~/miracl$ ./ecsver
signed file = MRI.jpeg
signature is verified
csestaff@pesu-G41MT-S2P:~/miracl$ cp MRI.jpeg MRI_before.jpeg
csestaff@pesu-G41MT-S2P:~/miracl$ convert MRI.jpeg -blur 5 MRI.jpeg
csestaff@pesu-G41MT-S2P:~/miracl$ cp MRI.jpeg MRI_after.jpeg
csestaff@pesu-G41MT-S2P:~/miracl$ ./ecsver
signed file = MRI.jpeg
signature is NOT verified
csestaff@pesu-G41MT-S2P:~/miracl$
    
```

Figure 4: Image verification using ECDSA

The figure 4 shows image verified value first and then after blurring the image using convert command from image magic package it shows signature = not verified” thereby showing the data is tampered.

II. LIMITATION

Only MRI brain images have been used in the study. It can be extended to include other image types.

III. CONCLUSION

Although there are many ways in which tampering can be avoided, the files have to be modified, changed to other formats and still it is not fool proof. Each has its own drawback. This paper invokes usage of the ECDSA algorithm for providing authentication of MRI images. The file size, file type, file format is not a limitation and can be extended to include other file types.

REFERENCES

1. ; Available from: 1.<https://www.hhs.gov/hipaa/for-professionals/security/laws-regulations>.
2. [cited 2019; Available from: https://en.wikipedia.org/wiki/General_Data_Protection_Regulation.
3. [cited 1994; Available from: <https://www.ncbi.nlm.nih.gov/books/NBK236546>.
4. Commons, C.; Available from: <https://cis-india.org/internet-governance/blog/privacy-in-healthcare-policy-guide>.
5. License, C.C.A.-S.; Available from: https://en.wikipedia.org/wiki/Medical_record.
6. 2019 Available from: <https://www.dicomstandard.org>.
7. Kahn, C.E., Jr., et al., DICOM and Radiology: Past, Present, and Future. Journal of the American College of Radiology, 2007. 4(9): p. 652-657.
8. Indrajit, I. and B. Verma, Digital imaging in radiology practice: An introduction to few fundamental concepts. Indian Journal of Radiology and Imaging, 2007. 17(4): p.230-236.
9. Unported, C.C.A.-N.-S.A.; Available from: <https://www.ncbi.nlm.nih.gov/pmc/articles/PMC3354356/>.
10. 10. P, S.R.S.R.B., Security System for Visitor Validation at Entrance using Raspberry Pi and Elliptical Curve Digital Signature. IIRTE, 2019. 8(4): p. 3777-3781

Efficient Medical Image Compression Based On Integer Wavelet Transform

R.Krishnaswamy

Assistant Professor,
Department of Electronics and
Communication Engineering
University college of engineering,
Ariyalur, Tamilnadu, India-621704

Dr. S. NirmalaDev iProfessor,

Department of Electronics and Communication Engineering,
Anna University,
Chennai, Tamilnadu, India-600 025

Abstract— Every day the amount of medical image generated grows rapidly so there is a need for efficient image compression for storing and managing the medical images. In this work, a suitable image codec is proposed for medical images. During the past few years, frequency domain analyzes such as Discrete Cosine Transform and Discrete Wavelet Transform (DWT) have been widely used in the field of image compression due to their well localized property of its coefficients in both space and frequency domain. This research work also deals with image compression based on frequency domain transformation. As the medical images are vital for diagnosis, they require lossless compression to store them. However, the coefficients of DWT are real numbers; lossless compression cannot be achieved. The Lifting Wavelet Transform (LWT) is used in proposed system to overcome limitation of DWT.

Keywords— ODCHS Algorithm, Lossless Compression, Signal Processing, Wavelet Transform

I. Introduction

The use of digital images in modern medical diagnosis has increased the need for large storage memory space images are represented in the form of matrix denotes the light intensity at the point .The number of pixel used to represent a image is based on resolution and quantization of gray level. a image has dimension 128*128 picture element each requiring 8 binary bits for gray level quantization To transmit or store such a image which contains five lakh bits of information requires enormous memory capacity. The modern diagnostic equipment produces high quality images that require good compression algorithm for storage and transfer The main aim of the image compression algorithm is reducing no of bits and reconstructed image is same as original image

II. LITERATURE SURVEY

An inventive scheme of discrete-color images for lossless compression is explained in Alzahir 2014 [1]. It consists of two important mechanisms. One is a fixed-size codebook incorporating the blocks in 8x8 bit of two-tone information alongside their related Huffman codes and their comparative probabilities of an event. The probabilities were acquired from an especially the big data set of two color images and are utilized for arithmetic coding. The next mechanism is the reductions coding of row-column, which can encode those blocks that are not in the codebook. The distinctive characteristics of the signal, for example, boundaries of sharp

object and gradually differing inside surfaces in Piecewise smooth (PWS) images.

Utilizing current advances in graph signal processing, a technique to reduce the PWS images using reasonable Graph Fourier Transforms (GFTs) to reduce the whole signal representation charge of every block of pixel is developed in WeiHu 2015 [2]. It allows both the sparsity of the transform coefficients of signal and the minimization of transform depiction.

Aranda et al. [5] have been developed the Logarithmical Hopping Encoding (LHE) scheme for an efficient image compression technique. It is a lossy compression scheme suitable for static images depends on the quantization algorithm. LHE has the capacity to achieve a low bit error rate and high PSNR. It also improved the quality of the image with reference and non-reference scheme. LHE can enhance the speed of compression with low perceptual relevance by downsampling the blocks. Image quality is improved in terms of improving the PSNR, FSIM, and pixel rate. A slight modification in the LHE algorithm is suitable for lossless image compression technique. This approach is applicable for video and audio compression.

Laplacian transparent composite model (LPTCM) is a method for DCT based image compression, it has been developed by Sun, C and yang, E [6]. An efficient non-predictive compression system with redesign the hard decision quantization, soft decision quantization and entropy coding scheme was proposed in the DCT based image compression technique. The main aim of the design is to reduce the distortion occurred in the images. The proposed scheme provides the multi-resolution capability, higher coding efficiency and low complexity. This method is more suitable for real time image processing applications.

Sierra, S et al. [7] has been developed the high dynamic range CMOS image sensor for image pixel compression. Histogram is the technique, which contain time information for estimation of the probability of illuminations impinging pixels. Tone mapping is the technique used to compress the High Dynamic range (HDR) scenes into Low dynamic range (LDR) output. Visual data size can be reduced by different orders of magnitude without any use of objectionable distortions. This kind of data size reduction is occurred in HDR tone mapping scheme. The proposed scheme is able to execute the fly in pixel adaptive tone mapping in the image, resulting it provides good quality images.

Sun, Y et al. [8] described the image encryption and compression method using fractal dictionary and Julia set.

The proposed scheme reduces the time consumption and provides quality image reconstruction with effective PSNR. For decompression, the restored image can be expert in the flash. Julia set keys are the method to improve the process of key conversion.

Zhang 2015 [9] presented the novel method for the semantic image compression based on the data hiding. In the given input original image, the various parts of the pixels are collected to create the compact image by the compressor. By using the data hiding techniques, the compressed image is generated by combining the errors into the compressed image. By using the data hiding methods, the compressed image are generated by using the small number of the pixels and also the visibility of the original image is highly efficient without using the decompression tool. By using the decompression tool the users are able to perform the image reconstruction with the given input original image. The proposed technology is able to perform the reversible and non-reversible data hiding techniques.

Rongchang Zhao and Yide Ma 2013 [10] presented the spiking cortical model based image compression technique. The quality reconstructed image was evaluated by Irregular segmentation region coding based on the spiking cortical model (ISRCS). ISRCS scheme performed based on the region and there are two main issues are focused in the performance. Image segmentation is the first issue in the proposed scheme to segment the image into the subdivisions and the coding method is used to concession with the image reconstruction and compression ratio. Segmentation based on the pulse image is mainly used for the efficient image compression. Segmented image is used to obtain some clear texture of the image for the image coding, and also, the method control the various numbers of the regions for the efficient compression ratio.

Cuiping Shi, Junping Zhang and Ye Zhang 2015 [11] described the vision based adaptive scanning for the remote sensing images. Mean square error is one of the important factors for the implementation of the various compression methodologies. In the field of the vision related applications, the high PSNR does not generate better visual quality. The conventional compression methodologies are involving on the natural images by the human visual system (HVS). A novel HVS based adaptive scanning based compression method is used for the efficient image compression ratio.

Jianquan Yang, Guopu Zhu 2015 [12] explained the local difference of the image intensity in the field of the JPEG compression. Local difference of the image intensity used to measure the image smoothness and also used in the field of the filtering length adjustment and image compression analysis. In the adaptive image compression and analysis, the image statistics is mainly used to estimate the local given input image characteristics. Local variance of the image intensity is one of the mostly used image statistics methods for efficient image compression analysis. Due to the efficient image smoothness, the local variance of the image intensity applied to the various image compression algorithms. A theoretical expression is derived to estimate the expectation of the local variance has quantified the expectation of the local variance of the JPEG compression and the variation of the local variance.

III. LOSSLESS COMPRESSION

In the field of the image compression, the lossless compression is consider as the major challenge. Lossless compression is applied in the medical applications. In medical applications , the image data is vital and cannot be discarded. It is where lossless compression comes as a major tool. The compression ratios of lossless compression algorithms are usually is of the order of 2:1 for lossy algorithms is around the order of 300:1. The image can be compressed to a maximum extent only if perpetual redundancy is discarded.

IV INTEGER WAVELET TRANSFORM

Integer wavelet transform(IWT) is a category of DWT. is used to find the frequency content as well as the time of occurrence of the frequency content in the signal. The wavelet transform in its discrete notation called DWT can be applied to discrete images. After taking DWT the band with least number of significant wavelet coefficients can be neglected. Such a band practically contains no information. In any image there will be several bands with least number of significant Discrete Wavelet Coefficients. This forms the basic principle of image compression. The drawback with d is the process of computation is intensive in nature, therefore it requires hardware acceleration. The lifting scheme method is used to implement the DWT efficiently. Finally, the IWT is applied as a lifting scheme. The forward and reverse IWT units are illustrated in Figure 1 and Figure 2 respectively.

In Figure 1, P is the prediction unit and U is the updation unit. The prediction unit transforms the image into a difference image using the prediction algorithm. Then the image is transformed using IWT.

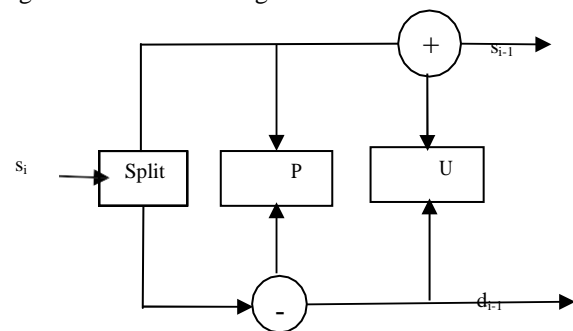


Fig. 1 Forward Integer Wavelet Transform Unit

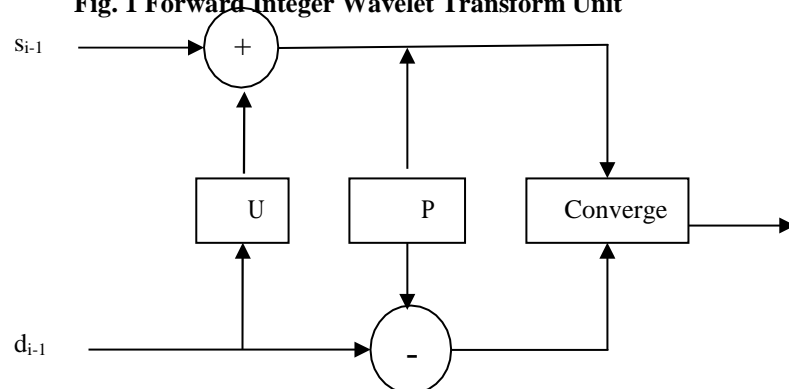


Fig. 2 Inverse Integer Wavelet Transform Unit

The IWT consists of three steps namely Split step, Compression step and Update step.

A. Split Step

The split step as the name implies splits the input data into even and odd Samples.

$$Split(x_i) = (even_{i-1}; odd_{i-1})$$

B. Compression Step

The subset of the difference can be obtained using the sample set of the image, because of high correlation between the odd and the even samples. Once prediction is made the current sample can be replaced by the previous sample of the subset.

C. Update Step

The update step is done to improve the subset after the prediction step is Complete. The final output of all the three steps is low pass co-efficients and highpass co-efficient. The transform can be changed by changing the prediction algorithm used in the transform.

VODCHS ALGORITHM

ODCHS stands for Orthogonal Diagonal Cross Hair Search. The algorithm searches for valid pixel in a range of Maximum and Minimum values. The maximum and minimum values are in powers of two. The maximum and minimum values are used as threshold for the entire encoding process. The algorithm divides the image into groups of 4x4, 8x8, 16x16, 32x32 pixels and so on from the top left corner. For each block it is checked, if at least any one of the pixel in the block exceeds the threshold level and is less than the maximum value. If it exceeds then the block is further divided into four sub blocks of equal size until the size becomes 4x4. For each 4x4 the procedure is repeated recursively. Each 4x4 sub pixels of the image are divided into two cross hairs and one octagon. First the entire 4x4 set is encoded. If at least one pixel exceeds threshold value a one is put in the encoded stream. Then the first cross hair in the 4x4 pixel subset is checked. Each pixel that exceeds the value of threshold encoded with a value one. The pixels that are less value of threshold is encoded with a value zero. The same procedure is repeated for the second crosshair. Then the octagon is encoded in a similar manner. Then the algorithm entered to another 4x4 subset. If on checking the entire 4x4 subset of pixels, no pixel exceeds the value the entire set is encoded with a value zero and the crosshairs and octagons are not checked.

The combination of compression (coding) and decompression (decoding) is called as CODEC architecture. The motive of Compression is reducing the number of bits. The size of the resulting bits from the compression system is always less than the input data entered into the compression system. The input data is represented as D, as well as the compressed data is represented as C(D). After the compression, the original bits can be retrieved from decompression system; the retrieved bits are represented as

Reconstructed data is purely depends on the algorithm used in the compression system. Lossy and lossless are the types of algorithm mostly used in the image compression

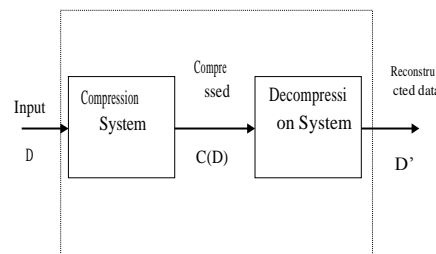


FIG 3 CODEC

technique. Lossy compression algorithm does not provide the exact replica of original data D. Lossless compression algorithm provide the exact reconstruction of original data. Data compression needs less space for data storage requirement. It effectively reduces the backup cost and data recovery in the system.

VI PERFORMANCE PARAMETERS

The quality of image is measured in terms of parameter such as Mean Square Error (MSE) Peak Signal to Noise Ratio (PSNR) and Bits Per Pixel (BPP),

1) Mean Square Error (MSE) is one of the parameter to evaluate the quality of compressed image.

$$MSE = \frac{1}{MN} \sum_{x=1}^M \sum_{y=1}^N [F(x,y) - F'(x,y)]^2$$

Where f(x, y) - original input image, f'(x, y)- compressed image, and M, N are no of rows and column of imagematrix

2) Peak Signal to Noise Ratio (PSNR) is ratio dimension of image to square mean square error . When MSE is zero the PSNR approaches infinity

$$PSNR = 10 \log_{10} \left[\frac{MXN}{MSE^2} \right]$$

Where, M is no of row ,N is number of coloum.

3) Bits per pixel ratio (BPP) gives the number of bits required to represent single pixel of image

$$BPP = \frac{Size\ of\ compressed\ file}{Total\ no\ of\ pxel\ in\ the\ image}$$

VIII EXPERIMENTAL RESULTS AND DISCUSSIONS

The performance of the proposed ODCHS compression algorithm is evaluated by comparing it with Embedded Zerotree Wavelet (EZW), Set partitioning in hierarchical trees(SPIHT), Set Partition Embedded block coder

(SPECK), ODCHS-IWT-HAAR, ODCHS-IWT-B4, ODCHS-DWT-HAAR, ODCHS-DWT-DB4, compression algorithms. In this work, the test images with size 256×256 is used. The Table 1 illustrates a comparison of the following compression algorithms: EZW, SPIHT, SPECK, ODCHS-IWT-HAAR, ODCHS-IWT-DB4, ODCHS-DWT-HAAR, ODCHS-DWT-DB4 in various bits per pixel.

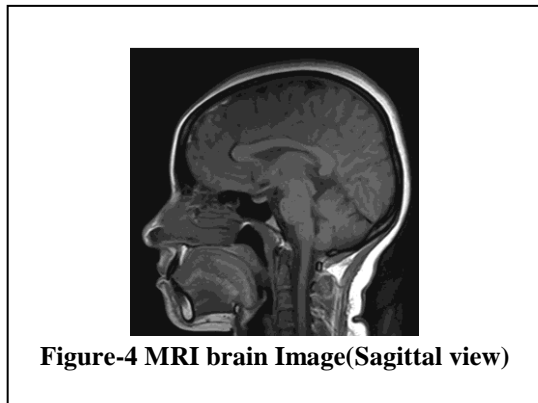


TABLE-1 PSNR VS BPP FOR VARIOUS ALGORITHMS

Bits per pixel	PSNR values (MRI brain Image(Sagittal view))									
	EZW	SPIHT	SPECK	ODCHS-DWT-DB4	ODCHS-DWT-Haar	ODCHS-IWT-DB4	ODCHS-IWT-Haar	DTMBWT	Bendlet	
MRI brain Image (Sagittal view)										
0.0625	27.82	27.8	27.82	28.55	28.41	27.78	31.04	27.94	30.08	
0.125	27.81	27.81	27.82	29.1	30.98	29.55	31.05	28.02	30.83	
0.25	28.53	28.52	28.53	30.72	31.25	30.75	32.35	28.02	30.87	
0.5	28.49	28.53	28.5	32.29	32.92	32.85	32.47	28.1	30.91	
1	28.72	33.09	32.82	33.79	34.37	33.55	35.05	28.17	30.95	
2	32.87	42.27	39.8	40.12	40.22	38.97	40.5	28.21	30.94	
3	39.07	42	43.88	45.26	45.96	43.49	49.36	28.21	30.97	

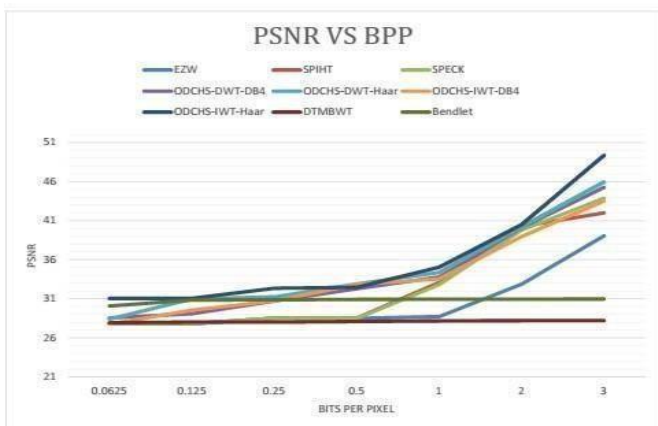


Figure 5 PSNR VS BITS PER PIXEL FOR VARIOUS ALGORITHM

The figure 6 and 7 shows the original image and histogram of the image at 1 bit per pixel the. from Figure 8 that the histogram plots of decompressed images at lossless bit rate are exactly match with the histogram of original image. the lossless bits per pixel for EZW, SPECK, ODCHS-IWT-DB4, and ODCHS-IWT- Haar are 5.9, 5.2, 6.2, and 5 respectively.

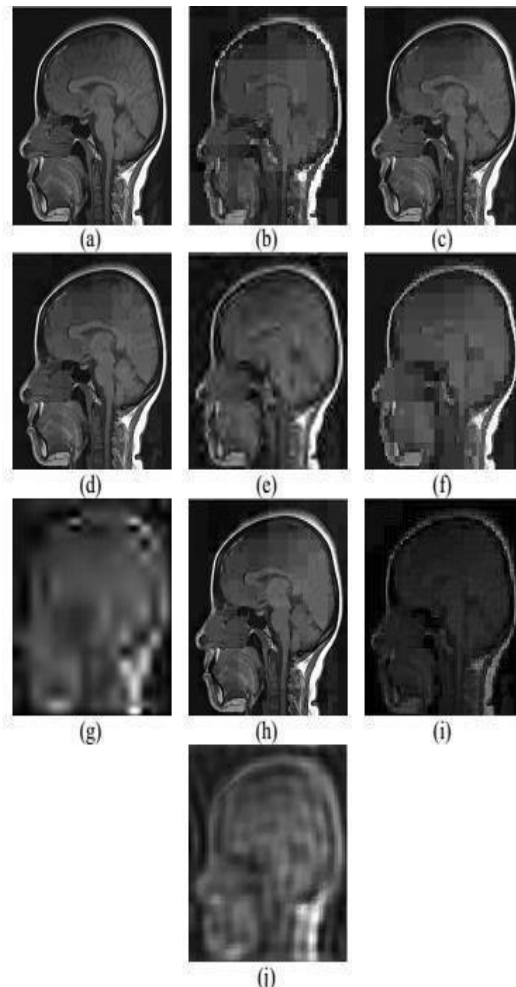


Figure 6 Compression at 1 bits per pixel (a) Input Image (b) EZW (c) SPIHT (d) SPECK (e) ODCHS-DWT-DB4 (f) ODCHS-DWT-Haar (g) ODCHS-IWT-db4 (h) ODCHS-IWT-Haar (i) DTMBWT (j) Bendlet

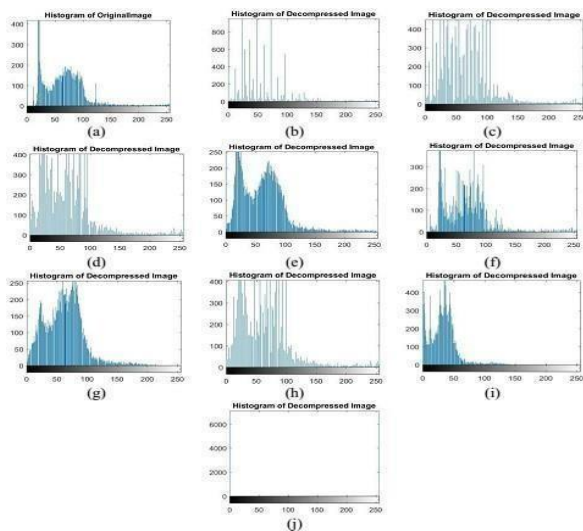


Figure 7 Image histograms at 1 bits per pixel (a) Input Image (b) EZW (c) SPIHT (d) SPECK (e) ODCHS-DWT-DB4 (f) ODCHS-DWT-Haar (g) ODCHS-IWT-db4 (h) ODCHS-IWT-Haar (i) DTMBWT (j) Bendlet

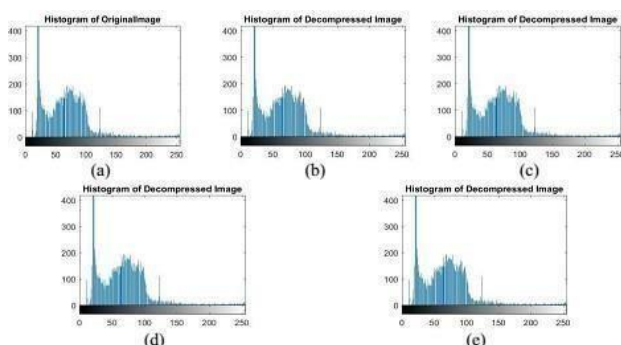


Figure 8 Image histograms at lossless (a) Input Image (b) EZW (c) SPECK (d) ODCHS-IWT-DB4 (e) ODCHS-IWT-Haar

The ODCHS algorithm is implemented with various wavelets and its performance is better than the EZW, SPIHT, SPECK in terms of PSNR values. The ODCHS algorithm with Haar and Daubechies 4 wavelet (db4) has higher PSNR in higher bit per pixel. From Table 1 it is inferred the ODCHS IWT Haar algorithm performs well in all bit per pixel due to its search pattern.

The dimension of decomposed images is more than the dimension of the input image for DTMBWT and Bendlet transform where as in DWT and IWT they are same size. Dual tree M-band wavelet transform (DTMBWT) and Bendlet provide more high frequency details than DWT and IWT. Hence, the decoding without high frequency details provides low PSNR. As the coefficients are integer in IWT, the PSNR is high for IWT when compared to DWT where the coefficients are floating numbers in DWT.

VII CONCLUSION

The archiving and transmission of medical images is the main application of image compression. In this paper, an efficient transform based image compression based on SPECK is presented. The proposed algorithm has the feature of progressive transmission and an embedded bitstream. The

result conveys that there is a notable enhancement in the performance of the proposed algorithm than algorithms such as EZW, SPIHT, SPECK.

REFERENCES

- [1] Alzahir, Saif, and Arber Borici. "An innovative lossless compression method for discrete-color images." *IEEE Transactions on Image Processing* 24.1 (2015): 44-56.
- [2] Hu, Wei, et al. "Multiresolution graph fourier transform for compression of piecewise smooth images." *IEEE Transactions on Image Processing* 24.1 (2015): 419-433.
- [3] Lee, Sung Kyu, Sung Gyun Kim, and Young Hwan Kim. "Multimode Image Compression Algorithm Employing Multiple-Choice Knapsack Problem-Based Encoding Mode Selection." *Journal of Display Technology* 12.6 (2016): 549-556.
- [4] Li, Yuanman, and Jiantao Zhou. "Anti-Forensics of Lossy Predictive Image Compression." *IEEE Signal Processing Letters* 22.12 (2015): 2219-2223.
- [5] Aranda, Jose Javier García, et al. "Logarithmical hopping encoding: a low computational complexity algorithm for image compression." *IET Image Processing* 9.8 (2015): 643-651.
- [6] Sun, Chang, and En-Hui Yang. "An efficient DCT-based image compression system based on Laplacian transparent composite model." *IEEE Transactions on Image Processing* 24.3 (2015): 886-900.
- [7] Vargas-Sierra, Sonia, Gustavo Liñán-Cembrano, and Ángel Rodríguez-Vázquez. "A 151 dB high dynamic range CMOS image sensor chip architecture with tone mapping compression embedded in-pixel." *IEEE Sensors Journal* 15.1 (2015): 180-195.
- [8] Sun, Yuanyuan, et al. "Image compression and encryption scheme using fractal dictionary and Julia set." *IET Image Processing* 9.3 (2015): 173-183.
- [9] Zhang, Xinpeng, and Weiming Zhang. "Semantic image compression based on data hiding." *IET Image Processing* 9.1 (2015): 54-61.
- [10] Zhao, Rongchang, and Yide Ma. "Novel region-based image compression method based on spiking cortical model." *Journal of Systems Engineering and Electronics* 26.1 (2015): 161-171.
- [11] Shi, Cuiping, Junping Zhang, and Ye Zhang. "A Novel Vision-Based Adaptive Scanning for the Compression of Remote Sensing Images." *IEEE Transactions on Geoscience and Remote Sensing* 54.3 (2016): 1336-1348.
- [12] Yang, Jianquan, Guopu Zhu, and Yun-Qing Shi. "Analyzing the Effect of JPEG Compression on Local Variance of Image Intensity." *IEEE Transactions on Image Processing* 25.6 (2016): 2647-2656.
- [13] Lessig C, Petersen P, Schäfer, M., (2017). Bendlets. A second-order shearlet transform with bent elements. *Applied and Computational Harmonic Analysis*, vol. 46, no. 2, pp. 384-399

Blood Vessel Segmentation on Retinal Fundus Image- A Review

P.Hosanna Princye,
Archana MK
SEA College of Engineering and
Technology, Bangalore,
hprincye@gmail.com,
archana.mk9@gmail.com

M.Lavanya,
Saveetha School of Engineering,
Saveetha Institute of Medical and
Technical Sciences, Saveetha
University, Chennai,

Sivasubramanian Karpagam College
of Engineering,
Coimbatore
laviraju88@gmail.com,
siva.ace@gmail.com

Abstract

—Automatic identification of blood vessels in CT images of retina has always been a big challenge since the contrast of images diminishes with respect to the increase in the pixel distance from the center of the image in retinal. The image segmentation blood vessels in retina helps in diagnosing the diseases that are associated with the changes in the retina. Most current techniques focus on developing Preprocessing and Image analysis. This Paper gives the survey on Retinal Image

Keywords— Retinal, Preprocessing and Segmentation

I. INTRODUCTION

In the field of ophthalmology the eye disease identification is very critical. The Conventional procedures available for retinal disease identification depend on perception that is exceedingly introverted and inclined to blunder. Henceforth, robotized methods are necessary along with traditional procedures which are fundamentally high in the medical field. The computerized disease identification proof procedures and its exactness is ought to be extreme. Other than being exact, the procedures likewise ought to have a quicker convergence rate that suits them to be reasonable for on-going applications. In view of these two execution measures, a few computerized systems are produced and actualized effectively for retinal disease identification.

II. RETINAL IMAGE PREPROCESSING TECHNIQUES

A. Text Font of Entire Document

Salem and Nandi [1] introduced a novel technique for the purpose of shading the retinal images with commitment towards the red channel which is versatile. On the premise of a circumstance that is created in this method, it utilizes the processing technique of both red and green channels in spite of only the green channel as it is normally done. The histogram coordinating is brought into utilization by changing the green channels histogram by enforcing the red channel histogram for acquiring another picture that is handled with the benefits of the two channels. This system can be used for redressing conflicting brightening in shading fundus images amid the programmed investigation of the fundus images. The results conclude that by using Histogram Matched (HM) picture gives preferable execution over influencing utilization of histogram of green channel to identify retinal veins to using two-dimensional matched filter.

Youssif et al. [2] presented three noteworthy pre-processing strategies like Mask Generation, Equalization of Illumination and impact of Color Normalization on distinguishing fundus Anatomy. Moreover, the extensive normalization technique is displayed which records the fulfilling output on the application for color normalization.

Salvatelli et al. [3] made the examination and tried numerous amendment approaches. Inconsistent illumination is balanced with the help of the morphology and homomorphism filtering; non-uniform differentiation is secured by utilizing morphology and nearby improvement. This work inspected the preparing stages, making utilization of Fuzzy C-Means segmentation technique and Local Hurst coefficient method for the programmed division of its strange veins. The expected outcomes of this method over a standard arrangement of Diabetic Retinopathy (DR) pictures are more efficient.

Salah-Eldin et al. [4] proposed another illumination normalization philosophy which depends on the improvement of the picture which is acquired from the Histogram Matching (HM) that uses gamma correction and compression function of Retinal filter's known as Gamma Histogram Matching Compression (GAMMA-HM-COMP) approach.

Rezatofighi et al. [5] identified a Retinal image which is obtained with the help of a fundus camera regularly comprises of low complexity, grey value. The work proposed is extraction of feature that use morphological method namely Local Binary Pattern (LBP) and spatial picture handling for division of the retinal veins in optic fundus pictures. The outcomes are numerically assessed for different calculations.

Miljkovic [6] clarified that the picture pre-processing was the term utilized for the procedures performed on the pictures with a reflection at the most reduced level and whose objective is enhancing the picture information to smother the superfluous contortions or upgrade few of the picture highlights noteworthy to proceed further. It doesn't provide an expansion in picture data content. These systems utilize considerable repetition in pictures. Pixels in the area identified with one object in real pictures have the same or comparative brilliance esteem and if there should arise an occurrence of a distorted pixel which is being browsed from the picture, it can be recovered as a normal estimation of pixels in theregion.

Akram et al. [7] presented a filter for upgrading and sharpening namely Gabor wavelet filter correspondingly. This method proceeds the vessel extraction from the sharpened

fundus images, utilizing an edge location algorithm after the morphological operation for their clarification.

Patil and Chaudhari [8] considered the development of a automated fundus picture preparing and examination framework for encouraging the analysis of the ophthalmologists. Color fundus photos are useful in the recognition of the hemorrhages, cotton wool spots, microaneurysms and hard exudates. Image Processing for digital images philosophy is worried about the computerized information change. This can recover the clearness of picture, sharpness and highlight subtle elements of enthusiasm from the extricated data and consequent investigation with the help of computer. This work presents an instrument for the opportune identification of Diabetic Retinopathy, with Image Enhancement system.

Trucco et al. [9] for the purpose of space and consistency examined the approval of Automatic Retinal Image Analysis (ARIA) algorithms, it focus on the approval of algorithms for preparing color retinal images. The investigation outlines the setting of ARIA validation, compressing the fundamental picture examination and approval procedures.

Raj and Devi [10] presented a correlation of the situations in which the pictures are presented as two sorts of noises like Salt and Pepper noise and Gaussian noises. Denoising should be done with the help of two distinct filters, in particular, Adaptive Wavelet and Modified Decision Based Unsymmetrical Trimmed Median Filter (MDBUTMF). At that point, with the help of Mathematical Morphology, the location of the vein and later the fovea region is finished.

III. RETINAL IMAGE ANALYSIS TECHNIQUES

Can et al. [16] clarified a straight, feature-based, and non-iterative system for joint computation of ceaseless changes of entire pictures onto the mosaic and termed them as the "grapple picture." Restraints of estimation are acquired from the available pairwise enlistment, incorporating both direct and indirect registration between pairs of non- anchor pictures. An added substance, graph-based method builds up the arrangement of enlisted picture sets which is used in the arrangement. The estimation system grants pictures that don't have any cover with the anchor frame for the mosaicing to be fruitful, an esteemed capacity for pictures mosaicing of the retinal periphery.

Sukkaewa et al. [17] presented a correlation among the edge detection approaches for the automated classification of veins in retinal images of child images. This system precision is evaluated by making a correlation among the outcomes with ground-truth pictures drawn by hand.

Candes et al. [18] examined a work of Curvelet Transform which is alluded to as multi-scale change that can be utilized for indicating to the edges along bends with much productivity. This clarifies the advancement of division innovation in the retinal vein picture processing got by utilizing non-mydratic shading photography. Exceptionally precise acknowledgment of veins for analyzing the varieties in the vessel system can be used for identifying the adjustments

Patil and Wankhede [11] presented about various preprocessing steps that incorporate central light reflex removal, foundation homogenization and vessel improvement to influence retinal picture to noise-free for post- processing. Mean and Gaussian filtering were utilized alongside Top-Hat transformation for extraction of noise.

Fiorini et al. [12] proposed a technique based on artificial and unique fundus images, qualities like a given informational collection, aside from the estimations of every morphological parameter. The work primarily concentrates on producing the non-vascular areas and it is adjusted by an examination done parallel with the production of structure and surface of the vessel network.

SagarAdatrao et al [13] presented the different preprocessing methods and comparison is made based on their ability of noise removal for the segmentation of the images.

Dilip Singh sisodia [14] presented the pre-processing steps of the acquired retinal fundus Images by Extraction process using green Channel histogram equalization, enhancement and resizing of image. For the purpose of quantative analysis fourteen features were extracted from the pre-processed images.

Sheeta Maruti Chougule [15] Presented new preprocessing approach for images in diabetic retinopathy screening. In this method pre-processing steps are illumination, equalisation, Denoising, Adaptive contrast equalisation and color normalisation. This method improved the ability to distinguish between lesions and nonlesions.

in the vein width identified with the way physiology of diabetes. The technique has the demerits of missing a couple of thin vessels because of use of a basic thresholding strategy. This work adds to the usage of a system which will likewise be appropriate for veins with little length.

Rezatofighi et al. [19] exhibited another multi-scale strategy for contrast enhancement in retinal images by using Contourlet Transforms. Here highlight extraction approach is used that has ses Local Binary Pattern (LBP), for dividing the retinal veins in optic fundus images morphological technique and spatial image processing. Moreover, for classification of images execution of Adaptive Neuro-Fuzzy Inference System (ANFIS) and Multilayer Perceptron (MLP) is examined.

Esmaili et al. [20] presented another curvelet based algorithm for the partition of red lesions in the staying color of the retinal picture. For avoiding the wrong assumption as red lesion, another illumination equalization algorithm is acquainted and connected with green plane of retinal picture.

Zahedi et al. [21] examined a procedure to repay the rotation effects which may happen amid scanning process. At that point, a Region of Interest (ROI) in circular form is chosen. Next a rotation invariant template is made from every ROI by a polar change. In the following stage, vessels from every format were upgraded. Radon transform is utilized for feature definition in this strategy.

Zahedi and Sadjedi [22] suggested Fourier change and special partitioning in this strategy optic disc is confined

utilizing template coordinating method and utilized for turning the retinal picture to reference position.

Miri and Mahloojifar [23] exhibited another way to deal with remove the veins with the help of the thresholding strategy and to recognize Optic Disc utilizing using circular Hough transform method. At last, identification of the exudates is finished with the help of versatile thresholding strategy in fundus picture.

Silvia and Poovizhi [24] proposed the Ripplet I transform which proficiently indicates that the edges and surfaces can likewise be used for catching the 2D singularities along a group of bends in pictures. The image segmentation is done with the help of morphological operators.

Chandani Nayak et al [25] proposed Curvelet transform for vessels enhancement. The two main features of curvelet transform are directionality and anisotropy scaling law. These features extracted represent the curves with its edges along with it that are more efficient than the traditional wavelet.

Nas gharaibeh Obadiah [26] proposed an effective method in image processing for identification of diabetic retinopathy disease using different techniques in image processing which gives high performance

Detecting Blood Vessels in fundus images is a successive procedure with great quality division. Before the segmentation procedure, picture preprocessing is important to expel the impact of ill-advised light and noise artifacts other than expanding the difference among the background of the blood vessels in retinal images. This research has determined that the nature of segmentation of image relies on the nature of fundus image. There are numerous strategies utilized for the identification and division of veins in the retina. Depending on few parameters like separation or gray level esteem pixels are relegated one cluster it can have as many clusters. In Supervised type of classification methods, this technique is a matter of first importance prepared utilizing the training information that comprise of the data sources and the comparing yields and then this method is connected to real time fundus images for the pixel classification.

IV. RETINAL VESSEL SEGMENTATION TECHNIQUES

Chaudhuri et al. [27] suggested a technique that approximates the profile of the intensity using Gaussian Curve. The profiles of gray level were figured the opposite way to the vessel length. Before division of vessels, picture upgrade is finished using $5 * 5$ mean filter that decreases spurious noise. The algorithm recognizes vessels in spite of the way that the neighborhood differentiate is low however the issue with this algorithm is that other brighter protests for example, injuries, optic disc ,edges etc., are additionally not look like any vessel section.

Soares et al. [28] built up a procedure which utilizes 2-D Morlet wavelet transformation for identification of vessel. 2-D Morlet transform was picked in light of its adaptability towards picking diverse introductions and capacity to choose specific recurrence. Before segmentation of image is done preprocessing of image is performed for reducing false identification of the edges of the images. Detection is carried

out with the help of the Bayesian classifier that is based on Gaussian Mixture Model (GMM). The strategy gave high Area under Curve (AUC). The significant issues were right for noise detection of in images.

Tsai et al. [29] exhibited Retinal Image Vessel Extraction and Registration System (RIVERS) that provides details about cutting edge digital fundus image analysis for retinal clinicians, specialists and work executives an incorporated suite of tools available over the Internet.

Chang et al. [30] proposed an algorithm extremely successful for the retinal veins segmentation. This method uses Retinal Blood Vessel Segmentation using Line and Edge detector (RBVSLE). The improved picture is then used to make an edge outline which is acquired by enforcing the canny edge locator to the upgraded picture. The proposed method is connected to wipe out this issue of misclassifying. Execution assessment of RBVSLE is done on both STructured Analysis of the Retina (STARE) and Digital Retinal Images for Vessel Extraction (DRIVE) databases.

Akram et al. [31] suggested a strategy for vein improvement in light of wavelet transform. Picture improvement is finished utilizing 2-D Gabor Wavelets. These types of wavelets are selected over different wavelets with respect to their introduction particularity selectiveness of feature and frequency adjustment. The improvement in vessel picture is fragmented utilizing Canny Edge Detection algorithm. Morphological dilation operation is filled for filling the holes in the vessel pixels.

Dua et al. [32] presented an techniques based on edge detection strategy based on hierarchical decomposition by using quad tree and limited distinction administrator for post filtration of edges. The work demonstrates that edges can be portrayed by an admirable power slope for medical pictures of normal birthplace, focal and/or penumbral blurred. This inclination additionally can be used for rejection of false cautions. A point by point approval and examination with related tasks away at Diabetic Retinopathy pictures and Computed Tomography (CT) filter pictures demonstrate that the suggested approach is productive and precise.

Jaafar et al. [33] suggested an algorithm for recognizing the grade and the seriousness of hard exudates. The identification procedure works on top-down picture division and its neighborhood thresholding by an algorithm based on hybridization of edge detection and region growing. The consequences of these identified hard exudate process were approved in view of clinician ground truth, with a general sensitivity of 93.2%. The predominant execution of this system recommends that it could be utilized for a PC helped mass screening of retinal diseases.

Marin et al. [34] built up a regulated strategy for the division of veins. The obtained picture is pre-processed first for evacuating vessel central light reflex issue and Gaussian kernel is used for noise smoothing. Vessel enhancement is performed by morphological Top Hat transformation. The component vector comprises of two minute invariants based features. The critical part of it is post preparing plays out for filling the gaps among the vessel pixels evacuating the

dishonestly identified by performing isolation of pixels. The system is straightforward, yet is computationally serious.

Onkaew et al. [35] performed retinal veins segmentation utilizing inclination introduction. In the first place subsidiary administrators in both x and y directions are utilized to for discovering gradient vectors which are normalized. As it has different features like sizes and width are different across a vein, first request subordinate, sobel administrator is utilized at three distinct scales. Results were distinguished with the help of Receiver Operating Curve (ROC), Area under Curve (AUC) and Maximum Average Accuracy (MAA).

Akram et al. [36] proposed a method for segmentation of veins in fundus images for distinguishing proliferative diabetic retinopathy. Vessel upgrade is finished utilizing Gabor Wavelets. Multilayered Thresholding strategy is utilized for the division of veins. In this the major work is by using sliding window system figuring the entropy and thickness and identifying the blood vessels. Execution assessment is carried out using database like DRIVE and STARE. Normal precision of the procedure is extremely equivalent in effectively existing comparable strategies that gives an average accuracy of 0.9469 and 0.9502.

Lazar and Hajdu [37] used directional height statistics for retinal blood vessels segmentation. In this technique a Gaussian like peak is obtained on the intensity profile if a direction is perpendicular to the length of vessel. To recognize vessel and non-vessel a score guide is utilized using standard deviation. Picture enhancement is carried out using Gaussian filter for an image using standard deviation.

Karasulu [38] examined the Sobel and Prewitt edge detectors using discrete differentiation operators. The proposed approach provided investigation to demonstrate an open source and productive usage of automatic blood vessel extraction and correlation of the execution of three distinctive edge detectors.

Ocbagabir et al. [39] built up another algorithm known as Star Networked Pixel Tracking algorithm, this algorithm for division and recognition of veins in fundus images. Blood vessel enhancement is done using the AHE alongside the morphological operations. Removal of noise is done using median filtering technique. Automatic thresholding is connected to the standardized fundus image to remove the veins. Execution assessment is done on the DRIVE database. The precision was observed to be 0.

Mehrotra et al. [40] suggested a new edge Preserving Filter (NEPF) and Gaussian smoothing filter connected for removal of impulse noise and Gaussian noise respectively. Clusters are formed using Kohonen Clustering Network (KCN) then connected to the resultant picture. The technique gives high exactness and sensitivity of 0.9802 and 0.9912 individually. False Positive Fraction (FPF) was observed to be 0.0415.

The estimation of Arterio-to-Venular Ratio (AVR) is a disputing task and requires optic disc identification on the sectioned veins. The detection optic disc is important for deciding the Region of Interest (ROI) where estimations of vessel are completed.

A self-loader strategy utilizing Gabor wavelet and morphological operations was suggested Ortiz et al. [41]. They exhibit the improvement of a model for measuring the vessel measurements to ascertain the AVR by utilizing diverse strategies. The width estimation depends on the picture skeleton and the opposite portion of the vessel. The strategy was tried on clinically obtained database of 30 pictures with 57% exactness.

Li et al. [42] introduced a computerized technique to ascertain AVR, yet the strategy still required couple of client contributions to distinguish supply arteries and veins. The coordinated Gaussian filter is used for recognizing the beginning stages of vessels. To depict the vessel profile an adjustable Gaussian model is used that considers the central light reflection of arterioles. The width calculation of vessel is done by information fitting.

Ruggeri et al. [43] introduced a vessel tracking algorithm on 50 clinically obtained pictures. Pictures are at first improvised to enhance the vessel network then followed by a algorithm based on vessel tracking. The optic disc position is inferred and the area inside which the AVR information is measured from the detected vessel structure, is resolved. Vessels inside are marked as arteries or veins and their caliber is assessed from tracing information. However, a portion of the vessels were missed by the following strategy in this manner gave inadmissible AVR esteems.

Manikis et al. [44] introduced a hessian based vessel division technique alongside thresholding and accomplished a precision of 93.71% and 93.18% for DRIVE and STARE separately. A Graphical User Interface (GUI) additionally underpins various techniques for the automatic measurement of width of the vessel at any chosen point region of interest. What's more, it gives strategies to altering the vessel portrayal keeping in mind the end goal to recoup from conceivable division misclassifications.

Muramatsu et al. [45] displayed a technique for retinal blood vessel segmentation, classification and selection of arteries and veins, optic disc segmentation alongside AVR. In spite of the fact that the normal mistake in the AVRs as for those in light of the manual vessel division comes about 0.11, the average error value in vessel measurement was found to be under 1 pixel.

Narasimhan et al. [46] proposed a technique for which veins are fragmented out at first from the pre-processed fundus images. Gray level and minute based highlights are extricated for characterizing the identified pixels as having a place with the vein class or not.

Khitran et al. [47] displayed another strategy for AVR calculation. They propose a computerized framework for discovery of HR by using arteriovenous (AV) ratio. The technique proposed framework comprises of unique strategy for arranging arteries and veins vessels by using new feature vector and hybrid type of classifier.

Agurto et al. [48] displayed a vessel segmentation technique namely multi-scale linear structure enhancement based on second order local entropy thresholding. The strategy was tried on 74 fundus images with 80% exactness. The AVR

computation was completed on (0.5-1) optic Disc Diameter (DD) which may give wrong outcomes.

Gehad Hassan et al [49] present a method based on segmentation of blood vessel using Mathematical morphology and K-means clustering for the segmentation of the vessels. For blood vessel enhancement and background image suppressing, smoothing of image is performed on the fundus image using mathematical morphology. Later the image that is enhanced is segmented using K-means clustering algorithm. This method had achieved an of 95.10% and 96.25% of accuracy.

V.Sathananthavathi et al [50] proposed dynamic shape features and SVM classifier to detect the disease. The first step from the background image pixel classification in which blood vessel and red lesions are separated. After removing the vasculature, the remaining part is considered as red lesions. Then the detected candidates are used for training using Support Vector Machine (SVM) classifier. The proposed method accuracy is about 80% for STARE database and 90 % for Diatteddb1 database.

V. CONCLUSION

An extensive survey of the present systems utilized for different phases of the retinal picture investigation process. The regularly utilized pre-preparing procedures, image processing techniques

REFERENCES

- [1] Salem, M.N & Nandi, A.K 2007, 'Novel and adaptive contribution of the red channel in pre-processing of colour fundus images', Journal of the Franklin Institute, Elsevier, vol. 344, no. 3, pp.243-256.
- [2] YoussifAliaa, AA, Atef, ZG &Ghoneim, AS 2007, 'A comparative evaluation of preprocessing methods for automatic detection of retinal anatomy', Proceedings of the Fifth International Conference on Informatics and Systems, vol. 2430, pp. 24-30.
- [3] Salvatelli, A, Bizai, G, Barbosa, G, Drozdowicz, B Delrieux, C 2007, 'A comparative analysis of pre-processing techniques in colour retinal images', Journal of Physics: Conference Series, IOP Publishing, vol. 90, no. 1, pp. 1-7.
- [4] Salah-ELDin, A, Nagaty, K &ELArif, T 2008, 'An Enhanced Histogram Matching Approach Using the Retinal Filter's Compression Function for Illumination Normalization in Face Recognition', Image Analysis and Recognition, Springer Berlin Heidelberg, pp.873-883.
- [5] Rezatofighi, SH, Roodaki, A & Noubari, HA 2008, 'An enhanced segmentation of blood vessels in retinal images using contourlet', Engineering in Medicine and Biology Society, EMBS International Conference of the IEEE, A new retinal image processing method for human identification using radon transform, vol. 30, pp.3530-3533.
- [6] Miljković, O 2009, 'Image pre-processing tool', Kragujevac Journal of Mathematics, vol. 32, no. 32, pp.97-107.
- [7] Akram, MU, Atzaz, A, Javed, MY Niazi, UAK 2009, 'Preprocessing and blood vessel segmentation of retinal images', IASTED Conference on Visualization, Imaging and Image Processing (VIIP), vol. 6, no. 1, pp. 13-18
- [8] Patil, JD &Chaudhari AL 2012, 'Tool for the Detection of Diabetic Retinopathy using Image Enhancement Method in DIP', International Journal of Applied Information Systems (IJ AIS), vol. 3, no. 3, pp. 54-56
- [9] Trucco, E, Ruggeri, A, Karnowski, T, Giancardo, L, Chaum, E, Hubschman, JP & Lim, G 2013, 'Validating retinal fundus image analysis algorithms: issues and a proposal', Investigative ophthalmology and visual science, vol. 54, no. 5, pp.3546-3559.
- [10] Raj, V & Devi, V 2013, 'Retinal Image Analysis Using Fovea Detection using Unsymmetrical Trimmed Median Filter (MDBUTMF)', International Journal of Engineering and Innovative Technology (IJ EIT), vol. 3, no. 3, pp. 263-269.
- [11] 11. Patil, JD &Chaudhari AL 2012, 'Tool for the Detection of Diabetic Retinopathy using Image Enhancement Method in DIP', International Journal of Applied Information Systems (IJ AIS), vol. 3, no. 3, pp. 54-56.
- [12] 12. Fiorini, S, De Biasi, M, Ballerini, L, Trucco, E & Ruggeri, A 2014, 'Automatic Generation of Synthetic Retinal Fundus Images', STAG: Smart Tools and Apps for Graphics, Andrea Giachetti (Editor), pp. 1-4.
- [13] 13. SagarAdatrao&MayankMittat ,2016 'An Analysis of Different Image Preprocessing Techniques for Determining the Centroids of Circular Marks Using Hough Transform', International Conference on Frontiers of Signal Processing , 2 pp.110-116
- [14] 14. Dilip singh sisodia, shruti nair and pooja khobragade 'Diabetic Retinal Fundus Images: Preprocessing and Feature Extraction For Early Detection of Diabetic Retinopathy', Biomedical & Pharmacology Journal Vol. 10(2), 615-626 (2017)
- [15] Ms. Sheetal Maruti Chougule and Prof. A. L. Renke , 'New Preprocessing approach for Images in Diabetic Retinopathy Screening' International Journal of Engineering Research and Technology. ISSN 0974-3154 Volume 10, Number 1 (2017)
- [16] Can, A, Stewart, CV, Roysam, B &Tanenbaum, HL 2002, 'A feature-based technique for joint, linear estimation of high-order image-to-mosaic transformations: mosaicing the curved human retina', IEEE Transactions on pattern analysis and machine intelligence, vol. 24, no. 3, pp. 412-419.
- [17] Sukkaewa, L, Uyyanonvarab, B &Barmanc, S 2005, 'Comparison of edge detection techniques on vessel detection of infant's retinal image', Proceedings of the International Conference on Computer and Industrial Management, ICIM, Bangkok, Thailand, pp. 6.1-6.5.
- [18] Candes, E, Demanet, L, Donoho, D & Ying, L 2006, 'Fast discrete Curvelet Transforms', Multiscale Modeling and Simulation, vol. 5, no. 3, pp. 861-899.
- [19] Rezatofighi, SH, Roodaki, A & Noubari, HA 2008, 'An enhanced segmentation of blood vessels in retinal images using contourlet', Engineering in Medicine and Biology Society, EMBS International Conference of the IEEE, A new retinal image processing method for human identification using radon transform, vol. 30, pp. 3530-3533.
- [20] Esmaeili, M, Rabbani, H, Dehnavi, AM & Dehghani, A 2010, 'A new curvelet transform based method for extraction of red lesions in digital color retinal images', 17th IEEE International Conference on Image Processing (ICIP), pp. 4093-4096.
- [21] Zahedi, A & Sadjedi, H 2010, 'A human identification system based on retinal image processing using partitioned Fourier spectrum', IEEE International Conference on Audio Language and Image Processing (ICALIP), pp. 435-438.
- [22] 22. Zahedi, A, Sadjedi, H & Behrad, A 2010, 'A new retinal image processing method for human identification using radon transform', IEEE Machine Vision and Image Processing (MVIP), Iranian, vol. 6, pp. 1-4.
- [23] Miri, MS &Mahloojifar, A 2011, 'Retinal image analysis using curvelet transform and multi structure elements morphology by reconstruction. IEEE Transactions on Biomedical Engineering, vol. 58, no. 5, pp. 1183-1192.
- [24] Silvia, MJ &Poovizhi, S 2012, 'Retinal image analysis using ripplelet-I transform and segmentation using morphological gradient', International Journal of Emerging Technology and Advanced Engineering, vol. 2, no. 12, pp. 719-724.
- [25] ChandaniNayak&LakhwinderKaur , 2015, ' Retinal Blood Vessel Segmentation for Diabetic Retinopathy Using Multilayered Thresholding', International Journal of Science and Research (IJSR) Volume 4 Issue 6, pp 1520-1527.
- [26] Nasr Gharaibeh; Obaida M. Al-Hazaimeh; Bassam Al-Naami; Khalid M.O. Nahar 'An effective image processing method for detection of diabetic retinopathy diseases from retinal fundus images' International Journal of Signal and Imaging Systems Engineering 2018 Vol.11 No.4, pp.206 – 216
- [27] Chaudhuri, S, Chatterjee, S, Katz, N, Nelson, M &Goldbaum, M 1989, 'Detection of blood vessels in retinal images using two-dimensional

- matched filters', IEEE Transactions on medical imaging, vol. 8, no. 3, pp. 263-269.
- [28] Soares, JV, Leandro, JJ, Cesar, RM, Jelinek, HF and Cree, MJ 2006, 'Retinal vessel segmentation using the 2-D Gabor wavelet and supervised classification', IEEE Transactions on medical Imaging, vol. 25, no. 9, pp. 1214-1222.
- [29] Tsai, CL, Madore, B, Leotta, MJ, Sofka, M, Yang, G, Majerovics, A & Roysam, B 2008, 'Automated retinal image analysis over the internet', IEEE Transactions on Information Technology in Biomedicine, vol. 12, no. 4, pp. 480-487.
- [30] Chang, CC, Lin, CC, Pai, PY & Chen, YC 2009, 'A novel retinal blood vessel segmentation method based on line operator and edge detector', IEEE Fifth International Conference on Intelligent Information Hiding and Multimedia Signal Processing, pp. 299-302.
- [31] Khitran, S, Akram, M, Usman, A & Yasin, U 2014, 'Automated system for the detection of hypertensive retinopathy', International Conference on Image Processing Theory, Tools and Applications (IPTA), vol. 4, pp. 1-6.
- [32] Dua, S, Kandiraju, N & Chowriappa, P 2010, 'Region quad-tree decomposition based edge detection for medical images', The Journal of open medical informatics, vol. 4, no. 50, pp. 50-57.
- [33] Jaafar, HF, Nandi, AK & Al-Nuaimy, W 2011, 'Automated detection and grading of hard exudates from retinal fundus images', In 19th European Conference on Signal Processing, pp. 66-70.
- [34] Marín, D, Aquino, A, Gegúndez-Arias, ME & Bravo, JM 2011, 'A new supervised method for blood vessel segmentation in retinal images by using gray-level and moment invariants-based features', IEEE Transactions on medical imaging, vol. 30, no. 1, pp. 146-158.
- [35] Onkaew, D, Turior, R, Uyyanonvara, B & Kondo, T 2011, 'Automatic extraction of retinal vessels based on gradient orientation analysis', Eighth international joint conference on Computer science and software engineering (JCSSE), pp. 102-107
- [36] Akram, MU, Atzaz, A, Javed, MY, Niazi, UAK 2009, 'Preprocessing and blood vessel segmentation of retinal images', IASTED Conference on Visualization, Imaging and Image Processing (VIIP), vol. 6, no. 1, pp. 13-18.
- [37] Lazar, I & Hajdu, A 2012, 'Segmentation of vessels in retinal images based on directional height statistics', IEEE Annual International Conference of the Engineering in Medicine and Biology Society (EMBC), pp. 1458-1461.
- [38] Karasulu, B 2012, 'Automatic extraction of retinal blood vessels: a software implementation', European Journal of Scientific, vol. 8, no. 30, pp. 47-57.
- [39] Ocbagabir, H, Hameed, I, Abdulmalik, S & Buket, DB 2013, 'A novel vessel segmentation algorithm in color images of the retina', In IEEE Conference on Long Island Systems Applications and Technology (LISAT), pp. 1-6
- [40] Mehrotra, A, Tripathi, S, Singh, KK & Khandelwal, P 2014, 'Blood Vessel Extraction for retinal images using morphological operator and KCN clustering', IEEE International Conference on Advance Computing (IACC), pp. 1142-1146.
- [41] Ortiz, D, Cubides, M, Suarez, A, Zequera, M, Quiroga, J, Gomez, J & Arroyo, N 2010, 'Support system for the preventive diagnosis of Hypertensive Retinopathy', Annual International Conference of the IEEE Engineering in Medicine and Biology, vol. 1, pp. 5649-5652.
- [42] Li, H & Chutatape, O 2004, 'Automated feature extraction in color retinal images by a model based approach', Transactions on Biomedical Engineering, vol. 51, pp. 246-254.
- [43] Trucco, E, Ruggeri, A, Karnowski, T, Giancardo, L, Chaum, E, Hubschman, JP & Lim, G 2013, 'Validating retinal fundus image analysis algorithms: issues and a proposal', Investigative ophthalmology and visual science, vol. 54, no. 5, pp. 3546-3559.
- [44] Manikis, GC, Sakkalis, V, Zabulis, X, Karamaounas, P, Triantafyllou, A, Douma, S, Zamboulis, C & Marias, K 2011, 'An image analysis framework for the early assessment of hypertensive retinopathy signs', IEEE Conference on E-Health and Bioengineering (EHB), vol. 1, pp. 1-6.
- [45] Muramatsu, C, Hatanaka, Y, Iwase, T, Hara, T & Fujita, H 2011, 'Automated selection of major arteries and veins for measurement of arteriolar-to-venular diameter ratio on retinal fundus images', Computerized Medical Imaging and Graphics, vol. 35, no. 6, pp. 472-480.
- [46] Narasimhan, K, Neha, V & Vijayarekha, K 2012, 'Hypertensive Retinopathy Diagnosis from Fundus Images by Estimation of AVR', Procedia Engineering, vol. 38, no. 1, pp. 980-993
- [47] Khitran, S, Akram, M, Usman, A & Yasin, U 2014, 'Automated system for the detection of hypertensive retinopathy', International Conference on Image Processing Theory, Tools and Applications (IPTA), vol. 4, pp. 1-6.
- [48] Agurto, C, Joshi, V, Nemeth, S, Soliz, P & Barriga, S 2014, 'Detection of hypertensive retinopathy using vessel measurements and textural features', Annual International Conference of the IEEE Engineering in Medicine and Biology Society, vol. 36, pp. 5406-5409.
- [49] Gehad Hassan, Nashwa El-Bendary, Aboul Ella Hassanien, Ali Fahmy, Abdullah M. Shueb, and Vaclav Snasel, 2015 'Retinal blood vessel segmentation approach based on mathematical morphology', International Conference on Communication, Management and Information Technology, pp. 612 - 622
- [50] Sathananthavathi V, G. Indumathi & R. Rajalakshmi, (2017), 'Abnormalities Detection in Retinal Fundus Images', International Conference on Inventive Communication and Computational Technologies (2017) pp. 89-93.

Analysis of Alzheimer Disease using Optimization Techniques

D. Chitradevi
Department of CSE
Hindustan Institute of Technology and Science
dcdevi@hindustanuniv.ac.in

S. Prabha
Department of ECE
Hindustan Institute of Technology and Science
sprabha@hindustanuniv.ac.in

Abstract— Alzheimer Disease (AD) is a neurodegenerative and most common form of disorder. Most of the researchers are concentrating on AD pathology for the past few decades since it is a major public health disease in the world wide. AD causes neuronal damage in the Brain Internal Regions (BIR) specifically Corpus Callosum (CC), White Matter (WM), Grey Matter (GM), Hippocampus (HC) and ventricle. The neuronal loss makes the changes in anatomical structure of the brain which affects the BIR. Identification of structural difference between the normal controls (NC) and AD of the brain is a challenging process due to its complex networks of nerves. Hence, there is a requirement of segmentation process to extract the BIR. The proposed work focused to segment the CC and ventricle regions using multi-level thresholding methods namely Ant colony Optimization (ACO) and Artificial Bee Colony (ABC) optimization techniques. These methods have been analyzed quantitatively and qualitatively using various measures with ground truth (GT) images. Artificial Bee Colony optimization techniques have been achieved the better accuracy of 93 % than ACO. Deep Learning (DL) classifier has been used to classify normal controls (NC) and AD and acquired the better accuracy of 78% in ABC than ACO. Finally the proposed pipeline provides the clinical evidence for analyzing AD.

Keywords—Alzheimer Disease, Brain Internal Regions, Deep Learning, Optimization Techniques

I. INTRODUCTION

Dementia can be categorized into different kinds of brain disorder namely cortical dementia, fronto-temporal dementia, vascular dementia, Alzheimer disease etc. AD is major form of disorder in and around the world. AD shows two typical abnormalities such as neurofibrillary tangles and amyloid plaques which leads neuronal loss. The loss begins from GM, and spreads into the regions of WM, CC, HC and ventricle. However, the ventricle chambers contain CSF and noticeably it is enlarged for AD patients [1]. The hallmarks to identify the AD are GM, WM, CC, hippocampus and ventricle. The changes in the shape of the ventricle cause the changes in GM due to its position of the Medial Temporal Lobe (MTL). The changes of ventricle are used to measure the hemispheric atrophy rates. The structural changes of the ventricular are highly associated with an increase in neurofibrillary tangles and senile plaques deposition in nerve cells [2]. In the same way, CC is related to left and right hemispheres since it makes the communication between them [3]. Various researchers have been reported as, the important atrophy in CC causes AD and it is responsible for WM degeneration [3]. AD diagnosis needs, segmentation process to extract the BIR and it should also observe the changes in the structures. The extraction/segmentation of ventricle and CC are very hectic task due to its homogeneous nature in nerve cells. The types of thresholding segmentation methods are bi-level thresholding (BT) and multi-level thresholding (MT). Various drawbacks were addressed from the BT technique due to the complexity of problem solving. BT method considers only one threshold to separate the regions namely foreground and background. Though, the MT

technique considers multiple thresholds in terms of separating the pixels into various numbers of groups. Hence, MT is strongly suggested for BIR segmentation. This aids to divide histogram image into number of classes [4]. The most widely used MT techniques are GA, Firefly Algorithm (FFA), CS, PSO and BFA etc. [5, 6]. There are various advantages observed from multi-level thresholding such as avoiding local optimum, finding global optimum solution, flexible, and simple. Therefore, this paper proposes an optimization method namely ACO and ABC to segment the ventricle and CC. The major intention of using this optimization is easy to implement, computationally efficient, flexible etc. The segmented regions (SR) are sending to the classifier as an input for classifying the normal and AD images. There are various classifiers which are available specifically K-Nearest Neighbour (KNN), Support Vector Machine (SVM) etc. However, the now-a-days trends for classification are deep learning due to its features of classification from the actual images [7]. In the proposed work, the real time MR images have given by Chettinad health city. Generally, the real time has the poor quality due to the homogeneous region of the pixels. Since, the pre-processing techniques are employed to maximize the contrast and removal of non-brain tissues. The optimization methods namely ACO and ABC are attempted for diagnosing the AD and the incessant structural changes. Overlapping and similarity measures are examined qualitatively and quantitatively to examine the performance of the segmentation. The power of ABC has been examined with DL classifier to identify NC and AD patients. Lastly, the DL classifier has been employed for ACO and ABC technique which helps to categorize NC and AD images. This process helps in medical analysis to diagnose AD.

II. MATERIALS AND METHODS

A. Workflow of this work

The entire workflow of this work is explained as follows. The procedure encompasses of five steps such as image acquisition, pre-processing, segmentation, GT validation and classification.

Step 1: The brain MR images has been generated by Chettinad Health City, Chennai.

Step 2: Next, to remove the skull and improve the contrast pre-processing techniques are implemented using Otsu's thresholding techniques and histogram equalization.

Step 3: Thirdly, the optimization techniques such as ACO and ABC were employed to extract the BIR such as CC and ventricle.

Step 4: Then, GT validation has been applied with segmented output. Step 5: Lastly, the deep learning classifier is implemented from the segmented output to classify the NC and AD patients which helps clinically to identify the level of disease.

B. MRI Dataset

The T2 weighted (flip angle = 90o, field of view=2.5cm x 2.5cm, matrix size=256x256, thickness=5mm) MR brain images are considered to extract ventricle and CC.

Table 1 Demographic details

	NC	AD
Number of Subjects	100	100
Sex (M/F)	73/27	68/32
Age	60.5 ± 5.5	67.5 ± 7.5
Clinical Dementia Rate (CDR)	0	1

Sagittal and axial slices of the brain images are collected from real time. The proposed work uses the screening scans from the 1.5 tesla. Totally 200 subjects (100: normal, 100: AD) with an age of 60 to 75 are considered for this work.

C. Pre processing

Generally, the real time images have homogeneous intensity value for both background region and object due to its deprived quality. Hence, the pre-processing is required to implement for improving the quality of an images. In this work, the pre-processing contains two steps: first one is contrast enhancement, and second is skull stripping. Adaptive histogram equalisation method has been applied for contrast enhancement and an Otsu thresholding technique is used for skull stripping.

D. Segmentation

Ant Colony Optimization (ACO):

ACO is a probabilistic method which is used to solve the complex problems by finding the good paths. Generally, ACO mimics the social life behaviour which is geared for survival of the group as a whole rather than individual or a subsection of the colony. The ant has distinctive characteristics in their behaviour which is the searching the food for their life. For searching the food, it will find the shortest path among the food sources and nest. The ants are having mass intelligence behaviour which makes the communication between the ants to find the food. The communication is not direct which is indirect by dropping the clinical substances called pheromone in their path. The substances will stay with short period of time which is recognized by ant. The ant selects the path based the pheromone rate for finding the food source [13]. The best path will be the optimum solution. Ants decide to move from node i to another j for finding the food through based on the probabilistic action rule which is as follows,

$$P_{ij}^k = \frac{[\tau_{ij}]^\alpha [\eta_{ij}]^\beta}{\sum_{l \in N_i^k} [\tau_{il}]^\alpha [\eta_{il}]^\beta}$$

: the amount of deposited pheromone between i and j

N_i^k : Neighbourhood nodes for ant k. α, β : constants which controls the pheromone rate and heuristic function.

The deposition of pheromone can be updated by the following formula:

$$\tau_{ij} = (1 - \rho)\tau_{ij} + \sum_k \Delta\tau_{ij}^k$$

: Pheromone evaporation coefficient,

$\Delta\tau_{ij}^k$: amount of pheromone deposited by kth ant.

Artificial Bee Colony Optimization (ABC):

ABC algorithm is a one of the meta-heuristic algorithm which consists of 3 types of bees: employed, onlooker and scout bees. In ABC algorithm, the food source position (optimal solution) search contains of three major stages: (1) place the employed bees into the food source locations and then calculate the amounts of nectar present in them; (2) select the best position of the food source with the assistance of onlooker bees after sharing the data attained from the employed bees and determined the fitness value of the food sources; (3) find the scout bees and place them at the randomly found out food source positions.

In initialization step, the food sources positions (employed bee populations) are randomly generated and fitness values are calculated. Next, employed bee identifies the new solution within neighbourhoods. The new fitness source position is higher than the old one means, it replaces the old values otherwise old one is taken. After finishing the search process, the employed bees share the fitness values of the best solution and food source position with onlooker bees. An onlooker bee selects the high probability food source location based on the nectar amounts and it calculates the fitness values. The unused food location is replaced by randomly produced food source location. The same procedure is repeated until it satisfies the condition. The probability can be calculated by using the following formula [18]:

$$p_i = \frac{fit_i}{\sum_{l=1}^n fit_l} \quad V_{ij} = X_{ij} + r * (X_{ij} - X_{k,j})$$

fit_i : fitness value of 'i', V_{ij} : new food source by onlooker bee, k: solution in the neighborhood of i, j, r: random number ranges from -1 to 1.

Fitness value is updated by the following:

$$fit_i = \begin{cases} \frac{1}{1 + f_i}, & \text{if } f_i \geq 0 \\ \frac{1}{1 + abs(f_i)}, & \text{if } f_i < 0 \end{cases} \quad \pi r^2$$

III RESULTS

The sagittal and axial slices of T2 weighted MRI has been considered for current process. Completely, 100 NC, 100 AD images are collected from the hospital. Extracting the BIR is a very demanding process due to its difficult structure. Initially, the contrast enhancement has been applied using histogram equalization, which helps to improve the resolution of the deprived images. Next step is to eliminate non brain tissues like skull, muscle and skin, the skull stripping is attempted using Otsu's thresholding which is depicted in Fig. 2. The axial and sagittal slices have been considered for this work to diagnose AD. The raw input image is having homogeneous pixel intensity value for both brain tissues as well as non-brain tissues since this reason there is an essential step to employ the skull stripping and contrast enhancement in Fig.2. Fig. 3 displays skull stripped and contrast enhanced images of normal and AD images of two slices. The segmentation of CC and ventricle are evaluated by using two multi thresholding methods such as

ACO and ABC techniques which are performed on real time input data.

The segmentation needs parameters to get optimal solution and to stop the execution. Hence, there is a necessity to select parameter values for the above optimization methods. The basic parameters for the above optimization methods are number of thresholds (NT),

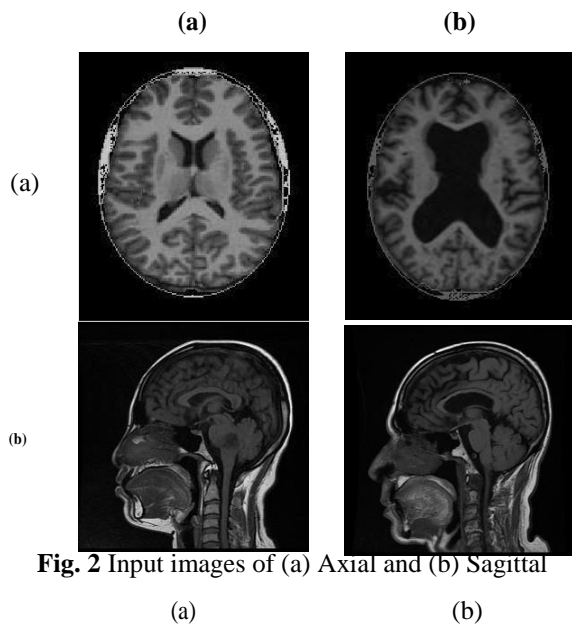


Fig. 2 Input images of (a) Axial and (b) Sagittal

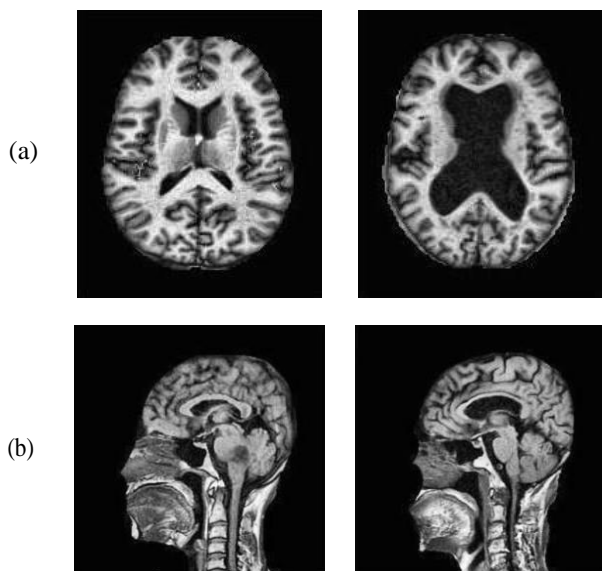


Fig.3 Pre-processed images of (a) Axial (b) Sagittal

population size and number of iterations (NI). The input parameter values are showed in the Table 2 and 3. The stopping criteria to segment the BIR such as ventricle and CC are NT and NI. Primarily, the NT value begins from lower values and it is incremented step by step. The lower values of T show extra regions which is the neighborhood region of the BIR and region loss. Then, the step by step parameter tuning has been evaluated to identify the correct NT. Optimal NT value provides the expected segmented region of the brain and also it avoids the extra regions of the brain. At the end of the parameter tuning, the sub regions are clearly acquired based on the comparison among the segmented and GT region. Finally, the analysis given the

true regions of the ventricle region by using the threshold at $T=8$ are shown in Fig. 4 and CC has been attained clearly in $T=10$ is shown in Fig. 5. These parameters are tuned depends on the optimum values which acquires optimal solution for BIR segmentation.

Table 2. Parameters for ACO and ABC techniques: Ventricle

Parameters	ACO	ABC
Population Size	20	20
NI	100	100
NT	8	8

Table 3. Parameters for ACO and ABC techniques: CC

Parameters	ACO	ABC
Population Size	20	20
NI	100	100
NT	10	10

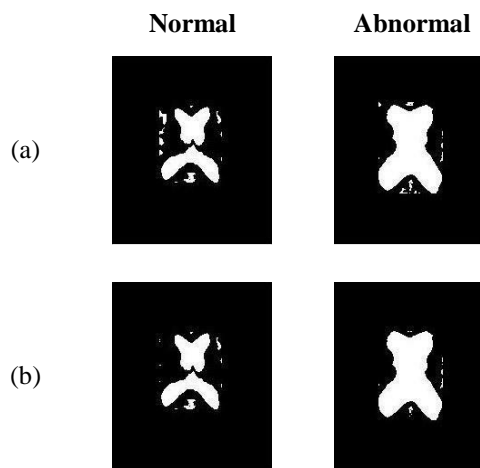


Fig. 4. SR of ventricles for normal and AD images (a) ACO (b) ABC

The proposed system is analyzed qualitatively for the above mentioned regions. In fig. 4 and 5, it is perceived that ABC shows good results than the ACO due to its own behavior of selecting the optimum solution. When comparing ABC and ACO, it has been understood that, the ACO requires high NI and it is verytough for theoretical analysis.

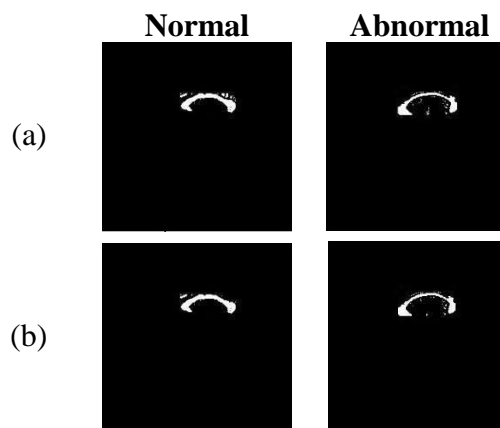


Fig. 5 SR of CC for NC and AD images using (a) ACO (b) ABC

Quantitative analysis has been evaluated for ACO and ABC methods for BIR segmentation by relating various metric values such as Feature Similarity Index (FSIM) and Structure Similarity Index (SSIM). The feature and structure similarity of an image have been computed by using FSIM and SSIM measures which is displayed in Fig. 6. The main intention of measuring these metric values is to identify the accuracy of BIR in segmentation for abnormal and normal patients. The GTs images are compared with SR to get accurate optimum results in segmentation. Comparatively, the proposed work shows greater performance with the accuracy of 93% in both SSIM and FSIM due to its similarity measures among segmented and GT of the BIR. After then, the similarity measures such as Jaccard Index (JC), Tanimoto (TN), Dice Similarity (DS) and volume Similarity (VS) are also examined for overlapped regions among GT and SR. These similarity measures are used to identify the ratio of the non-intersecting and intersecting regions of the GT and segmented images. Overlapping measures of GT and segmented BIR are displayed in the form of bar chart in Fig.7.

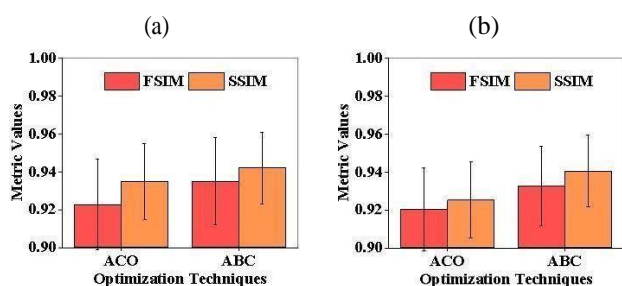


Fig. 6. FSIM and SSIM for (a) CC (b) Ventricle for ACO and ABC

From this plot, approximately 90% of similarity is observed among GT and segmented images. In the bar plot, the comparison measures such as JC, TN, DS and VS for ACO and ABC techniques were drawn. In this chart, X axis depicts the optimization techniques and Y axis shows the comparative measures of the GT and segmented images. From this graph ABC shows better segmentation accuracy than ACO. According to the work flow, the next step is the classification which is attempted to classify the NC and AD patients based on the features.

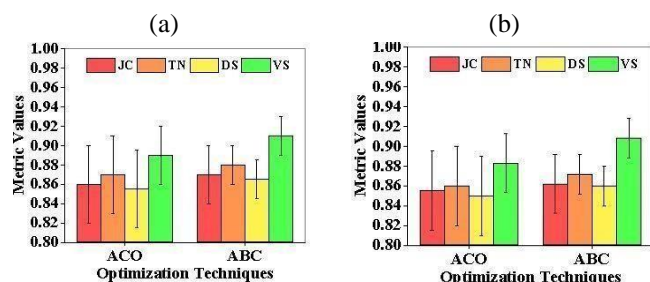


Fig. 7 overlapping measures using JC, TN, DS and VS for (a) CC (b) ventricle

The classification requires feature extraction process which is desirable to extract best features. The process of extracting the features is a very demanding process for every image in conventional approaches since; it involves 2 processes which are feature extraction and classification. Therefore, there is a need to use automated system for feature extraction and classification method such as

convolution neural network (CNN). The reason behind this CNN is that, the learning capability is used to select the exact features for every image automatically. Feature extractor and classification modules are combined in CNN process with set of layers. The convolution layer gets the input from the segmented BIR which helps to apply the mask for a particular region of the feature map for computing the weighted sum. The basic patterns of objects have been identified by applying the masking. To reduce the number of features, the convolution layers has been evaluated by applying subsampling layers which is called as feature extractor and it is fully linked. The results of the feature extractor layer are input to the classification layer and it is also fully connected. This helps to train the datasets to produce the output to the output layer. Fully connected layers are handled by using AlexNet in this proposed work. Then, the last fully connected layer will take responsibility to classify the NC and AD patients of the SR.

The performance analysis chart has been prepared for classifying NC and AD patients using ACO and ABC with statistical measures such as sensitivity, specificity and accuracy which is shown in Fig.8.

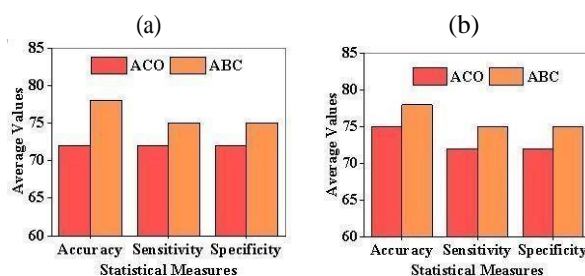


Fig. 8 CNN classification using ACO, ABC for (a) CC (b) Ventricle

In this figure, ABC achieved the maximum accuracy of 78% approximately from the above mentioned sub regions than the ACO due to the correct extraction of features from an image. Similarly, the maximum sensitivity of 74% and specificity of 74% is attained in ABC than ACO. These measures are used to examine the performance of the classifier since it is a very good feature extractor and filtering the features. From all the above measures, it is evidently witnessed that, the ABC showed better performance than ACO due to proper parameter tuning.

IV

DISCUSSIONS

Brain sub region extraction is the one of the major difficult task due to its anatomical variations of the brain. In recent years, the important bio-markers for AD are GM, WM, CC and ventricle due to its structural differences. CC is the largest white matter in the brain. The ventricle is placed at the centre of the brain which has a communicating network of cavities and it is filled inside the Cerebrospinal Fluid (CSF) [8, 9]. If any changes observed in the BIR, then it cause the reduction in size or shape enlargement, shrinkages of nerve cells etc. this leads to memory loss, functional activity problems, problems in judgment, skills, things misplacement etc. Hence, this work helps to analyse the clinical study in AD and which is used to classify the NC and AD.

In the proposed process, the optimization techniques such as ACO and ABC are proposed to segment the BIR. In this system, the input data are generated by Chettinad Health

City, Chennai. The segmentation of BIR is considered as major difficult task in analyzing AD. From the literature [10, 11], the proposed work outperform in ABC than ACO. The quantitative and qualitative analysis has been performed for ACO and ABC which proves that ABC provides the better results of an accuracy of 79% due to its ability in avoiding local minima. The analysis evidences that, ABC provides the promising results in terms of avoiding the local minima.

Numerous researchers have implemented the various classification methods such as SVM, KNN etc. [12, 13]. In the proposed work, to extract the features of segmented image and classification, CNN has been implemented to classify the NC and AD patients. Thus the pipeline provides study which can be extended to other neuro-degenerative disorders. This will support for the development of commercially viable automated computer aided disease diagnosis (CAD) environment for the screening of brain diseases.

V CONCLUSIONS

Quantification of structural variations of BIR is very difficult. In this work, the optimization techniques such as ACO and ABC are quantitatively analysed by using various measures. From this analysis, the ABC segmentation method provides better results than ACO due to its proper extraction of global optimal result. The DL classifier is applied to classify the NC and AD images in AD and acquired the accuracy of 79%. In the performance analysis, the proposed technique shows better accuracy for both segmentation and classification when compared to other techniques. The proposed process witnessed that, it is able to diagnose the AD via the changes observed from CC and ventricle. The proposed system demonstrates clinically which is useful for assessing and it work as a screening tool to study neurodegenerative disease especially AD.

REFERENCES

- [1] S. M. Nestor et al., "Ventricular enlargement as a possible measure of Alzheimer's disease progression validated using the Alzheimer's disease neuroimaging initiative database," *Brain*, 2008.
- [2] Dementia Australia 2002. <https://www.dementia.org.au/about-dementia/types-of-dementia/Alzheimer's-disease>, 2016.
- [3] H. Hampel et al., "Corpus callosum atrophy is a possible indicator of region- and cell type-specific neuronal degeneration in Alzheimer disease: A magnetic resonance imaging analysis," *Arch. Neurol.*, 1998.
- [4] X.S. Yang, S. Deb, Cuckoo search via Levy flights, in: 2009 World Congress. Nat. Biol. Inspired Computing NABIC 2009 - Proc., 2009. doi:10.1109/NABIC.2009.5393690.
- [5] S. Suresh, S. Lal, An efficient cuckoo search algorithm based multilevel thresholding for segmentation of satellite images using different objective functions, *Expert Syst. Appl.* (2016). doi:10.1016/j.eswa.2016.03.032.
- [6] A.K. Bhandari, V.K. Singh, A. Kumar, G.K. Singh, Cuckoo search algorithm and wind driven optimization based study of satellite image segmentation for MT using Kapur's entropy, *Expert Syst. Appl.* (2014). doi:10.1016/j.eswa.2013.10.059.
- [7] Mohsen, H., El-Dahshan, E.-S.A., El-Horbaty, E.-S.M., Salem, A.-B.M., 2017. Classification using Deep Learning Neural Networks for Brain Tumors, *Future Computing Informatics Journal*. <https://doi.org/10.1016/j.fcij.2017.12.001>
- [8] Hua X, Leow AD, Lee S, Klunder AD, Toga AW, Lepore N, Chou YY, Brun C, Chiang MC, Barysheva M, Jack CR Jr, Bernstein MA, Britson PJ, Ward CP, Whitwell JL, Borowski B, Fleisher AS, Fox NC, Boyes RG, Barnes J, Harvey D, Kornak J, Schuff N, Boreta L, Alexander GE, Weiner MW, Thompson PM, Alzheimer's Disease Neuroimaging Initiative: 3D characterization of brain atrophy in Alzheimer's disease and mild cognitive impairment using tensor-based morphometry. *Neuroimage* 2008; 41: 19–34.
- [9] Li J, Pan P, Huang R, Shang H: A meta-analysis of voxel-based morphometry studies of white matter volume alterations in Alzheimer's disease. *Neurosci Biobehav Rev* 2012; 36: 757–763.
- [10] C. Singh and A. Bala, A DCT-based local and non-local fuzzy C-means algorithm for segmentation of brain magnetic resonance images, *Applied Soft Computing*, (2018), 68 447-457.
- [11] T.X. Pham, P. Siarry, H. Oulhadj, Integrating fuzzy entropy clustering with an improved PSO for MRI brain image segmentation, *Appl. Soft Computing Journal* (2018). doi:10.1016/j.asoc.2018.01.003.
- [12] H. Mohsen, E.-S.A. El-Dahshan, E.-S.M. El-Horbaty, A.-B.M. Salem, Classification using Deep Learning Neural Networks for Brain Tumors, *Future Computing Informatics Journal* (2017). doi:10.1016/j.fcij.2017.12.001.
- [13] Y. Chen, T.D. Pham, Development of a brain MRI-based hidden Markov model for dementia recognition, *Biomedical Engineering Online*. (2013). doi:10.1186/1475-925X-12-S1-S2.

structures. *Biological cybernetics*, 65(3), 203-210.

[8]. Zhang, J., Wang, N., Kuang, H., & Wang, R. (2013). An improved method to calculate phase locking value based on Hilbert–Huang transform and its application. *Neural Computing and Applications*, 24(1), 125–132. doi: 10.1007/s00521-013-1510-z

[9]. Lachaux, J. P., Rodriguez, E., Martinerie, J., & Varela, F. J. (1999). Measuring phase synchrony in brain signals. *Human brain mapping*, 8(4), 194-208.

[10]. Ziehe, Andreas & Krämer, Nicole & Popescu, Florin & Müller, Klaus-Robert. (2010). Comparison of Granger Causality and Phase Slope Index. *Journal of Machine Learning Research - Proceedings Track*. 6. 267-276.

Vowel Identification from Neural Signals during Articulated Speech

Ashley Bishop¹, IEEE Member, Anandha Sree Retnapandian², Sandhya Chengaiyan², Kavitha Anandan, IEEE MEember,
¹Department of Biomedical Engineering, Drexel University, Philadelphia, PA, USA.

²Centre for Healthcare Technologies, Department of Biomedical Engineering, SSN College of Engineering, Chennai, India.
Email id : amb688@drexel.edu, anandha.sree@gmail.com, sandhyaaswathama@gmail.com, kavithaa@ssn.edu.in

Abstract— Speech interfaces have become widely accepted and are nowadays integrated in various real-life applications and devices for the impaired. The recent advances in EEG technology has made Brain Computer Interface (BCI) the most exciting field of biomedical research. The non-invasive nature of EEG has made researchers show interest towards it. In this paper, the conventional brain connectivity measures are employed to recognize the articulated vowels from the recorded brain activity. The work reveals that the brain activity registered from the temporal and parietal regions contain brimming information related to speech production and comprehension. Also the analysis showed that the comprehended information related to speech activities are packed within the theta, beta and alpha EEG sub-bands. The extracted functional connectivity parameters were used to train a Multi layer perceptron to identify the articulated vowel.

Keywords—Electroencephalography (EEG); Brain Computer Interface (BCI); Functional Connectivity Parameters; Multi Layer Perceptron (MLP);

I. INTRODUCTION

Brain-computer interactions (BCIs) focus on analyzing the physiological state of the brain to direct, augment, or control an external objective. BCIs are commonly used in assistive devices due to the direct communication between the brain and an external device. One promising potential application of BCIs is overcoming speech disorders that inhibit speech production. Many neurodegenerative diseases such as amyotrophic lateral sclerosis (ALS), can make it difficult for patients to speak by inhibiting muscle movement. BCIs could provide an easier means of communication for those with severe speech impairments by translating speech signals directly captured from the brain activity.

Speech is most commonly studied through voice signals and speech imagery is studied through electroencephalography (EEG), most famously through the “Thought Translation Device” [1]. However, while this project broke through many barriers, it brought to light a major tradeoff between speed and accuracy of BCI-based speech prostheses. Major advancements in computational power within the past several decades have also enabled a rise in machine-learning centered BCI speech prostheses [2]. Still the process lags behind in continuous processes. Hence

bridging the gap by decoding information from neural signals of the speech process is necessary. The conventional brain connectivity features specific to EEG signals were chosen. Thus, applying machine learning algorithms to studies of speech and imagery have also been an area of interest, testing to see whether it is possible for a program to differentiate between different words and letters from brain activity. One standard choice used in many different studies seems to be the support vector machine (SVM) algorithm which have been reported to typically perform on accuracies between 60 – 80% depending on the experimental protocol [3]. However, one of the highest reported algorithms developed for letter classification from brain signals is through an extreme learning machine (ELM) with an overall accuracy up to 98 – 99% [4]. In fact, this study further reported that when compared to an SVM, the ELM and its variations consistently performed better. However, these designs force a user to spell a word rather than determining a word from the way it is pronounced in natural speech.

Speech is the main characteristic that differentiate human from other animals. It is the ability to express thoughts and feelings by articulated sounds. On analyzing the background activity occurring in the brain during the speech process, it involves language processing, visualizing, hearing, comprehending, inner voice and preparation for articulation. Hence speech is considered as the brain’s higher cognitive activity. Even a minute malfunction in any of these functions might cause a speech disorder. Speech disorders can also be due to many other reasons, whereas these might be due to neuronal dysfunction or varied function. In recent years, researchers have been thriving to reveal the actual process happening in the brain during a speech production task, to build assistive devices to the differently functioned. Decoding brain signals during any specific speech tasks can be helpful to a limited extent. This work aims to analyse the brain signatures while articulating the English vowel phonemes ‘/a/’, ‘/e/’, ‘/i/’, ‘/o/’, ‘/u/’ which can be further incorporated in reconstructing the vowels from imagined speech.

II. METHODOLOGY

A. Data Acquisition

Twenty five healthy subjects with no observable speech impairments or severe disabilities volunteer and were used for this experiment.

The following protocol explains the experimental procedure for the speech imagery project. The total procedure has been divided into two major sub-procedures: one for the vowel speech protocol, one for the vowel speech imagery, where the vowels are defined as the set of letters ('/a/', '/e/', '/i/', '/o/', '/u/'). EEG signals were recorded using the Emotiv EPOC+ system, with the default sampling frequency of 128.

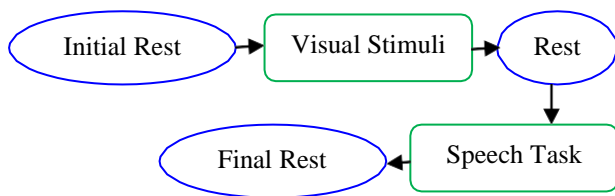


Figure 1. Speech protocol for vowels

Figure 1 describes the experimental protocol for the speech portion of the EEG data acquisition for each subject. This protocol was performed for each vowel for a total of 25 speech trials, 5 trials each for each vowel. The speech protocol also contained 3 states:

- **Rest:** Allows mental and physical preparation for the next. Initial and final rest was given for 30 seconds and 20 seconds between each trial.
- **Visual Stimulus:** Participant is shown visual representation of phoneme of one vowel which is displayed on a monitor placed before the subject indicating what vowel to say during each trial
- **Speech:** Where the participant articulates the given phoneme presented in the visual stage aloud; this phase is repeated for 5 trials after each 20 second rest period.

After all the data was recorded, the collective EEG data was segmented into respective electrodes, specifically for the electrodes of F7, F3, FC5, T7, P7, P8, T8, FC6, F4, and F8 [5]. Each electrode signal was then normalized and rescaled based on a min-max normalization that also rescaled the signal in-between the values of 0 to 1. The next step then included smoothening out the signal based on a moving average filter with a span of 5 units. Filtering then depended on what features were extracted, but all were some form of band pass filtering.

B. Feature Extraction

Brain-connectivity features extracted included phase locking value (PLV), partial directed coherence (PDC), directed transfer function (DTF), and phase slope index (PSI). For the brain-connectivity features, each signal first started through 3 different band pass filters: a 3rd order Butterworth filter, a 2nd order Type I Chebyshev filter with a ripple factor of 3, and a 2nd order Type II Chebyshev filter with a ripple factor of 3.

For PDC [6] and DTF [7], these band pass filters were applied for the band specified to run these calculations on, 1-4 Hz for delta waves, 4-8 Hz for theta waves, 8-13 for alpha waves, 13-30 for beta waves, and 30-44 for gamma waves. After being band pass filtered, these signals were then transformed using the fast Fourier transform and passed through a multivariate autoregressive (MVAR) model specifically with the Yule-Walker algorithm. The PDC and DTF were estimated using equations (1) and (2) respectively.

$$PDC(f) = \pi_{ij}(f) = \frac{\bar{a}_{ij}(f)}{\sqrt{d_j^H(f)a_j(f)}} \quad (1)$$

Where, $0 \leq |\pi_{ij}(f)| \leq 1$; 0: no coupling; 1: complete coupling; a_{ij} is the ij^{th} element of MVAR coefficient matrix.

$$DTF(f) = \frac{H_{ij}(f)}{\sqrt{h_j^H(f)h_j(f)}} \quad (2)$$

Where, $0 \leq DTF \leq 1$; 0 : no coupling; 1: complete coupling; H_{ij} being the ij^{th} element of the transfer function H.

For PLV, these band pass filters were in-between 1-44 Hz, to remove low-end and high-end noise. These signals were then decomposed using empirical mode decomposition into different intrinsic mode functions (IMF). Depending on the band, a specific IMF was chosen for the target frequency, by looking at the IMF in the frequency-domain and looking at power spectral density [8]. The two bands with the most activity were then passed through a function that first applied the Hilbert transform, then calculated instantaneous phase and the phase locking value. The PLV [9] is defined at time t as the average value:

$$PLV_t = \frac{1}{N} \left| \sum_{n=1}^N \exp(j\theta(t,n)) \right| \quad (3)$$

Where $\theta(t,n)$ is the phase difference $\phi_1(t,n) - \phi_2(t,n)$. PLV is a measure of synchronization between electrodes, a value between 0 to 1; where 1 represents complete synchronization and 0 suggests the signals are completely unsynchronized.

Finally, phase slope index (PSI) was also calculated by band pass filtering the signals used through three different filters: a 3rd order Butterworth filter, a 2nd order Type I Chebyshev filter with a ripple factor of 3, and a 2nd order Type II Chebyshev filter with a ripple factor of 3, for the target band. These filtered signals were then passed through another algorithm, as proposed in [10]. A positive PSI value suggests that signal one is ahead of the time series for signal two, and a negative value proposes the reverse relationship where signal two is ahead of signal.

C. Classification

A multilayer perceptron (MLP) algorithm have been created and tested for classification. MLP is a class of feed forward Artificial Neural Network composed of multiple layers of perceptrons, with threshold activation.

Currently, these algorithms are designed to test whether or not it is possible to differentiate between the different vowel phonemes. Each algorithm was trained for band-wise comparisons so that only the alpha features were tested against the other vowel phoneme alpha features, and so on. Data sets, with a twenty and eighty percent testing-training segmentation were used to train the algorithm with the functional brain-connectivity features. Figure 2 represents the structure of commonly used Multi Layer Perceptron structure.

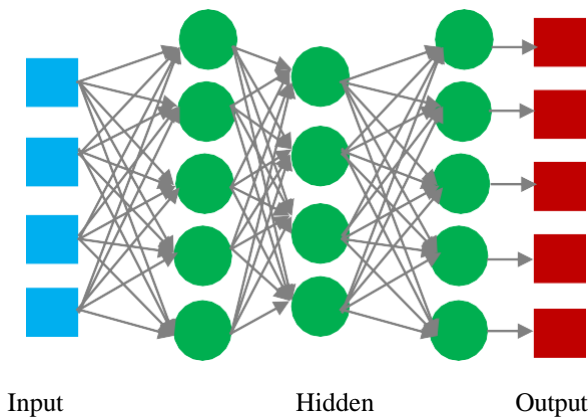


Figure 2. Structure of Multi Layer Perceptron (MLP)

III. RESULTS AND DISCUSSIONS

The articulated speech EEG signals were preprocessed to obtain artifact free signals. Figure 3 show the signal decomposed using Empirical Mode Decomposition to segment the signal into various sub-band frequencies. On comparing the frequencies of the IMFs, it was observed that the IMF1, IMF2, IMF3, IMF4 and IMF5 matched with the frequencies of gamma, beta, alpha, theta and delta respectively.

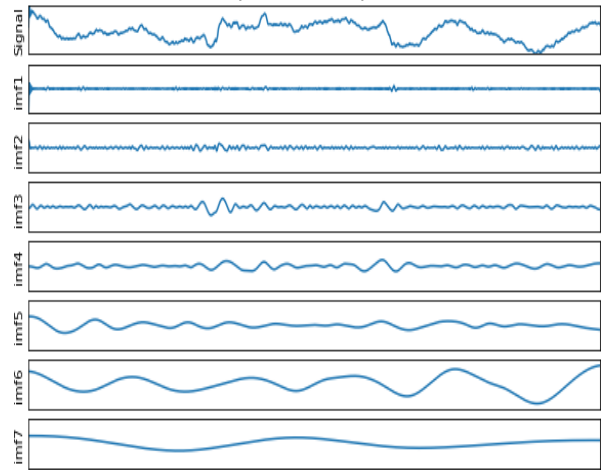
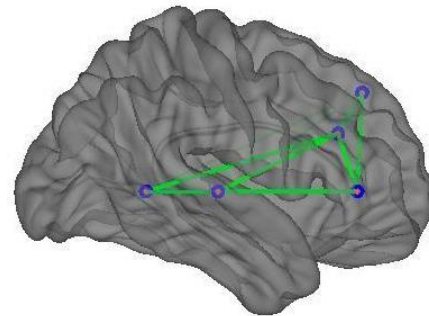
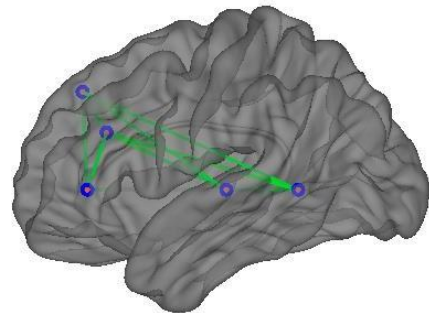


Figure 3. Empirical Mode Decomposed signal for a representative subject while speaking the phoneme of vowel 'a/'



(a)



(b)

Figure 4. The Phase Slope Index for a representative subject, while speaking the vowel 'a/'; (a) Left view (b) right view

The features extracted from the corresponding IMFs were used to train the MLP. On analyzing the features, prominent connectivity was found to be more in the left hemisphere of the brain when compared to the right hemisphere of the brain. Hence speech related tasks are performed by the left hemisphere of the brain.

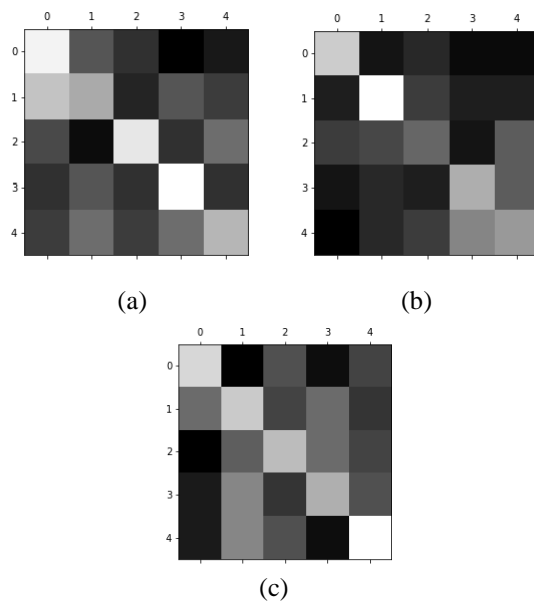


Figure 5. Confusion matrices for vowel identification using the functional connectivity features for the (a) alpha band; (b) beta band; (c) theta band.

The features from the different sub-band frequencies were separately used for analysis and classification. Based on the classification results, it is observed that the functional connectivity features obtained from the theta, beta and alpha bands were able to classify the articulated vowel. Figure 5 shows the confusion matrix for the classification of articulated vowel from the features obtained from alpha, beta and theta bands respectively. The brighter regions of the matrix represent higher classification accuracy and the darker regions represent lesser classification accuracy. Figure 6 shows the classification accuracies of the articulated vowels identified with the features extracted from theta, beta and alpha sub-bands.

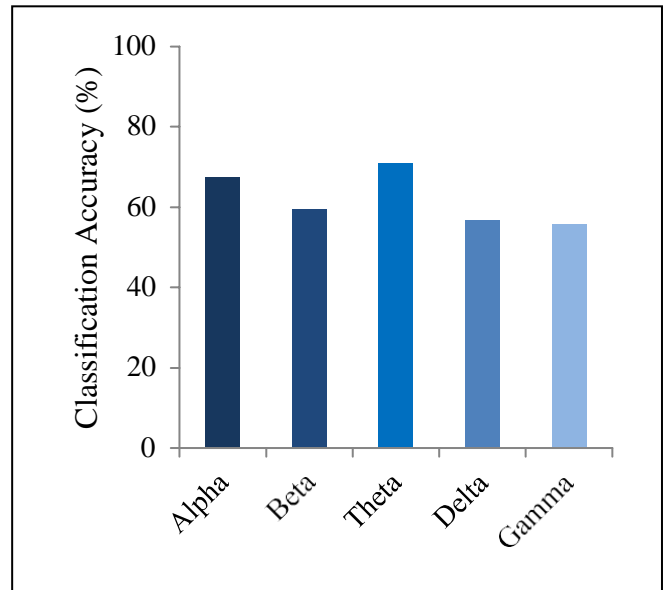


Figure 5. Classification Accuracy of the articulated vowels from theta, alpha and beta sub-bands

IV. CONCLUSION

The pre-processing routines and the connectivity analysis performed imply a better understanding about the interactions of the brain regions while speaking and imagining tasks. The conventional functional connectivity parameters were estimated for the segmented sub-band frequencies. EEG sub-band frequency analysis show higher activity in theta band during speech tasks. Also some relevant activation was observed in the alpha and beta sub-bands. The interaction between left hemispheric frontal and temporal lobes with occipital lobe was higher during speech task.

The observations prove that the brain has unique signatures during speaking every single vowel. Similar type of activations are expected to occur during the imagined speech processes. Results suggest that this non-invasive technique can be used as a method to retrieve verbal information from imagined speech. Speaking of different phoneme has different connectivity patterns in the brain that can be extracted from the EEG. Hence choosing the appropriate combination of features and machine learning technique can enable the extraction of information from the brain signals.

Acknowledgement

The authors would like to thank the Centre for Healthcare Technologies, SSN College of Engineering for the constant motivation and support towards this work. Also, we would like extend our thanks to the volunteers who participated in the study. This research did not receive any specific grant from funding agencies in the public, commercial, or not-for-profit sectors.

VI. REFERENCES

- [1]. Birbaumer, N., Kubler, A., Ghanayim, N., Hinterberger, T., Perelmouter, J., Kaiser, J., ... & Flor, H. (2000). The thought translation device (TTD) for completely paralyzed patients. *IEEE Transactions on rehabilitation Engineering*, 8(2), 190-193.
- [2]. DaSalla, C. S., Kambara, H., Koike, Y., & Sato, M. (2009, April). Spatial filtering and single-trial classification of EEG during vowel speech imagery. In *Proceedings of the 3rd International Convention on Rehabilitation Engineering & Assistive Technology* (pp. 1-4).
- [3]. Salama, M., ElSherif, L., Lashin, H., & Gamal, T. (2014). Recognition of unspoken words using electrode electroencephalographic signals. In *The Sixth International Conference on Advanced Cognitive Technologies and Applications* (pp. 51-55).
- [4]. Min, B., Kim, J., Park, H. J., & Lee, B. (2016). Vowel imagery decoding toward silent speech bci using extreme learning machine with electroencephalogram. *BioMed research international*, 2016.
- [5]. Chengaiyan, S., Retnapandian, A. S., & Anandan, K. (2019). Identification of vowels in consonant–vowel–consonant words from speech imagery based EEG signals. *Cognitive Neurodynamics*, 1-19.
- [6]. Baccalá, L. A., & Sameshima, K. (2001). Partial directed coherence: a new concept in neural structure determination. *Biological cybernetics*, 84(6), 463-474.
- [7]. Kaminski, M. J., & Blinowska, K. J. (1991). A new method of the description of the information flow in the brain structures. *Biological cybernetics*, 65(3), 203-210.
- [8]. Zhang, J., Wang, N., Kuang, H., & Wang, R. (2013). An improved method to calculate phase locking value based on Hilbert–Huang transform and its application. *Neural Computing and Applications*, 24(1), 125–132. doi: 10.1007/s00521-013-1510-z
- [9]. Lachaux, J. P., Rodriguez, E., Martinerie, J., & Varela, F. J. (1999). Measuring phase synchrony in brain signals. *Human brain mapping*, 8(4), 194-208.
- [10]. Ziehe, Andreas & Krämer, Nicole & Popescu, Florin & Müller, Klaus-Robert. (2010). Comparison of Granger Causality and Phase Slope Index. *Journal of Machine Learning Research - Proceedings Track*. 6. 267-276.

Effect of Virtual Reality on the EEG Sub-Band Frequency Powers of Autistic and Control groups

*Chrisilla S, **Anna Masciantonio, *Divya B, *Vidhusha S, *Kavitha A

*Centre for Healthcare Technologies, SSN College of Engineering, India.

**School of Biomedical Engineering, Science & Health Systems, Drexel University, Pennsylvania.

Abstract— *Cognitive load while performing a task indicates the magnitude of effort taken by the individual for the completion of the task. The effort taken by the control and autistic children vary depending on the task they perform. Virtual Reality (VR) is an emerging technology that has been considered as a learning tool for both the groups. EEG signals has been recorded and quantifiable parameters have been measured to assess the cognitive load while subjecting the children to VR platform. The derived features from theta and alpha oscillations have been considered for study. The results show that there were abnormal impairments in the theta and alpha band values in the autistic group compared to the controls. The relative power values obtained show an increase in delta band values due to enhanced neural processing and a gradual decrease in the power values of the other EEG sub-bands for both the groups. This suggests that VR can be used as a learning tool for improving the cognition of children with neurodevelopmental disorders.*

Keywords- *Virtual Reality, Autism, Band power, Relative power, Cognitive Load.*

I. INTRODUCTION

Evaluating the performance of the brain while performing a particular task is known as cognitive load analysis [2]. Load generally refers to the task given to the subject. The load can be intrinsic, extrinsic and germane depending on the difficulty. This analysis will be of great help in assessing the performance of the brain especially for children with brain disorders. Analysis of load in autistic children will help to quantify the effort taken by the group to complete a task.

Autism is a neuro developmental disorder which affects the ability of the child to interact, communicate and perform any activity [4]. These children have difficulty to learn things on their own. Researches have revealed that is changes in the brain surface and patterns of children with autism compared to the normal healthy brain. Autism may be high functioning and low functioning depending on the IQ level and social interaction. There are many special schools established to train autistic children along with parental guidance using flashcards, boards, charts and toys. Virtual Reality (VR) one among the flourishing

technologies have been found to be an effective rehabilitation tool to train autistic children.

In VR real world components can be generated as computerized figures and interactions can be made possible. Human interactions can also be made possible with the game components using VR [9]. Although VR training can be instrumental changes in bringing changes to improve the learning and communication skills the physiological changes were not assessed.

This study aims at assessing the cognitive ability of a child when they are exposed to VR environment using electroencephalogram (EEG). EEG signals were recorded using Emotiv Epoc 14 electrode system. Emotiv Epoch is a wireless technology and signals can be acquired with ease by placing the head mount over the scalp of the subject. These signals are predominant from 0.5-40 Hz and can be separated into five sub-bands delta, theta, alpha, beta and gamma depending on the frequency. From the band separated signals cognitive ability of the children were evaluated using band powers. The theta and alpha band powers were calculated to check for any cognitive impairment when the values are high [8]. Then the relative power values were obtained showing an increase in delta power. The delta band also modulates the working of neural process in the brain and carries most of the information regarding the cognitive load in this study [15]. More research work can be carried out on the deltaband functions related to cognition and working memory.

II. METHODOLOGY

Six participants comprising three autistic children between the age group 5-8 years were subjected to the VR environment developed and EEG signals were acquired correspondingly. Signals were acquired using the protocol shown in fig 1.

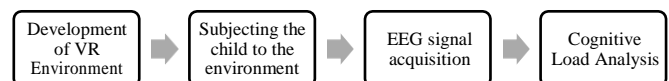


Figure 1. Methodology for signal acquisition from children

Signals were acquired from three healthy children and three autistic children at NIEPMD, Muttukadu, Chennai.

The children were accompanied by their parent and the experimental procedures were explained in detail. EEG signals were acquired using Emotiv Epoc using the protocol in fig 2. Before the acquisition it was ensured that the child was made comfortable to the wear the VR HMD and the EEG headset.

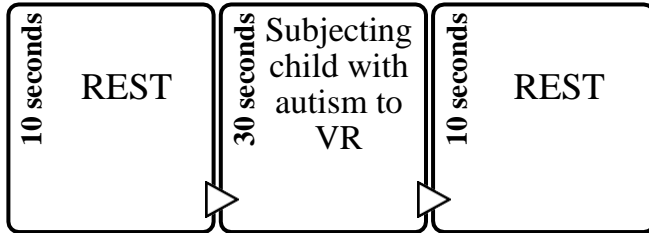


Figure 2. Protocol implemented

Signals were acquired when the child was subjected to the VR environment with a rest of 10 seconds at the beginning and end of the session. The same protocol was implemented to find the cognitive load for three normal children as control group. Fourteen electrodes AF3, F7, F3, FC5, T7, P7, O1, O2, P8, T8, FC6, F4, F8, AF4 were used for acquisition and analysis using Emotiv Epoch. Signals acquired were pre-processed using butterworth band pass filter and separated into delta, theta, alpha, beta and gamma bands. From the band separated signals, the theta to alpha ratio and the relative power values were estimated based on the electrode regions and were also analyzed for different EEG sub-bands.

A. Cognitive Load Analysis

In this study an intrinsic load is given to the children which evaluates the working memory for the controls and the autistic group and the cognitive load is evaluated.

From the filtered and band separated EEG signals the theta and alpha power values were determined to assess the working memory. Any alteration in the theta and alpha power were reported as impairment.

Along with Theta and Alpha band values the relative power is also determined for the various sub-bands.

$$\text{Relative Power} = \frac{\text{Band Power}}{\text{Total Power}} \quad (1)$$

Band power is the average of power values computed from the frequency spectrum of each sub-bands. It is one of the marker functions for cognitive load analysis. Total power is given by the sum of all the five EEG sub-band powers.

III. RESULTS

EEG signals acquired from three autistic and control groups were filtered using butterworth bandpass filter and separated into five EEG sub-bands. The corresponding power spectrum of the signals were also plotted.

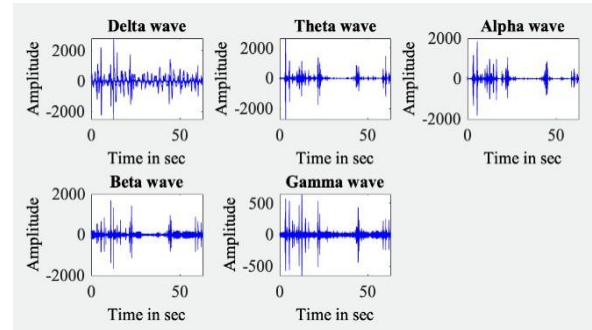


Figure 3. Band separated EEG signals

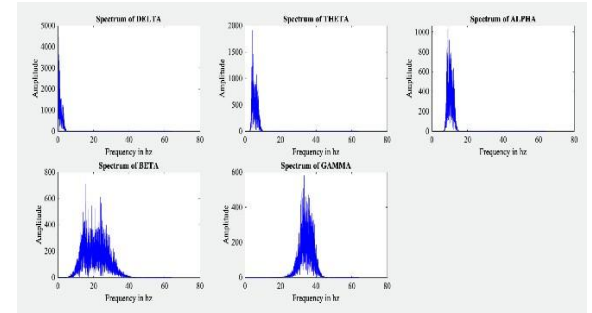


Figure 4. Power spectrum of the EEG sub-bands

From the filtered and band separated EEG signals separated into independent components to find out the active region while performing the task. The results obtained show that there is higher activity in most of the regions in normal children when compared to the autistic group. There are only few region activations in the autistic children when they are subjected to the VR environment. But in both the autistic and normal group there are activations in the frontal regions.

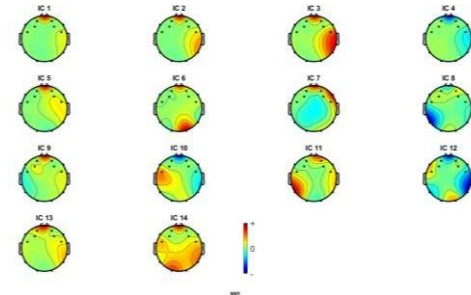


Figure 5. ICA of autistic children

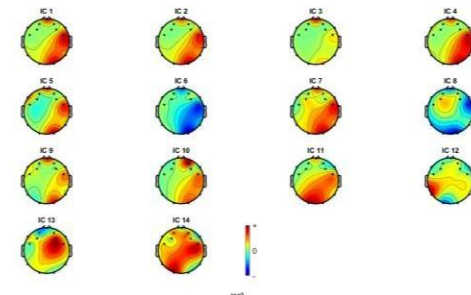


Figure 6. ICA of normal children

Fig 5 and 6 shows the active regions when the children are subjected to the VR. In order to determine the cognitive

load, theta and alpha power values was computed. This parameter estimates the amount of load given to the regions.

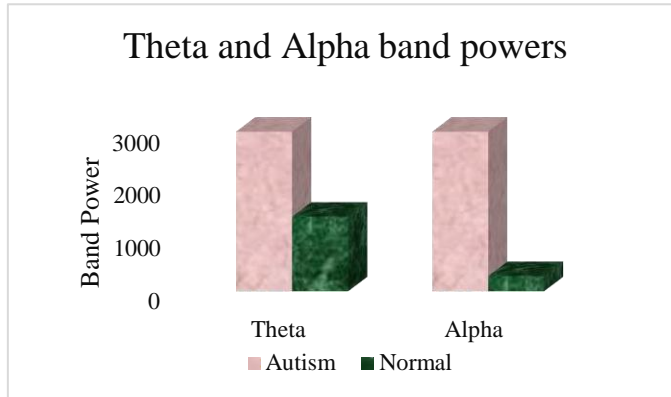


Figure 7. Theta and Alpha powers of autistic and normal children

The Theta and Alpha values from fig 7 shows that there is more load on the autistic brain when compared to the normal children. TAR values are obtained by the ratio of theta and alpha bands. This increase in the alpha and delta values show that there is cognitive impairment and can relate to the severity of autism with increase in work load.

The relative powers of the left and right hemisphere electrodes are also found and plotted to find the activation region during the task. From the results obtained it has been inferred that there is higher delta activity in both the autistic and normal children such that both exhibit similar cognitive functions. The relative power values gradually reduce from delta to the gamma for both the autistic and control groups. The values of the control group are found to be higher compared to the autistic group. The delta band which is predominantly present in the prefrontal cortex plays an important role in cognition and decision making hence the results infer that .

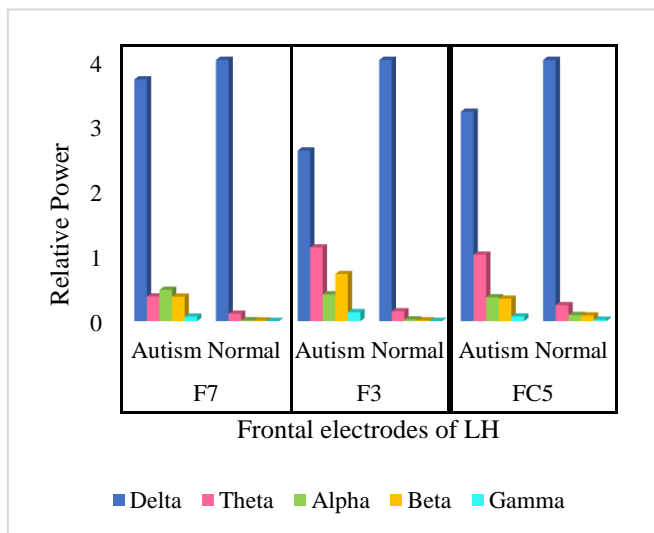


Figure 8. Left Hemisphere Frontal electrode relative power

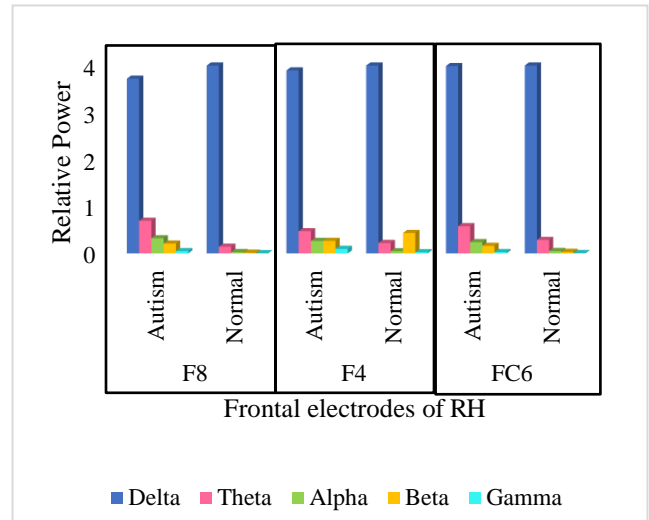


Figure 9. Right Hemisphere relative power values

Fig 8 and 9 shows the electrode activations in the right and left hemispheres of the autistic and control group respectively where the relative power of delta bands are high when compared to the other sub-bands.

IV. CONCLUSION

Cognitive load analysis is an important parameter to study the working of the brain when a task is performed. This paper discusses the effect of VR to evaluate the learning ability of normal and autistic children. The activations of the brain regions obtained show that during the performance of an intrinsic task, all the regions have equal activity in the control group but region-specific activation was observed in the autistic group. There was more activation in the frontal and occipital regions. Since frontal regions were activated there is a chance to help autistic children to learn from the VR environment when compared to the conventional methods. The occipital lobe activations suggest that there is an increased concentration among the autistic group. Thus, VR can be implemented as an effective and an alternative learning and training tool for children with autism.

The theta and alpha band powers is an important parameter in the cognitive load analysis. It estimates effective functioning of brain and increased values of autistic group indicate cognitive impairment. The value obtained was higher for autistic when compared to the control group indicating cognitive impairment.

The relative powers were estimated for the left hemisphere electrodes AF3, F7, F3, FC5, T7, P7, O1 and for the right hemisphere electrodes O2, P8, T8, FC6, F4, F8, AF4 separately. The delta band values were high for both the groups and gradually decreasing for the other sub-bands. The delta band present in the prefrontal region determines various effective cognitive processing. It is known that important decision-making neural processing tasks is primarily due to the delta band. The results show that when the controls and autistic children are subjected to the VR environment exhibit similar characteristics thus, VR can be

used as an effective learning tool. Hence VR can be thought as an alternative learning technology for autistic children to improve their cognitive abilities.

ACKNOWLEDGMENT

The authors would like to thank National Institute for Empowerment of Persons with Multiple Disabilities, Muttukadu, Chennai and the Department of Biomedical Engineering, SSN College of Engineering, Chennai for the successful completion of the research study.

REFERENCES

- [1] Alwedaie, Sayed Ahmed, Et Al. "Eeg-Based Analysis For Learning Through Virtual Reality Environment." *Journal Of Biosensors And Bioelectronics* 9.1 (2018): 249.
- [2] Amaral, C., Mougá, S., Simões, M., Pereira, H. C., Bernardino, I., Quental, H., ... & Castelo-Branco, M. (2018). A Feasibility Clinical Trial To Improve Social Attention In Autistic Spectrum Disorder (Asd) Using A Brain Computer Interface. *Frontiers In Neuroscience*, 12, 477
- [3] Başar, Erol, Et Al. "Gamma, Alpha, Delta, And Theta Oscillations Govern Cognitive Processes." *International Journal Of Psychophysiology* 39.2-3 (2001): 241-248.
- [4] De Vries, Marieke, And Hilde M. Geurts. "Cognitive Flexibility In Asd; Task Switching With Emotional Faces." *Journal Of Autism And Developmental Disorders* 42.12 (2012): 2558-2568.
- [5] Ferreira, Camila, Et Al. "Electroencephalographic Changes After One Nighth Of Sleep Deprivation." *Arquivos De Neuro-Psiquiatria* 64.2b (2006): 388-393.
- [6] Harmony, Thalia. "The Functional Significance Of Delta Oscillations In Cognitive Processing." *Frontiers In Integrative Neuroscience* 7 (2013): 83.
- [7] Israely, Inbal, Et Al. "Deletion Of The Neuron-Specific Protein Delta-Catenin Leads To Severe Cognitive And Synaptic Dysfunction." *Current Biology* 14.18 (2004): 1657-1663.
- [8] Larrain-Valenzuela, Josefina, Et Al. "Theta And Alpha Oscillation Impairments In Autistic Spectrum Disorder Reflect Working Memory Deficit." *Scientific Reports* 7.1 (2017): 1-11.
- [9] Maples-Keller, J. L., Bunnell, B. E., Kim, S. J., & Rothbaum, B. O. (2017). The Use Of Virtual Reality Technology In The Treatment Of Anxiety And Other Psychiatric Disorders. *Harvard Review Of Psychiatry*, 25(3), 103.
- [10] Mckinnon, Claire J., Et Al. "Restricted And Repetitive Behavior And Brain Functional Connectivity In Infants At Risk For Developing Autism Spectrum Disorder." *Biological Psychiatry: Cognitive Neuroscience And Neuroimaging* 4.1 (2019): 50-61.
- [11] Oberman, Lindsay M., Et Al. "Eeg Evidence For Mirror Neuron Dysfunction In Autism Spectrum Disorders." *Cognitive Brain Research* 24.2 (2005): 190-198.
- [12] Starr, Elizabeth M., Et Al. "How Are Schools Doing? Parental Perceptions Of Children With Autism Spectrum Disorders, Down Syndrome And Learning Disabilities: A Comparative Analysis." *Education And Training In Developmental Disabilities* (2006): 315-332.
- [13] Ulam, F., Et Al. "Cumulative Effects Of Transcranial Direct Current Stimulation On Eeg Oscillations And Attention/Working Memory During Subacute Neurorehabilitation Of Traumatic Brain Injury." *Clinical Neurophysiology* 126.3 (2015): 486-496.
- [14] Vogan, Vanessa M., Et Al. "The Neural Correlates Of Visuo-Spatial Working Memory In Children With Autism Spectrum Disorder: Effects Of Cognitive Load." *Journal Of Neurodevelopmental Disorders* 6.1 (2014): 19.
- [15] Zarjam, Pega, Julien Epps, And Fang Chen. "Characterizing Working Memory Load Using Eeg Delta Activity." 2011 19th European Signal Processing Conference. Ieee, 2011.

Analysis of Physiological Signals During Therapeutic Yoga Practice

R.Anandha Praba,
Department of Electronics and Communication
Engineering,
Meenakshi College of Engineering, Chennai, Tamilnadu,
India.
anuprem83@gmail.com

E.S.SelvaPriya L. Suganthi, T.Nandini, D.Sindu,
M.Muthu Vijay
Department of Bio-Medical Engineering,
Sri Sivasubramaniya Nadar college of Engineering,
Kalavakkam, Kancheepuram, - 603110, Tamil Nadu, India.
suganthil@ssn.edu.in

Abstract— Practicing yoga has become more effective among all kind of age groups, but researches focusing on the movement related yoga postures are limited. This work analysis the effect of therapeutic yoga on biosignals. Physiological parameter variations between yoga trainers and untrained subjects while performing the selected asanas including pranayama, dwipadapitham, apanasana, jathara parivrtti has been studied. ECG and EMG are acquired simultaneously before, during and after the specially framed yoga practice sequence. These signals are processed suitably to measure the time and frequency domain features and analyze their variations over the period of recording. HRV analysis shows variation of MHR, LF/HF and SD1/SD2 with increase during posture and decrease with rest. pNN50 shows decrease during posture and increase during rest. Further study will helpful in designing special yoga course for individuals based on their requirements and thus complementing their medical support as well.

Keywords— HRV analysis, EMG analysis, pranayama, dwipadapitham, apanasana, jathara parivrtti, therapeutic yoga practice.

I.INTRODUCTION

Yoga has many physiological and psychological benefits. Numerous studies have asserted that yoga practice improves flexibility and strength. Yoga also includes a physical component that, according to research, has many positive effects. Yoga therapy is tailor-made, suiting the specific needs of the individuals, delivered by specialized yoga therapists. Yoga practices generally involve systematic breathing and bodily movements that strengthen, stretch and stabilize the body, thereby improving blood circulation, respiratory functions, emotional and physiological balance, and specifically, targeting the natural recuperative bodily powers. [1].

There are various review articles in Yoga and its effects on brain signals, pulmonary function, management of chronic diseases, type 2 diabetes, cerebrovascular attack rehabilitation, prevention of cardiovascular disease and prevention of coronary heart disease and the hypertension [2-8].

Heart rate variability (HRV) is a noninvasive tool for assessment of cardiac autonomic status [9, 10]. It is found that yoga introduces consistent physiological changes in the Heart rate and the effect of suryanadi (SNP) and

Chandranadi pranayama (CNP) on Heart rate variability (HRV) was studied in healthy volunteers [11]. The study revealed that time domain analysis of SNP revealed an increased heart rate with a decreased RMSSD, However the SDNN was increased. Frequency domain analysis, increased LF power and decreased HF power and LF/HF ratio increased after the intervention.

Physiological activity of the motor unit was reflected in the parameters analysed with Surface EMG signals [12]. Researchers studied the effect of yoga on muscular activity and improvement in grip strength [13,14] The electromyographic activity of the rectus and external oblique abdominal muscles were studied while performing the pelvic tilt and other abdomen exercises. The abdomen-hollowing exercise was found to produce the least rectus and external oblique muscle activity compared to that with a pelvic tilt [15].

A study focussed on investigating the effect of Iyengar yoga and EMG biofeedback on the functional disability in patients suffering from chronic knee osteoarthritis. Results revealed that patients underwent Iyengar yoga showed increased resistance to pain and improved functional ability. The study concluded that Iyengar yoga, together with the conventional therapy offered better pain reduction and increased functional ability in patients suffering from chronic unilateral knee osteoarthritis. [16].

With the increase in population and diseases, the need for Yoga practice has gained popularity the recent decades. The main aim of the work is to analyse the variations in bodily physiological parameters before, during and after taking up therapeutic yoga practice. The results of this study can be used to boost the reliability and effectiveness of yoga practice.

II.METHODOLOGY

A. Data acquisition

This work was approved by at Krishnamacharya Yoga Mandiram (KYM), Mandaveli, Chennai.

Subjects who are under medication for any diseases, with mental illness, chronic smoking, and alcoholism were excluded from this study. The experimental protocol was approved by the Institutional Ethics

Committee. A written informed consent was obtained from each subject. The consent form had an explanatory attachment which gives the basic concepts of ECG and EMG easily understandable to the subjects are given before starting the experiment. The consent form itself had various statements acknowledging the subject's willingness to be a part of the study. After getting the consent of the subject a data collection form was filled. It had personal details about the subject and also basic clinical data like Blood pressure, Pulse, Body temperature measured using a Digital thermometer and OMRON digital blood pressure monitor.

We considered twelve yoga trainers and ten untrained subjects for this study. Subject physiological parameters have been given in table 1.

TABLE I. SUBJECT CHARACTERISTICS

Variable	Mean ± SD value of subject characteristics	
	Yoga trainers	Untrained subjects
Number of participants(n)	12	10
Age(years)	42±10	42±8
Weight(kgs)	64±7	66±10
Height(cms)	168.92±7.87	164.3±9.68
Body Temperature (F) Before	98.2±0.7	98.26±0.63
Blood pressure (mmHg) Before	130/79	117/75
Pulse(BPM) Before	78±6	75±11
Body Temperature(F) After	98.5±0.5	98.5±0.47
Blood pressure(mmHg) After	129/79	117/76
Pulse(BPM) After	75±5	80±8

B. Experimental protocol

We considered therapeutic effects for lower trunk problems like lower abdominal pain, back pain, spinal problems, digestive problems etc. So, the asanas were finalized after a demo and all further considerations. The recording procedure consisted of 4 practices with equal amounts of resting in between the postures. To consider conditions before and after the procedure, measurements were taken at sitting posture prior to the start and at complete lie down rest after the poses. The recording process is shown in Figure 1.

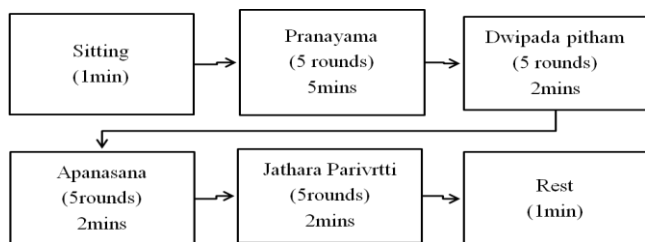


Fig. 1. Recording Setup

The procedure time is up to subject's individual variations. So, each asana was recorded for five rounds rather than exact time definitions. Every asana had individual effects. More than standing in the correct posture for long, synchronizing the body, breath and mind matters the most.

Dwipada pitham:

Dwipada pitham is a vinyasa, a dynamic movement that is coordinated with the inhalation and exhalation. This simple practice can be used in a variety of ways to release tension from the spine and breathing structures. It stimulates abdominal organs, lungs & thyroid glands. It is suggested as therapeutic asana for asthma, high BP, osteoporosis & sinusitis. Figure 2 shows the posture of Dwipadhapitham..

[Grab your reader's attention with a great quote from the document or use this space to emphasize a key point. To place this text box anywhere on the page, just drag it.]

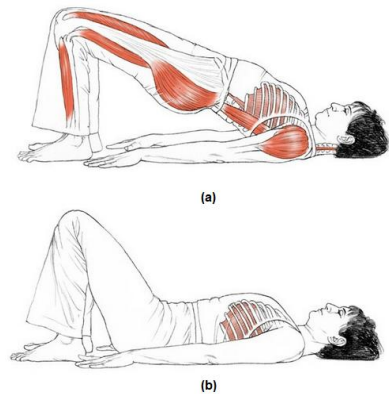


Fig. 2. Dwipadhapitham (a)Inhalation (b) Exhalation

Apanasana:

Apanasana is usually a movement into and out of the pose with the breath. Apanasana is frequently recommended to promote health and optimal functioning of the digestive, urinary, and sexual organs. This asana relieves the pressure of force, helping the body to efficiently reduce and expel waste, toxins, and tension. Figure 3 shows the posture of Apanasana during inhalation and exhalation. .

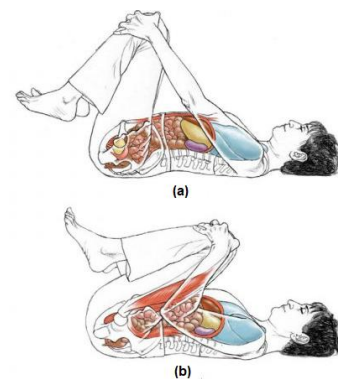


Fig. 3. Apanasana (a)Inhalation (b) Exhalation

Jathara parivritti:

Jathara parivritti is an asymmetrical supine twisting pose. Jathara parivritti is done for releasing lower back stiffness; helps to release tension for those people who have sedentary desk bound jobs. It tends to stimulate the abdomen. It assists in easy breathing. It helps in strengthening the digestive force. Figure 3 shows the posture of Jathara parivritti.

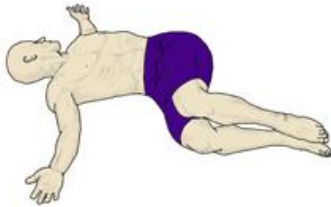


Fig. 4. Jatharaparivritti

Pranayama:

Pranayama is control of Breath. One can control the rhythms of pranic energy with pranayama and achieve healthy body and mind. Prana is upward flowing and Apana is downward flowing. Practice of Pranayama achieves the balance in the activities of these pranas, which results in healthy body and mind. We considered Nadi Shuddhi Pranayama or Anuloma - Viloma (Alternate nostril breathing -I). Figure 3 shows the posture of Pranayama.



Fig. 5. Pranayama

C. Electrode Placements and signal acquisition

Ag-AgCl surface electrodes were affixed to the skin surface of subjects with lead wires connected to the amplifier boards and then to the BITALINO kit. Initially, the skin was cleaned with spirit wipes after hair removal and electrodes were stuck. To record ECG activity electrodes were placed at chest collar bones and reference at neck spine bone. To monitor EMG activities in the abdominal area, Rectus abdominal position was selected. Figure 6 shows the arrangement of electrodes to record ECG and EMG.

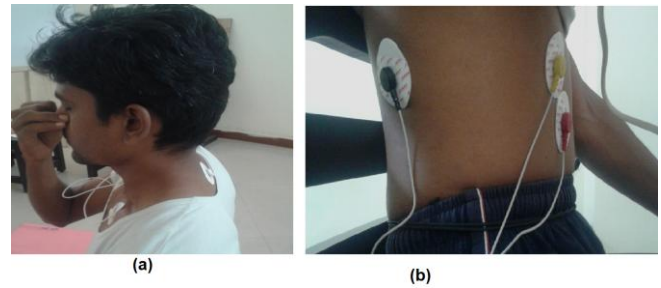


Fig. 6. (a) ECG electrode placements and EMG electrode placements

After explaining the procedure and collecting preliminary data from the subjects, the ECG and EMG signals were acquired using BITALINO kit and transmitted via bluetooth to a nearby laptop. It is visualised live as it is received using Opensignals software. These signals are recorded during sit, 4 yoga practices and rest and saved as text files for further processing. After the procedure, the subject's Blood pressure, body temperature and pulse were again measured.

III. SIGNAL PROCESSING AND PARAMETER EXTRACTION

A. Analysis of Electrocardiography (ECG)

The recorded ECG signal was measured from collar bone and had some amounts of baseline noise as well as DC offset added with it. To remove this we processed the signal by applying IIR high pass filter of 0.05Hz first which removed much of the noise. Then an IIR low pass filter of 20 Hz was applied to correct it further. This gave an almost clean signal without much distortion. The respiratory pattern variations were seen in the amplitude of the ECG signal. This could significantly show the cycle variations during the recording procedure. Then the time at R peaks were measured to obtain the R-R interval of the recording process. Figure 7 shows the raw ECG signal and filtered signal.

This file containing R-R intervals was processed using KUBIOS HRV ANALYSIS software to get the various Heart Rate Variability (HRV) parameters. The time-domain and geometrical parameters considered were Mean Heart Rate (MHR), pNN50.

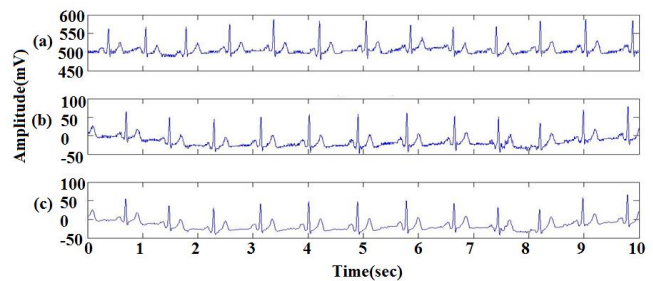


Fig. 7. (a) Raw ECG waveforms (b) High pass filtered ECG signal (c) High pass and low pass filtered ECG signal

The frequency-domain parameter considered was LF/HF ratio. Poincare plot parameter considered was

SD1/SD2 ratio to see R-R interval variation on long-term and short-term basis.

B. Analysis of Electromyography (EMG)

The EMG signal was recorded from Rectus abdominal position so there was ECG interference which was applied with a FIR high pass filter of 50Hz to be corrected. Much of this ECG noise was removed and then further processed using MATLAB software to detrend the signal and detect the linear envelope. The Power spectrum of the filtered signal was obtained in MATLAB and the frequency that divides the powers into two equal halves was noted as median frequency. From the linear envelope time-domain parameters like Peak amplitude, Mean amplitude, RMS value were obtained. These 4 parameters were compared for analysis.

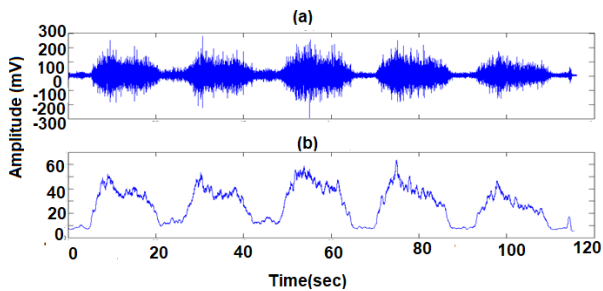


Fig. 8. (a) High pass filtered EMG signal (b)Envelope of EMG of Yoga trainer during apanasana
 Figure 8 (a) and (b) shows the High pass filtered EMG signal and envelope of EMG of Yoga trainer during apanasana. Similarly Figure 9 (a) and (b) shows High pass filtered EMG signal and envelope of EMG of untrained subjects during apanasana.

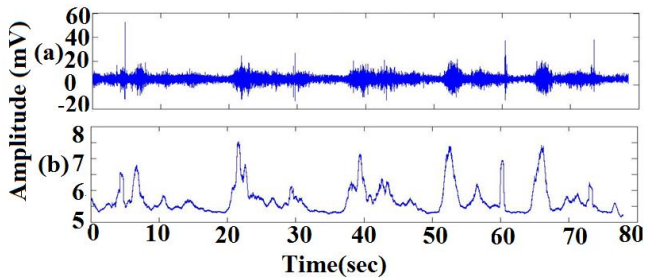


Fig. 9. (a) High pass filtered EMG signal (b)Envelope of EMG of untrained subject during apanasana

IV. RESULTS AND DISCUSSION

HRV analysis shows mean HR increases while performing the different asanas and reducing while come to rest for both yoga trainers and untrained subjects, But mean HR is less for Yoga trainers than untrained subjects. for yoga trainers PNN50 is reducing while performing the different assans and inceresing in rest condition. But it is not obsered in untrained subject. LF/HF is significantly high (P<0.05) while performing asanas than in rest for yoga trainers but LF/HF is less in untrained subjects in all the activity. Untrained subject group HRV parameters varies among individuals. Time domain analysis revealed an

increased heart rate with a decreased RMSSD, However the SDNN was increased. Frequency domain analysis, increased LF power and decreased HF power and LF/HF ratio increased after the intervention. Figure 10 shows the HRV analysis of various parameters with subject to Yoga trainers and untrained subjects.

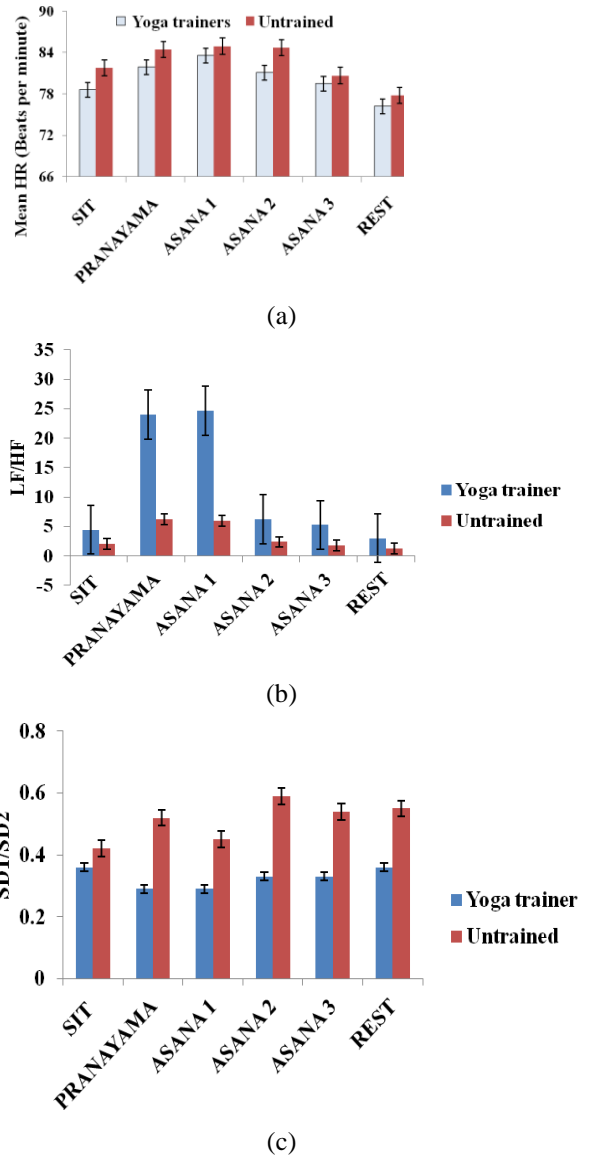
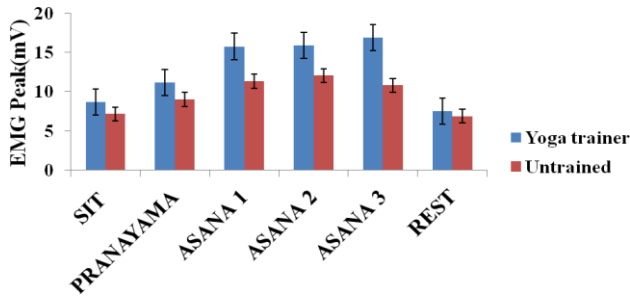
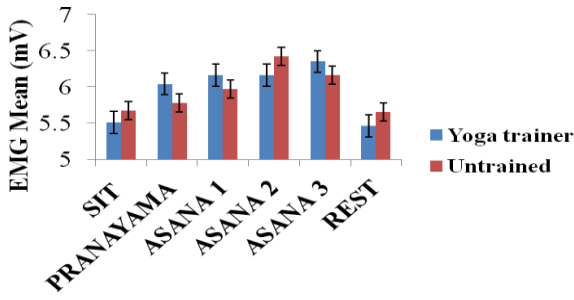


Fig.10. HRV Analysis of (a) Mean HR (b)LF/HF (c) SD1/SD2 for Yoga trainers and untrained subjects.

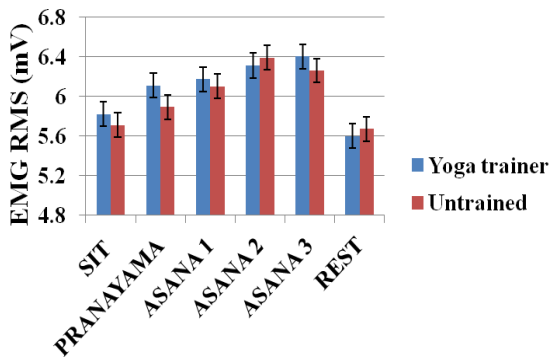
EMG signal analysis shows EMG peak value, and median frequency is high s while performing the different asanas and reducing while come to rest for both yoga trainers and un trained subjects, But EMG peak is significantly high (P<0.05) for Yoga trainers than untrained subjects. For yoga trainers EMG mean and RMS value is increasing consistantly while performing the different assans and reducing in rest condition. But it is not obsered in untrained subject. In untrained subject group EMG parameters varies among individuals. Figure 11 shows the analysis of various EMG parameters with subject to Yoga trainers and untrained subjects.



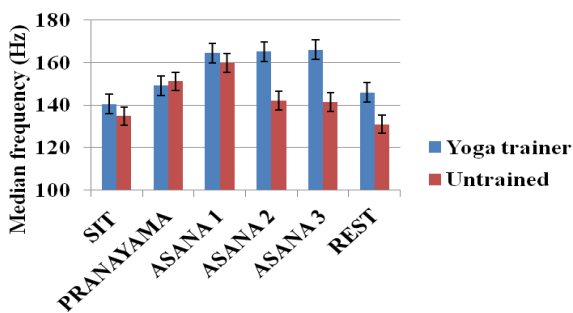
(a)



(b)



(c)



(d)

Fig.11. Analysis of EMG Parameters (a) EMG Peak (b)Mean (c) RMS (d) Median Frequency for Yoga trainers and untrained subjects.

V. CONCLUSION

Variations in HRV parameters and EMG parameters during yoga practices have been studied in this work. Yoga trainer's parameter variations show well-coordinated long-term regular practice while patient variations signify highly

variable short-term practice. In this study shows that consistent yoga practice can show significant parameter variations in physiological signals and also have improved therapeutic effects. In future the work can be extended to Inter-subject variability analysis for comparison and to analyse variations in various other parameters not considered in this study.

Conflicts of interest

There are no conflicts of interest.

Acknowledgment

We would like to thank. Dr. Latha Sathish, Research Head, and Yoga trainers of Krishnamacharya Yoga Mandiram (KYM) Chennai for their moral support in data collection.

REFERENCES

- [1] Woodyard C. Exploring the therapeutic effects of yoga and its ability to increase quality of life. *International journal of yoga*. 2011 Jul;4(2):49.
- [2] Desai R, Tailor A, Bhatt T. Effects of yoga on brain waves and structural activation: A review. *Complement Ther Clin Pract*. 2015;21:112–8.
- [3] Abel AN, Lloyd LK, Williams JS. The effects of regular yoga practice on pulmonary function in healthy individuals: A literature review. *J Altern Complement Med*. 2013;19:185–90.
- [4] Desveaux L, Lee A, Goldstein R, Brooks D. Yoga in the management of chronic disease: A systematic review and meta-analysis. *Med Care*. 2015;53:653–61.
- [5] Innes KE, Selfe TK. Yoga for adults with type 2 diabetes: A systematic review of controlled trials. *J Diabetes Res* 2016. 2016:6979370.
- [6] Lynton H, Kligler B, Shiflett S. Yoga in stroke rehabilitation: A systematic review and results of a pilot study. *Top Stroke Rehabil*. 2007;14:1–8.
- [7] Hartley L, Dyakova M, Holmes J, Clarke A, Lee MS, Ernst E, et al. Yoga for the primary prevention of cardiovascular disease. *Cochrane Database Syst Rev*. 2014;5:CD010072.
- [8] Cramer H, Lauche R, Haller H, Steckhan N, Michalsen A, Dobos G. Effects of yoga on cardiovascular disease risk factors: A systematic review and meta-analysis. *Int J Cardiol*. 2014;173:170–83.
- [9] Jovanov E. On spectral analysis of heart rate variability during very slow yogic breathing. In 2005 IEEE Engineering in Medicine and Biology 27th Annual Conference 2006 Jan 17 (pp. 2467-2470). IEEE.
- [10] Thanuja ES, Suganthi L. Effect of integrated yoga on cardiovascular parameters during pregnancy. In 2017 International Conference On Intelligent Computing And Control Systems (ICICCS) 2017 Jun 15 (pp. 804-809). IEEE.
- [11] Rajajeyakumar.M, Ananda Balayogi, Immediate effect of different Pranayama on Short term Heart rate variability in Health care students, ISSN-2320-6039 Vol-2, International journal of Physiology, Jan-June 2014.
- [12] Ruchika, Shalini Dhingra, An Explanatory Study of the Parameters to Be Measured From EMG Signal, International Journal Of Engineering And Computer Science ISSN:2319-7242, Volume 2 Issue 1 Jan 2013.
- [13] Petrofsky JS, Cuneo M, Dial R, Morris A. Muscle activity during yoga breathing exercise compared to abdominal crunches. *Journal of Applied Research in Clinical and Experimental Therapeutics*. 2005 Nov 1;5(3):501.
- [14] Dash M, Telles S. Improvement in hand grip strength in normal volunteers and rheumatoid arthritis patients following yoga training. *Indian journal of physiology and pharmacology*. 2001 Jul;45(3):355-60.
- [15] Cheri.L Drysdale,et al., Surface electromyographic activity of the abdominal muscle during pelvic tilt and abdominal hollowing exercises, *Journal of Athletic training*,39(1):32-36,2004.

- [16] Nambi GS, Shah AA. Additional effect of iyengar yoga and EMG biofeedback on pain and functional disability in chronic unilateral knee osteoarthritis. International journal of yoga. 2013 Jul;6(2):123.

A Novel VLSI Architecture of CORDIC Based Image Registration

Anirban Chakraborty

Electronics and Telecommunication Engineering
IIEST, Shibpur
Howrah, West Bengal -711103
acanirban@gmail.com

Ayan Banerjee

Electronics and Telecommunication Engineering
IIEST, Shibpur
Howrah, West Bengal -711103
ayan@telecom.iests.ac.in

Abstract— Now-a-days real-time image registration (IR) has been emerged as a potential field of research by virtue of its vast applicability. Despite such high demand, till now, most of the real-time IR based applications rely upon software based tools for performing the image registration task. Those software based tools need to be highly sophisticated to comply with the performance of any real-time system. Naturally, the real-time IR system is costly and power consuming in nature. The only cost-effective solution for this is to develop a dedicated hardware catering real-time IR. In this article, a novel VLSI architecture for real-time IR has been presented. With an ardent focus on making the proposed architecture cost-economic, the transform model estimation (TME) step of IR method is realized using co-ordinate rotation digital computer (CORDIC) technique which is popularly regarded as hardware efficient. The proposed CORDIC based TME architecture is utilized to realize the state of the art VLSI architecture of real-time IR in terms of dedicated hardware which has been implemented onto Zynq UltraScale+ MPSoC series FPGA. The performance of the proposed and FPGA-implemented VLSI architecture of the IR has been compared with its software based counterpart using MATLAB. The proposed VLSI architecture of IR has been proved to outperform the software based realizations in terms of area, power consumption and speed of operation, thereby emerging as a cost-economic solution for the real-time IR.

Keywords--- Image registration; TME; CORDIC; VLSI architecture; FPGA, Pipelining

I. INTRODUCTION

Image registration is the procedure of aligning two or more images of the same scene captured at different point of time, from different spatial positions or by different imaging equipment. The process of IR helps in eradicating certain imaging issues, like relative rotation, scaling and skew, which are commonly encountered while coalescing information scattered into different images of the same scene or the same object. By means of IR, a set of relatively rotated, translated, scaled and sheared images is brought into line with a particular reference frame. Most often, the reference frame or image itself is any constituent image of

the set of source images. The source images which are relatively rotated and translated with respect to the reference image are called moving images or floating images [1, 2]. In Fig. 1, the inputs and output of an arbitrary IR method have been exemplified. Fig. 1 (a) and (b) depict the reference and the floating image, which are inputs to the IR method, while Fig. 1 (c) is the output registered image. The images are taken from the ‘H2OPM Image Registration Dataset [3]’.

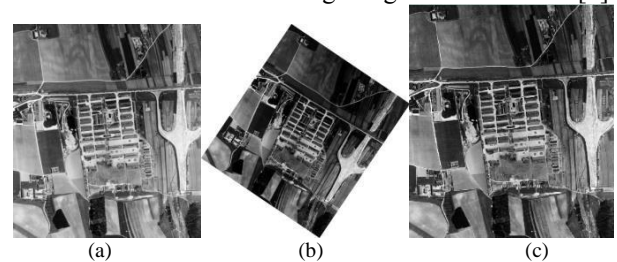


Fig.1. The inputs and output of a typical IR method; (a) reference image; (b) floating image; (c) registered image

The steps involving any standard IR consist of feature detection, feature matching, transform model estimation, and image transformation. The sequence of these integral steps is shown in Fig.2.

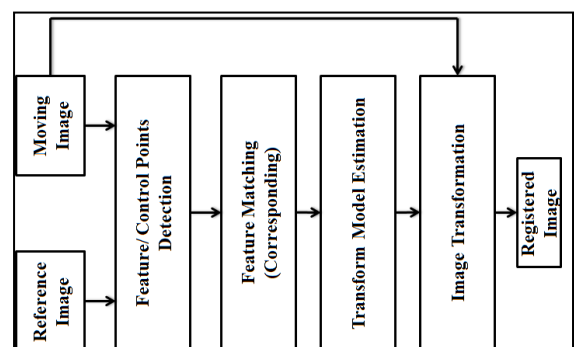


Fig. 2. General steps of standard IR technique

The transform model estimation (TME) step bears a large share of the total computational load of any IR algorithm. In another word, it can be stated that the

reduction of the computational load of the TME step, in turn, significantly reduces the computational complexity of the IR algorithm. As our research work is focused on the VLSI architecture design of IR algorithms, unsurprisingly, our hardware-oriented techniques are formulated by nurturing this TME step. Images can undergo several geometrical transformations like rotation, translation, and scaling, shearing, and projective transformation. According to the types of transformation an image experienced, there exist, certain transformation models, i.e., similarity transform, affine transform and projective transform [4-6]. Different types of 2D geometrical transformations along with the conventional matrix algebra based method to represent or model such transformation can be found in [6].

In this article, a novel and cost-effective VLSI architecture for real-time IR has been presented. The TME step of any standard IR method is the most time consuming one. In the proposed architecture, the TME step is realized using CORDIC based technique exploiting the inherent hardware efficiency of CORDIC. The CORDIC based first of its kinds IR architecture exhibits superiority over its software based counterpart and also over few hardware based IR realizations available in the literature.

The rest of the paper is organized as follows. Section II demonstrates the existing VLSI architectures for real-time IR applications. Section III presents the proposed CORDIC based VLSI architecture for real-time IR. The performance assessment of the proposed VLSI architecture is scripted in Section IV. Finally, Section V concludes the article.

II. LITERATURE REVIEW

In this section, the existing VLSI architectures for real-time IR are briefly described along with their advantages and disadvantages. In the year 2007, Gupta et. al. [7] designed a dedicated VLSI architecture for real-time exhaustive search technique based IR. The designed architecture also realized normalized cross-correlation function, mean square error and blue screen technique algorithm. The author developed the architecture following a data flow design approach that took inputs serially while performed parallel processing. The performance of the designed architecture had been comparatively evaluated with other existing architectures for establishing the supremacy. The author had designed the architecture by making provisions of being cascaded for reducing the computation time at the cost of proportional area and power overhead. The computation time of the presented architecture depends upon the size of both the reference as well as moving images.

In the year 2015, Mishra et. al. [8] developed a Demon approximation technique based non-rigid IR algorithm. The proposed algorithm is claimed to have achieved 15% better PSNR and 17% reduction in registration time for 256 X 256 sized images in comparison to other existing Demons

algorithm. After evaluating the performance of the algorithm in MATLAB, the authors synthesized the algorithm in Virtex XC6VLX760-2-FF1760 FPGA. The synthesized design was capable to be operated at a maximum operating speed of 174 MHz. The synthesized design was 30 to 40 times faster than the software counterpart. The advantage of the presented design was that the data path (computation time) would not change significantly with varying image size provided each pixel was represented by 8 bit. The computation time might increase notably with the bit precision. But the memory requirement of the design would change substantially with varying image size.

Though the works of [7, 8] developed VLSI architectures following some specific IR methods which are completely different to ours method, we have compared the performance of those architectures of [7, 8] as the main motto or applicability of those architectures are similar to our established VLSI architecture. Before performing the performance evaluation, we have deliberately realized the architectures of [7] and [8] using VHDL coding in Xilinx Vivado 18.2 tool and implemented those designs to the same platform as ours, i.e., Xilinx Zynq UltraScale+ MPSoC FPGA (XCZU7EV-2FFVC1156). After that, we have applied one reference and one floating (rotated and translated) images of size 256 X 256 images to the inputs of the FPGA. The pixel intensity for each image is represented using 16 bit fixed point binary representation. The images are taken from 'H2OPM Image Registration Dataset' [3] and resized to 256 X 256 using 'imresize' command of MATLAB before being applied to the inputs of the FPGA. The qualities of the output registered images for both the architecture of [7, 8] are assessed in MATLAB.

III. PROPOSED METHOD AND ARCHITECTURE

To fulfill our objective of designing dedicated VLSI architecture for real-time IR, at first, a unique 2D TME method is framed where the time complexity sub-linearly varies with the accuracy, i.e., bit precision. For formulating the proposed 2D TME method, the semi-iterative CORDIC method of the paper [9] is utilized. The CORDIC method of the paper [9] is termed by us, in the rest of this paper, as logarithmic CORDIC (LCORDIC) as its time complexity logarithmically varies with the accuracy. The proposed CORDIC based computation-efficient 2D TME technique is integrated with other standard IR steps to develop a low complexity and hardware realizable IR method. Then the proposed IR method is realized in terms of dedicated VLSI architecture. In this section, the procedure of formulating the proposed 2D TME method is illustrated followed by the descriptions of its respective VLSI architecture.

A. Proposed 2D TME Method (CORDIC Based)

Our formulated LCORDIC based maiden 2D TME method has such a low computational complexity that makes it possible to be realized in terms of dedicated VLSI

architecture. The pseudo-code of our TME technique is depicted in Table I below while the Fig. 3 pictorially illustrates the steps of our articulated TME method along with the respective computational complexity using 'big' notation.

In Fig. 3, there are two images which are rotated and translated with respect to one another in 2D Euclidean sub-space. The images are taken from the inbuilt 'Brain MRI' database that comes with the MATLAB R2015a. One of the MRI image is considered as the reference image (R) while the other is the floating image (F). 'P' numbers of feature points, denoted by green dots in Fig. 3, are detected and matched by an existing feature detection and matching technique [10]. The co-ordinates of the matched feature point are represented by x_r and y_r for the reference and the floating image respectively. Clearly, the problem depicted in Fig. 3 is a 2D problem (translation in two directions, i.e., x and y , and along with rotation in one direction, i.e., θ). Any of the feature points in R, along with its matched correspondence in F, are considered as 'Ground Nodes' (GNs). These GNs are denoted as R(1) and F(1) in Fig. 3. At first, the co-ordinates of these GNs are aligned with origin $(0,0)$. Likewise, the co-ordinates for all other feature points are adjusted to get translated feature points, x_s and y_s , following the simple subtraction operations, as expressed by the following equations,

$$(3.18)$$

$$(3.19)$$

$$(3.20)$$

$$(3.21)$$

$$(3.22)$$

Naturally, for 'P' numbers of feature points, total 'P' numbers of subtraction operations need to be performed following Eq. 3.19 to Eq. 3.22. The computational complexity for these subtraction operations can be represented by $O(P)$. It is to be noted that, by virtue of these subtraction operations, the 2D problem has been reduced to a 1D problem as both the images R and F are now linked to the origin through the GNs with the only misalignment being in direction. Now, any of the feature points along with its matched correspondence get virtually connected with GN by straight lines. In Fig. 3, R(2) and its matched corresponding F(2) are connected with GN, thus getting 'A' and 'B' vector. The vector 'A' is considered as reference, and the vector, 'B', gets overlapped with A by means of conventional CORDIC method in 'Vectoring Mode' (VM) [11, 12] with computational complexity for 'P' bit precision. Using this single CORDIC operation in VM, the required angle of rotation (θ) between R and F is grossly estimated. In the next step, the fine tuning is performed to accurately estimate θ and the translation. In the fine tuning step, the rest of the (P-2) feature points along with their respective matched correspondence points are

connected with GN to have (P-2) pairs of vectors. In Fig. 3, as an example, one pair of such vectors ('C' and 'D') is shown by green dotted line. The vector 'C' is rotated by the previously estimated approximate angle, to get a rotated vector FV. This rotation of the vector 'C' by θ is performed using our LCORDIC. In ideal case, considering θ been estimated accurately, FV should perfectly coincide with the vector 'D'. But, practically this will rarely happen due to error in estimating. So, to compute the error, the co-ordinates of the end points of the FV and 'D' get subtracted to have the respective errors in co-ordinate values [13]. This fine tuning process is repeated for all the (P-2) pairs of vectors to get (P-2) numbers of errors in co-ordinates values. Then, RMSE is calculated from these (P-2) error values. Finally, the floating image F is rotated by followed by subtraction of RMSE value from the co-ordinates of each pixels of the rotated F image to precisely align it with the R image. Basically, the fine tuning step consists of (P-2) numbers of LCORDIC operation in 'Rotation Mode' (RM) and 2(P-2) number of subtraction operation to correct the error in co-ordinate values. As, in this fine tuning step, we have utilised our LCORDIC 'P-2' number of times, the total computational complexity of this fine tuning step, can be considered

as $O(P^2)$. So, the overall computational complexity of our formulated LCORDIC based TME method amounts to

$O(P^2)$ which equals to $O(P^2)$. In any other existing conventional matrix

algebra based 2D TME technique, at least one matrix inversion and one matrix multiplication operations are involved [13-16]. The computation complexity of such conventional TME technique is considering $O(P^3)$ as the size of the input images. So, it is evident that we have been successful to radically reduce the computational load of 2D TME method which, in turn, will definitely bring down the computational load of any IR algorithm. Another noteworthy achievement is that our formulated LCORDIC based TME method has such a computational complexity that is completely independent to the size of the input images, thus invariably catering same timing performance irrespective of the imaging modality and size. In this sense, our TME method can be labelled as universal, unique and hardware realizable. The pseudo code for our formulated 2D TME method is briefed in Table I with necessary mathematical equations.

TABLE I: CORDIC BASED 2D TME METHOD

LCORDIC based 2D TME method
Inputs: Reference Image (R), Floating Image (F)
Outputs: F aligned onto R
Procedure:
For (i=0, i<P, i++) loop
If i=1 then
[Detailed procedure steps]
Else
Endif;

```

    End for;
    For(i=0, i<P, i++) loop
        If (i=1) then
            Apply conventional CORDIC in VM upon          to make
            it aligned with , thereby getting;
        Else
            Apply LCORDIC in RM upon          to rotate it by , thereby
            getting final vector .
        End if;
    End for;
     $\sqrt{\Sigma}$  and  $\sqrt{\Sigma}$ 
    [ ] [ ] [ ] [ ]
    
```

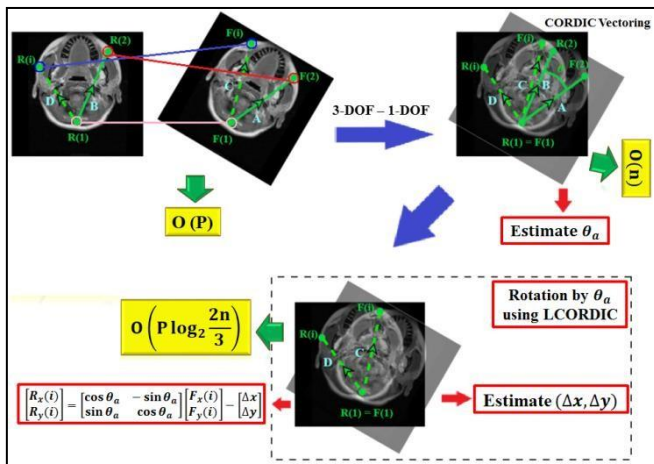


Fig. 3. Proposed 2D TME method using CORDIC

B. Proposed VLSI Architecture of IR

As our main aim is to design VLSI architecture for real-time IR, at first, our formulated first-of-its-kinds 2D TME method is realised in terms of dedicated hardware. The main hurdle (extensive computational load) for realising any TME method in terms of hardware has already been removed by the formulation of our computation-efficient CORDIC based 2D TME method, which has already been illustrated in the previous sub-section. In this sub-section, pipelined VLSI architecture for our established 2D TME method has been depicted. Our designed computation-efficient VLSI architecture of TME method has been integrated with the behavioral realizations of other standard IR steps using VHDL in Xilinx Vivado 18.2 tool for the implementation of real-time IR algorithm in terms of hardware. In the following, we have discussed the VLSI architecture of our formulated TME technique. Finally, we have described the hardware realization of real-time IR method involving our designed TME architecture in the form of a block diagram.

Our designed VLSI architecture of TME method is shown in Fig. 4 below. In Fig. 4, the dotted lines represent pipelining.

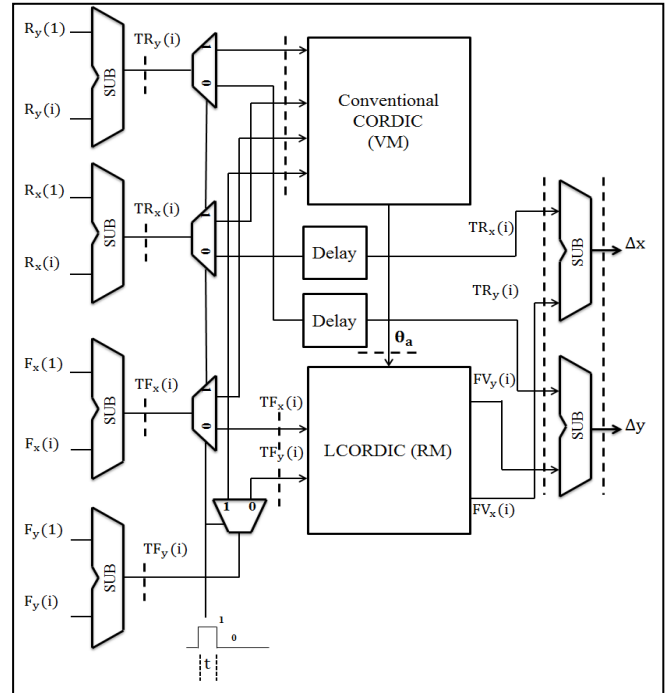


Fig. 4. Proposed VLSI architecture for our 2D TME method

From Fig. 4, it can be perceived that our designed VLSI architecture of 2D TME method only contains six subtractor denoted as ‘SUB’, four de-multiplexers and two delay blocks denoted as ‘Delay’ in addition to one conventional and one LCORDIC block. So, it can be said that the total area consumption of our designed TME architecture is almost similar to the area consumption of our LCORDIC architecture. In Fig. 4, the ‘Delay’ blocks are used for achieving synchronism in operations. Those ‘Delay’ blocks are realized in terms of D-flip-flops providing a delay equivalent to the sum of the delays of the ‘Conventional CORDIC (VM)’ and ‘LCORDIC’ blocks. In the above figure, the width of the trigger pulse connected to the select inputs of all the de-multiplexers is set equal to the delay of the ‘Conventional CORDIC (VM)’ block for proper synchronization. The outputs from our designed TME architecture is.

In this subsection, we have realized real-time IR method in terms of dedicated hardware. While realizing real-time IR method, we have utilized our designed VLSI architecture for 2D TME. All the other steps of any standard IR algorithms, apart from TME, are realized in behavioral VHDL coding following standard existing approach. The block diagram for the hardware realization of our formulated TME technique based IR method is shown in Fig. 5 below. In the Fig. 5, the hardware realization (using VHDL language in Xilinx Vivado 18.2) of the ‘Feature Detection’ and the ‘Feature Matching’ blocks are performed following the approach as mentioned in the paper [17]. The realization of ‘Image Resampling and Transformation’ is realized in VHDL following the approach of [18]. The inputs and outputs of our designed TME block are matched feature points denoted by ‘A’ and the transform vectors () respectively.

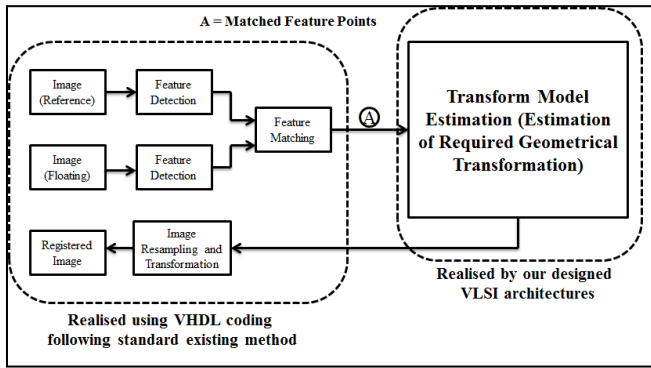


Fig. 5. Block diagram of the hardware realization of our TME technique based IR method.

IV. PERFORMANCE EVALUATION

The performance of VLSI architecture for real-time IR is extensively evaluated in terms of accuracy (SSIM), time complexity, hardware complexity and power consumption. The performance assessment has been performed in two phases. In the first phase, we have comparatively estimated the quality of our designed 2D TME architecture with respect to its software based counterpart using MATLAB. In this phase, we have implemented our prototype 16 bit TME architecture in the 16 nm FinFET+ technology based Xilinx Zynq UltraScale+ MPSoC series FPGA (XCZU7EV-2FFVC1156). Then we have interfaced the FPGA board (Xilinx ZCU104) with the host PC. After that, we have sent one reference and one floating images from host PC to the FPGA board for estimating the geometric transformation of the floating image with respect to the reference one in real-time. The accuracy and the computation speed of this estimation is measured and compared with respect to its software based counterpart. We have also proved that the computation time of our designed first-of-its-kinds 2D TME architecture is invariant to the input image sizes. In the next phase, we have moved on to comprehensively assess the quality of our developed IR architecture with respect to the existing works of [7, 8] The performance evaluation procedures for each of the phases are detailed in the following.

The performance of our developed TME architecture is estimated in terms of accuracy (SSIM), computation time, maximum operating frequency and power consumption. The power consumption is again measured using the integrated power analyzer tool of Xilinx Vivado 18.2. The performance of our developed LCORDIC based 2D TME architecture is compared with the MATLAB based 2D TME implementation running on our intel(R) Core(TM) i3-2310M ‘Central Processing Unit’ (CPU). For evaluating the performance of our developed 2D TME architecture in case of real-time operation, we have established connection between the host PC and FPGA board (Xilinx ZCU 104) to send the input from host PC to FPGA and to fetch the output from FPGA to hostPC.

After the Zynq UltraScale+ MPSoC FPGA has been configured with our 2D TME architecture, we have sent the

coordinates of the matched feature points between one 256 X 256 reference image, ‘Lena’ and its rotated version around axis. The transformation vectors (T_x and T_y) get calculated in the FPGA and the same is sent back to the host PC via the connection stated above. In the host PC, the transformation vectors are utilized to restore the rotated ‘Lena’ image using MATLAB R2015b. After that, 2D bi-cubic spline interpolation is performed on the restored image as this interpolation stage is necessary after any rotation operation performed on any image. This interpolation operation is performed using the standard bi-cubic spline command ‘interp2’ in MATLAB R2015b. Then 2D SSIM is calculated using the procedure stated in [1,2] using MATLAB R2015b. Then the accuracy (SSIM), computation time, maximum operating frequency and power consumption of our FPGA based TME architecture and its full MATLAB based realization are compared in case of the above-mentioned real-time operation as shown in the following Table II. In the Table II, we have also compared the performance of our established design for another image ‘image_1_1’ (taken from ‘H2OPM Image Registration Dataset’ [3]) in varying sizes. The size of the image ‘image_1_1’ has been made varying using ‘imresize’ command in MATLAB R2015b. The coordinates of the matched feature points between ‘image_1_1’ images of varying sizes with its respective rotated versions around axis are sent from the host PC to FPGA. The transformation vectors (T_x and T_y) get calculated in the FPGA and the same is sent back to the host PC for each of the sizes of the image ‘image_1_1’.

TABLE II: REAL-TIME COMPARATIVE PERFORMANCE EVALUATION OF OUR 2D TME

Image	MATLAB R2015b Based TME				Zynq UltraScale+ MPSoC FPGA Based TME			
	SSIM	CT (ms)	MOF (MHz)	PC (mW)	SSIM	CT (ms)	MOF (MHz)	PC (mW)
Lena (256 X 256)	0.86	372	2.10 GHz	77,000	0.83	0.0171	385	12.98
image_1_1 (256 X 256)	0.85	385	2.10 GHz	77,000	0.81	0.0173	385	12.98
image_1_1 (512 X 512)	0.91	692	2.10 GHz	77,000	0.88	0.0175	385	12.98
image_1_1 (1024 X 1024)	0.90	2453	2.10 GHz	77,000	0.87	0.0172	385	12.98
image_1_1 (2048 X 2048)	0.89	7562	2.10 GHz	77,000	0.86	0.179	385	12.98

From the above Table II, it can be inferred that the hardware realization of our TME architecture outperformed its software based counterpart (using MATLAB R2015b) in terms of CT, MOF and PC while exhibiting comparable performance in terms of accuracy. The accuracy can further be increased in case of TME architecture by increasing bit precision with very minimal timing overhead as our designed LCORDIC based TME architecture uniquely maintains sub-linear relationship between bit precision and time complexity. The notable fact, from the above table is that the computation time of the hardware realization of our established TME method is invariant to the image size which is not the case for its software based realization. Thus our established TME architecture is found to be effective for being utilized in case of real-time IR method.

Now, our established TME architecture is utilized to develop full hardware realization of our formulated TME based IR method. After that, the performance of the full hardware realization of IR is evaluated in comparison to the software based counterpart following the same evaluation approach as mentioned in the previous subsection 3.5.2. For evaluating the real-time performance we have sent one pair of images (reference image and floating image) to the FPGA from host PC. The pair of images considered here are 'image_1_1' (reference) and 'image_1_2' (floating). Both the images are taken from 'H2OPM Image Registration Dataset [3]'. The comparison is performed with respect to the software based counterpart as shown in Table III below.

TABLE III: REAL-TIME COMPARATIVE PERFORMANCE EVALUATION OF OUR 2D TME BASED IR

Image Size	MATLAB R2015b Based Realization				Zynq UltraScale+ MPSoC FPGA Based Realization			
	SSIM	CT (ms)	MOF (MHz)	PC (mW)	SSIM	CT (ms)	MOF (MHz)	PC (mW)
(256 X 256)	0.88	895	2.10 GHz	77.000	0.87	0.0413	257	23.59
(512 X 512)	0.85	1262	2.10 GHz	77.000	0.86	0.0497	257	23.59
(1024 X 1024)	0.87	2813	2.10 GHz	77.000	0.89	0.0582	257	23.59
(2048 X 2048)	0.85	8182	2.10 GHz	77.000	0.83	0.0701	257	23.59

From the above table, it can be seen that the hardware realization of our IR method outshines its software based counterpart. But this time an increase in CT can be noted with increasing image size. This increase in CT with varying image size can be attributed to the behavioral VHDL based realizations of standard IR steps integrated with our designed TME architecture. The MOF is also reduced in comparison to our designed TME architecture, as shown in Table III. The cause of such reduction in MOF can

also be attributed to the behavioral VHDL based realizations of standard IR steps integrated with our designed TME architecture.

We have compared the performance of our VLSI implementation of IR algorithm with that of the work of [7, 8] in the following Table IV. For that the works of [7, 8] are realized into bit fixed point format and implemented on the same FPGA platform as ours. Again, the same pair of images 'image_1_1' (reference) and 'image_1_2' (floating) [3] are considered as inputs.

TABLE IV: REAL-TIME COMPARATIVE PERFORMANCE EVALUATION OF OUR 2D TME BASED IR WITH THE WORKS OF [7, 8]

Works	Parameter	Image Size			
		(256 X 256)	(512 X 512)	(1024 X 1024)	(2048 X 2048)
[7]	SSIM	0.83	0.82	0.84	0.81
	CT	52.42	174.49	342.12	627
	MOF	80	80	80	80
	PC	123.34	123.34	123.34	123.34
[8]	SSIM	0.81	0.85	0.86	0.88
	CT	37	120	253.12	376.43
	MOF	174	174	174	174
	PC	67.12	67.12	67.12	67.12
Ours	SSIM	0.87	0.86	0.83	0.90
	CT	0.0413	0.0497	0.0582	0.0701
	MOF	257	257	257	257
	PC	23.59	23.59	23.59	23.59

From the above table, it is evident that the performances of our designed VLSI architecture for IR method surpass the work of [7, 8] in terms of CT, MOF and PC while maintain comparable accuracy in terms of SSIM. From the above discussion, it can be inferred that our designed LCORDIC based TME architecture and the complete hardware realization of IR are suitable to be employed in case of any real-time applications where both the accuracy and speed of operation are of prime importance.

V. CONCLUSION

In this article, a novel VLSI architecture for real-time IR has been proposed. At first, the time complexity of the most time consuming step of any IR method, i.e., TME, is reduced to make this TME step hardware resizable. The hardware efficient nature of CORDIC algorithm is exploited to realize the proposed computation efficient 2D TME method in terms of dedicated VLSI architecture. Then the uniquely designed CORDIC based 2D TME architecture is integrated with the standard VHDL realizations of the other steps of IR method to realize the whole IR method in terms of dedicated hardware. Finally, the performances of the proposed VLSI architecture of the 2D TME method along with the hardware for whole IR algorithm is extensively evaluated with software based counterpart and also with the

exiting architectures to prove the supremacy of our works. The designed architecture not only provides a ready cost effective solution for the real-time IR applications but also opens a new arena of research on CORDIC based IR realizations.

REFERENCES

- [1] Russ JC, Neal FB (2015) The Image Processing Handbook, 7th edn. CRC Press, Inc., Boca Raton, FL, USA
- [2] Bovik AC (2005). Handbook of Image and Video Processing (Communications, Networking and Multimedia). Academic Press, Inc., Orlando, FL, USA.
- [3] Zambanini, S. (2019). Feature-based groupwise registration of historical aerial images to present-day ortho-photo maps. *Pattern Recognition*, 90, 66-77. doi:10.1016/j.patcog.2019.01.024
- [4] Zitova, B., & Flusser, J. (2003). Image registration methods: a survey. *Image and vision computing*, 21(11), 977-1000.
- [5] Xiong, Z., & Zhang, Y. (2010). A critical review of image registration methods. *International Journal of Image and Data Fusion*, 1(2), 137-158.
- [6] [Online Available:] <https://in.mathworks.com/help/images/matrix-representation-of-geometric-transformations.html>
- [7] Gupta, N., & Gupta, N. (2007). A VLSI architecture for image registration in real time. *IEEE Transactions on Very Large Scale Integration (VLSI) Systems*, 15(9), 981-989. doi: 10.1109/TVLSI.2007.902210
- [8] Mishra, A., Mondal, P., & Banerjee, S. (2015). VLSI-Assisted nonrigid registration using modified demons algorithm. *IEEE Transactions on Very Large Scale Integration (VLSI) Systems*, 23(12), 2913-2921. doi: 10.1109/TVLSI.2014.2382134
- [9] A. Chakraborty and A. Banerjee, "Low Latency Semi-iterative CORDIC Algorithm using Normalized Angle Recoding and its VLSI Implementation," *2019 International Conference on Communication and Signal Processing (ICCSPP)*, Chennai, India, 2019, pp.0913-0920.
- [10] Ni, Q., Wang, F., Zhao, Z., & Gao, P. (2019). FPGA-based Binocular Image Feature Extraction and Matching System. arXiv preprint arXiv:1905.04890.
- [11] Lakshmi, B., & Dhar, A. S. (2010). CORDIC architectures: A survey. *VLSI design*, 2010, 2. doi: 10.1155/2010/794891
- [12] Banerjee, A., & Dhar, A. S. (2013). Pipelined VLSI architecture using CORDIC for transform domain equalizer. *Journal of Signal Processing Systems*, 70(1), 39-48. doi:10.1007/s11265-012-0657-7
- [13] Parkin A (2013) *Digital Imaging Handbook*, Springer Publishing Company, Incorporated.
- [14] Arthur R, Weeks J (1996) *Fundamentals of Electronic Image Processing*, IEEE Press, New York
- [15] Young IT, Gerbrands JJ, Van Vliet LJ (1998) *Fundamentals of image processing*, Delft, The Netherlands: Delft University of Technology
- [16] Bovik AC (2005). Handbook of Image and Video Processing (Communications, Networking and Multimedia). Academic Press, Inc., Orlando, FL, USA.
- [17] Ni, Q., Wang, F., Zhao, Z., & Gao, P. (2019). FPGA-based Binocular Image Feature Extraction and Matching System. arXiv preprint arXiv:1905.04890.
- [18] Zheng, J., Song, W., Wu, Y., & Liu, F. (2019). Weighted direct nonlinear regression for effective image interpolation. *IEEE Access*, 7, 8646-8659. doi:10.1109/ACCESS.2018.2890517

OUR SPONSORS



GLIMPSE OF 2019



**PROCEEDINGS OF 2020 IEEE SIXTH INTERNATIONAL CONFERENCE ON
BIOSIGNALS, IMAGES AND INSTRUMENTATION
(ICBSII 2020)**

Biomedical Engineering is a field of study that integrates two dynamic professions, Medicine and Engineering. It has recently established itself as an independent field with the objective of assisting medicine towards the betterment of society, through research.

Being an interdisciplinary science, it has associations with various other subjects such as Electrical Engineering, Mechanical Engineering, Chemical Engineering and Biotechnology. The spectrum of Bio-medical research aims to unite these disciplines in synergy, leading to new possibilities thus enabling the development of technology that could save lives.

The Sixth International Conference on Bio Signals, Images and Instrumentation (ICBSII-2020) was conceived with the thought of bringing together scientists, engineers and researchers from various domains all over the world. It has been a platform where some of the greatest minds of the country and abroad could interact, exchange ideas and work together towards a common goal.

Research papers were received from diverse areas such as Physiological Modeling, Medical Imaging, Medical Robotics, Biomechanics, Biomedical Instrumentation and Nano-materials amounting to a total of 103 papers. After a rigorous review process by an expert review committee, 24 papers that displayed quality in idea and work were selected for final presentation at the conference.

This conference is the fruit of a vision of the Management, faculty and students of the Department of Biomedical Engineering, SSN College of Engineering in association with the Centre for Healthcare Technologies (CHT), a multi-disciplinary R&D center, which works unanimously towards materializing it and they were instrumental in its success.

The Department of Biomedical Engineering, since its inception in 2005, has been a pioneer in the field of biomedical technology, instrumentation, and administration. The department has excellent infrastructure, experienced faculty members and motivated students. Department also has foreign collaborations which includes Birmingham City University, UK, Drexel University Philadelphia, and several industries such as L&T Medical System, Sri Ramachandra Medical College, Indian Biomedical Skill Consortium (IBSC), NIEPMD. Department has successfully conducted a retreat on "How to make India ready for 21st Century Medical device revolution?" with International and National delegates presenting their views on the topic. To add feather to the crown, the department has conducted three International conferences (ICBSII) in 2013, 2015, 2017, 2018, 2019 and two national conferences (NCABES) in 2014, 2016.

